

Chatham Island Paleocene fossils provide insight into the palaeobiology, evolution, and diversity of early penguins (Aves, Sphenisciformes)

Jacob C. Blokland, Catherine M. Reid, Trevor H. Worthy, Alan J.D. Tennyson, Julia A. Clarke, and R. Paul Scofield

ABSTRACT

Numerous skeletal remains recovered *in situ* from the late early to middle Paleocene Takatika Grit of Chatham Island, New Zealand, are among the oldest known fossils attributed to the penguin clade (Aves, Sphenisciformes). They represent a new medium-sized taxon, for which we erect a new genus and species, and a second, notably larger form. These new penguins are analysed in a parsimony and Bayesian framework using an updated and revised phylogenetic matrix, based on morphological and molecular characters, and interpreted as among the most basal of known sphenisciforms, closely related to *Waimanu*. While sharing numerous characteristics with the earliest wing-propelled divers, the novel taxon records the oldest occurrence of the characteristic penguin tarsometatarsus morphology. These ancient Chatham Island representatives add to a growing number and increased morphological diversity of Paleocene penguins in the New Zealand region, suggesting an origin for the group there. With their addition to other Paleocene penguins, these taxa reveal that sphenisciforms rapidly diversified as non-volant piscivores in the southern oceans following the end-Cretaceous mass extinction. They also provide further evidence for the hypothesis that their origin predates the Paleocene. This implies that stem Sphenisciformes and their sister group, the Procellariiformes, both originated in, and so may be expected to occur in, the Late Cretaceous.

Jacob C. Blokland. Biological Sciences, College of Science and Engineering, Flinders University, Bedford Park 5042, South Australia, Australia. jacob.blokland@flinders.edu.au
Catherine M. Reid. School of Earth and Environment, College of Science, University of Canterbury, Private Bag 4800, Christchurch 8140, New Zealand. catherine.reid@canterbury.ac.nz
Trevor H. Worthy. Biological Sciences, College of Science and Engineering, Flinders University, Bedford Park 5042, South Australia, Australia. trevor.worthy@flinders.edu.au

<http://zoobank.org/575B2ACF-4CB6-4C43-8F53-A62915EEB255>

Blokland, Jacob C., Reid, Catherine M., Worthy, Trevor H., Tennyson, Alan J.D., Clarke, Julia A., and Scofield, R. Paul. 2019. Chatham Island Paleocene fossils provide insight into the palaeobiology, evolution, and diversity of early penguins (Aves, Sphenisciformes). *Palaeontologia Electronica* 22.3.78 1-92. <https://doi.org/10.26879/1009>
palaeo-electronica.org/content/2019/2773-chatham-island-penguins

Copyright: December 2019 Society of Vertebrate Paleontology.

This is an open access article distributed under the terms of the Creative Commons Attribution License, which permits unrestricted use, distribution, and reproduction in any medium, provided the original author and source are credited.
creativecommons.org/licenses/by/4.0/
creativecommons.org/licenses/by-nc-sa/4.0/

Alan J.D. Tennyson. Museum of New Zealand Te Papa Tongarewa, PO Box 467, Wellington 6140, New Zealand. AlanT@tepapa.govt.nz

Julia A. Clarke. Department of Geological Sciences, Jackson School of Geosciences, University of Texas at Austin, 2305 Speedway Stop C1160, Austin, TX 78712-1692, USA. Julia_Clarke@jsg.utexas.edu.

R. Paul Scofield. Canterbury Museum, Rolleston Avenue, Christchurch 8013, New Zealand. pscofield@canterburymuseum.com

Keywords: new genus; new species; palaeontology; New Zealand; phylogenetics; waterbirds

Submission: 12 July 2019. Acceptance: 2 October 2019.

INTRODUCTION

There now exists a wealth of literature dedicated to the origin and diversification of crown group birds, or Neornithes, which has progressively elucidated the evolutionary history and framework of major modern bird clades (e.g., Feduccia, 1995; Ericson et al., 2006; Livezey and Zusi, 2007; Jarvis et al., 2014; Claramunt and Cracraft, 2015; Prum et al., 2015; Reddy et al., 2017; Houde et al., 2019; and references therein). Most modern birds are included within Neoaves, a clade which most recent molecular-based phylogenetic studies estimate emerged during the Late Cretaceous (Ericson et al., 2006; Pacheco et al., 2011; Jarvis et al., 2014; Lee et al., 2014; Claramunt and Cracraft, 2015; Prum et al., 2015; contra Brown et al., 2008). Subsequently, neoavian lineages are shown to have rapidly diversified into the abundance of ecological niches that immediately became available following the Cretaceous/Paleogene (K/Pg) mass extinction (Ericson et al., 2006; Jarvis et al., 2014; Claramunt and Cracraft, 2015; Ksepka and Phillips, 2015; Prum et al., 2015). Consistent with a lack of molecular support for their extensive diversification before the conclusion of the Cretaceous (Ericson et al., 2006), Late Cretaceous fossil neornithines—especially those proposed to have neoavian affinities—are particularly scarce and fragmentary (Chatterjee, 2000; Feduccia, 2003; Dyke and van Tuinen, 2004; Mayr, 2009; Agnolin, 2010; Longrich et al., 2011; Agnolin and Novas, 2012; Brocklehurst et al., 2012; Feduccia, 2014; Mayr, 2017; Mayr et al., 2018a; Tambussi et al., 2019; West et al., 2019). Comparatively, there are many definitive, well-preserved neoavian birds known from the early Paleogene onwards (see Mayr, 2017 and references therein). The fossil record evidences that stem group representatives of almost all modern neoavian orders were present in the early Eocene (Feduccia, 1995; Blondel and Mourer-Chauviré, 1998; Feduccia, 2003; Mayr, 2005; Ericson et al., 2006; Mayr, 2014), corroborated

by molecular estimates for divergence of most distinct lineages by 50 Ma (Jarvis et al., 2014).

Sphenisciformes (penguins), Procellariiformes (tubenoses), Gaviiformes (loons) and Phaethontiformes (tropicbirds) are diverse and early diverging clades in the radiation of waterbirds. The former three form part of the well-supported core waterbird assemblage, Aequornithes, sensu Mayr (2010), among Neoaves (e.g., Hackett et al., 2008; Mayr, 2017). Tropicbirds have also been shown to have a close relationship to this core waterbird clade (e.g., Prum et al., 2015; Houde et al., 2019). Late Cretaceous and early Paleogene fossils are well known for the Sphenisciformes (Tambussi et al., 2005; Slack et al., 2006; Jadwyszczak et al., 2013; Mayr et al., 2017a, 2017b, 2018b), Procellariiformes (Olson and Parris, 1987; Ksepka and Cracraft, 2008), and Phaethontiformes (Mayr and Scofield, 2016), though are not convincingly assigned for Gaviiformes (see Lambrecht, 1929; Chatterjee, 1989, 2000; Chiappe and Dyke, 2002; Mayr, 2004; Mayr et al., 2013; Mayr, 2014; Acosta Hospitaleche and Gelfo, 2015; Mayr, 2017; Mayr et al., 2018a).

Penguin fossils are relatively abundant in southern high-latitude Cenozoic sites, possibly due to their greater fossilisation potential, considering their shallow marine habitat and robust limb bones (Ksepka and Ando, 2011). Until recently sphenisciform fossils from the Paleocene were scarce (Jadwyszczak, 2009; Mayr et al., 2017a, 2017b, 2018b, 2019), however, the origin of basal stem-penguin evolution remains poorly resolved (Fordyce and Thomas, 2011). The oldest described sphenisciforms are from the Waipara Greensand in the Waipara River, Canterbury, New Zealand. These fossils include the larger and more basal (e.g., Gavryushkina et al., 2017) *Waimanu manneringi* Jones, Ando and Fordyce, 2006 in Slack et al. (2006), constrained between 60.5–61.6 Ma, and the slightly younger (58–60 Ma) and smaller *Muri-*

waimanu tuatahi (Ando, Jones, and Fordyce, 2006; in Slack et al., 2006). As aquatic wing-propelled divers, these fossils exhibit many derived characteristics of extant penguins, yet also display the most plesiomorphic morphology of Sphenisciformes to date (Mayr, 2017); superficially similar to diving alcids (Alcidae), and the extinct penguin-like plotopterids (Plotopteridae) (Slack et al., 2006; Fordyce and Thomas, 2011). Slightly more derived forms recovered from the same locality as remains attributed to *Waimanu* and *Muriwaimanu* include *Sequiwaimanu rosieae* Mayr, De Pietri, Love, and Mannering and Scofield, 2018b, described from a partial skeleton, and an unnamed giant form that is represented by distal leg bones, of middle Paleocene (~61 Ma) age (Mayr et al., 2017a, 2018b). Most recently, *?Crossvallia waiparensis* Mayr, De Pietri, Love, and Mannering and Scofield, 2019, was described from leg bones, representing an additional very large form, which was also recovered from the Paleocene Waipara Greensand (Mayr et al., 2019). The late Paleocene (59.5-55.5 Ma) giant penguin *Kumimanu biceae* Mayr, Scofield, De Pietri and Tennyson, 2017b, from the Moeraki Formation on Hampden Beach, Otago, New Zealand, further expands the known diversity of the oldest Sphenisciformes (Mayr et al., 2017b). Outside of New Zealand, the only representative of these earliest penguins is the giant *Crossvallia unienwillia* Tambussi, Reguero, Marensi and Santillana, 2005, from the late Paleocene (59.2-56 Ma) Cross Valley Formation of Seymour Island, Antarctica (Tambussi et al., 2005; Jadwiszczak et al., 2013). While *C. unienwillia* has been recovered in a basal position in a phylogenetic analysis (Chávez Hoffmeister, 2014), the fragmentary and incomplete nature of the fossils prohibits comparison with most stem group penguins.

Here we describe two novel basal penguins, from numerous fossils recovered from the Takatika Grit, Chatham Island, New Zealand. Specimens were recovered in situ from the same wave platform and relatively narrow “bird horizon”, overlying the ‘nodular phosphorite-bone package’ (sensu Stilwell et al., 2006), between 2006 and 2011 by Jeffrey D. Stilwell and parties, and likely represent numerous individuals. We taxonomically describe and examine the phylogenetic affinity of the medium-sized taxon and, due to its incompleteness, only comment on the second, larger form. Dated to the late early to middle Paleocene (62.5-60 Ma, New Zealand Teurian stage, Hollis et al., 2017), these specimens are among the oldest known fossils of Sphenisciformes and are signifi-

cant to the understanding of basal members of this clade, as well as early neoavian waterbird evolution. As some of the oldest avifauna recovered from the continental block associated with New Zealand, examination of these specimens is additionally important in understanding the ecology of early Zealandian seas.

GEOLOGICAL CONTEXT

The reported fossil specimens were recovered from main Chatham Island (Rēkohu), part of the Chatham Islands located 860 km off the east coast of New Zealand’s mainland on the largely submerged Chatham Rise (Figure 1) (Norris, 1964; Consoli and Stilwell, 2011). Collectively referred to as the Chatham Islands, Chatham and Pitt Island (Rangiaotea), and several smaller islands, are the only exposed land areas on the largely submerged Chatham Rise (Norris, 1964). The Chatham Islands, together with New Zealand and New Caledonia, and the interconnecting submerged Chatham Rise, Campbell Plateau, Lord Howe Rise, and Norfolk Ridge form the continental geological block that is referred to as Zealandia (Campbell et al., 1993; Consoli and Stilwell, 2011; Mortimer et al., 2017).

On northern Chatham Island, the Takatika Grit outcrops as steep, low-lying coastal cliffs and a 2 km span of wave-cut platforms and isolated blocks eroded from the cliff-line (between 43.743°S, 176.683°W and 43.750°S, 176.667°W) along the length of Maunganui Beach (Stilwell et al., 2006; Consoli, 2008; Consoli et al., 2009; Consoli and Stilwell, 2009). The Takatika Grit additionally occurs inland along Tutuiri Creek in a series of creek cuttings (Campbell et al., 1993; Consoli, 2008; Consoli and Stilwell, 2009). At a maximum thickness of 10 m (Stilwell et al., 2006; Stilwell, 2007; Consoli et al., 2009; Consoli and Stilwell, 2009) the Takatika Grit unconformably overlies the regional basement Chatham Schist and is conformably succeeded by the Tutuiri Greensand (Figure 1) (Campbell et al., 1993; Consoli and Stilwell, 2005). From an exclusively inland basal breccia, the Takatika Grit outcrops along Maunganui Beach as a fossiliferous, dark green-grey, well-bedded, poorly-sorted, glauconitic lithic wackestone (Consoli et al., 2009) with predominately fine glauconitic grains, quartz and metamorphic lithic inclusions, imbedded within a clay matrix, and often supported by siliceous cement (Consoli and Stilwell, 2009). A minor volcanic constituent is also observed (Stilwell et al., 2006; Stilwell, 2007). Three horizons containing macrofossils are known from the Taka-

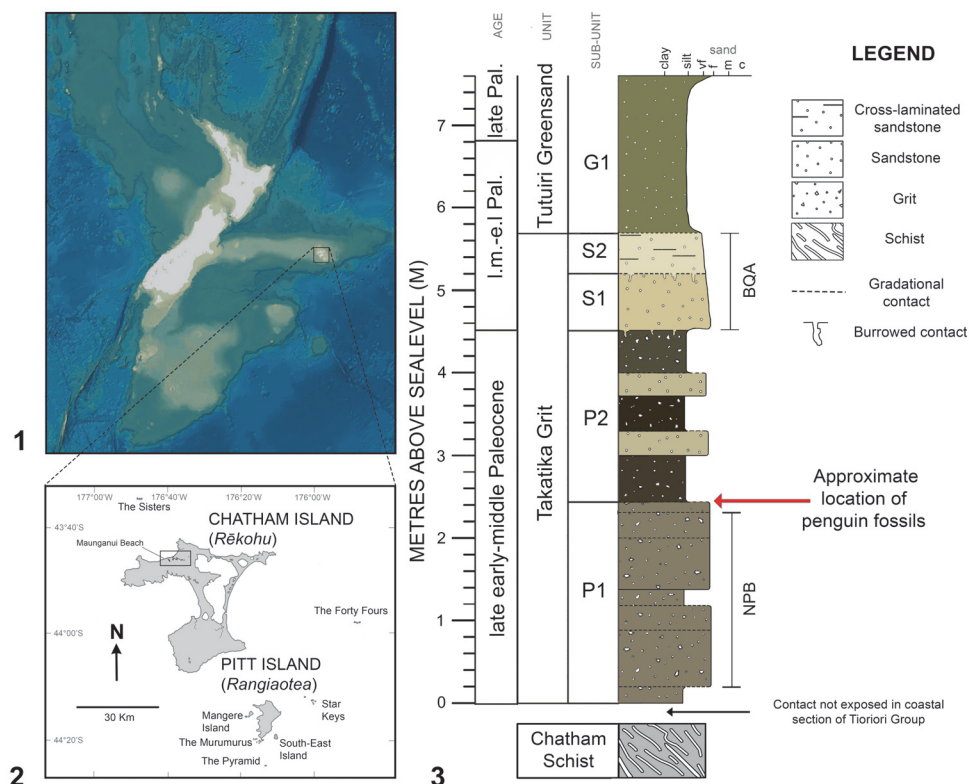


FIGURE 1. Locality information. **1**, Relative position of New Zealand and the Chatham archipelago; **2**, The locality on the Chatham Islands where the fossils were found; **3**, Stratigraphic column showing the Takatika Grit, from which the fossils were recovered. The stratigraphy is based on the same locality and stratigraphy illustrated in Hollis et al. (2017, figure 3) and also uses information from Consoli et al. (2009, figure 1). Ages, units, and sub-units refer to those specified in Hollis et al. (2017).

tika Grit, which show increasing fossil abundance up-section, and are laterally consistent across the areas the Takatika Grit outcrops (Stilwell et al., 2006). In the lower (Stilwell, 2007; Consoli et al., 2009) to mid-section (Consoli, 2008) of the glauconitic lithic wackestone, an abundance of differentially preserved fossils and authigenic phosphorite nodules of pebble to boulder size exist as a succinct package of several beds—together known as the nodular phosphorite-bone package (NPB) (Figure 1) (Consoli and Stilwell, 2005; Stilwell et al., 2006; Consoli, 2008; Consoli and Stilwell, 2009). Preserving the majority of fossils (Consoli and Stilwell, 2009), phosphorite nodules and skeletal elements in this package are almost conglomeratic in some areas (Consoli and Stilwell, 2005). The lower section of the NPB is characterised by poorly sorted, phosphatised grit among phosphate nodules and macrofossils, while the upper part is characterised by nodular-bedded sandstone and grit (Hollis et al., 2017). The Takatika Grit culminates in a bioclastic-quartz arenite package (BQA), suc-

ceeding the NPB, which lacks nodules, but is also fossiliferous (Figure 1) (Consoli et al., 2009).

Associated bird fossils, including the penguin material described herein, were recovered from a relatively narrow greensand horizon (Stilwell, personal commun., 2017, 2018), overlying the NPB, and distinguished from the NPB by a lack of phosphate nodules (Consoli, 2008). Specifically, these penguin fossils were found within crevasses and depressions created by the upper topography of the NPB in the uppermost P1, and in a narrow concretionary interval in the lowermost P2 (Figure 1.3) (Stilwell, personal commun. 2018). Fossils also recovered from this section include an abundant hexactinellid sponge fauna, teeth from the frilled shark *Chlamydoselachus tatere* Consoli, 2008, and isolated theropod dinosaur bones (Stilwell et al., 2006; Consoli, 2008; Consoli et al., 2009; Agnolin et al., 2010). Due to the presence of semi-articulated avian remains in these beds overlying the NPB, they are considered unlikely to have been reworked (Consoli et al., 2009).

The Takatika Grit formed as a product of extensional activity and progressive rifting from eastern Gondwana (Stilwell and Consoli, 2012), as Zealandia separated from West Antarctica c. 83-79 Ma (though possibly at or before 84 Ma, see Gaina et al., 1998; Laird and Bradshaw, 2004), and continued rifting from eastern Australia until the Eocene (Gaina et al., 1998; Sutherland, 1999; Bache et al., 2014; Rouillard et al., 2015; Tulloch et al., 2019). Through related post-rift thermal relaxation and subsidence, Zealandia experienced widespread marine transgression throughout this interval (Bache et al., 2014; Rouillard et al., 2015). In association with the oceanic inundation of the region, and the formation of a basin and basement range style landscape, the Takatika Grit formed as an accumulation of thin sandstones, greensands, and marine fossiliferous assemblages, deposited within half-grabens on the Chatham Rise simultaneously with intraplate volcanics (Campbell et al., 1993; Consoli and Stilwell, 2009; Consoli and Stilwell, 2011). Based on recent palynomorphic research, the Takatika Grit has been found to effectively preserve an initial marine transgression in the early Campanian (82-80 Ma), followed by an interval of non-deposition in the latest Cretaceous and earliest Paleocene, and renewed transgression and marine sedimentation in the late early to middle Paleocene (62.5-60 Ma) (Hollis et al., 2017).

MATERIALS AND METHODS

Appendix 1 should be referred to for details pertaining to undescribed elements, character definitions, states, ordering specifics, specimens used for character scoring, any coding changes, information relating to supplementary analyses, and associated figures (Figures A1-A10).

Nomenclature

Osteological and myological nomenclature follows Baumel et al. (1993) and Schreiweis (1982), except regarding the coracoid (Elzanowski et al., 2012; Worthy, 2012), distal femur morphology (Elzanowski, 2008), and that of the hypotarsus on the tarsometatarsus (Figure A10) (Mayr, 2016). All other osteological terminology used are followed by associated references. Directional and orientational language used here refers to the life-like positioning of bones in Sphenisciformes (e.g., Chávez Hoffmeister, 2014) and thus differs when compared to non-sphenisciform birds, particularly in regard to orientations of the forewing. Taxonomic nomenclature for extant and recently extinct taxa

follows Dickinson and Remsen (2013). Appropriate taxonomic authorities follow fossil taxa at their first mention.

Abbreviations

Institutions. AMNH, American Museum of Natural History, New York, United States of America; CM, Canterbury Museum, Christchurch, New Zealand; FUR, Flinders University Reference Collection, South Australia, Australia; IB/P/B, Institute of Biology, University of Bialystok; Poland; MACN, Museo Argentino de Ciencias Naturales; MLP, Museo de La Plata, La Plata, Argentina; ISAM, Iziko South African Museum, Cape Town, South Africa; MEF-PV, Museo Paleontológico Egidio Feruglio, Trelew, Argentina; MNHN, Muséum National d'Histoire Naturelle, Paris, France; MUSM Museo de Historia Natural, Universidad Nacional Mayor de San Marcos, Lima, Peru; NHMUK, Natural History Museum, London, United Kingdom; NMNZ, Museum of New Zealand Te Papa Tongarewa, Wellington, New Zealand; NMV B, Museum Victoria Ornithology Collection, Melbourne, Australia; NMV P, Museum of Victoria Palaeontology, Melbourne, Australia; NRM-PZ, Naturhistoriska Riksmuseet (Swedish Royal Museum of Natural History), Stockholm, Sweden; OM, Otago Museum, Dunedin, New Zealand; OU, Geology Museum, University of Otago, Dunedin, New Zealand; SAM P, South Australian Museum Palaeontology Collection, Adelaide, Australia; SGO-PV, Museo Nacional de Historia Natural, Santiago, Chile; UCMP, University of California Museum of Paleontology, Berkeley, CA; USNM, National Museum of Natural History, Smithsonian Institution, Washington DC, United States of America.

CT Scanning

The specimens NMNZ S.47303 and NMNZ S.47302 consist of fossils imbedded in a hard, lithological matrix (see Figures A1-A2). X-ray computed tomography (CT scanning) was utilised to allow non-destructive (Conroy and Vannier, 1984; Haubitz et al., 1988; Ketcham and Carlson, 2001), taxonomic assessment of these specimens without damaging the fossil material (e.g., Figure A3), to virtually separate and produce 3D models of the elements within the rocks (Lurino et al., 2013).

Both specimens were CT scanned at the Pacific Radiology, St Georges Hospital, Christchurch, New Zealand, using a SIEMENS/SOMATOM definition CT scanner, with the radiation setting of scans at 140 KVP. 411 virtual slices were made of NMNZ S.47302, and 821 slices were

made of NMNZ S.47303. Slices were taken in 0.2 mm increments and with a thickness of 0.4 mm. Three-dimensional segmentation and rendering was performed using *Materialise Mimics* (Materialise's Interactive Medical Image Control System) Innovation Suite 17.0.

Measurements

Measurements of the fossil elements in NMNZ S.47302 and S.47303 made using the integrated measurement tool in *Materialise Mimics*. Specimens NMNZ S.47308, S.47312, S.47339, and S.44729 were measured at NMNZ. Several elements in these specimens could not be confidently identified, or were not considered complete or informative enough to warrant quantitative and qualitative investigation (see Figures A1-A2, A5). All direct measurements of comparative material were carried out using a Mitutoyo 500-196-30CAL Absolute Advanced Onsite Sensor (AOS) digital calliper, accurate to 0.01 mm.

Phylogenetic Analyses

Data set. We constructed a phylogenetic data matrix to assess the relationships of the Chatham Island taxa in the framework of existing phylogenies from the matrices of Ksepka et al. (2012), Ksepka and Thomas (2012), Chávez Hoffmeister et al. (2014), Chávez Hoffmeister (2014), Park et al. (2016), Mayr et al. (2017a, 2017b, 2018b), and Degrange et al. (2018) using the most recent character definitions and states. GenBank accession numbers for molecular sequences are detailed in Table A1. Scored states from the most recent studies were used unless our examination showed otherwise. Where taxa could not be re-evaluated to assess more recent character definitions/states, scores were changed to “?” to avoid inaccurate coding. Unless indicated by coding changes in Table A2, character data (for example missing data) remains as presented by previous versions of the character matrix. In compiling our data matrix, we made key modifications as follows.

Outgroups. A volant distant outgroup taxon, *Phaethon rubricauda* (Phaethontiformes), was selected to better identify the evolutionary trajectory of character evolution as per the well-supported and commonly cited (e.g., Baker and Manwell, 1975; Raikow et al., 1988; Ksepka and Ando, 2011; Thomas et al., 2011; Ksepka et al., 2015) hypothesis that penguins are descended from aerially flighted ancestors (Simpson, 1946). Studies of higher avian phylogenies have long recovered Phaethontiformes among aquatic birds (Cracraft,

1981, 1988), part of a lineage sister to core water-bird clades (e.g., van Tuinen et al., 2001; Jarvis et al., 2014; Prum et al., 2015; Thomas, 2015; Houde et al., 2019). *Phaethon rubricauda* (Phaethontiformes) was scored for all osteological characters. As foot-propelled divers (Storer, 1971; Mayr, 2017), the taxa *Gavia immer* and *G. stellata* were subsequently excluded from all final analyses.

Characters. Two new characters were added to the resultant matrix: one relating tarsometatarsus trochlea metatarsi III morphology (character 266) as described in Mayr et al. (2018b: figure 2), and one pertaining to ulna shaft shape (character 203). While there is no certainty in assigning isolated elements to taxa named solely from tarsometatarsi (see Ksepka and Clarke, 2010), some character scores were inputted based on fossils from the Eocene La Meseta Formation, referred to taxa by Jadwiszczak (2006a, 2013, 2015) and Reguero et al. (2013). This increased character sampling for these taxa and potentially improved resolution of the phylogenetic dataset and facilitated assessment of the specific association of these elements (see Appendix 1, Figure A7). One character (character 242) was excluded from all analyses due to coding errors found in the matrix used by Chávez Hoffmeister (2014) and inability to re-score this character by direct examination of most of the taxa.

Taxa. The two new Chatham Island forms were added to the dataset, with NMNZ S.47302 and S.47304 tentatively associated based on size and source locality on Chatham Island, as a single unnamed parataxon (the larger Chatham Island form) (see Appendix 1, Figure A6). The recently described *?Crossvallia waiparensis* was also coded for and added to the data matrix. It is recognised that the holotype cast MLP 606 used in analyses by Chávez Hoffmeister (2014) referred to as *Arthrodytes grandis* (Ameghino, 1901)—a synonym of *Parapterodytes robustus* (Ameghino, 1895) as per Acosta Hospitaleche (2005) and Acosta Hospitaleche and Tambussi (2008)—actually refers to *Arthrodytes andrewsi* (Ameghino, 1901). In order to improve topological resolution, the following taxa were excluded from final analyses due to their irrelevance to the present study, incomplete character sampling, and also their high instability as determined through the taxon instability among trees module in Mesquite, version 3.04 (Maddison and Maddison, 2015): *Hydrobates tethys*, *Ardenna grisea*, *Dunroonornis parvus* Marples, 1952, *Pachydyptes simpsoni* Jenkins, 1974, *Palaeodyptes antarcticus* Huxley, 1859, *Eudyptes calauina* Chávez Hoffmeister, Carrillo Briceño and

Nielsen, 2014, and Sphenisciformes indet. SAM P10863. Both *Gavia* species were also excluded from final analyses (as per above). Removal of additional taxa further to those listed above resulted in more poorly resolved consensus trees, and so were deemed necessary to include to maximise phylogenetic signal (e.g., Wiens, 2003, 2005, 2006; Wiens and Tiu, 2012). Despite having relatively incomplete character sampling, such fossil taxa as *Crossvallia unienwillia* and the giant Waipara Greensand penguin CM 2016.158 were also retained in final analyses for their importance in understanding of stem group topologies. The resultant matrix that underlies our final analyses has 89 included taxa and is referred to hereafter as the Chatham matrix.

The Chatham matrix includes 8,429 characters—284 of which are morphological/standard characters, and 8,145 molecular characters. Molecular sequence data was used as per some aforementioned studies involving penguin phylogenetics (e.g., Ksepka et al., 2012; Ksepka and Thomas 2012), to resolve morphology-based fossil taxa more accurately among a relatively robust molecular and morphological data informed framework for extant taxa, and includes five genes (RAG-1, cytochrome b, COI, 12S and 16S, see Table A1). This matrix includes 89 taxa, with 73 ingroup taxa, consisting of 54 fossil and 19 extant Sphenisciformes. The outgroups consist of 16 extant taxa, composed of one phaethontiform, and 15 Procellariiformes.

Primary search strategy. Parsimony analyses were conducted using PAUP* version 4.0a165 (Swofford, 2003), using a heuristic search strategy. This included 10,000 replicates of random taxon addition, holding 10 trees per step, where no more than 100 trees of a score/length greater than or equal to 1 were saved in each replicate. TBR branch-swapping algorithm, with a reconnection limit of 8, was also in effect. Parsimony optimality criterion was used, all characters were equally weighted, and gaps in the matrix were treated as “missing”. Character ordering was applied for 49 characters in all analyses. Multistate characters within the matrices were treated variably as polymorphisms or ambiguous, and branches with a minimum length of zero were collapsed to create polytomies. Bootstrap support values were calculated using 1,000 replicates, with 10 random taxon addition replicates, holding 10 trees per step and TBR branch-swapping. All trees were rooted to the outgroup, defined as all Procellariiformes and *Phaethon rubricauda*.

After heuristic analysis of the Chatham matrix, taxa which were highly unstable across the most parsimonious trees (MPTs) were subsequently pruned from these MPTs prior to the generation of consensus trees: *Nucleornis insolitus* Simpson, 1979, *Korora oliveri* Marples 1952, and Sphenisciformes indet. NMV P221273. The resultant MPTs thus included 86 taxa (see 1009_chatham_matrix_89_8428_paup.nex in Supplementary Materials).

Bayesian analyses. The Chatham matrix was based on data matrices developed for parsimony analyses and therefore autapomorphic characters, known to be especially informative in Bayesian analyses (see Lee and Palci, 2015), are relatively undersampled. Nevertheless, we analysed the Chatham matrix in a Bayesian framework to assess how a different phylogenetic inference method would affect evolutionary interpretations (see Wright and Hillis, 2014; O'Reilly et al., 2016). Bayesian analysis has been conducted on an alternate version of this dataset (Ksepka et al., 2012), to assess whether fossil taxa may be ancestral to geologically younger forms, and was informative on the timing of the crown group penguin radiation (Gavryushkina et al., 2017). In contrast to Gavryushkina et al. (2017), however, we chose not to undertake tip-dated analyses of the current dataset due to the lack of autoapomorphies sampled (see Lee and Palci, 2015).

The program MrBayes 3.2.6 (Ronquist and Huelsenbeck, 2003) was utilised to determine posterior probabilities for clades within the phylogenetic tree. An analysis was performed for the Chatham matrix, where all modifications and exclusions regarding characters, taxa, and ordering assumptions were tested as per the primary search strategy (86 included taxa, 8,429 characters, see 1009_chatham_matrix_89_8428_undated.nex in Supplementary Materials). Analysis of the output from each Bayesian analysis was performed using Tracer v1.7 (Rambaut et al., 2018).

PhyML 3.0 (Guindon et al., 2010), and PartitionFinder 2.1.1 (Lanfear et al., 2017) were used, implementing unlinked branch lengths, BIC (Bayesian Information Criterion) model selection, and the “greedy” algorithm (Lanfear et al., 2012), where only MrBayes compatible models were tested, to generate an appropriate partitioning scheme and to select models for molecular data. The Mk model was assigned to morphological characters (Lewis, 2001), assuming only variable characters have been included (coding = variable), and rate variability is distributed according to gamma parameter (rates = gamma). Parameters

including state frequencies, substitution rates, shape parameter of gamma distribution of rate variation, proportion of invariable sites, and branch lengths, were unlinked across all partitions. Four independent analyses were performed simultaneously to check for sufficient convergence—a combined total of 50,000,000 generations, which was sampled every 5,000 generations. To improve exploration of tree topology space, the heating parameter was set to 0.1, and one cold and three incrementally heated chains were used per analysis (totalling four chains per analysis). Using relative burn-in, the first 20% of sampled trees were discarded after the analysis of each dataset was completed, and a consensus tree was produced.

Comparisons

A focus is made on comparing the taxon described herein, the notably larger form, and fossil elements pertaining to each (from specimens NMNZ S.47302, S.47303, S.47308, S.47312, S.47339 and S.47339) with coeval Paleocene sphenisciforms. Comparisons are also made with Eocene penguins where appropriate, due to their relatively close association with Paleocene taxa phylogenetically and temporally. While Antarctic Eocene penguins are immediately relevant due to the existence of an Antarctic Paleocene penguin (*Crossvallia unienwillia*), comparisons with South American Eocene penguins are also deemed appropriate and important, owing to their relative completeness compared to Antarctic Eocene taxa, age, and basal morphologies. Moreover, the phylogenetic interrelationships of Eocene taxa are also commented on, in recognition of their relevant basal morphologies, and their importance in understanding the early radiations of the penguin clade.

SYSTEMATIC PALAEONTOLOGY

Class AVES Linnaeus, 1758
Order SPHENISCIFORMES Sharpe, 1891
Genus *KUPOUPOU* gen. nov.
Figures 2-8

zoobank.org/4576CB2A-AB34-46DE-B198-4B6BBE219901

Type species. *Kupoupou stilwelli*, sp. nov.

Included species. Type species.

Etymology. From Te Re Miori, the native language of Chatham Island, in recognition of where the fossils were recovered. “Kupoupou” meaning “diving bird”. The gender is nominated as neuter.

Diagnosis. *Kupoupou*, n. gen. is referred to Sphenisciformes because it shares the synapomorphy of having flattened long bones of the forewing/flip-

per. *Kupoupou*, n. gen. is characterised by the combination of the following osteological apomorphies: a bifurcated processus transversus of the axis with a dorsally protruding torus dorsalis; the processus acrocoracoideus has a rounded and protruding omal crista acrocoracoidea of the coracoid, the insertion for ligamenti acrocoraco-procoracoidale on the facies articularis clavicularis is weakly hooked with a rounded facies apicalis, a weakly defined tuberculum for the insertion of plica synovialis coracoidea, joined by a low ridge to the impressio ligamenti acrocoraco-acromiale, the latter of which is separated by the impressio ligamenti acrocoraco-procoracoidale by a groove; a well-defined labrum internum of the coracoid that is compressed in the sternal-omal direction; the distal margin of the crista bicipitalis on the humerus is nearly perpendicular to the long axis of the shaft; the distal caudal border of the olecranon of the ulna is distinctly angled, with a marked bony caudal protuberance; a dorsocaudally situated sub-triangular insertion scar for the musculus supinator on the proximal radius; a distinct caudally projecting tuberculum aponeurosis ventralis from the ventral caudal margin of the distal radius and an associated prominent ulnar depression; a proximally directed process on the phalanx III-1; a marked laterally protruding epicondylus lateralis on the femur; the sulcus for the tendon to the muscle flexor hallucis longus is bounded by medial and lateral hypotarsal crests of distinct subequal plantar projection on the tarsometatarsus; a strongly plantar projecting flange on the lateral rim of trochlea metatarsi IV.

Comparisons. *Kupoupou*, n. gen. is distinguished from *Waimanu* in that the tarsometatarsus is shorter and stouter, and the lateral margin is more linear than concave. It differs from *Muriwaimanu* as follows: the insertion point of the plica synovialis coracoidea is less distinct; the impressio ligamenti acrocoraco-procoracoidale is not as distinctly hooked overhanging the sulcus musculi supracoracoidei; the impressiones ligamenti acrocoraco-acromiale and ligamenti acrocoraco-procoracoidale are separated by a groove; the facies apicalis on the processus acrocoracoideus is more rounded; the apex of the humeral head located caudal to the midline of the shaft and crista deltopectoralis more distally located; olecranon more distally located on the caudal border of the ulna, and processus cotylaris dorsalis less cranially projected; the radius is more dorsoventrally flattened, has a craniocaudally wider shaft, and the proximal end is more angled and deflected; carpometacar-

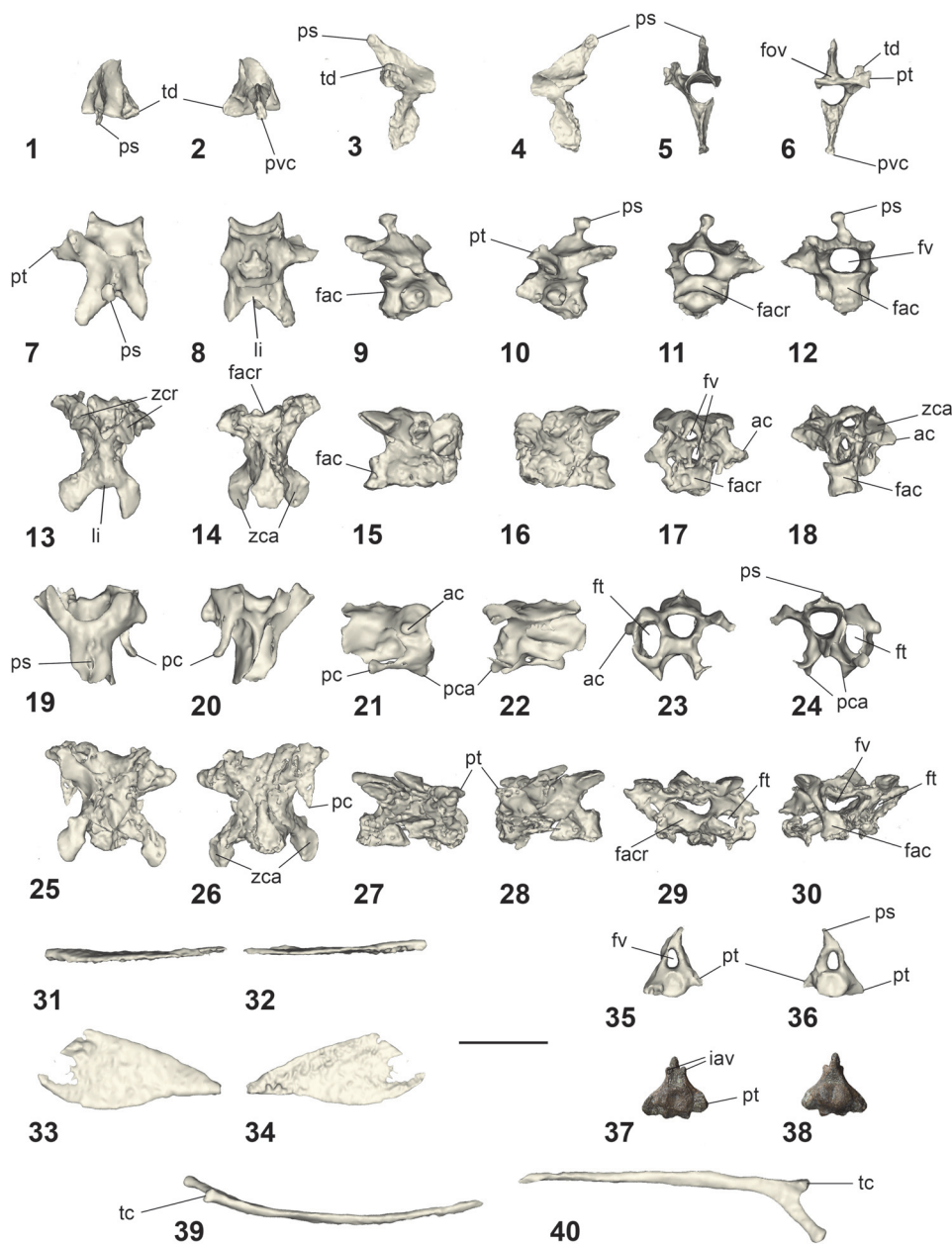


FIGURE 2. Axis vertebra (1-6), cervical vertebrae (7-30), pelvis (31-34), caudal vertebrae (35-38), and rib elements (39, 40) referred to *Kupoupou stilwelli* n. gen. et sp. Axis, NMNZ S.47303 in 1, dorsal; 2, ventral; 3, right lateral; 4, left lateral; 5, cranial; 6, caudal. Cervical vertebra (i), possibly third in vertebral column, NMNZ S.47303 in 7, dorsal; 8, ventral; 9, right lateral; 10, left lateral; 11, cranial; 12, caudal. Cervical vertebra (ii), NMNZ S.47303 in 13, dorsal; 14, ventral; 15, right lateral; 16, left lateral; 17, cranial; 18, caudal. Cervical vertebra (iii), NMNZ S.47303 in 19, dorsal; 20, ventral; 21, right lateral; 22, left lateral; 23, cranial; 24, caudal. Cervical vertebra (iv), NMNZ S.47303 in 25, dorsal; 26, ventral; 27, right lateral; 28, left lateral; 29, cranial; 30, caudal. A partial ischium, from the right side of the pelvis, NMNZ S.47303, 31, dorsal; 32, ventral; 33, medial; 34, right lateral. Caudal vertebra, NMNZ S.47303, 35, cranial and 36, caudal. Caudal vertebra, NMNZ S.47312, interpreted to have been located further caudally in the vertebral column compared to the caudal vertebra in NMNZ S.47303, in 37, cranial and 38, caudal. A left rib, NMNZ S.47303 in 39, lateral and 40 caudal. **Abbreviations:** ac, ansa costotransversaria; fac, facies articularis caudalis; facr, facies articularis cranialis; fov, fovea at base of processus spinosus; ft, foramen transversarium; fv, foramen vertebrale; iav, incipient projections of the arcus vertebrae; li, lacuna interzygapophysialis; pc, processus costalis; pca, processus caroticus; ps, processus spinosus; pt, processus transversus; pvc, processus ventralis corporis; tc, tuberculum costae; td, torus dorsalis; zca, zygapophysis caudalis; zcr, zygapophysis cranialis. Scale bars equal to 20 mm.

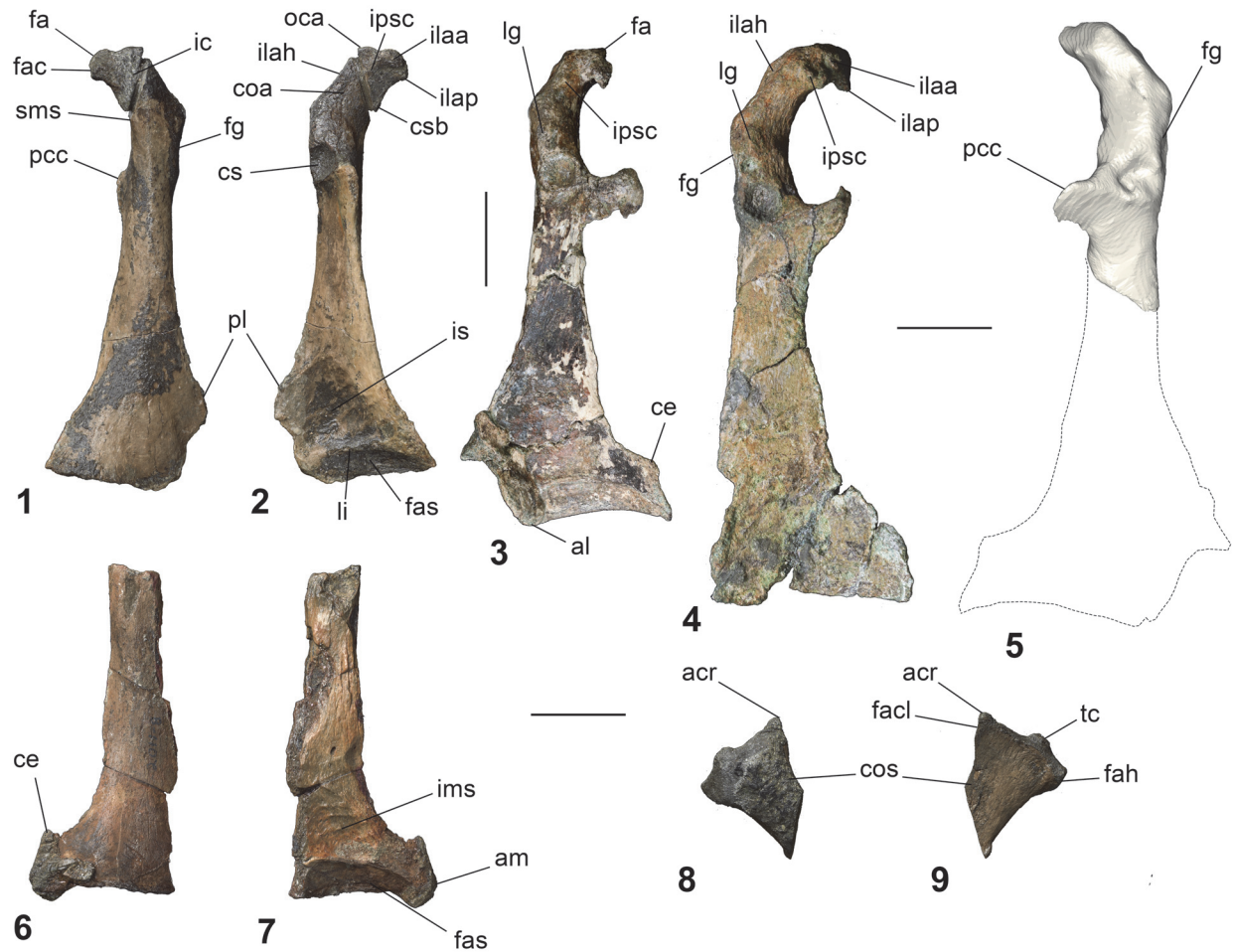


FIGURE 3. Coracoids and scapula referred to *Kupoupou stilwelli* n. gen. et sp. (1-2, 6-7, 8-9) compared to other Paleocene taxa (3-5). Two left coracoids assigned to *K. stilwelli* n. gen. et sp., NMNZ S.44729, in 1, ventral and 2, dorsal; and NMNZ S.47308 in 6, ventral and 7, dorsal. Dorsal perspectives of left coracoids of *Muriwaimanu tuatahi*, CM zfa 34 in 3, and *Sequiwaimanu rosieae*, CM 2016.6.1 in 4; right omal part coracoid of NMNZ S.47302 (larger Chatham Island form), in 5. Left cranial part scapula referred to *K. stilwelli* n. gen. et sp. NMNZ S.47339, 8, medial and 9, lateral. **Abbreviations:** **acr**, acromion; **al**, angulus lateralis; **am**, angulus medialis; **ce**, crista epimarginalis; **coa**, collum acrocoracoidei; **cos**, collum scapulae; **cs**, cotyla scapularis; **csb**, crista subcapitalis; **fa**, facies apicalis; **fac**, facies articularis clavicularis; **fas**, facies articularis sternalis; **fg**, facies glenoidalis (facies articularis humeralis); **ic**, impressio coracobrachialis; **ilaa**, insertion for ligamenti acrocoraco-acromiale; **ilah**, impressio ligamenti acrocoracohumeralis; **ilap**, insertion for ligamenti acrocoraco-procoracoidale; **is**, impressio sternocoracoidea; **ipsc**, tuberculum for the insertion of plica synovialis coracoidea; **lacs**, insertion for ligamenti acrocoraco-claviculare superficiale; **lg**, labrum glenoidale (facies articularis humeralis); **li**, labrum internum; **not**, notch adjacent to the facies articularis clavicularis; **oca**, protruding omal extremity of crista acrocoracoidea; **pac**, processus acrocoracoideus; **pcc**, processus procoracoideus; **pl**, processus lateralis; **sms**, sulcus musculi supracoracoideus; **tc**, tuberculum coracoideum. Scale bars equal to 20 mm. Note that 5 is a tomographic rendering image. The images in 3.3 and 3.4 are reprinted from Mayr et al. (2018b, fig. 3B, 3A) by permission of the publisher (Taylor & Francis Ltd, <http://www.tandfonline.com>) and by permission of the Society of Vertebrate Paleontology (<http://www.vertpaleo.org>).

pus more flattened distally; femur with a more angled medial margin of the crista supracondylaris medialis, a proportionally less enlarged condylus medialis proximodistally, and a more distally rounded condylus lateralis; and tarsometatarsus less elongate.

Kupoupou n. gen. differs from *Sequiwaimanu rosieae* where it is overall smaller; particularly in humerus morphology where it possesses a narrower and more slender humeral shaft (ratio of 0.12 of minimum shaft width to maximum length, compared to 0.15); a more prominent proximal

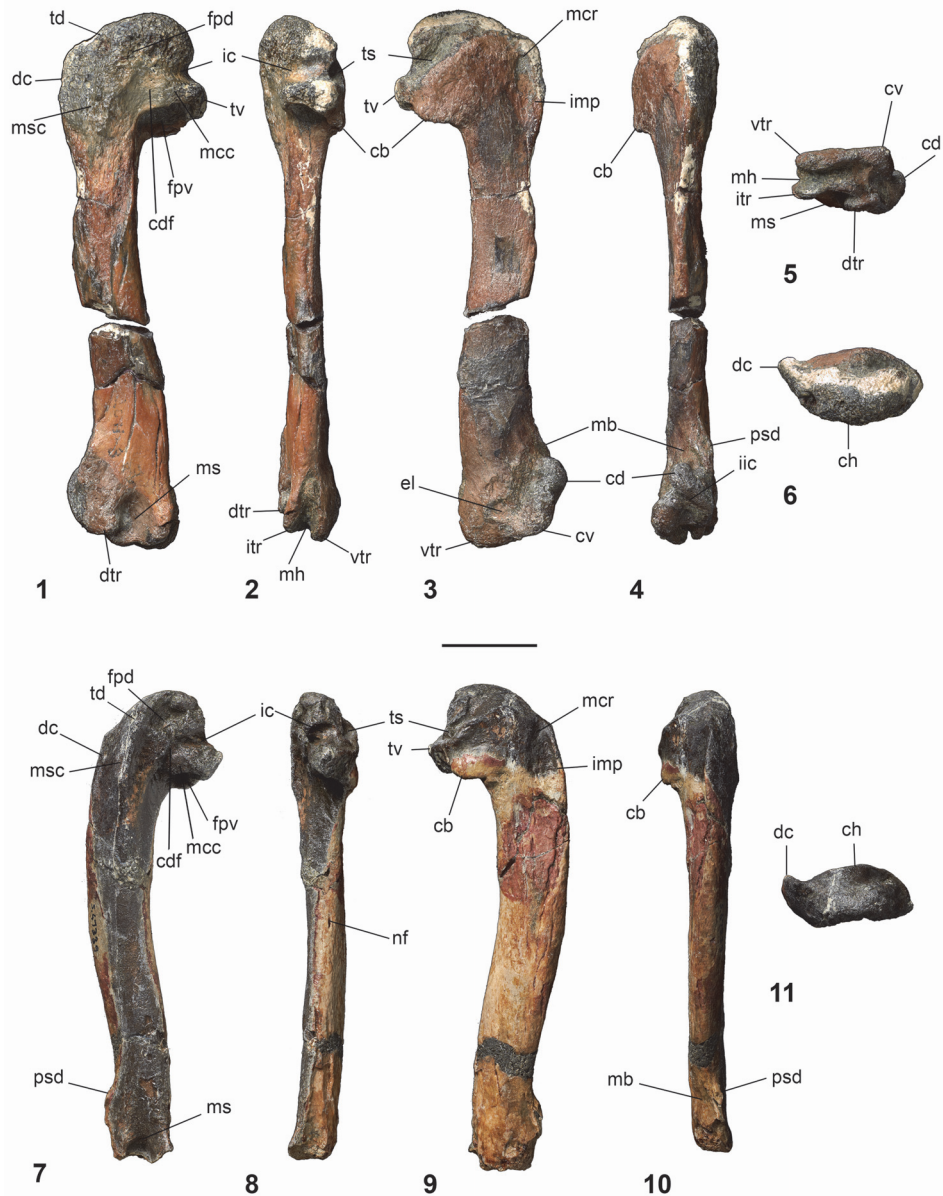


FIGURE 4. The humeri of *Kupoupou stilwelli* n. gen. et sp. Left humerus of NMNZ S.47308 in **1**, dorsal; **2**, caudal; **3**, ventral; **4**, cranial; **5**, distal; **6**, proximal. Left humerus of NMNZ S.47339 in **7**, dorsal; **8**, caudal; **9**, ventral; **10**, cranial; **11**, proximal. **Abbreviations:** **cb**, crista bicipitalis (bicipital crest); **cd**, condylus dorsalis (radial condyle); **cdf**, crus dorsale fossa; **ch**, caput humeri (humerus head); **cv**, condylus ventralis (ulnar condyle); **dc**, crista deltopectoralis (deltopectoral crest) and insertion of the musculus deltoideus major; **dtr**, dorsal trochlear ridge; **el**, insertion for entepicondylar ligament; **fpd**, fossa pneumotricipitalis dorsalis (secondary tricipital fossa); **fpv**, fossa pneumotricipitalis ventralis (tricipital fossa); **ic**, incisura capituli (capital incisura); **iic**, incisura intercondylaris; **imp**, impressio musculus pectoralis; **itr**, intermediate trochlear ridge; **mb**, fossa musculus brachialis; **mcc**, attachment scar of musculus coracobrachialis caudalis; **mcd**, margo caudalis; **ms**, trochlea for tendon musculus scapulothoracalis; **mcl**, margo cranialis; **mcr**, insertion for musculus coracobrachialis cranialis (impressio coracobrachialis); **mh**, trochlea for tendon musculus humerotricipitalis; **msc**, crista musculus supracoracoidei as an accessory insertion site for the tendon of the musculus supracoracoideus, extending distally from the tuberculum dorsale; **nf**, nutrient foramen; **psd**, processus supracondylaris dorsalis (dorsal supracondylar tubercle); **td**, tuberculum dorsale (dorsal tubercle) the attachment site of the musculus deltoideus minor and the principal part of the musculus supracoracoideus; **ts**, sulcus transversus (transverse sulcus); **tv**, tuberculum ventrale (ventral tubercle/internal tuberosity); **vtr**, ventral trochlear ridge. Scale bars equal to 20 mm.

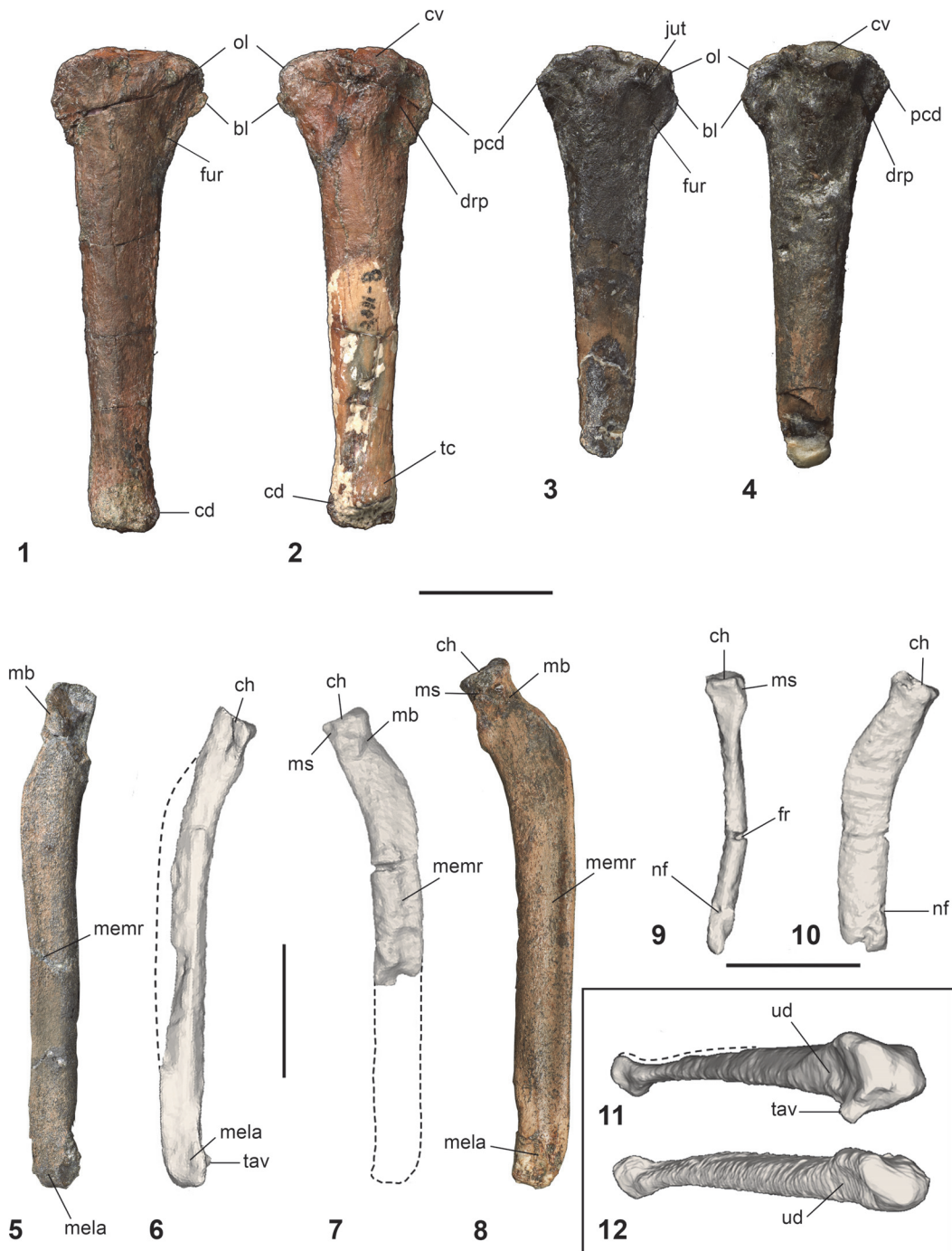


FIGURE 5. Long bones of the forewing of *Kupoupou stilwelli* n. gen. et sp. Left ulna of NMNZ S.47308 in **1**, dorsal; **2**, ventral. Left ulna of NMNZ S.47339 in **3**, dorsal; **4**, ventral. Dorsal view of radii, **5**, left NMNZ S.47312; **6**, left NMNZ S.47303; **7**, right NMNZ S.47303; **8**, right NMNZ S.47339. Right radius of NMNZ S.47303 (without suggested eroded extent) in caudal (**9**), and ventral (**10**) views. Caudodistal view of left radius of NMNZ S.47303, **11**, and *Muriwaimanu tuatahi*, right radius (mirrored) CM 2009.99.1, **12**. **Abbreviations:** **bl**, bony lobe; **cd**, condylus dorsalis; **ch**, cotyla humeralis; **cv**, cotyla ventralis; **drp**, incisura radialis (depression radialis proximalis); **fr**, fracture; **fur**, furrow; **jut**, edge-like jut on dorsal ulna face; **mb**, scar for insertion of musculus brachialis; **mela**, groove for musculus extensor longus alulae; **memr**, groove for the musculus extensor metacarpi radialis; **ms**, insertion scar for musculus supinator; **nf**, nutrient foramen; **ol**, olecranon; **pcd**, processus cotylaris dorsalis; **tav**, tuberculum aponeurosis ventralis; **tc**, tuberculum carpale; **ud**, depressio ligamentosa (ulnar depression). Dotted lines represent suggested erosion to respective elements. Scale bars equal to 20 mm. **11** and **12** are not to scale.

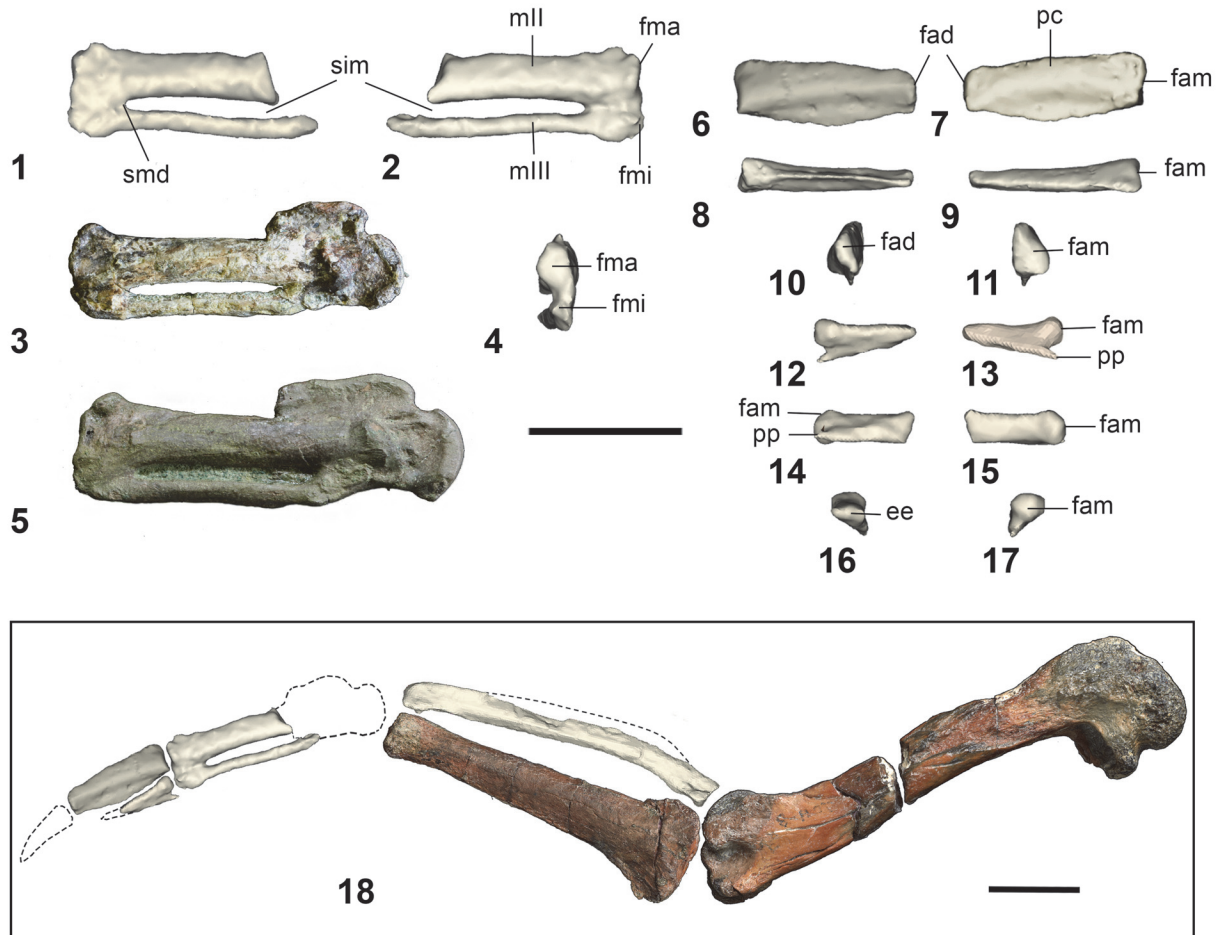


FIGURE 6. Images of the distal right-wing elements in NMNZ S.47303 (**1-2, 4-17**). Distal carpometacarpus in **1**, ventral, **2**, dorsal, and **4**, distal aspects. Left carpometacarpi of *Muriwaimanu tuatahi*, **3** (CM zfa 34, mirrored, Slack et al., 2006), and *Sequiwaimanu rosieae*, **5** (CM 2016.6.1, mirrored, Mayr et al., 2018b) are presented for comparison, in ventral aspect. The right proximal manus phalanx of the second digit is shown in **6**, dorsal, **7**, ventral, **8**, caudal, **9**, cranial, **10**, distal, and **11**, proximal views. The right manus phalanx of the third digit is presented in **12**, dorsal, **13**, ventral, **14**, caudal, **15**, cranial, **16**, distal, and **17**, proximal aspects. A left-wing reconstruction of *Kupoupou stilwelli* n. gen. et. sp. is shown in **18**, using mirrored carpometacarpus and phalanges. Scale bars are equal to 20 mm. **Abbreviations:** **ee**, eroded end; **fad**, facies articularis digitalis major; **fam**, facies articularis metacarpalis; **fma**, facies articularis digitalis major; **fmi**, facies articularis digitalis minor; **mll**, os metacarpale majus (metacarpal II); **mlll**, os metacarpale minus (metacarpal III); **pc**, pila cranialis phalangis; **pp**, proximally directed process; **si**, sulcus interosseous; **sim**, spatium intermetacarpale; **smd**, symphysis metacarpalis distalis. The images in **6.3** and **6.5** are reprinted from Mayr et al. (2018b, fig. 4G, 4F) by permission of the publisher (Taylor & Francis Ltd, <http://www.tandfonline.com>) and by permission of the Society of Vertebrate Paleontology (<http://www.vertpaleo.org>).

crista deltopectoralis, and a more notched (rather than rounded) proximocranial margin between the caput humeri and proximal extremity of the crista deltopectoralis; the crista bicipitalis is not as distally extended; there is no bulge proximal to the condylus dorsalis on the cranial margin; the condylus ventralis is continuous with the ventral trochlear process; a shallower sulcus humerotricipitalis. Differences in the femur include a more rounded proximal crista trochanteris, a more concave facies

articularis antitrochanterica in cranial and caudal views; a larger and more sub-spherical condylus medialis on the cranially and caudally; a mediolaterally larger crista tibiofibularis, and the trochlea fibularis is restricted to a proximal position on the condylus lateralis. Furthermore, the furrow for the musculus extensor longus alulae runs proximodistally rather than transversing the distal dorsal radius; and the facies articularis sternalis of the

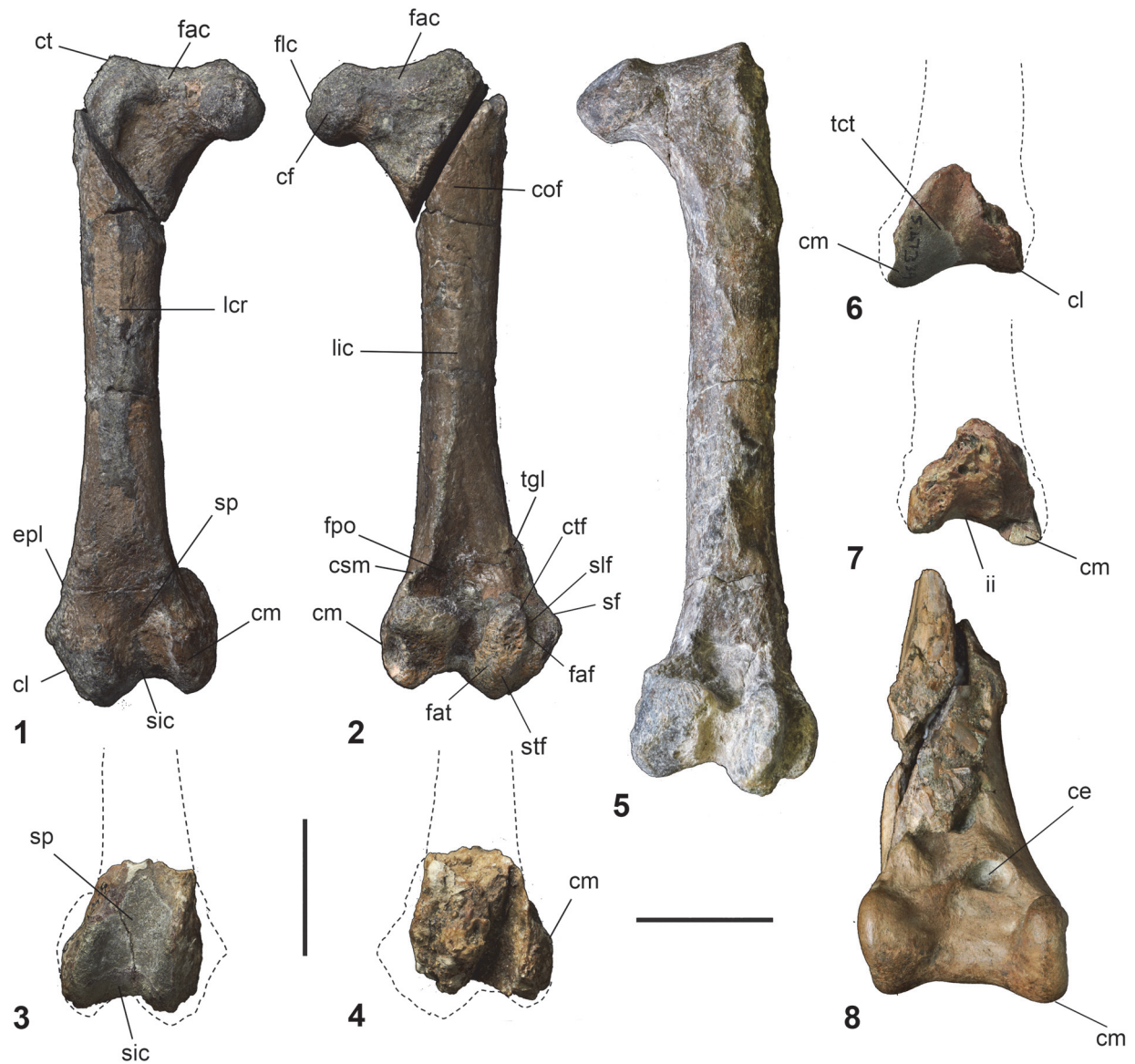


FIGURE 7. Hindlimb elements. Right femur of *Kupoupou stilwelli* n. gen. et sp. NMNZ S.47308 in **1**, cranial and **2**, caudal views. Left distal femur of NMNZ S.47339 in **3**, cranial and **4**, caudal aspects. Right femur of *Sequiwaimanu rosieae* in caudal view (holotype, CM 2016.6.1), **5**, for comparison. Fragmentary right distal tibiotarsus of NMNZ S.47339 in **6**, caudal and **7**, cranial aspects, compared to cranial view of right distal tibiotarsus of *Waimanu manneringi* (holotype, CM zfa 34), **8**. **Abbreviations:** **ce**, distal opening of canalis extensorius; **cf**, caput femoris; **cl**, condylus lateralis; **cm**, condylus medialis; **cof**, collum femoris; **csm**, crista supracondylaris medialis; **ct**, crista trochanteris; **ctf**, crista tibiofibularis; **stf**, semicondylus tibiofibularis; **sf**, semicondylus fibularis; **epl**, epicondylus lateralis; **fac**, facies articularis antitrochanterica; **faf**, facies articularis fibularis; **fat**, facies articularis tibialis; **flc**, fovea ligamenti capitis; **fpo**, fossa poplitea; **ii**, incisura intercondylaris; **lcr**, linea intermuscularis cranialis; **lic**, linea intermuscularis caudalis; **sic**, sulcus intercondylaris; **sf**, semicondylus fibularis; **slf**, sulcus fibularis; **sp**, sulcus patellaris; **stf**, semicondylus tibiofibularis; **tct**, trochlea cartilaginis tibialis; **tgl**, tuberculum musculus gastrocnemialis lateralis. Scale bars equal to 20 mm. The image in **7.5** is reprinted from Mayr et al. (2018b, fig. 11A) by permission of the publisher (Taylor & Francis Ltd, <http://www.tandfonline.com>) and by permission of the Society of Vertebrate Paleontology (<http://www.vertpaleo.org>). The image in **7.8** is reprinted from Mayr et al. (2017b, fig. 2j), which was published under a Creative Commons Attribution 4.0 International License (<http://creativecommons.org/licenses/by/4.0/>).

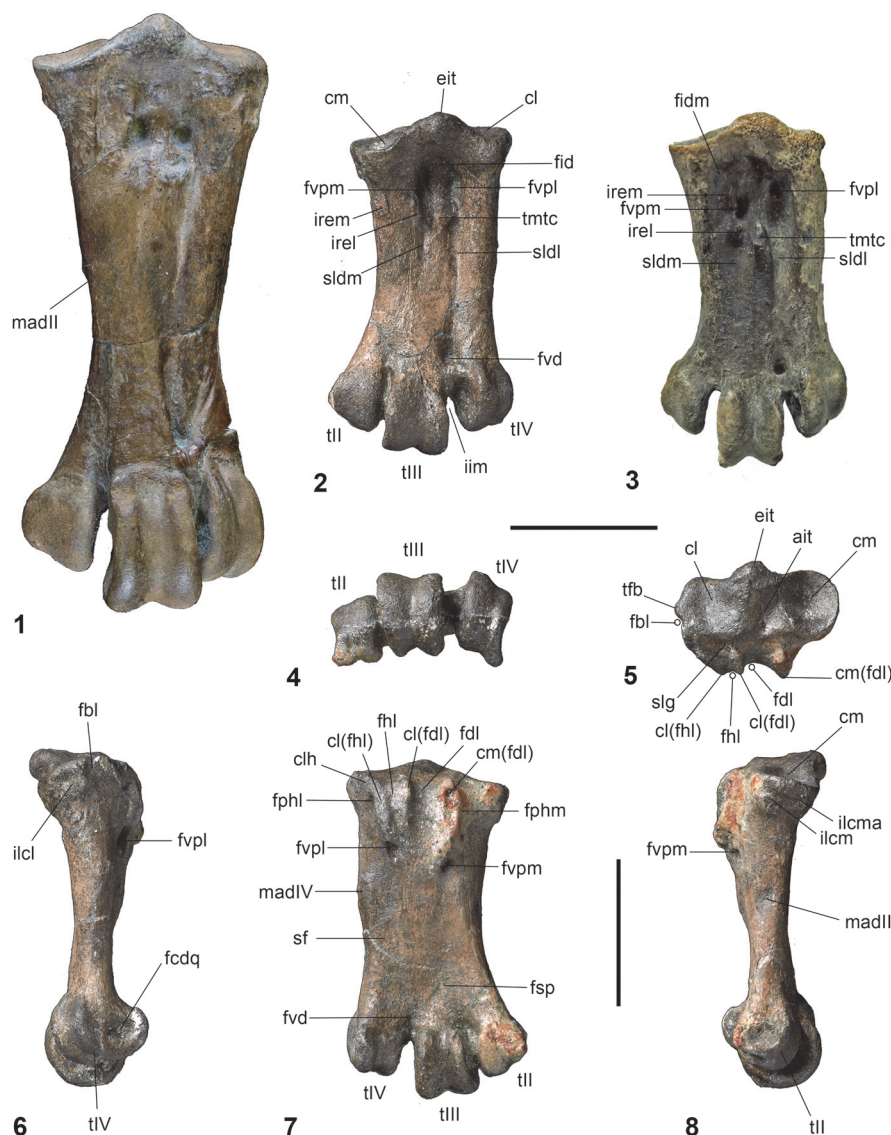


FIGURE 8. Tarsometatarsus of *Kupoupou stilwelli* n. gen. et sp. compared to other fossil taxa. Tarsometatarsi in dorsal aspect, **1**, Paleocene *Waimanu manningi*, right (mirrored), holotype CM zfa 35; **2**, Paleocene *Kupoupou stilwelli* n. gen. et sp. left, NMNZ S.47312, **3**, Eocene *Delphinornis larseni*, left, IB/P/B-0062. Left tarsometatarsus of NMNZ S.47312 in **4**, distal, **5**, proximal, **6**, lateral, **7**, plantar, and **8**, medial views. **Abbreviations:** ait, area intercotylaris; cl, cotyla lateralis; cl(fdl), crista lateralis flexoris digitorum longus; cl(fhl), crista lateralis flexoris hallucis longus; clh, crista lateralis hypotarsi; cm, cotyla medialis; cm(fdl), crista medialis flexoris digitorum longus; eit, eminentia intercotylaris; fbl, sulcus for muscularis fibularis longus; fcdq, fovea ligamentae collateralis digitorum quarti; fdl, sulcus for tendon of musculus flexor digitorum longus; fhl, sulcus for tendon of musculus flexor hallucis longus; fid, fossa intercotylaris dorsalis; fidm, fossa intercotylaris dorsalis medialis; fphl, fossa parahypotarsalis lateralis; fphm, fossa parahypotarsalis medialis; fsp, fossa supratrochlearis plantaris; fvd, foramen vasculare distale; fvpl, foramen vasculare proximale laterale; fvpm, foramen vasculare proximale laterale; iim, incisura intertrochlearis medialis; ilcl, impressio ligamentosae collateralis laterale intertarsi; ilcm, impressio ligamentosae collateralis mediale intertarsi; ilcma, impressio ligamentosae collateralis mediale intertarsi accessorium; irel, impressiones retinaculi extensorii lateralis; irem, impressiones retinaculi extensorii medialis; madII, insertion site of musculus adductor digiti II; madIV, insertion site of musculus adductor digiti IV; sf, sulcus flexorius; sldl, sulcus longitudinalis dorsalis lateralis; sldm, sulcus longitudinalis dorsalis medialis; slg, sulcus ligamentosus; tII, trochlea metatarsi II; tIII, trochlea metatarsi III; tIV, trochlea metatarsi IV; tfb, tuberculum muscularis fibularis brevis; tmtc, tuberositas muscularis tibialis cranialis. Scale bars equal to 20 mm.

coracoid is narrower and the omally bounding ridge is more prominent.

Differences with other Paleocene taxa such as *Crossvallia unienwillia* include its markedly smaller size, a more elongate humerus with a less extensive impression for the musculus pectoralis and lacking a marked supracondylar tubercle, and a less robust femur with a deeper intercondylar sulcus. *Kupoupou* n. gen. further differs from ?*Crossvallia waiparensis* in its smaller size, the presence of a shallower sulcus patellaris of the distal femur with more rounded medial and lateral margins, and features of the tarsometatarsus, such as the absence of an angled dorsal edge and a markedly medially extended medial margin of cotyla medialis, and a more linear and dorsoplantarily rounded lateral shaft margin. It differs from *Kumi-manu* in its smaller size, and also where it has a flattened cranial border of the scapula between the acromion and the tuberculum coracoideum, the tuberculum coracoideum is also not as cranially projected.

Kupoupou n. gen. differs from the Eocene *Kaiika maxwelli* Fordyce and Thomas, 2011, known only from a humerus, by the impression for the musculus coracobrachialis and pectoralis thoracica being proportionally smaller, the crista bicipitalis does not form a pronounced distally directed process and associated groove, and the supracondylar tubercle is less distinct. *Kupoupou* n. gen. differs from all post-Paleocene Sphenisciformes (excluding *Kaiika*) in that the humerus length exceeds that of the coracoid; the crista supracoracoidei is situated nearer the cranial margin rather than close to the midline of the humerus; the humerus shaft is sigmoidal and slender; the sulcus scapulothoracalis and dorsal trochlear ridge on the distal humerus are located dorsally, rather than caudally; shafts of the ulna and radius are relatively craniocaudally narrow; the processus cotylaris dorsalis projects caudally on the proximal ulna; the carpometacarpus is relatively straight and broad and not cranially bowed on metacarpal II; the margin of the lateral cotyla projects beyond the lateral border of the tarsometatarsus; the lateral-most trochlear rim of metatarsi IV is markedly plantarly projected on the distal tarsometatarsus.

Kupoupou stilwelli sp. nov.

zoobank.org/414D797D-0C75-46DF-977D-91FB12515AFB

Diagnosis. As for genus.

Etymology. The type species "*stilwelli*" honours palaeontologist Jeffrey D. Stilwell, who led and organised the parties to recover the holotype and the only known referred specimens.

Holotype. NMNZ S.47312; associated left tarsometatarsus, left radius, and caudal vertebra.

Referred material. NMNZ S.44729; a left coracoid. NMNZ S.47303 (Figure A2); associated partial skeleton comprising of a distal right carpometacarpus, left radius, proximal right radius, right proximal phalanx of the second digit, right phalanx of the third digit, an almost complete axis, four cervical vertebrae, a caudal vertebra, a left rib, and a partial worn ilium. NMNZ S.47308; a right femur, a left humerus, a sternal section of a left coracoid, a left ulna. NMNZ S.47339; omal part scapula, distally eroded left humerus, right ulna, right radius, distal left femur, distal left tibiotarsus, two cervical vertebrae and five other vertebrae in differing degrees of preservation and exposure at the rock surface, and two partial ribs.

Measurements (mm). Holotype NMNZ S.47312: Tarsometatarsus, total proximodistal length, 46.4; proximal mediolateral width, 22.1; midshaft mediolateral width, 16.9; proximal dorsoventral width, 16.1. Radius, proximodistal length, c.75; breakage prevents meaningful proximal width and depth measurements; craniocaudal width of mid-shaft 7.6, dorsoventral depth of mid-shaft c. 3; distance from cotylaris humeralis to the bend on the cranial margin c.17. Caudal vertebra, diameter of centrum/corpus 8.3; maximum dorsoventral height, 14.4, maximum lateral width 15.5, maximum craniocaudal depth of corpus/centrum 7.7. Referred material – see Table 1. Note that measurements of the femur and tibiotarsus of NMNZ S.47339 were not made due to the incomplete nature of the elements.

Type locality, horizon, and age. Maunganui Beach, east of Tahatika Creek, north western Chatham Island, near 43°45'10.1"S, 176°40'46.8"W; New Zealand. The fossils come from a narrow greensand layer in outcrop on the wave platform that overlies the Upper nodular-phosphate and bone package horizon (NPB, Figure 1.3), Takatika Grit (late early-middle Paleocene, 62.5-60 Ma) (Consoli et al., 2009; Consoli and Stilwell, 2009; Hollis et al., 2017).

DESCRIPTION AND COMPARISONS

Kupoupou stilwelli n. gen. et sp.

Kupoupou stilwelli n. gen. et sp. is a medium-sized sphenisciform (relative to all known fossil and extant penguins), likely slightly smaller than a modern adult *Aptenodytes patagonicus*. The referred specimens are assigned to *Kupoupou stilwelli* n. gen. et sp. based on similarity of overlapping skele-

TABLE 1. Measurements of skeletal elements of referred specimens of *Kupoupou stilwelli* n. gen. et sp. Refer to Figures 2 and A2 for relating numerals associated with each cervical vertebra to images of their corresponding element.

Specimen/Element	Measurement distance	Measurement (mm)
NMNZ S.44729/Coracoid	Maximum omal-sternal length	91.4
	Maximum omal-sternal distance of sulcus musculi supracoracoidei	12.1
	Maximum diameter of scapular condyle	7.7
NMNZ S.47303/Carpometacarpus	Total length	31.9
	Distal craniocaudal width	11.73
	Distal dorsoventral depth	4.16
NMNZ S.47303/Left radius	Total proximodistal length	69.16
	Proximal craniocaudal width	7.33
	Mid-shaft craniocaudal width	6.38
	Proximal dorsoventral depth	4.61
	Mid-shaft dorsoventral depth	3.35
	Distance from cotylaris humeralis to bend on cranial margin	24.82
	NMNZ S.47303/Right radius (broken)	Total proximodistal length (broken)
Proximal craniocaudal width		7.06
Mid-shaft craniocaudal width		7.58
Proximal dorsoventral depth		5.75
Mid-shaft dorsoventral depth		3.3
Distance from cotylaris humeralis to bend on cranial margin		17.5
NMNZ S.47303/Manus phalanx II-1	Total length	24.14
	Proximal craniocaudal width	6.54
	Proximal dorsoventral depth	3.66
	Distal craniocaudal width	5.05
	Distal dorsoventral depth	1.85
	Maximum craniocaudal width	8.51
NMNZ S.47303/Manus phalanx III-1	Total length	13.17
	Proximal facet craniocaudal width	4.3
	Proximal facet dorsoventral depth	3.75
	Mid-shaft craniocaudal width	4.65
NMNZ S.47303/Axis	Craniocaudal length of neural canal	12.28
	Lateral diameter of neural canal	5.5
	Total distance between tips of ventral process and neural spine	25.9
NMNZ S.47303/Cervical (i)	Craniocaudal length of neural canal	13.9
	Lateral diameter of neural canal	7.14
	Total distance between tips of ventral process and neural spine	23.42
NMNZ S.47303/Cervical (ii)	Craniocaudal length of neural canal	19.07
	Maximum lateral width between caudal zygapophyses	17.99
	Maximum lateral width between cranial zygapophyses	14.1
NMNZ S.47303/Cervical (iii)	Craniocaudal length of neural canal	17.45
	Lateral diameter of neural canal	7.27
	Maximum lateral width between cranial zygapophyses	18.15
NMNZ S.47303/Cervical (iv)	Craniocaudal length of neural canal	16.8
	Lateral diameter of neural canal	7.95

TABLE 1 (continued).

Specimen/Element	Measurement distance	Measurement (mm)
NMNZ S.47303/Caudal vertebra	Maximum lateral width between cranial zygapophyses	24.47
	Maximum lateral width between caudal zygapophyses	24
	Lateral diameter of centrum/corpus	7.34
	Maximum lateral width	13.89
	Maximum dorsoventral height	15.57
NMNZ S.47303/Rib	Maximum craniocaudal length of centrum/corpus	7.45
	Maximum length	70.42
NMNZ S.47303/Ischium	Maximum craniocaudal length	41.42
	Maximum dorsoventral width	14.99
	Maximum mediolateral depth	2.36
NMNZ S.47308/Femur	Maximum proximodistal length	c. 96.0
	Maximum mediolateral width of distal end	25.7
	Maximum mediolateral width of proximal end	26.7
NMNZ S.47308/Humerus	Maximum proximodistal length	106.8
	Mid-shaft craniocaudal width	13.3
	Maximum craniocaudal width of caput humeri	20.6
NMNZ S.47308/Coracoid	Maximum omal-sternal length	-
NMNZ S.47308/Ulna	Maximum proximodistal length	69.9
	Proximal craniocaudal width	22.6
	Proximal dorsoventral depth	11.0
	Mid-shaft craniocaudal width	10.5
	Mid-shaft dorsoventral depth	6.5
	Distal craniocaudal width	10.0
NMNZ S.47339/Scapula	Distance from facies articularis humeralis to acromion	22.0
NMNZ S.47339/Humerus	Maximum proximodistal length	-
	Mid-shaft craniocaudal width	14.4
	Maximum craniocaudal width of caput humeri	18.6
NMNZ S.47339/Ulna	Maximum proximodistal length	-
	Proximal craniocaudal width	22.1
	Proximal dorsoventral depth	11.3
	Mid-shaft craniocaudal width	11.0
	Mid-shaft dorsoventral depth	6.8
NMNZ S.47339/Radius	Total proximodistal length	77.3
	Proximal craniocaudal width	8.5
	Mid-shaft craniocaudal width	8.2
	Proximal dorsoventral depth	7.1
	Mid-shaft dorsoventral depth	-
	Distance from cotylaris humeralis to bend on cranial margin	16.3

tal elements (Figure A4), size, and their origin in the same horizon of the same bed in the Takatika Grit. The dimensions of the forewing elements reveal that *Kupoupou stilwelli* n. gen. et sp. was likely smaller than both *Muriwaimanu tuatahi* and

Sequiwaimanu rosieae. Its humeri and coracoids show that it was smaller than the larger Chatham Island form described later in the text (Figure 3).

New Zealand stem penguins of broadly comparable age examined directly included *Waimanu*

manneringi, *Muriwaimanu tuatahi*, ?*Crossvallia waiparensis*, and *Sequiwaimanu rosieae*. Additionally, other similarly aged taxa including the giant Waipara Greensand penguin, *Kumimanu biceae*, *Kaiika maxwelli*, and *Crossvallia unienwillia*, were compared from relevant literature (Tambussi et al., 2005; Fordyce and Thomas, 2011; Jadwiszczak et al., 2013; Mayr et al., 2017a, 2017b, 2019).

Cervical vertebrae. The axis and an articulated set of four cervical vertebrae were preserved in NMNZ S.47303 (Figure A2). Because the vertebrae were not in contact with the axis, the former presence of an intervening vertebra cannot be discounted, so the exact positions of these cervical vertebra along the vertebrae column are unknown. Another seven vertebrae are also preserved in NMNZ S.47339, two of which are cervical vertebrae, yet are not described here due to their poor preservation, and/or because they are poorly exposed and have not been excavated from the dense surrounding matrix.

The axis (Figure 2.1-6) is proportionally similar to *Sequiwaimanu rosieae* (see Mayr et al., 2018b: figure 7F-G), yet the processus spinosus in NMNZ S.47303 is more dorsally tapered and the processus ventralis corporis is not as craniocaudally expanded. Extending dorsally and caudally, the dorsal extremity of the processus spinosus does not preserve a pronounced knob-like structure, as reported for *S. rosieae* (see Mayr et al., 2018b), nor is it similar to that of *Icadyptes salasi* Ksepka, Clarke, DeVries, and Urbina, 2008, however, erosion to the left lateral side of NMNZ S.47303 prevents accurate comparison. A fovea exists at the base of the processus spinosus in caudal view, which is absent in extant penguins and not as deeply excavated as in *S. rosieae*. The extremity of the processus ventralis corporis is bifurcated, although broken on the left side. The ventral-most processus ventralis corporis is bilaterally narrower than the relatively thickened and robust form of *I. salasi* (see Ksepka et al., 2008). The left processus transversus and arcus vertebrae are missing, leaving the foramen vertebrale exposed. The right processus transversus is well-preserved and is proportionally shorter in lateral length, compared to the dorsoventral lengths of the processus spinosus and processus ventralis corporis, relatively more so than in *S. rosieae*, but not as short as *I. salasi* (Ksepka et al., 2008: figure 8). The processus transversus is bifurcated at its extremity and presents a distinctly dorsally protruding torus dorsalis, unlike in *S. rosieae*, *I. salasi*, extant *Pterodroma* (Procellariidae), and *Eudyptula*.

The closest cervical vertebra to the axis (Table 1 cervical (i); Figure 2.7-12) in NMNZ S.47303 is partially exposed at the rock surface, is not in contact with any of the other cervical vertebrae, and appears heavily eroded. Its structure is typical of more cranial vertebrae and is identified as possibly cervical vertebrae III based on the position of the facies articularis caudalis relative to the rest of the vertebra body and the probable ventral extent of the processus ventralis corporis. The eroded processus spinosus extends dorsocaudally. While the right processus transversus is missing, the left one is bifurcated and eroded at its extremity. The lacuna interzygapophysialis preserves a “v”-shape. The foramen vertebrale is relatively well-preserved and is ovoid in shape, with greatest diameter across width. Both the facies articularis cranialis et caudalis are well-preserved.

A diagenetically deformed and severely fractured cervical vertebra (Table 1 cervical (ii); Figure 2.13-18) of NMNZ S.47303 is partially in contact with another cervical vertebra, however, this may be a result of post-mortem disturbance rather than an indication of real articulation. Like the preceding vertebra, it appears to have been cranial in the vertebral column. Both processus transverses preserve the foramen transversarium and ansa costotransversarium. The zygapophyses caudales are well formed, yet deformed in dorsal and ventral aspects, and enclose a “v”-shaped lacuna interzygapophysialis. The zygapophyses craniales et caudales are widely expanded and ovate.

Another cervical vertebra (Table 1 cervical (iii); Figure 2.19-24) in NMNZ S.47303 is nearly articulated with the subsequent cervical vertebra caudally. This vertebra is partially preserved, limited to mainly the cranial section of the vertebra, and is perhaps from the mid-series in the cervical vertebral section based on its structure, shape, and features. The processus spinosus has been almost completely eroded away. While the left side of the corpus vertebrae has been eroded, the shape of the foramen vertebrale is visible in cranial and caudal aspects, and is sub-triangular and widest dorsally. The right processus transversus is complete, preserving the ansa costotransversarium as well as the foramen transversarium—which is ovoid in shape, narrowest between the right and left sides, and is widest between the dorsal and ventral surfaces of the foramen. The right processus transversus also has a long processus costalis extending posteriorly off the ventral part of the structure. The left processus transversus is only partially complete, and the foramen transversarium is not

enclosed, however, it appears similar in shape to that of the right side. Both processus transverses have preserved flat, oval zygapophyses craniales. Two processus carotici extend at an acute angle ventrally on the cranio-ventral surface of the vertebra.

The last cervical vertebra (Table 1 cervical (iv); Figure 2.25-30) of NMNZ S.47303 is severely damaged and flattened. Despite being crushed, the vertebra appears almost complete, and may have also been a mid-cervical vertebra. The foramen vertebrale is intact, albeit deformed, and has had the facies articularis cranialis forced through it by ventrodorsal compression. The facies articularis caudalis is better preserved. Both cranial processus transverses appear to have been broken, yet both present compressed and entirely enclosed foramina transversaria. The left processus transversus is in relatively better condition compared to the right equivalent, and is only broken where it connects to the corpus vertebrae. Both processus carotici and the left processus costalis are intact. The left processus transversus exhibits an oval, flat zygapophysis cranialis. Both zygapophyses caudales are preserved, extending posterolaterally, and have large, flat, oval zygapophysial articular facets on each.

Caudal vertebrae. One largely intact free caudal vertebra is preserved in NMNZ S.47303 (Figure 2.35-36), separate from other fossil elements. The vertebra has a prominent triangular-shaped, dorsally extending processus spinosus. While the right side of the processus spinosus is eroded, it appears it was bifurcated at its extremity, comparable to the caudal vertebra of *Waimanu manneringi*, *Sequiwaimanu rosieae*, and also in modern *Eudyptula minor*. The foramen vertebrale is completely enclosed by the arcus vertebrae and oval in shape—greatest in diameter through its depth. Both processus transverses are present, extending cranially, laterally and ventrally, yet both are eroded; the left transverse process to the most extent. The corpus of the vertebra is well-preserved, presenting a shallow concavity on both cranial and caudal facies, with flattened surfaces in lateral, dorsal, and ventral views.

Another caudal vertebra was recovered as part of NMNZ S.47312 (Figure 2.37-38) and is similar to the caudal vertebra from NMNZ S.47303. However, a small incipient dorsal projection of the arcus vertebrae is present on both sides of, and cranial to, the processus spinosus, which may be homologous with a vestigial zygapophyses cranialis. The processus spinosus is not bifurcated, and it

is interpreted that this vertebra was more caudal than the purportedly bifurcated caudal vertebra of NMNZ S.47303, as exists in modern *Eudyptula minor*. Both processus transverses are present yet eroded. Similarly, two processus haemali project ventrally from the corpus vertebrae, but are heavily weathered.

Ribs. A single left rib is well-preserved and almost completely intact in NMNZ S.47303 (Figure 2.39-40). Another two partial ribs were recovered in NMNZ S.47339, but are poorly preserved (Figure A5.9-10).

Coracoid. A left coracoid is preserved in NMNZ S.44729, and a sternal part of a left coracoid is present in NMNZ S.47308 (Figure 3.1-2, 3.6-7). As in *Muriwaimanu tuatahi* and *Sequiwaimanu rosieae* the coracoid is shorter than the humerus. This is in contrast to all known post-Paleocene Sphenisciformes, where the coracoid length exceeds the humerus. The coracoid is elongate with a concave medial margin and medioventrally directed processus acrocoracoideus at its omal end, largely resembling the shape of the aforementioned Paleocene taxa, and additionally *Kumimanu biceae*. In contrast, geologically younger penguin taxa such as *Anthropornis grandis*, *Icadyptes salasi*, *Kairuku grebneffi* Ksepka, Fordyce, Ando and Jones, 2012, and some extant forms like *Pygoscelis*, and *Spheniscus*, possess a proportionally a more medially extended acrocoracoid process relative to the shaft, almost perpendicular to the coracoid's long axis (Jadwyszczak, 2006a; Ksepka et al., 2008, 2012).

In NMNZ S.44729 the facies apicalis is angled normal to the alignment collum acrocoracoidea, at its terminus, and has a relatively rounded surface, similar to *Sequiwaimanu rosieae*, as compared to the sharply angled shape in *Muriwaimanu tuatahi*, while the facies articularis clavicularis exists sternal to it. The impressio ligamenti acrocoracohumeralis is distinct upon the lateral edge of the acrocoracoid process, bounded dorsally by the crista acrocoracoidea—the omal extremity of which forms a marked lobe (Figure 3.1-2 oca) that is more strongly protruding than in any other Paleocene taxon. Sternal on the facies articularis clavicularis, the medial insertion for ligamenti acrocoracoprocoracoideale is rounded, overhanging the sulcus musculi supracoracoidei, producing a weak hook-like appearance in dorsal and ventral views. This is unlike the state in all extant and extinct known sphenisciforms, except *Icadyptes salasi* and the large Chatham form described later, where prominent sternally directed “hooking” of the medial

extremity of the acrocoracoid is contrarily observed. The tuberculum for insertion of plica synovialis coracoidea is poorly defined on the dorsal facies of collum acrocoracoidei, compared to a more strongly protruded ridge in *M. tuatahi* and *S. rosieae*. It is joined by a low ridge to the insertion for ligamenti acrocoraco-acromiale, which forms a rounded structure upon the dorsal side of the facies articularis clavicularis. The acrocoraco-acromiale ligament insertion is separated from the insertion for the ligamenti acrocoraco-procoracoideale by a groove that does not distinctly occur on either *M. tuatahi* or *S. rosieae*. The impressio coracobrachialis is indistinct across the omal-ventral surface of the acrocoracoid process, bounded sternally by a low ridge. The fossa sternal to this ridge is shallow unlike the deepened feature observed for Eocene *I. salasi*. There is no identifiable impressio bicipitalis. The musculus biceps brachii is absent or vestigial in extant sphenisciforms (Schreiweis, 1982), and weak in procellariiforms, which may relate to the lack of distinction of this impression in these groups (Elzanowski et al., 2012).

Alike to living and extinct penguins, the omal end of the coracoid of NMNZ S.44729 is flat ventral to the acrocoracoid process. The facies glenoidalis (for the facies articularis humeralis) exists on the lateral edge of the omal coracoid, sternal to the acrocoracohumeralis ligament impression, and has a poorly defined labrum glenoidale ventrally. Dorsal and sternal to the facies glenoidalis, the cotyla scapularis is deeply concave and rounded.

The processus procoracoideus projects medially, ending on a broken edge near to the medio-dorsal surface of the corpus coracoideum, restricting comparisons. As in *Muriwaimanu tuatahi*, *Kumimanu biceae*, and *Sequiwaimanu rosieae*, the foramen nervi supracoracoidei is absent, whereas it is present in all Eocene and Oligocene penguins for which this area of the coracoid is preserved.

The extremitas sternalis is preserved in both specimens, is flared mediolaterally with a well-defined angulus medialis (obtuse in NMNZ S.47308 and acute in NMNZ S.44729—though possibly eroded), but the extent of the processus lateralis is unknown due to breakage in both specimens. Insofar as preservation allows, the mediolateral width of the sternal end in these specimens shows a lesser degree of flaring than in specimens of *Muriwaimanu tuatahi*. The sternal margin is slightly concave in dorsal aspect in both specimens and is more incurvate (especially medially) in

NMNZ S.47308 where the facies articularis sternalis meets the angulus medialis. The impressio sternocoracoidei is large, deeply dorsoventrally concave, and separated from the facies articularis sternalis by a thin, distinctly raised labrum internum. Sternal of the labrum internum, the facies articularis sternalis dorsalis is concave and dorsoventrally deep. In both specimens this facet is lost laterally, and thus it is unknown if a second more laterally situated facet existed, as it did in the Oligocene *Kairuku* (see Ksepka et al., 2012). The facies articularis sternalis in *Kupoupou stilwelli* n. gen. et sp. is different to that in *Sequiwaimanu rosieae* in that the labrum internum is more prominent, and the facet is narrower in the sternal-omal direction, yet not as narrow as in extant penguins. In this respect, its proportions are more alike *M. tuatahi*. The medial border the extremitas sternalis of NMNZ S.44729 is relatively straight and uniform compared to the convexly bulging sternal medial margin of the right coracoid in *S. rosieae* (see Mayr et al., 2018b: figure 9). While the medial margin of the coracoid in NMNZ S.47308 is incompletely preserved, the angular crista epimarginalis is similar to some specimens of *M. tuatahi* (Figure 3.3). The crista epimarginalis is not prominent in NMNZ S.44729, in comparison.

Scapula. An incomplete left scapula in NMNZ S.47339 (Figure 3.8-9), preserves the extremitas cranialis, and is broken caudal to the collum scapulae. Its shape resembles that of *Muriwaimanu tuatahi* and *Sequiwaimanu rosieae*, where the acromion is dorsally projected, and the facies articularis humeralis is rounded on the ventral margin. While the cranial margin between the acromion and the tuberculum coracoideum is relatively flattened in NMNZ S.47339, *M. tuatahi*, and *S. rosieae*, this area is shallowly incurvate in *Kumimanu biceae* and even more concave in the Eocene *Icadyptes salasi* and *Inkayacu paracasensis* Clarke, Ksepka, Salas-Gismondi, Altamirano, Shawkey, D'Alba, Vinther, DeVries and Baby, 2010, and is prominently concavely notched in extant sphenisciforms (Ksepka et al., 2008; Clarke et al., 2010; Mayr et al., 2017b). Compared to *K. biceae* and extant penguins, the tuberculum coracoideum does not project as far cranially, and a less prominently angled profile exists on the processus glenoidalis scapulae from lateral and medial aspects. Associated with this, the facies articularis humeralis is dorsoventrally wider in extant penguins. The cranial margin between the tuberculum coracoideum and facies articularis humeralis is also shallower in NMNZ S.47339 than

M. tuatahi and *S. rosieae*. Caudal on the corpus scapulae, a ventrally projecting ridge on the ventral edge of NMNZ S.47339 may suggest an expanded blade-like caudal scapula, compared to the proportionally narrow dorsoventral width observed in *M. tuatahi*. A dorsoventrally wider caudal scapula blade is observed in *S. rosieae* and even more so in *K. biceae*, yet not to the extent of the distinct paddle-like shape of phylogenetically crownward penguins (Mayr et al., 2017b; Mayr et al., 2018b).

Humerus. A distally eroded left humerus was recovered from NMNZ S.47339, in addition to a more complete and slightly larger humerus from NMNZ S.47308, which has been broken at mid-length and subject to erosion along the cranial margin (Figure 4.1-11). These humeri show dorsoventral flattening typical of sphenisciforms, are gracile, and do not widen distally. The humeri show sigmoidal curvature in dorsal and ventral aspects, also observed in the humeri of other Paleocene penguins (Slack et al., 2006; Jadwiszczak, 2013), and Eocene forms such as *Kaiika maxwelli* (see Fordyce and Thomas, 2011), whereas more crownward taxa possess relatively straighter shafts. The shaft is elongate, with a ratio of proximodistal length to mid-shaft craniocaudal width (shaft robustness index) value of 7.78 for NMNZ S.47308, markedly narrower than other extant and extinct penguin taxa, except *Muriwaimanu tuatahi* (see phylogenetic data matrix). The missing distal end of the NMNZ S.47339 humerus precluded calculation of the shaft robustness index, however, its shape and surviving proportions are similar to NMNZ S.47308. The humeri of both NMNZ S.47308 and NMNZ S.47339 appear slightly proportionally wider craniocaudally than in *M. tuatahi*, consistent with a more derived morphology, yet are also subtly narrower than, and less robust compared to, other Paleocene taxa including *Sequiwaimanu rosieae* and *Crossvallia unienwillia*. This is supported by the ratio of minimum humerus width to maximum humerus length of ~0.12 (0.12 in *M. tuatahi* and 0.15 in *S. rosieae*, Mayr et al., 2018b).

Like other penguins, the caput humeri is very enlarged, and hemispherical in dorsal and ventral aspects. The caput is positioned dorsocaudally, rather than more caudally oriented in the humeri of modern penguins. The proximal dorsal and ventral profile of the caput is asymmetric, with a prominent apex positioned caudal to the midline of the shaft, yet not as reniform as in extant penguins. In comparison, Paleocene penguins *Muriwaimanu tuatahi*, *?Crossvallia waiparensis*, and *Sequiwaimanu*

rosieae have apices positioned closer to the midline of the shaft. The proximal extremity of the crista deltopectoralis on the cranial margin is markedly distal to the apex of the humerus head—more so in NMNZ S.47339. On the proximal edge, both NMNZ S.47339 and NMNZ S.47308 have a notch separating the caput humeri from the crista deltopectoralis, similar to *Kaiika maxwelli*, yet not as deep as in some specimens referred to *M. tuatahi*, where the proximal crista deltopectoralis is more cranially projected (CM zfa 34, Slack et al., 2006: figure 1 A o). In contrast, other humeri assigned to *M. tuatahi* and those of *S. rosieae* and *?C. waiparensis* have a more rounded and convex proximocranial profile in dorsal and ventral aspects. On the proximal cranioventral face of both specimens a distinct, shallow, well-defined oblong fossa, elongated proximodistally along the proximocranial margin, marks the insertion of the musculus coracobrachialis cranialis, which is adjacent to the attachment surface for the musculus pectoralis thoracica on the proximal cranioventral border (Schreiweis, 1982). This fossa is proportionally small compared to *Crossvallia unienwillia* and *K. maxwelli*. Typical of basal penguins, the incisura capitis is located caudally in both NMNZ S.47339 and NMNZ S.47308, and is aligned with, yet distinct from the sulcus transversus, but not as far separated as in specimens of *M. tuatahi*. The caudal margin of the fossa pneumotricipitalis ventralis extends further caudally relative to the caput humeri in dorsal and ventral profiles, corresponding with similar proportions of *M. tuatahi* and early Eocene *K. maxwelli*, rather than *S. rosieae*, *C. unienwillia*, and phylogenetically crownward penguins. An ovoid impression on the dorsal margin of the fossa pneumotricipitalis ventralis, and bounded cranially by the crus dorsale fossa, is described as the attachment scar for musculus coracobrachialis caudalis in both specimens. The caudal coracobrachialis muscle attachment tubercle is similarly shaped and located in *M. tuatahi*, and *S. rosieae*, yet is proportionally larger in NMNZ S.47308 and NMNZ S.47339, and is similarly located in *K. maxwelli* (see Fordyce and Thomas, 2011). In more crownward sphenisciforms, such as *Icadyptes salasi* and *Kairuku grebneffi*, this feature is an obliquely orientated, distally projected protrusion, on the cranial dorsal margin of the tricripital fossa (Ksepka et al., 2008, 2012). The crista bicipitalis is a subtly rounded shelf, distally extends almost perpendicular to the shaft in both specimens, similar to that in *?C. waiparensis*, and is not as distally convex as in *M. tuatahi*, nor does it exhibit the same

distal extension of *S. rosieae*. The crista bicipitalis is not as flat as observed in *Kumimanu biceae*, and unlike *K. maxwelli* there is no distally directed prominence of the ventral tubercle and associated groove. The fossa pneumotricipitalis ventralis is deep, singular, and lacking pneumatic foramina as in other Sphenisciformes. A dorsally located shallow depression more cranial to the incisura capitis is identified as the fossa pneumotricipitalis dorsalis and is distally continuous with the shaft facies. While the fossa pneumotricipitalis dorsalis is distinct in NMNZ S.47339, erosion to NMNZ S.47308 has partially obscured it, although it is still visible immediately caudal to the insertion scar for musculus supracoracoideus and distal to the caput humeri. In *K. maxwelli* this feature is similarly located, immediately caudal to the supracoracoideus muscle insertion scar, and is also apparent in some specimens of *M. tuatahi* (CM zfa 34, CM 2008.145.3, CM 2008.145.4), but is absent in *S. rosieae*. Dorsally, near the proximal end of the crista deltopectoralis, the tuberculum dorsale marks the insertion of musculus deltoideus minor and the principal part of the musculus supracoracoideus, the attachment surface for the latter of which has been raised and distally elongated in penguins to form the crista musculi supracoracoidei (Schreiweis, 1982; Baumel et al., 1993). This supracoracoideus muscle scar is distinct and raised near the cranial margin of the dorsal facies in NMNZ S.47339, but abraded in NMNZ S.47308, as it is in basal sphenisciforms *M. tuatahi*, *S. rosieae*, *C. uienwillia*, *?C. waiparensis*, and *K. maxwelli*. In geologically younger and phylogenetically more crownward penguins, this feature is located closer to the mid-line of the proximal humerus shaft.

Features of the distal end are well-preserved and described from NMNZ S.47308. The tuberculum supracondylare dorsale is a poorly defined small projection on the distal cranial border and is similarly indistinct in *Sequiwaimanu rosieae*. A small compact tuberculum supracondylare dorsale has been recognised in several penguin taxa, including *Perudyptes devriesi* Ksepka and Clarke, 2010, *Muriwaimanu tuatahi* and *Kaiika maxwelli* (Slack et al., 2006; Ksepka and Clarke, 2010; Fordyce and Thomas, 2011).

In both dorsal and ventral aspects, the sub-hemispherical radial condyle (condylus dorsalis) is distinct from *Muriwaimanu tuatahi* in its relatively more rounded profile and different to *Sequiwaimanu rosieae* in that it is proportionally larger and continuous with the distal cranial shaft margin—rather than exhibiting an indentation and sub-

sequent “bulge” proximal to it (Mayr et al., 2018b). The ulnar condyle (condylus ventralis) is positioned caudal and ventral compared to the radial condyle and extends slightly more distally. In ventral aspect, the ulnar condyle is cranially bounded by the impression for the insertion of the entepicondylar ligament. In ventral view, the ulnar condyle is continuous with the ventral trochlear process, like *M. tuatahi*, whereas they are separated in *S. rosieae*. In distal aspect, the ulnar condyle is proportionally more extensive craniocaudally, and more tubular than that of *S. rosieae*, yet the radial condyle is shorter and more rounded. The angle between the shaft and the tangent of the radial and ulnar condyles is greater than 40°.

The sulcus scapulotricipitalis and sulcus humerotricipitalis are deep excavations on the distal humerus of NMNZ S.47308. Common to all penguins, these humerotricipital sulci are delimited by distinct trochlear ridges, consisting of a dorsal, intermediate and ventral processes (trochlear processes in Marples 1952; Ksepka et al., 2006; Acosta Hospitaleche et al., 2007; process-like crests in Göhlich, 2007; trochlear ridges in Ksepka and Clarke, 2010). The sulcus scapulotricipitalis is present as a dorsally located deep sub-spheroid concavity, as it is in *Muriwaimanu tuatahi* and *Sequiwaimanu rosieae*, bordered by the dorsal trochlear ridge cranially and the intermediate trochlear ridge caudally, in NMNZ S.47308, rather than caudally situated as it is in phylogenetically crownward penguins. Like all other penguins, the sulcus humerotricipitalis is present on the caudal face of the distal humerus, delimited by the ventral and intermediate trochlear ridges. The groove for the sulcus humerotricipitalis is markedly shallower compared to *S. rosieae* and most other penguins. The distal end of the humerus is missing in NMNZ S.47339, however, the proximal remains of the grooves of these trochleae are still visible in dorsal and caudal views. The dorsal trochlear ridge is located dorsally in NMNZ S.47308 and does not reach the caudal margin in dorsal view, alike to *M. tuatahi*, and *S. rosieae*, compared to a more caudally located and extended process in geologically younger penguins. The intermediate trochlear ridge is more dorsally situated than ventrally on the caudal margin, is rounded, and projects further caudally and distally than both ventral and dorsal trochlear ridges. Relatively extensive distal projection of the intermediate trochlear ridge is common to other penguins, except *Perudyptes devriesi* where the dorsal trochlear ridge extends further than the intermediate trochlear ridge (Ksepka and

Clarke, 2010). The ventral trochlear ridge is more caudally extended than the dorsal trochlear ridge in distal view, but less than the intermediate trochlear ridge. In contrast, the caudal extension of these trochlear ridges is subequal in *S. rosieae*, and in most phylogenetically younger penguins the caudal extent of the ventral trochlear ridge surpasses that of the other trochlear ridges. This is true except for the Miocene *Paraptenodytes antarcticus* (Moreno and Mercerat, 1891), where the intermediate trochlea ridge extends most caudally, followed by the dorsal trochlea ridge, and the ventral trochlea ridge with the least caudal projection.

Ulna. *Kupoupou stilwelli* n. gen. et sp. is represented by two ulnae, an almost complete left ulna in NMNZ S.47308, eroded on the ventral face distally, and another left ulna missing its distal portion in NMNZ S.47339 (Figure 5.1-4). These ulnae are typical of that in basal penguins such as *Muriwaimanu tuatahi* and *Sequiwaimanu rosieae*, as they are craniocaudally widest proximally and tapered distally and are less dorsoventrally flattened and relatively craniocaudally narrow than all other geologically younger, more derived sphenisciforms. The olecranon is a caudally extending tab-like projection with a convex dorsal and ventral profile, similar to that in *M. tuatahi* and *S. rosieae*. However, the distal caudal margin of the olecranon in NMNZ S.47308 and NMNZ S.47339 is uniquely angled, accentuated by a bony prominence that projects caudally from the distal border of the olecranon and is more protuberant in NMNZ S.47308. The apex of the olecranon is slightly more distally located than in *M. tuatahi*—more so in NMNZ S.47339. Similarly, the apex of the olecranon in *S. rosieae* is also slightly distally situated compared to *M. tuatahi*. In more phylogenetically derived penguins such as *Icadyptes salasi*, the apex of the olecranon is even further displaced from the cotyla ventralis, and in even more geologically younger sphenisciforms the shaft expands towards the olecranon from approximately one fourth of the length to the distal end of the ulna.

A plesiomorphic feature common to the aforementioned described Paleocene taxa, but absent from post-Paleocene counterparts, the processus cotylaris dorsalis exists on the cranioproximal ulnar margin as a rounded, cranially projecting convex structure (Mayr et al., 2017b, 2018b). In contrast to both *Muriwaimanu tuatahi* and *Sequiwaimanu rosieae*, the processus cotylaris dorsalis is not as pronounced, less cranially projected, and is instead more confluent with the cranial margin of the ulna in both NMNZ S.47339 and NMNZ S.47308. The

cranial profile of the processus cotylaris dorsalis is more angled in NMNZ S.47339 than in NMNZ S.47308 and has a cranially protrusive apex more proximally situated. Like *M. tuatahi* and *S. rosieae* the olecranon and processus cotylaris dorsalis on both NMNZ S.47308 and NMNZ S.47339 dorsalis are expanded distally along the margin of the dorsal face, resulting in a flattened proximal dorsal surface and a relatively sub-cylindrical shaped proximal ventral ulna. Morphological features upon the proximal dorsal surface in NMNZ S.47339 and especially NMNZ S.47308 are comparatively more flattened and less well-defined than on the ulnae of *M. tuatahi* and *S. rosieae*. As in *M. tuatahi* and *S. rosieae*, a shallow fossa exists proximocaudally on the dorsal face of both ulnae and is caudally bounded by an “edge-like jut” (Mayr et al., 2018b) in NMNZ S.47339, which is less prominent compared to the same feature in ulnae of *M. tuatahi* and *S. rosieae*. A narrow furrow is present on the dorsal face of the distal olecranon near the caudal margin in NMNZ S.47339 and NMNZ S.47308, which is more distinct in the ulnae of *S. rosieae*, and absent in all other sphenisciforms.

The distal end of the ulna is not preserved in NMNZ S.47339, and in NMNZ S.47308 features are obscured by abrasion. However, the overall shape of the distal end bears a resemblance to that of *Muriwaimanu tuatahi* and *Sequiwaimanu rosieae*. A projecting caudal convexity on the distal end of NMNZ S.47308 is consistent with the positioning of the condylus dorsalis of *M. tuatahi* and *S. rosieae*, but lacks the definition observed in these species. Additionally, a poorly defined ventral protuberance on the distal end may represent the tuberculum carpale. The condylus ventralis is indiscernible. While still visible in Paleocene sphenisciforms such as *M. tuatahi* and *S. rosieae*, a reduction of these distal features is observed in geologically younger penguins with stiffened flippers more adapted to aquatic locomotion (Mayr et al., 2018b).

Radius. *Kupoupou stilwelli* n. gen. et sp. is represented by four radii: a complete right radius in NMNZ S.47339, a left (with an eroded cranial margin) and a proximal right radius in NMNZ S.47303, and a fractured and proximally worn left radius in NMNZ S.47312 (Figure 5.5-11). While of similar general size, the radii in NMNZ S.47303 are slightly relatively shorter than the others. The radii are flattened dorsoventrally as for all known Sphenisciformes. The overall shape of the radii closely resembles those of *Muriwaimanu tuatahi* and *Sequiwaimanu rosieae*, rather than more phyloge-

netically derived penguins, but they are generally shorter. Compared to those of *M. tuatahi* they also are more dorsoventrally flattened and have a proportionally craniocaudally wider shaft—although considerably narrower than radii associated with Eocene penguins such as *Delphinornis larseni* (see Jadwiszczak, 2006a: figure 13 c, d) and *Icadyptes salasi* (Ksepka et al., 2008). As in other Paleocene sphenisciforms, the proximal end of the radius is markedly deflected caudally relative to the shaft, when viewed in dorsal/ventral aspects. The radii of *K. stilwelli*, n. gen. et sp. are more prominently bent in this way than those associated with *M. tuatahi* and bear similar proximal angulation to that in *S. rosieae*. Greater proportional proximal displacement of the cotyla humeralis relative to the proximal radius bend is also observed in *K. stilwelli*, n. gen. et sp. compared to Eocene penguins such as *Delphinornis larseni*, *Anthropornis Wiman*, 1905a, and *Icadyptes salasi* (Jadwiszczak, 2006a; Ksepka et al., 2008; Jadwiszczak, 2012), and geologically younger penguins. Common to *M. tuatahi* and *S. rosieae*, and most Eocene sphenisciforms, *K. stilwelli* n. gen. et sp. has a rounded cranial margin where the proximal bend meets the radius shaft and differs from Eocene *Palaeudyptes gunnari* (Wiman, 1905a) more phylogenetically derived penguins where the cranial border is relatively angular and crest-like in comparison (see Jadwiszczak, 2012: figure 2B). As in *S. rosieae*, distal to the proximal facet, a sulcus extends proximodistally on the dorsal face marking the scar for the proximal insertion of the musculus brachialis (Mayr et al., 2018b). Geologically younger penguins, such as the Oligocene *Kairuku*, instead have a shallow incurvate depression or notch along the cranial margin marking this insertion (Ksepka et al., 2012), while in recent penguins such as *Pygoscelis*, *Eudyptula*, and *Eudyptes*, this notch is distinctly concave in comparison.

Located dorsocaudally, immediately distal to the cotyla humeralis, the insertion scar for musculus supinator is sub-triangular in shape. The musculus supinator scar is distinct on the right radii of NMNZ S.47308 and NMNZ S.47339 but is not visible on the other radii due to erosion. This structure is similarly located, yet smaller, oval-shaped and not as clearly defined in *Muriwaimanu tuatahi* (referred specimen CM 2009.99.1), whereas the scar is not distinctly visible in *Sequiwaimanu rosieae* (see Mayr et al., 2018b). In geologically younger penguins such as *Icadyptes salasi*, *Kairuku* and extant species (Ksepka et al., 2008, 2012), the musculus supinator scar is more dor-

sally situated on the proximal end, and is a larger, more prominent sub-triangular mark.

A furrow for the musculus extensor metacarpi radialis tendon is well-defined on the dorsal surface of the right radius of NMNZ S.47303, NMNZ S.47339, and NMNZ S.47312, whereas erosion to the surface of the left radius of NMNZ S.47303 has obscured this feature. The furrow extends proximodistally on the dorsal face, immediately cranial to the mid-line of the radius, as it does in *Sequiwaimanu rosieae* and *Muriwaimanu tuatahi* (albeit only distally well-defined). In contrast, the furrow is located closer to the cranial border in more phylogenetically derived sphenisciforms such as *Delphinornis larseni*, *Icadyptes salasi*, *Kairuku* (Jadwiszczak, 2006a; Ksepka et al., 2008, 2012), and extant forms.

The sulcus for the musculus extensor longus alulae runs proximodistally, caudal to the mid-line, at the distal end of the radius in dorsal aspect, but cannot be viewed on the right radius of NMNZ S.47303 as only the proximal half of the element was preserved. It is similarly located and shaped in the Paleocene *Muriwaimanu tuatahi* (CM 2009.99.1). The furrow is not as proximodistally oriented in *Sequiwaimanu rosieae*, instead transversing at an angle from the caudal margin to the central distal radius in comparison. This is similar to extant penguins, where the musculus extensor longus alulae produces a groove across the dorsal radius to insert on the cranial proximal articulation facies of the carpometacarpus (Ksepka et al., 2008). On the left radius of NMNZ S.47303, a bony tubercle projects caudally from the ventrodiscal margin, which is absent in all other extant and extinct sphenisciforms, and may be representative of the tuberculum aponeurosis ventralis. In caudal aspect, the distal radius forms a marked ulnar depression (depressio ligamentosa) in conjunction with the bony tubercle on the caudal ventral edge, and the caudally protruding lip of the dorsal margin, which is more prominent than that of *M. tuatahi* (Figure 5.11-12). The ligamenti interosseum radioulnare occupies this space of the ulnar depression, and prevents direct contact between the distal ulna and radius, in extension and flexion of the wrist joints (Baumel et al., 1993).

Carpometacarpus. A distal right carpometacarpus is preserved in NMNZ S.47303 (Figure 6.1-2, 6.4). The element has subtle dorsoventral flattening and an ovoid cross-section. The spatium intermetacarpale is long and ovoid. The carpometacarpus is relatively straight and broad, and metacarpal II (os metacarpale majus) does not show distinct anterior

bowing. The distal articular surface also broadens anteriorly in distal aspect. Metacarpals II and III (os metacarpale minus) are sub-equal in distal extent, which is characteristic of many penguins including *Muriwaimanu tuatahi*, *Sequiwaimanu rosieae*, middle Eocene *Perudyptes devriesi*, and late Eocene *Pachydyptes ponderosus* Oliver, 1930. For comparison, in some recent penguins metacarpal III extends significantly distal to metacarpal II, including early Miocene *Palaeospheniscus patagonicus* Moreno and Mercerat, 1891, latest Oligocene-earliest Miocene *Platydyptes marplesi* Simpson, 1971, and crown group penguins. The preserved portion largely resembles that of *M. tuatahi* and *S. rosieae*, only differing notably where the carpometacarpus of *M. tuatahi* has a more rounded distal end, whereas in NMNZ S.47303 and *S. rosieae* the distal face is relatively flattened and angular in section.

Proximal manus phalanx of the second digit.

The right manus phalanx II-1 is intact and well-preserved in NMNZ S.47303 (Figure 6.6-11). The bone is dorsoventrally flattened, with the proximal facet wider and with greater dorsoventral depth than the distal facet. The cranial border from the mid-line of the phalanx is particularly thin and flattened relative to the rest of the bone, and it is craniocaudally widest around the mid-point of the length of the bone.

Manus phalanx of the third digit. What is interpreted as the right manus phalanx III-1 is partially preserved in NMNZ S.47303 (Figure 6.12-17), with the articulation facet for the carpometacarpus and most of the corpus preserved except for part of the caudal edge and the distal extremity (shown in Figure A2). While the original length of the bone is unknown, precluding accurate comparison with manus phalanx II-1, the complete bone is estimated to be shorter than phalanx II-1, as typical of avian morphology. This is similar to the proportions between phalanx II-1 and III-1 observed in Eocene *Icadyptes salasi* (Ksepka et al., 2008; Ksepka and Ando, 2011), yet unlike the subequal lengths observed in extant penguins. Proximally, separate from the carpometacarpal facet, a proximally projected process or tubercle is preserved, as typifies extant penguins, but this has not been reported from any fossil stem penguins.

Pelvis (ischium). A fragment of the right side of the pelvis is preserved in NMNZ S.47303, which is identified as part of the ischium (Figure 2.31-34). It is wide, flat, and ovoid and does not differ markedly from that of extant penguin species.

Femur. A complete right femur is preserved in NMNZ S.47308, but separated into two parts by a saw cut obliquely traversing the shaft at the trochanteral end (Figure 7.1-2). An incomplete distal left femur was recovered in NMNZ S.47339 (Figure 7.3-4). Overall, the femur closely resembles that of *Muriwaimanu tuatahi* and is more gracile than the relatively robust femora of larger penguins such as *Crossvallia unienwillia*, *Inkayacu paracasensis*, and *Kairuku grebneffi* (see Slack et al., 2006; Clarke et al., 2010; Ksepka et al., 2012; Jadwyszczak et al., 2013). The crista trochanteris is weakly projected proximally, although exceeds that of the caput femoris. This contrasts with procellariiforms such as *Diomedea nigripes*, and Eocene penguins like *Perudyptes devriesi*, *Delphinornis gracilis* (Wiman, 1905a), *Palaeudyptes gunnari* and *Notodyptes wimani* Marples, 1953, where the caput projects equally or slightly further proximally than the crista trochanteris (Jadwyszczak, 2006a; Ksepka and Clarke, 2010). The proximal surface of the facies articularis antitrochanterica is slightly concave in cranial and caudal profile, but not as pronounced nor deep as in phylogenetically more crownward penguins such as *Kairuku grebneffi* and extant forms (Ksepka et al., 2012). In *Sequiwaimanu rosieae*, the crista trochanteris is more proximally tapered and the facies articularis antitrochanterica is even less concave in cranial and caudal views. The caput is similar to that of *Inkayacu paracasensis*, being sub-circular in cranial and caudal aspects (Clarke et al., 2010), rather than the relatively more proximomedially sloped ovoid shape observed in *M. tuatahi* and *S. rosieae*. The lateral border of the shaft is weakly concave in dorsal view, as it is in procellariiforms and *Crossvallia unienwillia* (see Jadwyszczak et al., 2013), rather than being straight or slightly convex as observed in most other sphenisciforms. Proximally, the linea intermuscularis cranialis is located close to the midline of the long axis of the bone in NMNZ S.47308, as it is in *Hydrobates leucorhous*, *S. rosieae*, and *Delphinornis gracilis*, rather than more laterally in *Diomedea nigripes* and *M. tuatahi* (see Jadwyszczak, 2006a; Slack et al., 2006; Mayr et al., 2018b). While the proximal linea intermuscularis cranialis is sharply defined and prominent in *S. rosieae*, it is less so in NMNZ S.47308. The linea intermuscularis cranialis continues distally in a central position along the shaft, comparable with the aforementioned Paleocene and Eocene sphenisciforms. In caudal view, the medial margin of the crista supracondylaris medialis abruptly joins the shaft, although this is less angular in profile than that

observed in *S. rosieae*, and *Marambiornis exilis* Myrcha, Jadwiszczak, Tambussi, Noriega, Gaździcki, Tatur, and Del Valle, 2002 (see Jadwiszczak, 2006a), and less convex than in *M. tuatahi*. In comparison, in many geologically younger penguins, the transition between the shaft and the condylus medialis along the medial profile is relatively smooth.

Distally, the fossa poplitea is deeper than that in *Muriwaimanu tuatahi*, and more comparable to *Sequiwaimanu rosieae*. Cranially, the sulcus patellaris is relatively shallow and is not as distinctly bounded as that of *?Crossvallia waiparensis*. Both the condylus medialis and condylus lateralis are prominently bulbous and flare mediolaterally, similar to in *Inkayacu paracasensis* and *Kairuku grebneffi* (see Clarke et al., 2010; Ksepka et al., 2012), rather than narrower profile reported for *Delphinornis gracilis* (see Jadwiszczak, 2006a). The condylus medialis in caudal aspect is more sub-spherical and is proportionally larger than in *S. rosieae*, but not as proximodistally extensive as in *M. tuatahi*. In caudal aspect, the condylus lateralis extends further distally than the condylus medialis, more so than in *M. tuatahi*, *S. rosieae*, *Crossvallia unienwillia* and *Delphinornis gracilis* (see Jadwiszczak, 2006a; Jadwiszczak et al., 2013). The epicondylus lateralis in cranial view projects laterally as a rounded tubercle, and is more distinctive than in other extinct or extant sphenisciforms. Caudally, the sulcus fibularis is relatively proximally situated between the semicondylus tibiofibularis and the semicondylus fibularis, giving the condylus lateralis a more rounded distal profile in caudal view than in *M. tuatahi*, *S. rosieae*, and *?C. waiparensis*. Additionally, the sulcus fibularis is not as prominent compared to all geologically younger penguins. The crista tibiofibularis is mediolaterally wide, more-so than observed in *S. rosieae*, or as reported in *Delphinornis gracilis* (see Jadwiszczak, 2006a). The proximal semicondylus fibularis is angular in caudal and cranial views, similar to *M. tuatahi* (Slack et al., 2006: figure 1 A w), rather than the rounded profile in *S. rosieae*.

Tibiotarsus. A distal right tibiotarsus fragment was recovered in NMNZ S.47339 (Figure 7.6-7). It shows that the trochlea cartilaginosa tibialis is a smooth, wide trough caudally, between sharply projecting crests of the condyli medialis et lateralis, and an overall shape similar to that of *Waimanu manneringi* (Figure 7.8) and *Sequiwaimanu rosieae*.

Tarsometatarsus. A complete, left tarsometatarsus is well-preserved in the holotype, NMNZ

S.47312 (Figure 8.2, 8.4-8). It is relatively short and wide; a stout morphology typical of modern penguins. This contrasts to the relatively more elongated tarsometatarsi of Paleocene penguins *Waimanu manneringi* and *Muriwaimanu tuatahi*, and instead converges on an overall shape typical of geologically younger Eocene penguins, particularly to *Delphinornis larseni* (Figure 8.2-3; Wiman, 1905a; Myrcha et al., 2002; Slack et al., 2006; Jadwiszczak and Mörs, 2019). While being much smaller, it is proportionally similar to the tarsometatarsus associated with the giant mid-Paleocene penguin recovered from the Waipara Greensand (Mayr et al., 2017a), and that of *?Crossvallia waiparensis* (see Mayr et al., 2019).

In dorsal view, the eminentia intercotylaris is rounded and prominent proximally, contrasting with the relatively more angular and more proximally projecting morphology of both *Waimanu manneringi*, *Muriwaimanu tuatahi*, and *?Crossvallia waiparensis*, and is comparatively more dorsally projected than in *Delphinornis larseni* (NRM-PZ A.994, Jadwiszczak and Mörs, 2019: figure 2.6). The cotylae are sub-circular depressions of sub-equal size, in contrast to a proportionally more medially enlarged cotyla medialis in *?C. waiparensis*. The lateral margin of the cotyla lateralis projects beyond the lateral edge of the tarsometatarsus, in dorsal and plantar views, similar to *W. manneringi* and *M. tuatahi*, and the unnamed giant Waipara Greensand taxon (Mayr et al., 2017a), yet unlike many more phylogenetically crownward penguin species (Chávez Hoffmeister, 2014). The cotyla medialis is dorsodistally deflected, slightly exposing the articular surface in dorsal view. In contrast to *?C. waiparensis*, the tarsometatarsus of NMNZ S.47312 lacks a large and prominent medial projection on the medial margin of the cotyla medialis.

The tarsometatarsus shaft has a concave medial border and is straight laterally when viewed from plantar and dorsal aspects. The lateral border is straight in geologically younger sphenisciforms such as *Delphinornis larseni*, *Inkayacu paracasensis*, and *Kairuku* (Myrcha et al., 2002; Clarke et al., 2010; Ksepka et al., 2012), and convex in *Archaeospheniscus lopdellorum* Marples, 1952, and *Dunstroornis parvus* (see Marples, 1952), but is concave in the basal penguins *Waimanu manneringi*, *Muriwaimanu tuatahi*, and *?Crossvallia waiparensis*. The margo lateralis is rounded dorsoplantarly, in comparison with a more sharply angled edge in *?C. waiparensis*. Dorsally, the fossa infracotylaris dorsalis is deep, in contrast to the rel-

atively shallow state exhibited by other Paleocene taxa, however, it is not as excavated to the extent observed in *D. larseni*, whereby marked depressions for the fossa infracotyloidalis dorsalis medialis et lateralis exist (sensu Myrcha et al., 2002). Two scars are visible dorsomedially; the impressio retinaculi extensorii medialis near the medial margin, and the impressio retinaculi extensorii lateralis adjacent to the sulcus longitudinalis dorsalis medialis (Figure 8.2; labelled as per Myrcha et al., 2002). Comparatively, in *D. larseni* both impressio retinaculi extensorii are less far separated, more laterally situated and strongly protruding, one immediately medial to the foramen vasculare proximale mediale, and other which is slightly more laterally located and distally bounds the foramen (Figure 8.3; Jadwiszczak and Mörs, 2019: figure 2.2). The sulcus longitudinalis dorsalis medialis is proximally deep near the foramen vasculare proximale mediale and shallows towards the mid-shaft. In contrast, the sulcus longitudinalis dorsalis lateralis is relatively deep, and stretches from distal to the foramen vasculare proximale laterale to the foramen vasculare proximale distale. Both foramina vascularia proximalia mediale et laterale are small oval-shaped and elongate openings on the proximodorsal facies, and both open plantarly. Both foramina are located proximal to the mid-shaft on the plantar surface. Plantarly, the foramen vasculare proximale laterale opens distal to the crista lateralis flexor hallucis longus and is situated more proximally than its medial equivalent. The plantar foramen vasculare proximale mediale perforates the crista medialis flexoris digitorum longus at its distal-most extremity. The tuberositas muscularis tibialis cranialis forms a low protuberance separating the foramina vasculare proximale on the dorsal facies, in comparison to a more marked, dorsally protruding structure in *D. larseni* (Figure 8.2-3). A small ovoid depression on the medial margin marks the origin surface for musculus adductor digiti II, which is much less marked than that in *W. manneringi* (Figure 8.1), *M. tuatahi* (CM 2009.99.1) and *D. larseni* (IB/P/B-0547, Jadwiszczak and Mörs, 2019: figure 2.8). Comparatively, the lateral abductor scar for digit IV in NMNZ S.47312 is indistinct.

The cristae hypotarsi are well-defined and although the crista medialis flexoris digitorum longus is abraded, it projects plantarly more so than the other crista hypotarsi. Lateral to the crista medialis flexoris digitorum longus the sulcus hypotarsus for flexor digitorum longus is deeply excavated. The sulcus hypotarsus for flexor hallu-

cis longus is groove-like and is delimited by the crista lateralis flexoris digitorum longus and the crista lateralis flexoris hallucis longus, which are connected and sub-equally projected. The crista lateralis hypotarsi continues as a ridge lateral to these crests, on the border of the proximal articulation area. The presence of a distinct sulcus for tendon of muscle flexor hallucis longus is atypical of many penguins, where the groove is usually vestigial or absent (Chávez Hoffmeister, 2014). However, it is present in many primitive penguins including *Waimanu manneringi*, *Muriwaimanu tuatahi*, *Delphinornis gracilis*, and *Marambiornis exilis* (see Appendix 1, Figure A10; Jadwiszczak, 2015), but is bounded by a plantarly prominent intermediate crest, and a lesser projecting lateral crest, making the groove laterally open (Chávez Hoffmeister, 2014). Proximal to the crista hypotarsi, a depression along the plantar-proximal border is interpreted as the sulcus ligamentosus. A sulcus for the musculus fibularis longus is distinct on the proximal lateral margin and is bounded dorsally by a projecting tuberculum muscularis fibularis brevis (Figure 8.5-6). The fossa parahypotarsalis lateralis is larger and deeper than the fossa parahypotarsalis medialis, which is relatively shallow and indistinct. On the lateral edge of the tarsometatarsus the impressio ligamentosae collaterale laterale intertarsi (as per Zinoviev, 2010, 2015) is well-marked and creates a notch on the proximolateral vertex. The impressio ligamentosae collaterale mediale intertarsi is also well-defined on the medial border and is accompanied by an accessory collateral ligament scar dorsally. The attachment area of both of these medial ligaments is associated with a prominently ridged surface that projects from and overhangs the proximomedial shaft, which is observed in Paleocene *W. manneringi* and *M. tuatahi*, but is substantially reduced and relatively confluent with the medial margin in Eocene forms such as *D. larseni* (Figure 8.1-3). In modern penguins a protruding prominence associated with these medial collateral ligaments is variably expressed, but is not as sharply ridged.

Dorsally, the foramen vasculare distale penetrates the bone at the distal end of a groove between metatarsals III and IV and exits plantarly. A canalis interosseus distalis is also present within the incisura intertrochlearis lateralis. Trochlea metatarsi III extends more distally than trochleae metatarsorum IV and II, which have subequal distal extent. In plantar view, the rims of the trochlea metatarsi III are not distinctly proximally convergent as in *Waimanu manneringi* but are closer to

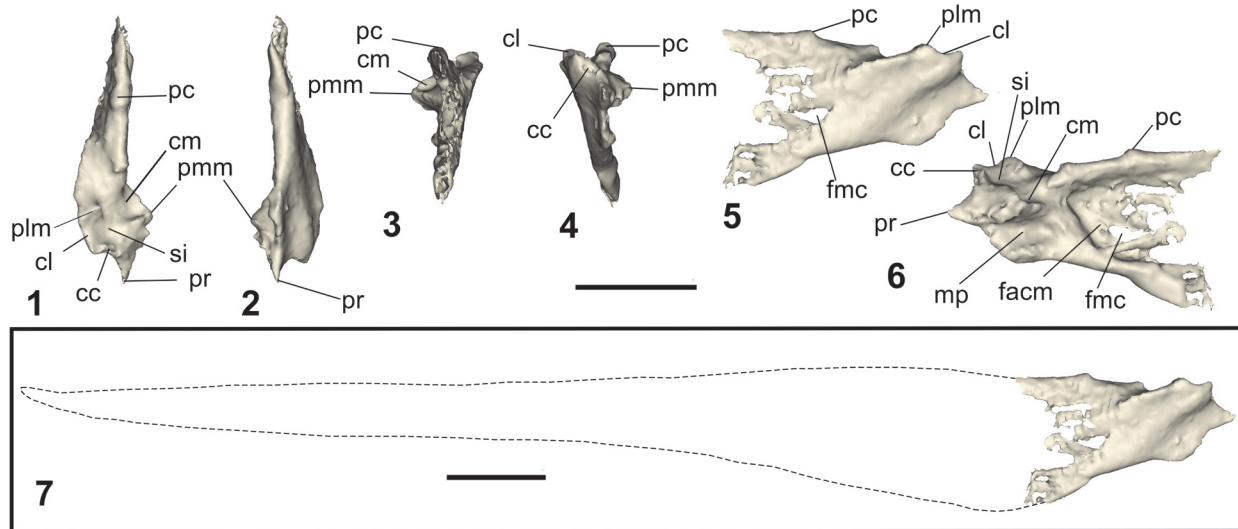


FIGURE 9. Views of the caudal end left mandible of NMNZ S.47302. **1**, dorsal; **2**, ventral; **3**, rostral; **4**, caudal; **5**, left lateral; **6**, left medial aspects. Reconstruction assuming proportions similar to Paleocene penguins in **7**, in left lateral view. **Abbreviations:** **cc**, cotyla caudalis; **cl**, cotyla lateralis; **cm**, cotyla medialis; **facm**, fossa aditus canalis mandibulae; **fmc**, fenestra mandibulae caudalis; **mp**, insertion of musculus pterygoideus; **pc**, processus coronoideus; **plm**, processus lateralis mandibulae; **pmm**, processus mandibulae medialis; **pr**, processus retroarticularis; **si**, sulcus intercotylaris. Scale bars equal to 20 mm.

parallel as they are in *Muriwaimanu tuatahi* (see Mayr et al., 2018b). A deep furrow exists between the rims on trochlea metatarsi III of NMNZ S.47312, deeper than *M. tuatahi*, but not as deep as in *Delphinornis larseni*. The incisura intertrochlearis lateralis extends more proximally and is wider than the medial equivalent, as it is in *M. tuatahi*. The trochlea metatarsi IV is strongly deflected laterally, accentuating the size of the incisura intertrochlearis lateralis from dorsal aspect, more so than in *M. tuatahi* and *D. larseni*. The trochlea metatarsi IV is dorsally directed in distal aspect, comparable that seen in *M. tuatahi* and *D. larseni* (Myrcha et al., 2002). A marked plantar projecting flange of the lateral rim of trochlea metatarsi IV is also observed on NMNZ S.47312 and extends further plantarly than the other trochlea (Figure 8.4). This flange is relatively more sharply angled in *W. manneringi*, and a reduced form exists in *M. tuatahi*, but is not observed in other sphenisciforms. The trochlea metatarsi II is projected medially, in contrast to more crownward penguins, where it is aligned closer to the shaft (Chávez Hoffmeister, 2014). The trochlea metatarsi II is relatively aligned with trochlea metatarsi III in distal view, comparable to *D. gracilis*, rather than the strong plantar deflection observed in *W. manneringi* and *M. tuatahi*, and noticeable deflection of Eocene forms including *D. larseni*, *D. arctowskii*, *Marambiornis*

exilis, *Mesetaornis polaris*, and *Palaeodyptes klekowskii* Myrcha, Tatur and Del Valle, 1990.

Larger Chatham Island Form

Besides *Kupoupou stilwelli* n. gen. et sp., we recognise another markedly larger form of penguin from the Takatika Grit, of the same late early to middle Paleocene age (Figures 9-12). This form is represented by specimens NMNZ S.47302 and NMNZ S.47304, recovered from the same wave platform and horizon of the Takatika Grit as the specimens of *Kupoupou stilwelli* n. gen. et sp. NMNZ S.47302 (Figure A1) is one of four blocks preserving parts of one skeleton, the other three of which (whereabouts unknown) were unavailable to study and was collected February 2008. NMNZ S.47302 is an associated partial skeleton comprising of a caudal portion of the left mandible (Figure 9), a partial furcula (Figure 10.11-16), a fourth cervical vertebra (Figure 10.1-6), an omal part of the right coracoid (Figure 10.7-10), a portion of the sternum (Figure 11), and a vertebra fragment (Figure A5.8). The second specimen, NMNZ S.47304, is a single humerus (Figure 12.1-2). While markedly larger than *Kupoupou stilwelli* n. gen. et sp., the lack of overlap in skeletal elements between the two specimens, means their association as one taxon is only tentative. Furthermore, their relative incompleteness precludes a formal taxonomic description. Nevertheless, some comparative

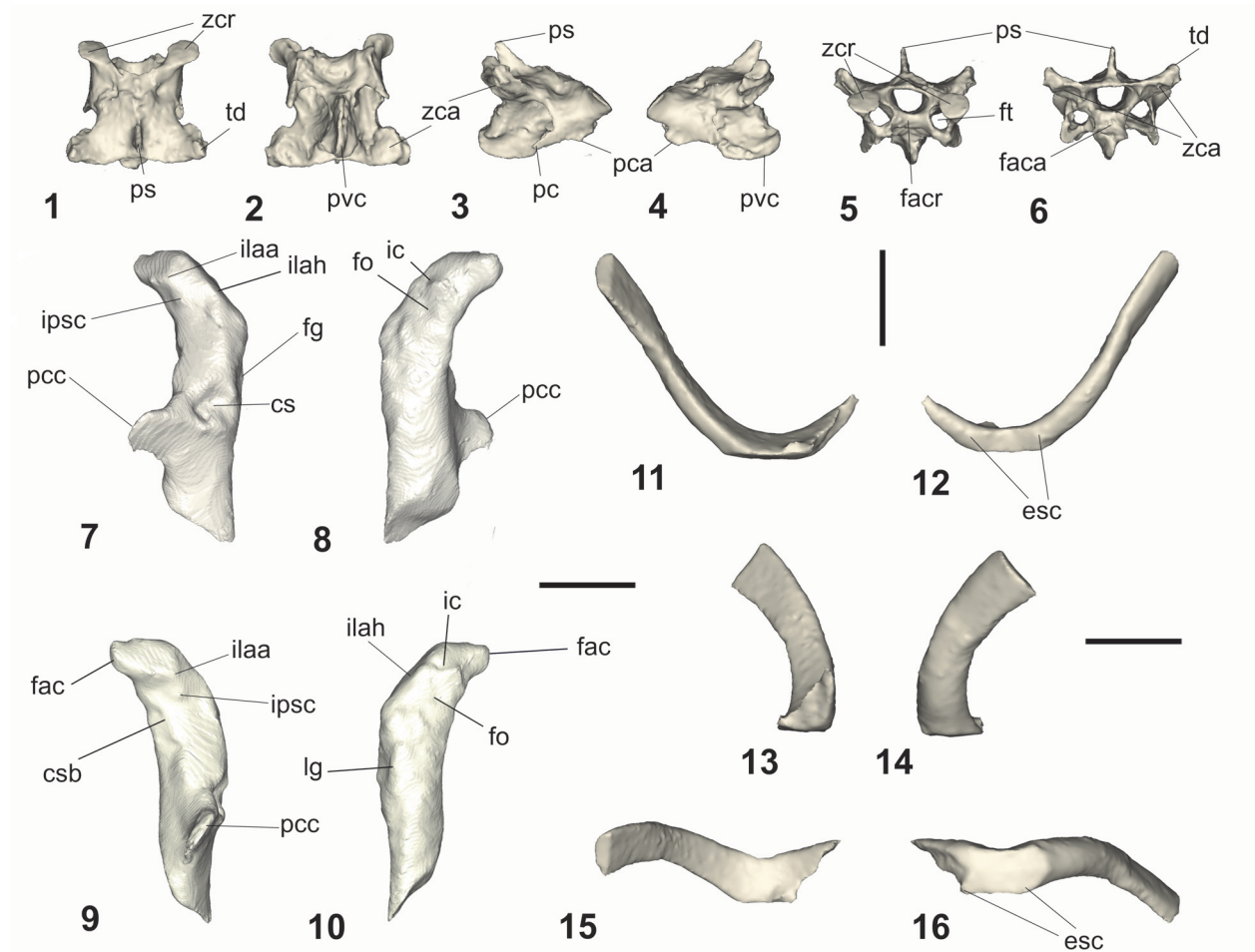


FIGURE 10. Cervical vertebra IV (1-6), coracoid (7-10), and furcula (11-16) of NMNZ S.47302, as part of the larger Chatham Island form. Cervical vertebra IV in **1**, dorsal; **2**, ventral; **3**, right lateral; **4**, left lateral; **5**, cranial; **6**, caudal. Omal right coracoid in **7**, dorsal; **8**, ventral; **9**, medial; **10**, lateral. Partial furcula in **11**, caudal; **12**, cranial; **13**, right lateral; **14**, left lateral; **15**, dorsal; **16**, ventral. **Abbreviations:** **cs**, cotyla scapularis; **esc**, extremitas sternalis clavicularae; **fac**, facies articularis clavicularis; **fac**, facies articularis caudalis; **facr**, facies articularis cranialis; **fg**, facies glenoidalis (facies articularis humeralis); **fo**, fossa (see text); **ft**, foramen transversarium; **ic**, impressio coracobrachialis; **ilaa**, impressio ligamenti acrocoraco-acromiale; **ilah**, impressio ligamenti acrocoracohumeralis; **ipsc**, tuberculum for insertion of plica synovialis coracoidea; **lg**, labrum glenoidale (facies articularis humeralis); **pc**, processus costalis; **pca**, processus caroticus; **pcc**, processus procoracoideus; **ps**, processus spinosus; **pvc**, processus ventralis corporis; **td**, torus dorsalis; **zca**, zygapophysis caudalis; **zcr**, zygapophysis cranialis. Scale bars equal to 20 mm.

observations are made assuming they are of one taxon. Based on the humerus length, this larger Chatham Island form was between the size of an adult *Aptenodytes forsteri* and *A. patagonicus*. Measurements for this form are available in Table 2.

The mandible NMNZ S.47302 (Figure 9) represents a large form distinct from all other sphenisciforms in that it has a short, caudally projected, and sharply tapered retroarticular process. In extant penguins, a thin sheet of bone connects the processus mandibulae medialis with the processus retroarticularis (Bertelli et al., 2006), however

(while the processus mandibulae medialis is eroded), this characteristic is not visible on NMNZ S.47302, where this sheet is consistently thick in contrast, with no clear separation. The coracoid in NMNZ S.47302 (Figures 3.5, 10.7-10) possesses a shallow fossa sternal to the indented and ventromedially crested impressio coracobrachialis on the ventral processus acrocoracoideus, which may be analogous to a deeper ovoid depression that is present on the ventral face of the processus acrocoracoideus in *Icadyptes salasi*, and a slight indentation is present on some extant penguin species (Ksepka et al., 2008). Otherwise, however, both liv-

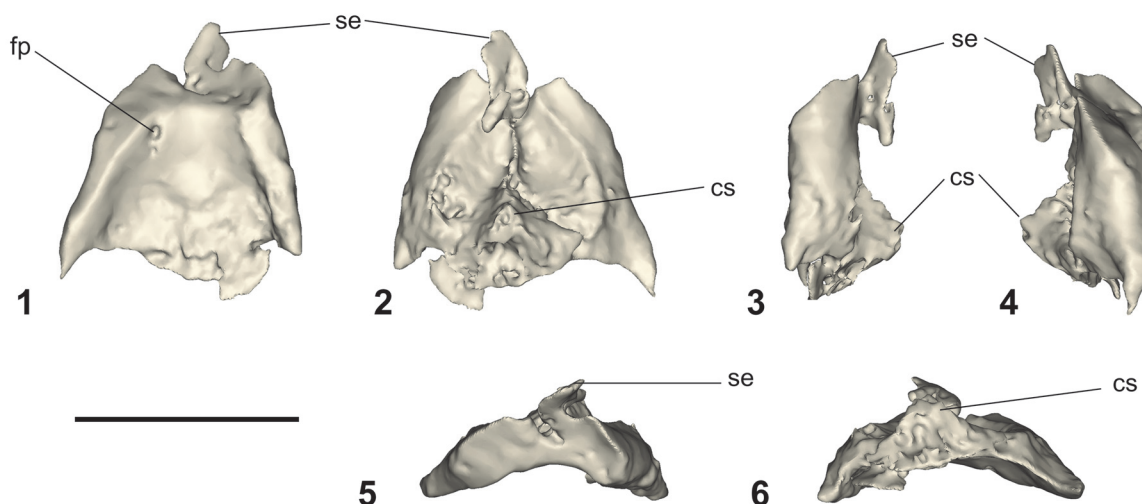


FIGURE 11. Partial sternum of NMNZ S.47302, of the larger Chatham Island form. Dorsal, **1**; ventral, **2**; right lateral, **3**; left lateral, **4**; cranial, **5**; caudal, **6**. **Abbreviations:** **cs**, carina sterni; **fp**, foramen pneumaticum; **se**, spina externa. Scale bar equals 20 mm.

ing and extinct penguins have a flat surface on the ventral side of the processus acrocoracoideus. The furcula in NMNZ S.47302 (Figure 10.11-16) is relatively “U”-shaped and rounded in dorsal and ventral aspects. A ventrally projecting hypocleidium (lamina intercalvicularis) at the symphysis of the furcula, is not preserved, similar to Paleocene Sphenisciformes *Muriwaimanu tuatahi* (see Slack et al., 2006: fig. 1h) and *Sequiwaimanu rosieae*, however, this may be a product of erosion. In contrast, in Eocene *Inkayacu paracasensis* the hypocleidium is blade-like (Clarke et al., 2010), and in a taxonomically unassigned Eocene sphenisciform IB/P/B-0889 from Seymour Island, Antarctica, it is poorly developed (Jadwiszczak, 2006a). A cavity, possibly representative of a foramen pneumaticum is observed on the dorsal surface of the partial sternum (Figure 11). The humerus in NMNZ S.47304 (Figure 12.1-2), length 116.3 mm, displays a strong sigmoid curvature, is distinctly robust with a shaft robustness index of 5.88 (which comparatively ranges from 7-6 in *S. rosieae*, *M. tuatahi* and *Kupoupou stilwelli* n. gen. et sp.), and has a ratio of minimum humerus width to maximum humerus length of 0.16, compared to 0.15 in *S. rosieae*, and 0.12 in *M. tuatahi* and *K. stilwelli* n. gen. et sp. The proximal humerus has an incurvate crista deltopectoralis on the cranial margin accentuating its sigmoid shape and a sharply protruding proximal extremity. The notch between the caput and the crista deltopectoralis is shallow and poorly demarcated. A processus supracondylaris dorsalis is absent on the distal cranial margin, and the condy-

lus ventralis is sub-spheroid condylus ventralis on the ventral face is confluent with the ventral trochlear ridge, giving the humerus a markedly hemispherical distal ventral profile. The angle between the main axis of the shaft and the tangent of the ulnar and radial condyles on the distal humerus is close to 30°, compared to a much larger angle (exceeding 40°) in *K. stilwelli* n. gen. et sp., *M. tuatahi*, and *S. rosieae*.

These bones minimally represent one larger taxon than *Kupoupou stilwelli* n. gen. et sp. It differs from *K. stilwelli* n. gen. et sp. in coracoid morphology including: a proportionally smaller diameter of cotyla scapularis; a collum acrocoracoidei (acrocoracoid neck, see Ballmann, 1969; Elzanowski et al., 2012) that is proportionally mediolaterally thinner and slender sternal to the processus acrocoracoideus; a more gracile shape of the corpus coracoideum sternal to the processus procoracoideus; a pronounced depression for the impressio coracobrachialis and a fossa sternal to it, and the lack of a rounded and omally directed apex of the crista acrocoracoidea; a better defined labrum glenoidale. The humerus of the larger Chatham Island form (NMNZ S.47304) differs from *K. stilwelli* n. gen. et sp. in its more robust form; the proximal apex of the caput humeri located nearer to the midline of the humerus shaft; and a crista deltopectoralis that is proximally incurvate and extends more proximally. The extremitas sternalis claviculae is narrower and more curved in dorsal and ventral views.



FIGURE 12. Humeri of sphenisciforms from the Chatham Island, compared to those of various early penguins. Right humerus NMNZ S.47304 of unnamed large form in **1**, dorsal, **2**, ventral. Humeri in ventral aspect, left *Sequiwaimanu rosieae*, CM 2016.6.1, **3**; left *Kupoupou stilwelli* n. gen. et sp. NMNZ S.47308, **4**; left *K. stilwelli* n. gen. et sp., NMNZ S.47339, **5**; right *Muriwaimanu tuatahi*, CM zfa 34, **6**; right *M. tuatahi*, 2008.145.4, **7**; right *M. tuatahi*, 2008.145.3, **8**; left *M. tuatahi*, 2008.145.4, **9**; right *M. tuatahi*, CM 2010.108.3, **10**; left *Kaiika maxwelli*, OU 22402, **11**. **Abbreviations:** **cb**, crista bicipitalis (bicipital crest); **cd**, condylus dorsalis (radial condyle); **ch**, caput humeri (humerus head); **cv**, condylus ventralis (ulnar condyle); **dc**, crista deltopectoralis (deltopectoral crest) and attachment site for musculus propatagialis (dorsally) and musculus pectoralis; **fpd**, fossa pneumotricipitalis dorsalis (secondary tricipital fossa); **fpv**, fossa pneumotricipitalis ventralis (tricipital fossa); **ic**, incisura capitis (capital incisura); **imp**, impressio musculus pectoralis, particularly for insertion of musculus pectoralis thoracica; **itr**, intermediate trochlear ridge; **mcc**, attachment scar of musculus coracobrachialis caudalis; **ms**, trochlea for tendon musculus scapulotricipitalis; **mcr**, insertion for musculus coracobrachialis cranialis; **mh**, trochlea for tendon musculus humerotricipitalis; **msc**, crista musculus supracoracoidei as an accessory insertion site for the tendon of the musculus supracoracoideus, extending distally from the tuberculum dorsale; **psd**, processus supracondylaris dorsalis (dorsal supracondylar tubercle); **td**, tuberculum dorsale (dorsal tubercle) and attachment site of musculus deltoideus minor and the principal part of the musculus supracoracoideus; **ts**, sulcus transversus (transverse sulcus); **tv**, tuberculum ventrale (ventral tubercle/internal tuberosity); **vtr**, ventral trochlear ridge. Scale bar equal to 20 mm. The image in **12.3** is reprinted from Mayr et al. (2018b, fig. 4C) by permission of the publisher (Taylor & Francis Ltd, <http://www.tandfonline.com>) and by permission of the Society of Vertebrate Paleontology (<http://www.vertpaleo.org>).

TABLE 2. Measurements of skeletal elements of specimens associated with the larger Chatham Island form.

Specimen/Element	Measurement distance	Measurement (mm)
NMNZ S.47302/Mandible	Maximum rostrocaudal length	45.65
	Maximum mediolateral width	13.23
	Maximum dorsoventral depth	24.94
NMNZ S.47302/Furcula	Maximum length of left clavicle from omal end to extremitas sternalis claviculae	46.99
	Distance between omal-most ends of each clavicle	59.85
	Maximum omal-caudal width	5.45
	Maximum dorsoventral depth	11.32
NMNZ S.47302/Cervical vertebra IV	Length of neural canal	19.28
	Lateral diameter of neural canal	6.09
	Maximum lateral width between cranial zygapophyses	25.73
	Maximum lateral width between caudal zygapophyses	26
	Total distance between tips of ventral process and neural spine	24.09
NMNZ S.47302/Coracoid	Diameter of scapular condyle	8.45
	Maximum omal-sternal length	62.02
	Maximum omal-sternal distance of sulcus musculi supracoracoidei	29.25
NMNZ S.47302/Sternum	Maximum length	24.48
	Maximum width	22.23
	Maximum depth of carina sterni	6.09
NMNZ S.47304/Humerus	Maximum proximodistal length	116.3
	Mid-shaft craniocaudal width	20.0
	Maximum craniocaudal width of caput humeri	27.0

The bones of this larger Chatham Island form are differentiated from Paleocene taxa such as *Muriwaimanu tuatahi* and *Kumimanu biceae* by their larger and smaller size, respectively, and the mandibular differences noted above. NMNZ S.47302 is further differentiated from *M. tuatahi* by: a dorsally and ventrally more curved and narrow extremitas sternalis claviculae of the furcula; and a more robust humerus in NMNZ S.47304, with an incurvate cranial margin of the proximal crista deltopectoralis.

While of similar size to *Sequiwaimanu rosieae*, the larger Chatham Island form differs by the following features: its unique mandibular morphology (as above), in that the facies articularis humeralis is distinctly flattened and wider omal-sternally on the coracoid; the processus acrocoracoideus on the omal end of the coracoid is rounded without a hook-like appearance corresponding to the insertion for ligamenti acrocoraco-procoracoideale (however, these morphologies may have been influenced by abrasion to the dorsomedial acrocoracoid extremity however, rather than a real mor-

phology); the ligamenti acrocoraco-acromiale and the tuberculum for the insertion of plica synovialis coracoidea of the tuberculum brachialis are not distinct and shallowly linked dorsally, in contrast to being prominent and separated by a distinct groove in *S. rosieae*; the extremitas sternalis claviculae of the furcula is wider and shallower and does not possess ventral projections (however, they may have been lost due to erosion); the humerus of NMNZ S.47304 differs from *S. rosieae* in its more sturdy build and associated lack of elongation; a sharp proximal projection of the proximal crista deltopectoralis; a distally joined condylus ventralis and ventral trochlear ridge.

RESULTS

Primary Phylogenetic Analyses

The heuristic parsimony analysis of the Chatham matrix resulted in 16,300 MPTs, with a treelength (L) score of 5,278 steps, consistency index (CI) = 0.5218, retention index (RI) = 0.7151, and homoplasy index (HI) = 0.4793. Following

pruning and subsequent condensing of duplicate trees, 6,590 MPTs were retained, $L = 5,234$, $CI = 0.5250$, $RI = 0.7018$, $HI = 0.4750$. Procellariiformes and Sphenisciformes were recovered as monophyletic clades in 100% of MPTs, with high bootstrap support (94% and 99%, respectively). The better resolved majority-rule (50%) consensus tree is depicted here (Figure 13), rather than the strict consensus tree (see Figure A8), to show relationships between taxa that are recovered in a large percentage of MPTs, but which are collapsed to form polytomies in the strict consensus program.

Preliminary analysis where *Kupoupou stilwelli* n. gen. et sp., NMNZ S.47302 and NMNZ S.47304 were treated as separate taxa, resulted in their basal positioning in the tree (see Appendix 1; Figure A6). This further justified merging NMNZ S.47302 and NMNZ S.47304 into one parataxon, labelled here as “larger Chatham Island form”.

The exact relationships of the basal-most sphenisciforms will be focused on here. In the strict consensus tree (Figure A8) *Waimanu manningi* and *Muriwaimanu tuatahi* have a sister taxon relationship in a clade separate to one, which includes all other Sphenisciformes. *Kupoupou stilwelli* n. gen. et sp. occupies a position one node crownwards of Sphenisciformes base, in an unresolved polytomy alongside Waipara Greensand giant CM 2016.158.1, *Sequiwaimanu rosieae*, *Crossvallia unienwillia*, ?*Crossvallia waiparensis*, the larger Chatham Island form and *Kaiika maxwelli*. All MPTs recovered *Kumimanu biceae* one node crownwards of this polytomy. This node was found one node more basal to the position of Eocene *Delphinornis larseni*, which is the sister taxon to a clade that consists of all geologically younger sphenisciforms. The majority-rule (50%) consensus tree provided greater resolution to the unresolved polytomy of Paleocene taxa (Figure 13), where the Waipara Greensand giant CM 2016.158.1 exists most basally one node crownwards of the basal-most node of Sphenisciformes. 70% of MPTs resolved *K. stilwelli* n. gen. et sp., *S. rosieae*, ?*C. waiparensis* and *C. unienwillia* one node crownwards of this position, *K. maxwelli* one node crownwards of this unresolved polytomy in 51% of MPTs, and the larger Chatham Island form another node crownwards of *K. maxwelli* in 93% of MPTs. All interrelationships between Paleocene taxa received low bootstrap support values, the best supported of which being the sister pairing of *Waimanu + Muriwaimanu*, which was recovered in 51% of bootstrap replicates.

The phylogenetic position of *Kupoupou stilwelli* n. gen. et sp. is distinguished relative to other taxa by supporting character state changes including the presence of an asymmetric caput humeri with a caudal apex that is slightly prominent, compared to the more primitive semi-circular shape (character 158); a nutrient foramen on the caudal face of the humerus shaft (character 180); a tab-like and squared olecranon caudal margin of the ulna, compared to the rounded primitive state (character 199); the presence of a proximally directed process on phalanx III-1 (character 213); a slightly dorsodistally deflected medial cotyla of the tarsometatarsus (character 237); the impressio ligamenti collaterale lateralis forming a well-defined notch on the tarsometatarsus, rather than inconspicuous or depressed (character 246); a medial infracotylar depression proximal to the dorsal opening for the foramen vasculare proximale mediale (character 254); a more pronounced sulcus longitudinalis dorsalis medialis on the dorsal tarsometatarsus face (character 256); and medial and lateral carinae on the plantar-most articulation surface of trochlea metatarsi III that are parallel to one another, as opposed to tapered (character 266).

The larger Chatham Island form (NMNZ S.47302 and NMNZ S.47304) is defined phylogenetically by apomorphies such as: a moderately long and narrow processus retroarticularis of the mandible, compared the broad primitive state (character 118); and the humerus shaft is markedly more robust compared to the elongate shaft of more basal forms (character 183).

Bayesian Analyses

The four independent Bayesian analyses on the Chatham matrix achieved stationarity and convergence: the average Potential Scale Reduction Factor (PSRF) was 1.000 for all runs; for runs 1 through to 4, respectively, the log likelihood statistics were -33279.68, -33280.27, -33280.07 and -33278.21; Effective Sample Size (ESS) for runs 1 to 4 after Burn-in of 20% were 1163, 1500, 1546, and 1586, respectively. After 50,000,000 generations each the average Standard Deviation of Split Frequencies (SDSF) across runs was 0.029187, and the convergence diagnostic approached 0.0 as runs converged.

In the majority-rule consensus tree produced (Figure 14), both Sphenisciformes and Procellariiformes are recovered as well-supported monophyletic clades with a posterior probability of 1.0. As with parsimony-based analyses, only the topology

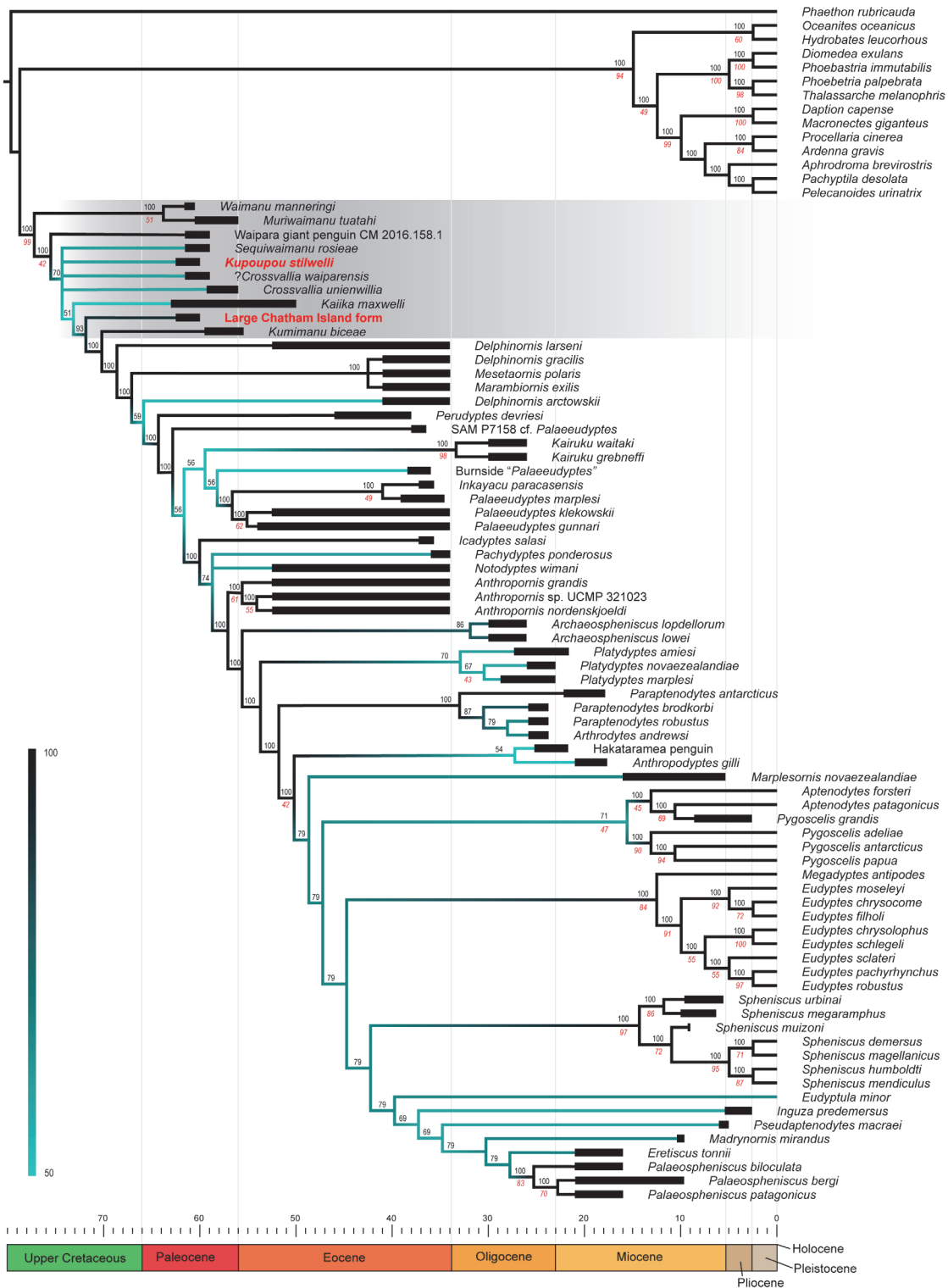


FIGURE 13. Parsimony majority-rule (50%) consensus tree of 16,300 MPTs (length = 5,234). Percentage of MPTs recovering each node is indicated at each internode in the consensus tree, and bootstrap support values (over 40% only) are numbered below them italicised in red. Legend and branch colouration correspond to percentage of MPTs that recovered each node. Darkened area indicates the topological region occupied by Paleocene taxa. Ages associated with taxa are shown in thickened black lines, the references of which are given in Appendix 1. Nodes illustrated are not calibrated in association with age.

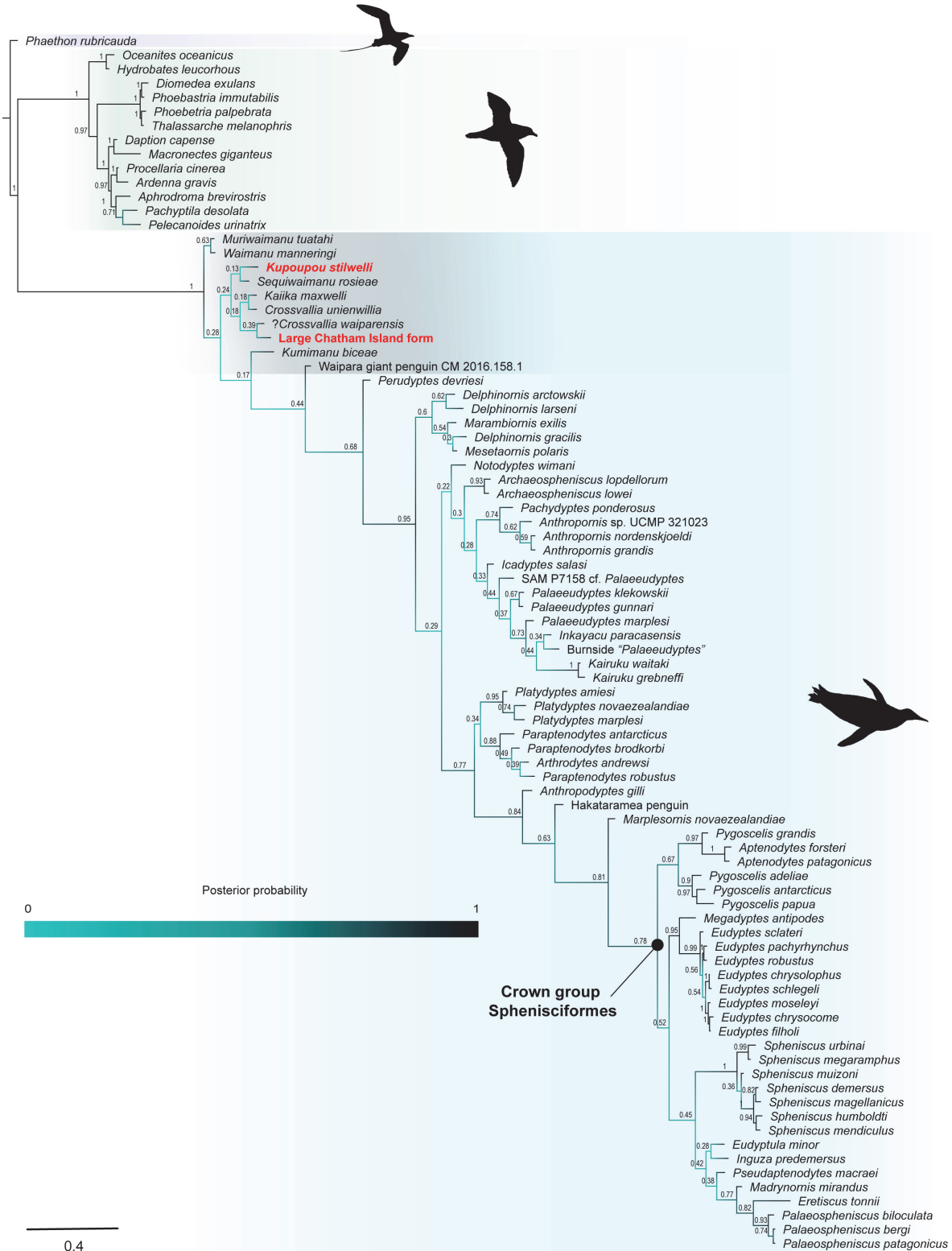


FIGURE 14. Phylogenetic tree based on Bayesian inference (majority-rule consensus, undated). Colour of branches indicate the gradient of posterior probability values (see legend), the numbers of which are specified next to their respective branches. Darkened area at base of Sphenisciformes indicates the topological region occupied by Paleocene taxa. Scale bar corresponds to the given degree of change across branch lengths.

of Paleocene penguins and close counterparts is detailed here. The base of the Sphenisciformes clade is characterised by a poor-moderately supported clade consisting of both *Waimanu manneringi* and *Muriwaimanu tuatahi* (posterior probability of 0.63), and a poorly supported clade, which includes all other Sphenisciformes (posterior probability of 0.28). At the most basal node in the latter, one node crownwards of the Sphenisciformes base, the posterior distribution supports a monophyletic clade including the majority of all Paleocene forms with a posterior probability of 0.24. This is with the exception of *Kumimanu biceae*, which exists most basally in a sister-clade that includes all other penguins (posterior probability 0.17), and the Waipara Greensand giant penguin, which is positioned one node crownwards of *K. biceae* (0.44). The exact interrelationships of taxa within the clade that includes the majority of Paleocene penguins similarly receive very low posterior probabilities, including a sister taxon relationship between *Kupoupou stilwelli* n. gen. et sp. and *Sequiwaimanu rosieae* (0.13), which itself is sister to a clade (0.18) consisting of the larger Chatham Island form and *?Crossvallia waiparensis* as sister taxa in a nested clade (0.39), and similarly for *Kaiika maxwelli* and *Crossvallia unienwillia* (0.18). The middle Eocene *Perudyptes devriesi* exists one node crownwards of the Paleocene Waipara Greensand giant penguin (poor-moderately supported, posterior probability 0.68), and is the sister taxon to a highly supported clade which includes all other Sphenisciformes (0.95 posterior probability).

DISCUSSION

Phylogenetic Inferences and Implications

Kupoupou stilwelli n. gen. et sp. and the specimens belonging to a larger Chatham Island form are among the oldest described representatives of the penguin clade, from deposits that are dated to late early to middle Paleocene (62.5-60 Ma). Fittingly, they are recovered in basal positions across both phylogenetic analyses (Figures 13, 14), alongside similarly-aged New Zealand Paleocene counterparts *Waimanu manneringi*, *Muriwaimanu tuatahi*, *Sequiwaimanu rosieae*, *Kumimanu biceae*, the unnamed Waipara Greensand giant penguin (Slack et al., 2006; Mayr et al., 2017a, 2017b, 2018b), *?Crossvallia waiparensis* (see Mayr et al., 2019), *Crossvallia unienwillia* from Seymour Island (Tambussi et al., 2005; Jadwiszczak et al., 2013), and *Kaiika maxwelli* reportedly from the early Eocene (Fordyce and Thomas, 2011). Importantly,

however, support values for placement of fossil taxa, including Paleocene forms, are notably low. This is perhaps expected given many fossil taxa have much missing data, including a complete lack of molecular data (Gavryushkina et al., 2017); e.g., *Kaiika* and the unnamed Waipara Greensand giant penguin are represented by a nearly complete humerus and a partial tarsometatarsus with pedal phalanges, respectively. Effectively, relatively incomplete fossils can impede on topologic resolution, including potential obfuscation of relationships among relatively more complete taxa (Gauthier et al., 1988; Huelsenbeck, 1991; Wilkinson, 1995; Anderson, 2001; Wiens, 2003), leading to reduced branch support across the tree (Cobbett et al., 2007). Conversely, a variety of research using both parsimony and Bayesian methodology supports that, irrespective of the amount of missing data, including highly incomplete taxa can be beneficial for topological resolution and accuracy where an adequate sample of phylogenetically informative characters are scored (e.g., Wiens, 2003, 2005, 2006; Wiens et al., 2005; Wiens and Moen, 2008; Wiens and Morrill, 2011; Wiens and Tiu, 2012). Indeed, preliminary heuristic parsimony analyses in this study that omitted a greater number of relatively incomplete taxa from the matrix resulted in more poorly resolved consensus trees than when they were included, suggesting these fossils possessed unique combinations of character states that increased phylogenetic signal (see also Wilkinson, 1995; Wiens, 2003, 2005). The subsequent pruning of unstable taxa from most parsimonious trees provided greater topological resolution in the consensus tree as well as better bootstrap support (see Goloboff and Szumik, 2015).

Nonetheless, although the consensus trees depicted here may show particular topologies, specific placement of fossil taxa in these trees with low support values should be treated tentatively, while those recovered in a supermajority of trees may be hypotheses more confidently interpreted as approaching reality. This is especially relevant for the majority-rule consensus tree (Figure 13) under parsimony criterion, where even though a topological relationship may be recovered in more than 50% of MPTs, in the case of Paleocene taxa, no justification exists for the preference of one topology over an alternate equally parsimonious topology (see equally parsimonious trees, Figure A9).

The implication is that using both parsimony and Bayesian inference methods a clade including both *Waimanu* and *Muriwaimanu* branching from the most basal Sphenisciformes node, and sister to

all other ingroup taxa, may be treated with a degree of confidence. However, the specific arrangement of nodes and branches pertaining to other Paleocene forms (and the majority of other fossil penguins) should be viewed more tentatively. This topological uncertainty is also illustrated by the posterior distribution favouring the recovery of most Paleocene taxa within a monophyletic clade sister to a clade leading to the crown group in the Bayesian analysis (albeit with very low support, Figure 14), compared to their various taxonomic groupings or stepwise relationships commonly found under parsimony (Figures 13, A9; unresolved when comparing across all MPTs, Figure A8). Their phylogenetic placement does, however, support the interpretation that *Kupoupou stilwelli* n. gen. et sp., the larger Chatham Island form and other Paleocene taxa possess more derived morphologies compared to *W. manneringi* and *M. tuatahi* (see previous; Mayr et al., 2017a, 2017b, 2018b). The fossil humerus of *Kaiika maxwelli* from South Canterbury, New Zealand, commonly reported as early Eocene in age was found nested among Paleocene taxa in all analyses, supporting recognition that it may have been derived from older sediments (Fordyce and Thomas, 2011). Except for *K. maxwelli*, MPTs consistently recovered *Delphinornis larseni* as the most basal of Eocene taxa, with low bootstrap support (Figures 13, A8). While *Delphinornis* is still recovered in a relatively basal position among Eocene penguins in the Bayesian majority-rule consensus tree, the poor-moderately supported position of middle Eocene *Perudyptes devriesi* one node crownwards of the Paleocene Waipara Greensand giant penguin (Figure 14), implies a contrasting evolutionary scenario to that depicted in most parsimonious trees where it is one node more basal to a node that supports a clade including *Delphinornis*, *Marambiornis exilis* and *Mesetaornis polaris* Myrcha, Jadwyszczak, Tambussi, Noriega, Gaździcki, Tatur, and Valle, 2002, and another clade that includes all other geologically younger sphenisciforms. The consistency of close relationships between Paleocene taxa, and their absence from Eocene clades across both Bayesian and parsimony trees, however, does support their phylogenetic restriction to the base of Sphenisciformes.

While phylogenetic relationships of more crownward sphenisciforms are not the focus of this research, the topology of other Eocene penguins are commented on here due to their closer relationship to the Paleocene taxa, and relevance in documenting an early penguin evolutionary stage,

before the onset of continental glaciation in Antarctica (Myrcha et al., 2002; Gaździcki, 2004; Jadwyszczak, 2006a). The South American Eocene penguin *Inkayacu paracasensis* of Peru is consistently found nested within a clade consisting of species of *Palaeudyptes* in both parsimony and Bayesian analyses, although low support values underpin this morphological relationship. Similarly, close affinities between these taxa were also suggested by Mayr (2017: 170), and comparable topologies have also been recovered in some other phylogenetic studies (e.g., Clarke et al., 2010; Chávez Hoffmeister, 2014). In Bayesian analysis *Icadyptes salasi* of Peru occupies a poorly supported position as the basal-most taxon of a clade including species of *Palaeudyptes*, *Inkayacu*, and Oligocene *Kairuku*, in a clade separate to that, which includes crown group sphenisciforms (contra Gavryushkina et al., 2017). In contrast with the results of this Bayesian analysis, *Icadyptes salasi* is recovered with a closer association to both *Notodyptes wimani* Marples, 1953, and *Pachydyptes ponderosus* in MPTs, and falls within the range of topological variation shown in other studies (e.g., Clarke et al., 2010; Ksepka et al., 2012; Chávez Hoffmeister, 2014). The New Zealand giant *Pachydyptes ponderosus* is recovered with moderate support as the sister taxon to *Anthropornis* in Bayesian analysis, in a clade that is sister to one that includes species of *Icadyptes*, *Palaeudyptes*, *Inkayacu* and *Kairuku*. The phylogenetic position of *Pachydyptes ponderosus* is less resolved in parsimony analysis however, and receives low bootstrap support, in an unresolved polytomy crownwards of *Icadyptes salasi*, with *Notodyptes wimani*, one node basal to a node that branches to the *Anthropornis* clade and another branch leading to a clade that includes all geologically younger penguins, with the exception of *Kairuku*.

Eocene taxa from the La Meseta Formation in Seymour Island of Antarctica are equally important in the evolution of stem penguins, yet are especially problematic having been predominately named based on individual bones, rather than partial/complete skeletons (Myrcha et al., 2002), creating taxonomic and phylogenetic uncertainty (Ksepka and Clarke, 2010). While other elements have been subsequently referred to these taxa based largely on morphology and sized groupings (Wiman, 1905b; Simpson, 1971; Jadwyszczak, 2006a), their assignment in most cases remains uncertain (Jadwyszczak, 2006a, 2006b; Ksepka and Clarke, 2010). Here we opted to include referred elements in analyses in an attempt to

resolve overall topologies between these otherwise relatively incomplete fossil taxa (however, see Appendix 1; Figure A7). It is noted that the Bayesian analysis of this study recovered species of *Marambiornis* and *Mesetaornis* nested within a clade including all *Delphinornis* species, which is sister to all other Eocene sphenisciforms (except *Perudyptes devriesi* and *Kaiika maxwelli*), which contrasts with the sampled ancestor Bayesian analysis of Gavryushkina et al. (2017), the parsimony-based analysis of this study, and that of others, where these genera occupy one node more crownwards of a monophyletic *Delphinornis* clade (e.g., Ksepka and Clarke, 2010; Ksepka et al., 2012; Chávez Hoffmeister et al., 2014). In all heuristic searches and Bayesian analyses *Notodyptes wimani* is also recovered in close association with the *Anthropornis* clade, similar to as reported by Chávez Hoffmeister (2014), rather than nested within *Delphinornis* (contra Ksepka and Clarke, 2010; Ksepka et al., 2012). Phylogenetic investigation by Jadwiszczak (2013) also supported the exclusion of this taxon from *Delphinornis*. Oligocene *Archaeospheniscus* of New Zealand (however, see Jadwiszczak, 2006b; Tambussi et al., 2006, regarding the possibility of a late Eocene Antarctic representative) is crownwards of all aforementioned Eocene taxa in parsimony analysis, as recovered in other phylogenetic studies (Ksepka and Clarke, 2010; Ksepka et al., 2012; Ksepka and Thomas, 2012; Chávez Hoffmeister et al., 2014; Gavryushkina et al., 2017), yet is contrastingly recovered within a predominately Eocene clade in Bayesian analysis. As with the Paleocene penguins, however, even with referred elements and known partial skeletons included (e.g., Acosta Hospitaleche and Reguero, 2010; Jadwiszczak, 2012; Acosta Hospitaleche, 2016; Jadwiszczak and Mörs, 2019), many of these Eocene taxa are comprised of relatively incomplete skeletons compared to extant taxa, resulting in low relational support values, and tentative phylogenetic positions.

Underlying the phylogenies presented, the content of the morphological character matrix is paramount in the interpretation of the evolutionary relationships between the various fossil sphenisciforms (see Poe and Wiens, 2000; Simões et al., 2017). Given the numerous fossil penguin discoveries subsequent to the creation of the base matrix, and a greater understanding of penguin evolution, as well as improvements in phylogenetic methods, revision of the penguin data matrix is necessary. While we compiled characters and taxa from numerous studies (see Materials and Methods),

and modified some character descriptions and codings, a more thorough reassembly of the phylogenetic data matrix was beyond the scope of this study. Of note, Bayesian inference methods are advantageous in allowing the combination of prior known information such as age data to be implemented when estimating phylogenies, and have been shown to outperform parsimony-based analyses using discrete morphological data (Wright and Hillis, 2014; O'Reilly et al., 2018). Autapomorphies are required to be adequately sampled to most accurately estimate evolutionary changes along branches and divergence dates in a Bayesian framework (Lee and Palci, 2015), and are largely absent in the current matrix due to it being developed for parsimony-based research. Many additional apomorphic characters could also be defined and scored from the taxonomic descriptions and comparisons of fossil taxa, and differential observations throughout the literature, to optimise the recovery of information from fossils and accurately describe morphological variation among all taxa involved. Further possible improvements are outlined by Gavryushkina et al. (2017).

While the relatively poor representation of most fossil taxa in the datamatrix compared to extant counterparts effectively precludes a robust phylogenetic hypothesis for stem relationships, this result is considered more beneficial than not having one at all (see Wiens and Reeder, 1995; Wiens, 2003). Until further fossil discoveries provide additional material, or the character matrix is appropriately reassembled and analysed, a greater understanding of basal topologies and more exact relationships between Paleocene taxa as *Kupoupou stilwelli* n. gen. et sp., *Sequiwaimanu rosieae*, the larger Chatham Island form, *Crossvallia unienwillia*, ?*Crossvallia waiparensis*, the giant Waipara Greensand penguin, *Kumimanu biceae*, as well as *Kaiika maxwelli* and definitive Eocene forms will remain obscured.

Palaeobiological Interpretations for Paleocene Chatham Island Penguins

The close association of *Kupoupou stilwelli* n. gen. et sp. and the larger Chatham Island penguin with other Paleocene forms in phylogenetic simulations reflects the numerous anatomical similarities drawn between these similarly aged species (see Descriptions and Comparisons). *Kupoupou stilwelli* n. gen et sp. is further phylogenetically distinguished from other Paleocene taxa by morphological characters of the humerus, ulna, proximal manual phalanx of digit three, and the tarsometatarsals.

tarsus, while the larger Chatham form is distinguished with regard to mandibular (NMNZ S.47302) and humeral (NMNZ S.47304) characters (see Results). With the material available, clear plesiomorphic features are observed in these early penguins, which do not persist in geologically younger taxa, and which we and others (Livezey, 1989; Ksepka and Clarke, 2010; Ksepka and Ando, 2011; Mayr et al., 2018b) consider ancestral in Sphenisciformes. These include: the lack of a coracoidal fenestra on the medial margin of the coracoid (character 149), a relatively slender (character 183), and less dorsoventrally flattened humerus (Livezey, 1989; Ksepka and Clarke, 2010) that is longer than the coracoid (character 146), dorsoventral flattening of forelimb elements (character 155)—but not as broad and as heavily flattened as in more crownward spheniscids, and the presence of a processus cotylaris dorsalis on the proximal ulna (character 201; Mayr et al., 2018b).

Modern penguins are well known for the assortment of specialised adaptations they possess in association with a subaquatic lifestyle (see Kaiser, 2007; Ksepka and Ando, 2011, and references therein). However, this morphological transition towards the modern form has been a gradual one (Bannasch, 1994), where the aforementioned differences observed in basal counterparts reflect an earlier stage in this evolution. Given the various structures preserved it is possible to make broad functional inferences with regards to the Paleocene Chatham Island penguins, and their adaptive significance.

Both *Kupoupou stilwelli* n. gen. et sp. and the larger Chatham Island form possess a caudally directed and blade-like processus spinosus on cervical vertebrae, that is directly linked to mechanical ability of the cervical system in bringing the head back to the body (Guinard et al., 2010). Mechanical folding of the cervical series in the neck is observed in many birds, and in extant penguins is especially important in the formation of a more hydrodynamic shape for pelagic aqueous flight, as well as maintaining erect posture on land (Gaina et al., 1998; Guinard and Marchand, 2010; Guinard et al., 2010). This shared characteristic may infer that neck length reduction, associated reduction of drag, and acquisition of hydrodynamic form may have been present in these Chatham Island Paleocene penguins.

Modern penguins are known for having a very specialised flight apparatus (Bannasch, 1994; Ksepka and Ando, 2011). The coracoid is a key

element in underwater penguin locomotion, where the acrocoracoid process, furcula, and scapula create the canalis triosseum, which acts as a pulley for the musculus supracoracoideus to raise the wing in the upstroke (Baumel et al., 1993; Bannasch, 1994). The coracoids of *Kupoupou stilwelli* n. gen. et sp. and the larger Chatham Island form display a medioventrally directed processus acrocoracoideus that is more elongate compared to aerially flighted birds, but not as long as some phylogenetically more derived penguins (e.g., *Palaeudyptes klekowskii*, *Spheniscus demersus*) (Bannasch, 1994; Acosta Hospitaleche and Di Carlo, 2010). The musculus supracoracoideus is relatively enlarged in extant penguins (Clark and Bemis, 1979; Kovacs and Meyers, 2000), allowing them to raise their wing and produce greater forward thrust against the resistance of water (Clark and Bemis, 1979; Bannasch, 1994; Kovacs and Meyers, 2000), 800 times the density of air (Penny-cuick, 1987). Similarly, greater acrocoracoid process elongation in *K. stilwelli* n. gen. et sp. and the larger Chatham Island form compared to volant counterparts may relate to an increased space for this muscle and confer aquatic locomotory advantages.

A shorter coracoid relative to the length of the humerus is a plesiomorphic character *Kupoupou stilwelli* n. gen. et sp. shares with other Paleocene penguins *Muriwaimanu tuatahi* and *Sequiwaimanu rosieae* and aerially flighted birds. By contrast, the opposite is true for the hyper-elongate coracoid of modern penguins, which acts to displace the canalis triosseum relative to the sternum, increasing space for the pectoralis muscles, and leverage for the supracoracoideus muscle for the upbeat of the wing (Jenkins, 1974; Bannasch, 1994). The length of the coracoids associated with *K. stilwelli* n. gen. et sp., *M. tuatahi* and *S. rosieae* implies an intermediate adaptation towards diving proficiency, compared to the more specialised hyper-elongated coracoids of extant penguins. While the full length of the coracoid associated with the larger Chatham Island form (NMNZ S.47302) is not preserved, approximate length extrapolation and comparison to the humerus of the larger form reveals that the coracoid may have been equal in size or longer than the humerus of NMNZ S.47304. Should they represent the same taxon, this would be the earliest occurrence of more elongate coracoid proportions within Sphenisciformes and may have indicated increased diving efficiency.

The pronounced dorsoventral flattening and shortening of the forewing is another notable

example of the morphological transition to aquatic life in penguins (Shufeldt, 1901; Ksepka and Ando, 2011), related to more efficient aquaflight with increasing body mass (Bannasch, 1994; Habib, 2010). Indeed, the reduced marrow cavity observed in radii of *Kupoupou stilwelli* n. gen. et sp., provides evidence of a more robust and dense bone structure than volant birds, approaching that of modern forms (Figure A3). This adaptation acts to counteract buoyancy and allows greater ability for diving and underwater foraging (Meister, 1962; Watanuki and Burger, 1999). Basal penguins had more elongate and less flattened humeri than extant forms (Livezey, 1989; Ksepka and Clarke, 2010) and would have been less resistant to torsion imposed by the stresses of swimming in the dense water medium (Kaiser, 2007; Habib, 2010). In this way, the Paleocene Chatham Island penguins bear closer resemblance to the other earliest penguins, however, the humerus of the larger Chatham Island form (NMNZ S.47302) is markedly more robust than *K. stilwelli* n. gen. et sp., which may be reflected in aquatic flight potential. Compared to *Muriwaimanu tuatahi*, it is observed that *K. stilwelli* n. gen. et sp. had proportionally shorter, wider, and more flattened ulnae and radii converging on the morphologies of Eocene penguins such as species of *Anthropornis*. These structural modifications likely increased bone mass and strength, potentially enhanced flight stroke rate, and submarine propulsion ability during the up and downstroke, and lowered energetic costs (Johansson and Wetterholm Aldrin, 2002; Habib, 2010), yet are still far removed from the broader, more specialised, forewing elements of modern penguins.

In addition, the humeral condylus ventralis in *Kupoupou stilwelli* n. gen. et sp. and the larger Chatham Island form are rounded with a shelf-like articular surface adjacent to it, reminiscent of other basal sphenisciforms (Ksepka, 2007). This joint morphology would have increased relative rigidity of the wing in the downstroke, but would have been less effective at counteracting the ventrodistal flexion against water during the upstroke (Ksepka, 2007). The humerus-ulna joint of modern penguins is a comparatively flat surface, contributing to a relatively narrow range of wing motion, and allowing it to act as an efficient hydrofoil (Shufeldt, 1901; Clark and Bemis, 1979; Raikow et al., 1988; Bannasch, 1994; Ando, 2007). Effectively, Paleocene penguins such as *K. stilwelli* n. gen. et sp. and the larger Chatham Island form may have had a greater wing flexibility and movement range at

the elbow than in modern counterparts (Ando, 2007; Ksepka, 2007).

In a rare circumstance amongst fossil penguins (Ksepka and Ando, 2011), a manus phalanx II-1 and manus phalanx III-1 were recovered with the *Kupoupou stilwelli* n. gen. et sp. material. The manus phalanx III-1 has a proximally directed tubercle similar to that in extant penguins, in contrast to its absence from all known fossil taxa (Ksepka et al., 2008). While incomplete, preserved distal tapering of manus phalanx III-1 indicates that it may not have exceeded the length of manus phalanx II-1 (Figure 6), which would be indicative of a more tapered wing tip like *I. salasi* and volant birds, than in modern penguins (Ksepka et al., 2008). Such morphology is correlated with an increased wing loading and a higher aspect ratio compared to extant penguins, reflective of primitive proportions, though contribution to aquatic flight efficiency was likely almost negligible (Ksepka, 2007; Ksepka and Ando, 2011).

Another distinctive morphological change in penguins through their evolution is the progressive shortening and widening of the tarsometatarsus. Among penguins, *Waimanu manneringi* and *Muriwaimanu tuatahi* have the most primitive and elongate proportions in this element (see Slack et al., 2006). The complete tarsometatarsus of *Kupoupou stilwelli* n. gen. et sp. however, as well as that of the less complete and less well-preserved unnamed giant penguin and *?Crossvallia waiparensis* from the Waipara Greensand (Mayr et al., 2017a, 2019), present the earliest occurrence of a relatively shortened, stout, and robust morphology. In particular, the specific morphology of the tarsometatarsus in *K. stilwelli* n. gen. et sp. seems to approach that of Eocene penguins of Seymour Island, especially those of similar inferred body size such as species of *Delphinornis*, *Mesetaornis*, and *Marambiornis* (Myrcha et al., 2002), in a transition to the characteristic modern penguin hind-limb.

While ancient penguins (including some of the largest, e.g., species of *Anthropornis*) are recognised to have had relatively more elongate tarsometatarsi compared to recent forms (Wiman, 1905b; Simpson, 1946), Simpson (1946) notes that a more robust structure is also mechanically required to support a greater mass and would imply that shortened tarsometatarsi of penguins may be an adaptation related to supporting their increased weight relative to volant ancestors. Contrarily, the elongate tarsometatarsi that some of the heaviest birds (e.g., ratites) bear suggest that shortened tarsometatarsi in penguins may have an

additional functional significance. Modern penguins use their cornified feet and tarsometatarsi for much more than walking or resting, including propelling themselves in prone positions on land or ice, gripping and holding onto icy surfaces, and are also very important in underwater flight, assisting with steering the bird as it swims (Simpson, 1946; Stonehouse, 1967; Bedford, 1970; Hui, 1985; Parfitt and Vincent, 2005). It has also been observed that the presence, shape, and position of feet in extant penguins during underwater flight reduced drag and completed a more hydrodynamic shape (Parfitt and Vincent, 2005), and may potentially facilitate heat retention when feet are placed in line with the body (Willener et al., 2016). Effectively, the evolution of the distinctive shortened tarsometatarsi in some of the earliest penguins may have evolved as an adaptation that augmented swimming capabilities (Willener et al., 2016). While this likely led to greater reproductive success (Willener et al., 2016), a consequence of such shortened-hind limbs may have meant *Kupoupou stilwelli* n. gen. et sp., *?Crossvallia waiparensis* and the Waipara Greensand giant were prone to high metabolic costs while walking, but also large lateral displacement of their feet, characteristic of an energetically conservative waddling gait observed in modern forms (Pinshow et al., 1977; Gauthier-Clerc et al., 2000), compared to the relatively less phylogenetically derived *Waimanu manneringi* and *Muriwaimanu tuatahi*.

Further distinguishing the tarsometatarsus of *Waimanu manneringi* and *Muriwaimanu tuatahi* from *Kupoupou stilwelli* n. gen. et sp. is the comparatively reduced plantar deflection of trochlea metatarsi II observed in *K. stilwelli* n. gen. et sp. and the giant Waipara Greensand penguin. Definitive and reliable comparisons relating to this feature in *?Crossvallia waiparensis* are limited, however, due to damage to the plantar surface of trochlea metatarsi II. The plantar deflection and medial ridge of trochlea metatarsal II is typical of foot-propelled diving birds (Olson, 1992; Ando, 2007), facilitating the movement of the inner toe behind the other toes in the recovery stroke while swimming at the surface of and within the water (Galton and Martin, 2002; Ando, 2007). This morphology is exhibited to a small degree in *W. manneringi* and *M. tuatahi* relative to birds that use foot-propelled diving as a primary form of locomotion, allowing the postulation that these early penguins may have utilised foot-propelled propulsion in underwater locomotion, in conjunction with their comparatively less specialised flippers (Ando,

2007; Mayr et al., 2017a). The contrastingly shortened tarsometatarsus, with more dorsally aligned toes may support that early penguins such as *K. stilwelli* n. gen. et sp. and the giant Waipara Greensand taxon used their feet in a more similar way to modern penguins than *W. manneringi* and *M. tuatahi*, perhaps in underwater steering. Indeed, differing locomotory function and behaviour may have promoted ecological separation and niche partitioning in these Paleocene penguins, considering their likely co-existence (Mayr et al., 2017a).

Early Penguin Evolution and Diversification

The abandonment of aerial flight in penguin evolution can be viewed as the elimination of volancy-related constraints (Ksepka, 2007), to allow specialised adaptations for underwater propulsion efficiency (Raikow et al., 1988; Elliott et al., 2013). In turn, numerous morphological adaptations (e.g., see Livezey, 1989; Kaiser, 2007; Ksepka and Ando, 2011) have allowed penguins to better exploit the marine realm, many of which were in place by the middle Paleocene (see above).

Unrestricted from aerial body mass constraints, penguins attained larger sizes early in their evolution (e.g., Mayr et al., 2017a, 2017b, 2019). In addition to being associated with greater muscle mass required for more powerful aquatic wing-propulsion (Ksepka and Ando, 2011), larger size is hypothesised to be related to increased mating success (Kingsolver and Pfennig, 2004; Mayr et al., 2017b), capacity to dive longer and to a wider range of depths (e.g., Walker and Boersma, 2003; Elliott et al., 2013 and references therein), to facilitate niche separation (Ksepka et al., 2006), and confers advantages in catching more prey (see Adams and Brown, 1989; Walker and Boersma, 2003). This evolution does not, however, seem to be correlated with migration into higher latitudes or cooler temperatures (Simpson, 1971; Clarke et al., 2007). While early penguins like *Muriwaimanu tuatahi* were likely capable wing-propelled divers (Ksepka, 2007), their forewing structure suggest that they and other Paleocene forms were neither as powerful nor efficient as their modern relatives (Ando, 2007). Although *Kupoupou stilwelli* n. gen. et sp. was not a giant penguin, a potential higher body mass, and a more hydrodynamic morphology may have given it a competitive advantage in diving capabilities, and may have permitted foraging at greater depths, or allowed a wider exploitation of marine environments and ecological niches compared to coexist-

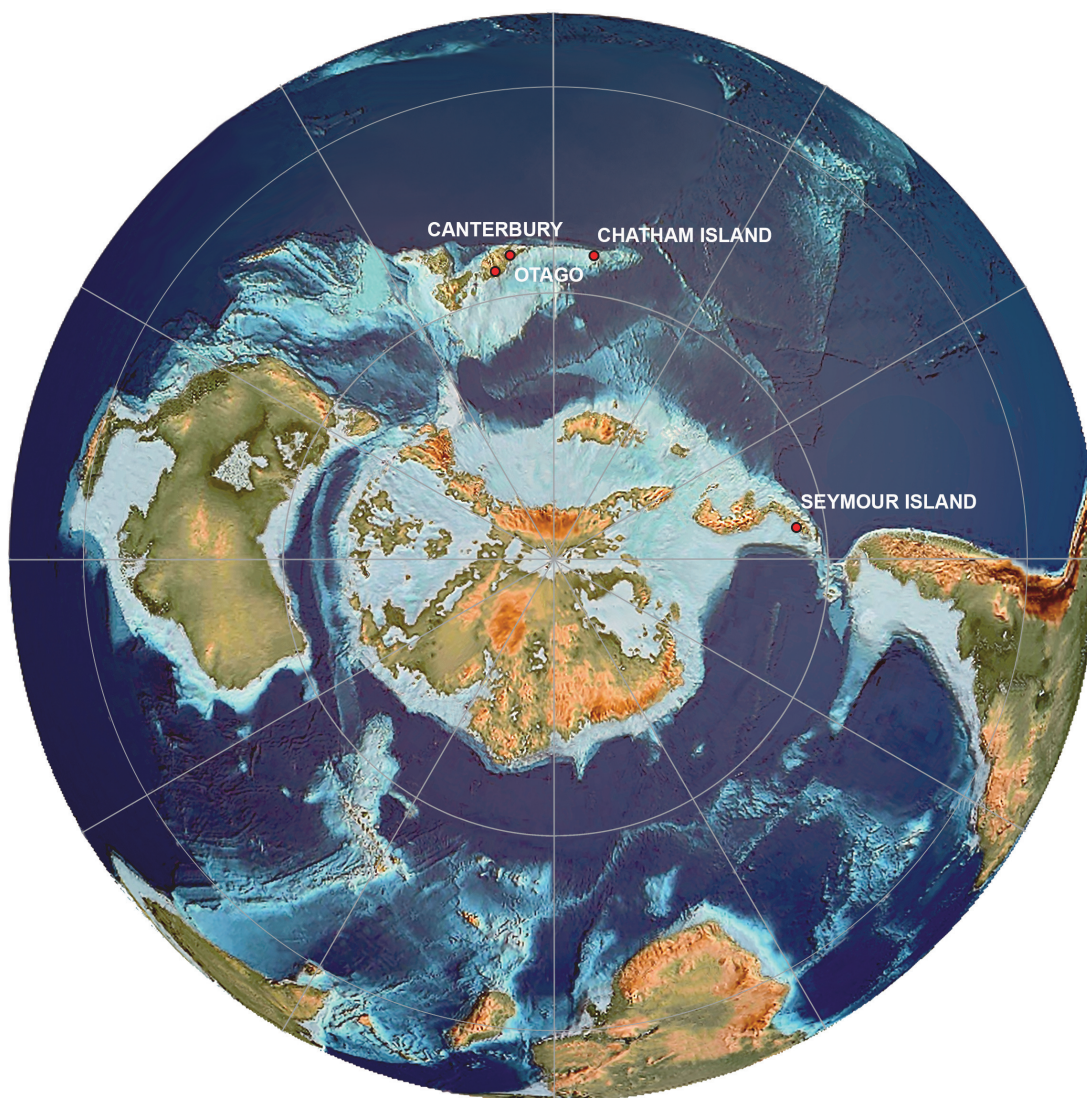


FIGURE 15. A south polar orthographic projection of the Earth around 60 Ma. Approximate site locations of Paleocene penguin fossils are indicated. Locations are associated with following fossils: CANTERBURY, Waipara Greensand = *Waimanu manneringi*, *Muriwaimanu tuatahi* (Slack et al., 2006), *Sequiwaimanu rosieae* (Mayr et al., 2018b), giant Waipara Greensand penguin (Mayr et al., 2017a), *?Crossvallia waiparensis* (Mayr et al., 2019); OTAGO, Moeraki Formation = *Kumimanu biceae* (Mayr et al., 2017b); CHATHAM ISLAND, Takatika Grit = *Kupoupou stilwelli* n. gen. et sp. and larger Chatham Island form; SEYMOUR ISLAND, Cross Valley Formation = *Crossvallia unienwillia* (Tambussi et al., 2005; Jadwiszczak et al., 2013). Adapted from palaeogeographic maps of the PALEOMAP PaleoAtlas for GPlates (Scotese, 2002; 2016), used with permission. Reconstruction was implemented using GPlates 2.0 software (<http://www.gplates.org/>).

ing penguins such as *M. tuatahi*. Effectively, other, more massive Paleocene forms such as *?Crossvallia waiparensis*, and the unnamed Waipara Greensand giant penguin, that also had stout tarsometatarsi, may have explored and exploited the water column to an even greater extent.

Until recently, archaic penguins such *Waimanu manneringi* and *Muriwaimanu tuatahi*,

from the Canterbury area in New Zealand, were thought to be the oldest sphenisciforms. Recent discoveries reveal that similarly aged taxa including *Sequiwaimanu rosieae*, *?Crossvallia waiparensis*, and the morphologically dissimilar giant Waipara Greensand penguin shared the same environment (Mayr et al., 2017a, 2018b, 2019). Less than 300 kilometres away from these Canterbury penguins, an additional giant species, *Kumi-*

manu biceae (see Mayr et al., 2017b), revealed further Paleocene diversity (Figure 15). Only 800 km from Canterbury, on the Chatham Peninsula of Zealandia, *Kupoupou stilwelli* n. gen. et sp. and the larger Chatham Island form would have inhabited marine or nearshore environments, in areas where we know mainland penguins regularly visit today (e.g., Cole et al., 2019), likely from ephemeral oceanic islands (Consoli and Stilwell, 2011), surrounded by deep ocean to the north and south (Figure 15) (Stilwell and Consoli, 2012). Also from Canterbury, *Kaiika maxwelli* may have also coexisted alongside these Paleocene penguins (Fordyce and Thomas, 2011). This unprecedented diversity of Paleocene penguins living in a relatively close proximity (Figure 15) implies that numerous ecological niches must have been present in the region now known as the eastern coast of New Zealand's South Island during this time (Mayr et al., 2017a). Ecological segregation for an area such as this is not unparalleled, however, in consideration that some sub-Antarctic islands and the Antarctic Peninsula today are known to host breeding populations of several modern penguin species sympatrically (e.g., Adams and Brown, 1989).

While still connected to Australia (Bache et al., 2014), early Cenozoic Zealandia had drifted north after it had completely separated from the eastern Gondwanan margin becoming increasingly isolated (Figure 15), and geographically and biologically distinct (Stilwell and Consoli, 2012; Stilwell, 2016). As a unique and important sector of the south-west Pacific (Crampton and Cooper, 2010; Stilwell, 2016), and with the discoveries of an apparently diverse assemblage of archaic penguins on this landmass, Zealandia—and by extension the exposed landmass of present day New Zealand—is currently recognised as the apparent cradle in which Sphenisciformes evolved (Ksepka and Thomas, 2012; Mayr, 2017). The lack of exposed outcrops available to study, however, may obscure the true nature of their origin. The only non-Zealandian sphenisciform of this early interval is represented by the late Paleocene *Crossvallia unienwillia*, and while fossils attributed to it are relatively fragmentary and incomplete (Tambussi et al., 2005; Jadwyszczak et al., 2013), visual observations and phylogenetic analyses (this study, albeit poorly supported) find it closely associated with Zealandian Paleocene penguins. Taxa such as these would have lived in a greenhouse interval with exceptionally warm poles (Zachos et al., 2008), predating the formation of the Circum-Ant-

arctic Current, in a world before the southern polar ice cap; when ocean circulation and climate was drastically different as a result (Campbell and Hutching, 2007). While sub-tropical to tropical surface water temperatures existed (Hollis et al., 2009) in the warmer early Cenozoic (Zachos et al., 2008), the sub-surface water would have still been cooler than penguin body temperature (Ponganis et al., 2003; Thomas et al., 2011). Indeed, modern penguins have geographic distributions that are largely correlated with specific aquatic temperature ranges (see Stonehouse, 1967; Simpson, 1971: 374), and also possess numerous thermoregulatory adaptations related to survival in cooler waters (e.g., Frost et al., 1975; Kooyman et al., 1976; Thomas and Fordyce, 2007). Thomas et al. (2011) hypothesised that the evolution of the rete mirabile of the forelimb in early penguins would have promoted greater foraging duration at cooler sub-surface water temperatures, and increased their ability to forage for longer durations and greater distances. Evidence of a humeral plexus of this fashion has not been confidently observed in any Paleocene penguin, and the observation that the majority of these early taxa have been recovered in a relatively close proximity, near the east coast of New Zealand's South Island, may imply that a humeral plexus may not have yet evolved, effectively restricting them to a relatively near-shore foraging habitat (Thomas et al., 2011). Adaptations such as this, in conjunction with giant size and greater hydrodynamic body shape, may have been significant in the dispersal of Paleocene penguins from inshore habitats and their radiation across the ocean to Antarctic shores (Figure 15). Unfortunately, while of massive proportions, the highly weathered bones attributed to *C. unienwillia* limit the evolutionary inferences that can be made surrounding the presence of this species in the late Paleocene Antarctic.

The ecological release provided by the vacuum in the aftermath of the K/Pg mass extinction allowed near simultaneous divergence of neoavian birds into newly available niches, followed by rapid population isolations, specialisations, and speciation events (e.g., Feduccia, 2003; Jarvis et al., 2014; Prum et al., 2015). It has been hypothesised that the lineage of birds leading to penguins evolved flightlessness in the wake of the K/Pg mass extinction, whereby penguins may have inherited a world devoid of many marine predators such as large sharks and marine reptiles (Simpson, 1976; Jadwyszczak, 2000; Ando, 2007; Ksepka and Ando, 2011). While reptilian predators

were subsequently replaced in the earliest Cenozoic (Kriwet and Benton, 2004; Mannering and Hiller, 2008), this event potentially facilitated the transition to flightlessness in the ancestors of penguins, especially in areas largely free of predation pressures (Ando, 2007; Ksepka and Ando, 2011; Mayr, 2017). The large and growing diversity of early penguins (Figure 12) may coincide with the niche availability following the mass extinction, and a rapid radiation of early penguin forms into the early Cenozoic. The large osteological variation observed within some species may fall within the range of sexual dimorphism and other intraspecific variation (Jadwiszczak and Mörs, 2011; Jadwiszczak and Acosta Hospitaleche, 2013), significant levels of which have been recognised for modern sphenisciforms (e.g., Forero et al., 2001; Ksepka and Bertelli, 2006; Ksepka and Clarke, 2010). This could explain morphological differentiation across elements assigned to *Kupoupou stilwelli* n. gen. et sp. (e.g., Figures 3-5) and in specimens attributed to *Muriwaimanu tuatahi* (Figure 12.6-10). Conversely, the disparities evident across Paleocene forms may reflect the existence of hitherto unrecognised taxonomic diversity of Paleocene species.

Recent genomic studies have implied a mid-Paleocene divergence of the Sphenisciformes clade from its sister taxon, the Procellariiformes (Jarvis et al., 2014; Prum et al., 2015), in contrast, however, some earlier molecular estimates had suggested that this split occurred within the Late Cretaceous (Baker et al., 2006; Slack et al., 2006; Brown et al., 2008). Paleogene procellariiforms are scarce, and fossils from deposits of the latest Cretaceous or earliest Paleocene have only been tentatively referred to the Procellariiformes (Olson and Parris, 1987; Ksepka and Cracraft, 2008; Mayr, 2015; Acosta Hospitaleche and Gelfo, 2017). However, the earliest penguin fossils from the Paleocene are relatively well-preserved and are diverse in size and form. The existence of at least two Chatham Island penguin taxa, in addition to an already diverse sphenisciform fauna on what is now the eastern coast of New Zealand's South Island, with morphologies significantly dissimilar to the earliest procellariiforms during the early-middle Paleocene suggests that origin of both sphenisciforms and procellariiforms occurred before the Paleocene.

We agree with Mayr et al. (2017a), that a deeper, Late Cretaceous divergence of the penguin lineage from that leading to Procellariiformes better conforms with the fossil record, whereby the earliest Sphenisciformes intensely radiated in the South Pacific oceans following the K/Pg mass extinction. Freed from aerial flight constraints, these non-volant archaic sphenisciforms evolved numerous adaptations and morphologically disparate forms related to exploiting the aquatic realm and diving efficiency, culminating in the highly specialised penguins of today.

ACKNOWLEDGEMENTS

Importantly, we are deeply grateful to T. and D. Tuanui and family for allowing access to the fossil site, their invaluable logistic support, and enthusiasm for the Chatham Islands palaeontology. We thank J.D. Stilwell and parties, for instigating this research through the discovery and collection of the fossils for this study. We are also grateful to A.A. Mannering for the preparation of specimens NMNZ S.47303 and NMNZ S.47302, and to J.-C. Stahl for the photography of many of the specimens used in this study. Additionally, we would like to thank G. Mayr for numerous photos of specimens and granting permission for their use within this work. The specimens in this study were acquired by the Museum of New Zealand Te Papa Tongarewa under acquisition number #3120. We extend our thanks to the Hokotehi Moriori Trust for their aid in Te Re Moriori vocabulary, and also D.M. Richards, in relation to the name of the taxon described in this study. We are grateful to J.D. Stilwell, M.S.Y. Lee, V.L. De Pietri, P. Jadwiszczak, and G. Guinard for their helpful communication, feedback, and sharing of information, and five anonymous reviewers for their useful comments. This research would not have been possible without the use of the materials and facilities of Canterbury Museum, Museum of New Zealand Te Papa Tongarewa, the Department of Geological Sciences, University of Canterbury, and financial support from the Mason Trust Fund. Additionally, we greatly appreciate the use of the equipment at St. George's Radiology and the CT scanning of the fossils. Thank you all.

REFERENCES

- Acosta Hospitaleche, C. 2005. Systematic revision of *Arthrodytes* Ameghino, 1905 (Aves, Spheniscidae) and its assignment to the Paraptenodytinae. *Neues Jahrbuch für Geologie und Paläontologie-Abhandlungen*, 7:404–414.
- Acosta Hospitaleche, C. 2016. Paleobiological remarks on a new partial skeleton of the Eocene Antarctic penguin *Palaeudyptes klekowskii*. *Ameghiniana*, 53:269–281. <https://doi.org/10.5710/AMGH.27.08.2015.2890>
- Acosta Hospitaleche, C. and Di Carlo, U. 2010. The coracoids in functional and morphological studies of penguins (Aves, Spheniscidae) of the Eocene of Antarctica. *Rivista Italiana di Paleontologia e Stratigrafia*, 116:23–34. <https://doi.org/10.13130/2039-4942/5938>
- Acosta Hospitaleche, C. and Gelfo, J.N. 2015. New Antarctic findings of Upper Cretaceous and lower Eocene loons (Aves: Gaviiformes). *Annales de Paleontologie*, 101:315–324. <https://doi.org/10.1016/j.annpal.2015.10.002>
- Acosta Hospitaleche, C. and Gelfo, J.N. 2017. Procellariiform remains and a new species from the latest Eocene of Antarctica. *Historical Biology*, 29:755–769. <https://doi.org/10.1080/08912963.2016.1238470>
- Acosta Hospitaleche, C. and Reguero, M. 2010. First articulated skeleton of *Palaeudyptes gunnari* from the late Eocene of Isla Marambio (Seymour Island), Antarctica. *Antarctic Science*, 22:289–298. <https://doi.org/10.1017/S0954102009990769>
- Acosta Hospitaleche, C. and Tambussi, C. 2008. South American fossil penguins: A systematic update. *Oryctos*, 7:109–127.
- Acosta Hospitaleche, C., Tambussi, C., Donato, M., and Cozzuol, M. 2007. A new Miocene penguin from Patagonia and its phylogenetic relationships. *Acta Palaeontologica Polonica*, 52:299–314.
- Adams, N.J. and Brown, C.R. 1989. Dietary differentiation and trophic relationships in the sub-Antarctic penguin community at Marion Island. *Marine Ecology Progress Series*, 57:249–258. <https://doi.org/10.3354/meps057249>
- Agnolin, F.L. 2010. An avian coracoid from the Upper Cretaceous of Patagonia, Argentina. *Studia Geologica Salmanticensia*, 46:99–119.
- Agnolin, F.L., Ezcurra, M.D., Pais, D.F., and Salisbury, S.W. 2010. A reappraisal of the Cretaceous non-avian dinosaur faunas from Australia and New Zealand: Evidence for their Gondwanan affinities. *Journal of Systematic Palaeontology*, 8:257–300. <https://doi.org/10.1080/14772011003594870>
- Agnolin, F.L. and Novas, F.E. 2012. A carpometacarpus from the Upper Cretaceous of Patagonia sheds light on the ornithurine bird radiation. *Paläontologische Zeitschrift*, 86:85–89. <https://doi.org/10.1007/s12542-011-0112-2>
- Ameghino, F. 1895. Sur les oiseaux fossiles de Patagonie. *Boletín del Instituto Geográfico de Argentina*, 15:501–602.
- Ameghino, F. 1901. L'âge des formations sédimentaires de Patagonie. *Anales de la Sociedad Científica Argentina*, 51:20–39, 65–91.
- Anderson, J.S. 2001. The phylogenetic trunk: Maximal inclusion of taxa with missing data in an analysis of the Lepospondyli (Vertebrata, Tetrapoda). *Systematic Biology*, 50:170–193. <https://doi.org/10.1080/10635150119889>
- Ando, T. 2007. *New Zealand Fossil Penguins: Origin, Pattern, and Process*. Unpublished PhD Thesis, University of Otago, Dunedin, New Zealand.
- Bache, F., Mortimer, N., Sutherland, R., Collot, J., Rouillard, P., Stagpoole, V., and Nicol, A. 2014. Seismic stratigraphic record of transition from Mesozoic subduction to continental breakup in the Zealandia Sector of eastern Gondwana. *Gondwana Research*, 26:1060–1078. <https://doi.org/10.1016/j.gr.2013.08.012>
- Baker, A.J., Pereira, S.L., Haddrath, O.P., and Edge, K.-A. 2006. Multiple gene evidence for expansion of extant Penguins out of Antarctica due to global cooling. *Proceedings of the Royal Society of London B: Biological Sciences*, 273:11–17. <https://doi.org/10.1098/rspb.2005.3260>
- Baker, C.M.A. and Manwell, C. 1975. Penguin proteins: Biochemical contributions to classification and natural history. In Stonehouse, B. (ed.), *The Biology of Penguins*. MacMillan, London.

- Ballmann, P. 1969. Les oiseaux Miocènes de La Grive-Saint-Alban (Isère). *Geobios*, 2:157–204. [https://doi.org/10.1016/S0016-6995\(69\)80005-7](https://doi.org/10.1016/S0016-6995(69)80005-7)
- Bannasch, R. 1994. Functional anatomy of the flight apparatus in penguins. *Mechanics and Physiology of Animal Swimming*, 99:163–192. <https://doi.org/10.1017/CBO9780511983641.013>
- Baumel, J.J., King, A.S., Breazile, J.E., Evans, H.E., and Vanden Berge, J.C. 1993. *Handbook of Avian Anatomy: Nomina Anatomica Avium, 2nd Edition*. Nuttall Ornithology Club, Cambridge, Massachusetts.
- Bedford, J.J. 1970. A little blue penguin in captivity. *Tane*, 16:115–119.
- Bertelli, S., Giannini, N.P., and Ksepka, D.T. 2006. Redescription and phylogenetic position of the early Miocene penguin *Parapterodytes antarcticus* from Patagonia. *American Museum Novitates*, 3525:1–36.
- Blondel, J. and Mourer-Chauviré, C. 1998. Evolution and history of the western Palaearctic avifauna. *Trends in Ecology & Evolution*, 13:488–492. [https://doi.org/10.1016/S0169-5347\(98\)01461-X](https://doi.org/10.1016/S0169-5347(98)01461-X)
- Brocklehurst, N., Upchurch, P., Mannion, P.D., and O'Connor, J. 2012. The completeness of the fossil record of Mesozoic birds: Implications for early avian evolution. *PLoS ONE*, 7:e39056. <https://doi.org/10.1371/journal.pone.0039056>
- Brown, J.W., Rest, J.S., García-Moreno, J., Sorenson, M.D., and Mindell, D.P. 2008. Strong mitochondrial DNA support for a Cretaceous origin of modern avian lineages. *BMC Biology*, 6:6. <https://doi.org/10.1186/1741-7007-6-6>
- Campbell, H. and Hutching, G. 2007. *In Search of Ancient New Zealand*. Penguin, Auckland, New Zealand.
- Campbell, H.J., Andrews, P.B., Beu, A.G., Maxwell, P.A., Edwards, A.R., Laird, M.G., Hornibrook, N.d.B., Mildenhall, D.C., Watters, W.A., Buckeridge, J.S., Lee, D.E., Strong, C.P., Wilson, G.J., and Hayward, B.W. 1993. *Cretaceous-Cenozoic Geology and Biostratigraphy of the Chatham Islands, New Zealand*. Institute of Geological & Nuclear Sciences, Lower Hutt, New Zealand.
- Chatterjee, S. 1989. The oldest Antarctic bird. *Journal of Vertebrate Paleontology*, 9:16A.
- Chatterjee, S. 2000. The morphology and systematics of *Polarornis*, a Cretaceous loon (Aves: Gaviidae) from Antarctica. *Proceedings of the 5th Symposium of the Society of Avian Paleontology and Evolution*, Beijing, p. 125–155.
- Chávez Hoffmeister, M.F. 2014. Phylogenetic characters in the humerus and tarsometatarsus of penguins. *Polish Polar Research*, 35:469–496.
- Chávez Hoffmeister, M.F., Carrillo Briceño, J.D., and Nielsen, S.N. 2014. The evolution of seabirds in the Humboldt Current: New clues from the Pliocene of central Chile. *PLoS ONE*, 9:e90043 (90041–90012). <https://doi.org/10.1371/journal.pone.0090043>
- Chiappe, L.M. and Dyke, G.J. 2002. The Mesozoic radiation of birds. *Annual Review of Ecology and Systematics*, 33:91–124. <https://doi.org/10.1146/annurev.ecolsys.33.010802.150517>
- Claramunt, S. and Cracraft, J. 2015. A new time tree reveals Earth history's imprint on the evolution of modern birds. *Science Advances*, 1:e1501005. <https://doi.org/10.1126/sciadv.1501005>
- Clark, B.D. and Bemis, W. 1979. Kinematics of swimming of penguins at the Detroit Zoo. *Journal of Zoology*, 188:411–428. <https://doi.org/10.1111/j.1469-7998.1979.tb03424.x>
- Clarke, J.A., Ksepka, D.T., Salas-Gismondi, R., Altamirano, A.J., Shawkey, M.D., D'Alba, L., Vinther, J., DeVries, T.J., and Baby, P. 2010. Fossil evidence for evolution of the shape and color of penguin feathers. *Science*, 330:954–957. <https://doi.org/10.1126/science.1193604>
- Clarke, J.A., Ksepka, D.T., Stucchi, M., Urbina, M., Giannini, N., Bertelli, S., Narváez, Y., and Boyd, C.A. 2007. Paleogene equatorial penguins challenge the proposed relationship between biogeography, diversity, and Cenozoic climate change. *Proceedings of the National Academy of Sciences*, 104:11545–11550. <https://doi.org/10.1073/pnas.0611099104>
- Cobbett, A., Wilkinson, M., and Wills, M.A. 2007. Fossils impact as hard as living taxa in parsimony analyses of morphology. *Systematic Biology*, 56:753–766. <https://doi.org/10.1080/10635150701627296>
- Cole, T.L., Ksepka, D.T., Mitchell, K.J., Tennyson, A.J., Thomas, D.B., Pan, H., Zhang, G., Rawlence, N.J., Wood, J.R., and Bover, P. 2019. Mitogenomes uncover extinct penguin taxa and reveal island formation as a key driver of speciation. *Molecular Biology and Evolution*, 36:784–797. <https://doi.org/10.1093/molbev/msz017>

- Conroy, G.C. and Vannier, M.W. 1984. Noninvasive three-dimensional computer imaging of matrix-filled fossil skulls by high-resolution computed tomography. *Science*, 226:456–458. <https://doi.org/10.1126/science.226.4673.456>
- Consoli, C.P. 2008. A rare Danian (early Paleocene) *Chlamydoselachus* (Chondrichthyes: Elasmobranchii) from the Takatika Grit, Chatham Islands, New Zealand. *Journal of Vertebrate Paleontology*, 28:285–290. [https://doi.org/10.1671/0272-4634\(2008\)28\[285:ARDEPC\]2.0.CO;2](https://doi.org/10.1671/0272-4634(2008)28[285:ARDEPC]2.0.CO;2)
- Consoli, C.P., Pisera, A., and Stilwell, J.D. 2009. Siliceous sponges of the Takatika Grit (Cretaceous–Paleogene), Chatham Islands, South Pacific. *Journal of Paleontology*, 83:811–819. <https://doi.org/10.1666/08-120.1>
- Consoli, C.P. and Stilwell, J.D. 2005. Late Cretaceous Cephalopoda (Mollusca) from the Takatika Grit, Chatham Islands, Southwest Pacific. *New Zealand Journal of Geology and Geophysics*, 48:389–393. <https://doi.org/10.1080/00288306.2005.9515121>
- Consoli, C.P. and Stilwell, J.D. 2009. Late Cretaceous marine reptiles (Elasmosauridae and Mosasauridae) of the Chatham Islands, New Zealand. *Cretaceous Research*, 30:991–999. <https://doi.org/10.1016/j.cretres.2009.02.009>
- Consoli, C.P. and Stilwell, J.D. 2011. Palaeontology of the Chatham Islands, SW Pacifica review. *Alcheringa: An Australasian Journal of Palaeontology*, 35:285–301. <https://doi.org/10.1080/03115518.2011.532326>
- Cracraft, J. 1981. Toward a phylogenetic classification of the recent birds of the world (class Aves). *The Auk*, 98:681–714.
- Cracraft, J. 1988. The major clades of birds, p. 339–361. In Benton, M.J. (ed.), *The Phylogeny and Classification of the Tetrapods*. Systematics Association by the Clarendon Press, Oxford.
- Crampton, J.S. and Cooper, R.A. 2010. The state of paleontology in New Zealand. *Palaeontologia Electronica* 13.2.4A:1–9. https://palaeo-electronica.org/2010_2/commentary/zealand.htm
- Degrange, F.J., Ksepka, D.T., and Tambussi, C.P. 2018. Redescription of the oldest crown clade penguin: Cranial osteology, jaw myology, neuroanatomy, and phylogenetic affinities of *Madrynornis mirandus*. *Journal of Vertebrate Paleontology*, 38:e1445636 (1445631–1445625). <https://doi.org/10.1080/02724634.2018.1445636>
- Dickinson, E.C. and Remsen, J.V. 2013. *The Howard and Moore Complete Checklist of the Birds of the World, 4th Edition, Vol. One Non-passerines*. Aves Press Limited, Eastbourne.
- Dyke, G.J. and van Tuinen, M. 2004. The evolutionary radiation of modern birds (Neornithes): Reconciling molecules, morphology and the fossil record. *Zoological Journal of the Linnean Society*, 141:153–177. <https://doi.org/10.1111/j.1096-3642.2004.00118.x>
- Elliott, K.H., Ricklefs, R.E., Gaston, A.J., Hatch, S.A., Speakman, J.R., and Davoren, G.K. 2013. High flight costs, but low dive costs, in auks support the biomechanical hypothesis for flightlessness in penguins. *Proceedings of the National Academy of Sciences*, 110:9380–9384. <https://doi.org/10.1073/pnas.1304838110>
- Elzanowski, A. 2008. The avian femur: Morphology and terminology of the lateral condyle. *Oryctos*, 7:1–5.
- Elzanowski, A., Bieńkowska-Wasiluk, M., Chodyń, R., and Bogdanowicz, W. 2012. Anatomy of the coracoid and diversity of the Procellariiformes (Aves) in the Oligocene of Europe. *Palaeontology*, 55:1199–1221. <https://doi.org/10.1111/j.1475-4983.2012.01187.x>
- Ericson, P.G.P., Anderson, C.L., Britton, T., Elzanowski, A., Johansson, U.S., Kallersjo, M., Ohlson, J.I., Parsons, T.J., Zuccon, D., and Mayr, G. 2006. Diversification of Neoaves: Integration of molecular sequence data and fossils. *Biology Letters*, 2:543–U541. <https://doi.org/10.1098/rsbl.2006.0523>
- Feduccia, A. 1995. Explosive evolution in Tertiary birds and mammals. *Science*, 267:637–638. <https://doi.org/10.1126/science.267.5198.637>
- Feduccia, A. 2003. 'Big bang' for Tertiary birds? *Trends in Ecology & Evolution*, 18:172–176. [https://doi.org/10.1016/S0169-5347\(03\)00017-X](https://doi.org/10.1016/S0169-5347(03)00017-X)
- Feduccia, A. 2014. Avian extinction at the end of the Cretaceous: Assessing the magnitude and subsequent explosive radiation. *Cretaceous Research*, 50:1–15. <https://doi.org/10.1016/j.cretres.2014.03.009>

- Fordyce, R.E. and Thomas, D.B. 2011. *Kaiika maxwelli*, a new early Eocene archaic penguin (Sphenisciformes, Aves) from Waihao Valley, South Canterbury, New Zealand. *New Zealand Journal of Geology and Geophysics*, 54:43–51. <https://doi.org/10.1080/00288306.2011.536521>
- Forero, M.G., Tella, J.L., Donazar, J.A., Blanco, G., Bertellotti, M., and Ceballos, O. 2001. Phenotypic assortative mating and within-pair sexual dimorphism and its influence on breeding success and offspring quality in Magellanic penguins. *Canadian Journal of Zoology*, 79:1414–1422. <https://doi.org/10.1139/z01-088>
- Frost, P.G.H., Siegfried, W.R., and Greenwood, P.J. 1975. Arterio-venous heat exchange systems in the Jackass penguin *Spheniscus demersus*. *Journal of Zoology*, 175:231–241. <https://doi.org/10.1111/j.1469-7998.1975.tb01398.x>
- Gaina, C., Müller, D.R., Royer, J.Y., Stock, J., Hardebeck, J., and Symonds, P. 1998. The tectonic history of the Tasman Sea: A puzzle with 13 pieces. *Journal of Geophysical Research: Solid Earth*, 103:12413–12433. <https://doi.org/10.1029/98JB00386>
- Galton, P.M. and Martin, L.D. 2002. Postcranial anatomy and systematics of *Enaliornis* Seeley, 1876, a foot-propelled diving bird (Aves: Ornithurae: Hesperornithiformes) from the Early Cretaceous of England. *Revue de Paléobiologie*, 21:489–538.
- Gauthier-Clerc, M., Le Maho, Y., Clerquin, Y., Drault, S., and Handrich, Y. 2000. Penguin waddling is not wasteful. *Nature*, 408:929. <https://doi.org/10.1038/35050167>
- Gauthier, J., Kluge, A.G., and Rowe, T. 1988. Amniote phylogeny and the importance of fossils. *Cladistics*, 4:105–209. <https://doi.org/10.1111/j.1096-0031.1988.tb00514.x>
- Gavryushkina, A., Heath, T.A., Ksepka, D.T., Stadler, T., Welch, D., and Drummond, A.J. 2017. Bayesian total-evidence dating reveals the recent crown radiation of penguins. *Systematic Biology*, 66:57–73. <https://doi.org/10.1093/sysbio/syw060>
- Gaździcki, A. 2004. Eocene–Pliocene ecosystems of South Shetlands and Antarctic Peninsula. *Bolletino di Geofisica Teorica ed Applicata*, 45:258–260.
- Göhlich, U.B. 2007. The oldest fossil record of the extant penguin genus *Spheniscus* – a new species from the Miocene of Peru. *Acta Paleontologica Polonica*, 52:285–298.
- Goloboff, P.A. and Szumik, C.A. 2015. Identifying unstable taxa: Efficient implementation of triplet-based measures of stability, and comparison with Phyutility and RogueNaRok. *Molecular Phylogenetics and Evolution*, 88:93–104. <https://doi.org/10.1016/j.ympev.2015.04.003>
- Guinard, G. and Marchand, D. 2010. Modularity and complete natural homeoses in cervical vertebrae of extant and extinct penguins (Aves: Sphenisciformes). *Evolutionary Biology*, 37:210–226. <https://doi.org/10.1007/s11692-010-9097-0>
- Guinard, G., Marchand, D., Courant, F., Gauthier-Clerc, M., and Le Bohec, C. 2010. Morphology, ontogenesis and mechanics of cervical vertebrae in four species of penguins (Aves: Spheniscidae). *Polar Biology*, 33:807–822. <https://doi.org/10.1007/s00300-009-0759-2>
- Guindon, S., Dufayard, J.-F., Lefort, V., Anisimova, M., Hordijk, W., and Gascuel, O. 2010. New algorithms and methods to estimate maximum-likelihood phylogenies: Assessing the performance of PhyML 3.0. *Systematic Biology*, 59:307–321. <https://doi.org/10.1093/sysbio/syq010>
- Habib, M. 2010. The structural mechanics and evolution of aquaflying birds. *Biological Journal of the Linnean Society*, 99:687–698. <https://doi.org/10.1111/j.1095-8312.2010.01372.x>
- Hackett, S.J., Kimball, R.T., Reddy, S., Bowie, R.C., Braun, E.L., Braun, M.J., Chojnowski, J.L., Cox, W.A., Han, K.-L., and Harshman, J. 2008. A phylogenomic study of birds reveals their evolutionary history. *Science*, 320:1763–1768. <https://doi.org/10.1126/science.1157704>
- Haubitz, B., Prokop, M., Döhring, W., Ostrom, J., and Wellnhofer, P. 1988. Computed tomography of *Archaeopteryx*. *Paleobiology*, 14:206–213. <https://doi.org/10.1017/S0094837300011921>
- Hollis, C.J., Handley, L., Crouch, E.M., Morgans, H.E., Baker, J.A., Creech, J., Collins, K.S., Gibbs, S.J., Huber, M., and Schouten, S. 2009. Tropical sea temperatures in the high-latitude South Pacific during the Eocene. *Geology*, 37:99–102. <https://doi.org/10.1130/G25200A.1>
- Hollis, C.J., Stickley, C.E., Bijl, P.K., Schiøler, P., Clowes, C.D., Li, X., and Campbell, H. 2017. The age of the Takatika Grit, Chatham Islands, New Zealand. *Alcheringa: An Australasian Journal of Palaeontology*, 41:383–396. <https://doi.org/10.1080/03115518.2017.1296189>
- Houde, P., Braun, E.L., Narula, N., Minjares, U., and Mirarab, S. 2019. Phylogenetic signal of indels and the neoavian radiation. *Diversity*, 11:108. <https://doi.org/10.3390/d11070108>

- Huelsenbeck, J.P. 1991. When are fossils better than extant taxa in phylogenetic analysis? *Systematic Biology*, 40:458–469. <https://doi.org/10.2307/2992240>
- Hui, C.A. 1985. Maneuverability of the Humboldt penguin (*Spheniscus humboldti*) during swimming. *Canadian Journal of Zoology*, 63:2165–2167. <https://doi.org/10.1139/z85-318>
- Huxley, T.H. 1859. On a fossil bird and a fossil cetacean from New Zealand. *Quarterly Journal of the Geological Society of London*, 15:670–677. <https://doi.org/10.1144/GSL.JGS.1859.015.01-02.73>
- Iurino, D.A., Danti, M., Della Sala, S.W., and Sardella, R. 2013. Modern techniques for ancient bones: Vertebrate palaeontology and medical CT analysis. *Bollettino della Societa Paleontologica Italiana*, 52:i–xi.
- Jadwiszczak, P. 2000. The fossil record of Antarctic penguins. *Polish Polar Studies, 27th International Polar Symposium*, Toruń, Poland, p.39–45.
- Jadwiszczak, P. 2006a. Eocene penguins of Seymour Island, Antarctica: Taxonomy. *Polish Polar Research*, 27:3–62.
- Jadwiszczak, P. 2006b. Eocene penguins of Seymour Island, Antarctica: The earliest record, taxonomic problems and some evolutionary considerations. *Polish Polar Research*, 27:287–302.
- Jadwiszczak, P. 2009. Penguin past: The current state of knowledge. *Polish Polar Research*, 30:3–28.
- Jadwiszczak, P. 2012. Partial limb skeleton of a “giant penguin” *Anthropornis* from the Eocene of Antarctic Peninsula. *Polish Polar Research*, 33:259–274.
- Jadwiszczak, P. 2013. Taxonomic diversity of Eocene Antarctic penguins: A changing picture, p. 129–138. In Hambrey, M.J., Barker, P.F., Barrett, P.J.B., Davies, V. B., Smellie, J.L., and Tranter, M. (eds.), *Antarctic Palaeoenvironments and Earth-Surface Processes*. The Geological Society, London. <https://doi.org/10.1144/SP381.7>
- Jadwiszczak, P. 2015. Another look at tarsometatarsi of early penguins. *Polish Polar Research*, 36:343–354.
- Jadwiszczak, P. and Acosta Hospitaleche, C. 2013. Distinguishing between two Antarctic species of Eocene *Palaeudyptes* penguins: A statistical approach using tarsometatarsi. *Polish Polar Research*, 34:237–252.
- Jadwiszczak, P., Hospitaleche, C.A., and Reguero, M. 2013. Redescription of *Crossvallia unienwillia*: The only Paleocene Antarctic penguin. *Ameghiniana*, 50:545–553. <https://doi.org/10.5710/AMGH.09.10.2013.1058>
- Jadwiszczak, P. and Mörs, T. 2011. Aspects of diversity in early Antarctic penguins. *Acta Palaeontologica Polonica*, 56:269–278.
- Jadwiszczak, P. and Mörs, T. 2019. First partial skeleton of *Delphinornis larseni* Wiman, 1905, a slender-footed penguin from the Eocene of Antarctic Peninsula. *Palaeontologia Electronica* 22.2.32A:1–31. <https://doi.org/10.26879/933>
palaeo-electronica.org/content/2019/2574-skeleton-of-an-eocene-penguin
- Jarvis, E.D., Mirarab, S., Aberer, A.J., Li, B., Houde, P., Li, C., Ho, S.Y.W., Faircloth, B.C., Nabholz, B., Howard, J.T., Suh, A., Weber, C.C., da Fonseca, R.R., Li, J., Zhang, F., Li, H., Zhou, L., Narula, N., Liu, L., Ganapathy, G., Boussau, B., Bayzid, M.S., Zavidovych, V., Subramanian, S., Gabaldon, T., Capella-Gutierrez, S., Huerta-Cepas, J., Rekepalli, B., Munch, K., Schierup, M., Lindow, B., Warren, W.C., Ray, D., Green, R.E., Bruford, M.W., Zhan, X., Dixon, A., Li, S., Li, N., Huang, Y., Derryberry, E.P., Bertelsen, M.F., Sheldon, F.H., Brumfield, R.T., Mello, C.V., Lovell, P.V., Wirthlin, M., Cruz Schneider, M.P., Prodocimi, F., Samaniego, J.A., Vargas Velazquez, A.M., Alfaro-Nunez, A., Campos, P.F., Petersen, B., Sichteritz-Ponten, T., Pas, A., Bailey, T., Scofield, P., Bunce, M., Lambert, D.M., Zhou, Q., Perelman, P., Driskell, A.C., Shapiro, B., Xiong, Z., Zeng, Y., Liu, S., Li, Z., Liu, B., Wu, K., Xiao, J., Yinqi, X., Zheng, Q., Zhang, Y., Yang, H., Wang, J., Smeds, L., Rheindt, F.E., Braun, M., Fjeldsa, J., Orlando, L., Barker, F.K., Jonsson, K.A., Johnson, W., Koepfli, K.-P., O'Brien, S., Haussler, D., Ryder, O.A., Rahbek, C., Willerslev, E., Graves, G.R., Glenn, T.C., McCormack, J., Burt, D., Ellegren, H., Alstrom, P., Edwards, S.V., Stamatakis, A., Mindell, D.P., Cracraft, J., Braun, E.L., Warnow, T., Jun, W., Gilbert, M.T.P., and Zhang, G. 2014. Whole-genome analyses resolve early branches in the tree of life of modern birds. *Science*, 346:1320–1331. <https://doi.org/10.1126/science.1253451>
- Jenkins, R.J.F. 1974. A new giant penguin from the Eocene of Australia. *Paleontology*, 17:291–310.

- Johansson, L.C. and Wetterholm Aldrin, B.S. 2002. Kinematics of diving Atlantic puffins (*Fratercula arctica* L.): Evidence for an active upstroke. *Journal of Experimental Biology*, 205:371–378.
- Kaiser, G.W. 2007. *The Inner Bird: Anatomy and Evolution*. UBC Press, Vancouver, Toronto.
- Ketcham, R.A. and Carlson, W.D. 2001. Acquisition, optimization and interpretation of X-ray computed tomographic imagery: Applications to the geosciences. *Computers & Geosciences*, 27:381–400. [https://doi.org/10.1016/S0098-3004\(00\)00116-3](https://doi.org/10.1016/S0098-3004(00)00116-3)
- Kingsolver, J.G. and Pfennig, D.W. 2004. Individual-level selection as a cause of Cope's rule of phyletic size increase. *Evolution*, 58:1608–1612.
- Kooyman, G.L., Gentry, R.L., Bergman, W.P., and Hammel, H.T. 1976. Heat loss in penguins during immersion and compression. *Comparative Biochemistry and Physiology Part A: Physiology*, 54:75–80. [https://doi.org/10.1016/S0300-9629\(76\)80074-6](https://doi.org/10.1016/S0300-9629(76)80074-6)
- Kovacs, C.E. and Meyers, R.A. 2000. Anatomy and histochemistry of flight muscles in a wing-propelled diving bird, the Atlantic puffin, *Fratercula arctica*. *Journal of Morphology*, 244:109–125. [https://doi.org/10.1002/\(SICI\)1097-4687\(200005\)244:2<109::AID-JMOR2>3.0.CO;2-0](https://doi.org/10.1002/(SICI)1097-4687(200005)244:2<109::AID-JMOR2>3.0.CO;2-0)
- Kriwet, J. and Benton, M.J. 2004. Neoselachian (Chondrichthyes, Elasmobranchii) diversity across the Cretaceous–Tertiary boundary. *Palaeogeography, Palaeoclimatology, Palaeoecology*, 214:181–194. <https://doi.org/10.1016/j.palaeo.2004.02.049>
- Ksepka, D.T. 2007. *Phylogeny, Histology and Functional Morphology of Fossil Penguins (Sphenisciformes)*. Unpublished PhD Thesis, Columbia University, New York, USA.
- Ksepka, D.T. and Ando, T. 2011. Penguins past, present, and future: Trends in the evolution of the Sphenisciformes, p. 155–186. In Dyke, G. and Kaiser, G.W. (eds.), *Living Dinosaurs: The Evolutionary History of Modern Birds*. John-Wiley & Sons Ltd, Hoboken, New Jersey. <https://doi.org/10.1002/9781119990475.ch6>
- Ksepka, D.T. and Bertelli, S. 2006. Fossil penguin (Aves: Sphenisciformes) cranial material from the Eocene of Seymour Island (Antarctica). *Historical Biology*, 18:389–395. <https://doi.org/10.1080/08912960600658376>
- Ksepka, D.T., Bertelli, S., and Giannini, N.P. 2006. The phylogeny of the living and fossil Sphenisciformes (penguins). *Cladistics*, 22:412–441. <https://doi.org/10.1111/j.1096-0031.2006.00116.x>
- Ksepka, D.T. and Clarke, J.A. 2010. The basal penguin (Aves: Sphenisciformes) *Perudyptes devriesi* and a phylogenetic evaluation of the penguin fossil record. *Bulletin of the American Museum of Natural History*, 337:1–77. <https://doi.org/10.1206/653.1>
- Ksepka, D.T., Clarke, J.A., DeVries, T.J., and Urbina, M. 2008. Osteology of *Icadyptes salasi*, a giant penguin from the Eocene of Peru. *Journal of Anatomy*, 213:131–147. <https://doi.org/10.1111/j.1469-7580.2008.00927.x>
- Ksepka, D.T. and Cracraft, J. 2008. An avian tarsometatarsus from near the K-T boundary of New Zealand. *Journal of Vertebrate Paleontology*, 28:1224–1227. <https://doi.org/10.1671/0272-4634-28.4.1224>
- Ksepka, D.T., Fordyce, R.E., Ando, T., and Jones, C.M. 2012. New fossil penguins (Aves, Sphenisciformes) from the Oligocene of New Zealand reveal the skeletal plan of stem penguins. *Journal of Vertebrate Paleontology*, 32:235–254. <https://doi.org/10.1080/02724634.2012.652051>
- Ksepka, D.T. and Phillips, M.J. 2015. Avian diversification patterns across the K-Pg boundary: Influence of calibrations, datasets, and model misspecification. *Annals of the Missouri Botanical Garden*, 100:300–328. <https://doi.org/10.3417/2014032>
- Ksepka, D.T. and Thomas, D.B. 2012. Multiple Cenozoic invasions of Africa by penguins (Aves, Sphenisciformes). *Proceedings of the Royal Society of London B: Biological Sciences*, 279:1027–1032. <https://doi.org/10.1098/rspb.2011.1592>
- Ksepka, D.T., Werning, S., Sclafani, M., and Boles, Z.M. 2015. Bone histology in extant and fossil penguins (Aves: Sphenisciformes). *Journal of Anatomy*, 227:611–630. <https://doi.org/10.1111/joa.12367>
- Laird, M.G. and Bradshaw, J.D. 2004. The break-up of a long-term relationship: The Cretaceous separation of New Zealand from Gondwana. *Gondwana Research*, 7:273–286. [https://doi.org/10.1016/s1342-937x\(05\)70325-7](https://doi.org/10.1016/s1342-937x(05)70325-7)
- Lambrecht, K. 1929. *Neogaeornis wetzeli* ngn sp. der erste Kreidevogel der südlichen Hemisphäre. *Palaeontologische Zeitschrift*, 11:121–129.

- Lanfear, R., Calcott, B., Ho, S.Y., and Guindon, S. 2012. PartitionFinder: Combined selection of partitioning schemes and substitution models for phylogenetic analyses. *Molecular Biology and Evolution*, 29:1695–1701. <https://doi.org/10.1093/molbev/mss020>
- Lanfear, R., Frandsen, P.B., Wright, A.M., Senfeld, T., and Calcott, B. 2017. PartitionFinder 2: New methods for selecting partitioned models of evolution for molecular and morphological phylogenetic analyses. *Molecular Biology and Evolution*, 34:772–773. <https://doi.org/10.1093/molbev/msw260>
- Lee, M.S.Y., Cau, A., Naish, D., and Dyke, G.J. 2014. Morphological clocks in paleontology, and a mid-Cretaceous origin of crown Aves. *Systematic Biology*, 63:442–449. <https://doi.org/10.1093/sysbio/syt110>
- Lee, M.S.Y. and Palci, A. 2015. Morphological phylogenetics in the genomic age. *Current Biology*, 25: R922–R929. <https://doi.org/10.1016/j.cub.2015.07.009>
- Lewis, P.O. 2001. A likelihood approach to estimating phylogeny from discrete morphological character data. *Systematic Biology*, 50:913–925. <https://doi.org/10.1080/106351501753462876>
- Linnaeus, C. 1758. *Systema Naturæ per Regna Tria Naturæ, Secundum Classes, Ordines, Genera, Species cum Characteribus, Differentiis, Synonymis, Locis* Vol. 1 (10). Laurentius Salvius, Holmiæ. <https://doi.org/10.5962/bhl.title.542>
- Livezey, B.C. 1989. Morphometric patterns in recent and fossil penguins (Aves, Sphenisciformes). *Journal of Zoology*, 219:269–307. <https://doi.org/10.1111/j.1469-7998.1989.tb02582.x>
- Livezey, B.C. and Zusi, R.L. 2007. Higher-order phylogeny of modern birds (Theropoda, Aves: Neornithes) based on comparative anatomy. II. Analysis and discussion. *Zoological Journal of the Linnean Society*, 149:1–95. <https://doi.org/10.1111/j.1096-3642.2006.00293.x>
- Longrich, N.R., Tokaryk, T., and Field, D.J. 2011. Mass extinction of birds at the Cretaceous–Paleogene (K–Pg) boundary. *Proceedings of the National Academy of Sciences of the United States of America*, 108:15253–15257. <https://doi.org/10.1073/pnas.1110395108>
- Maddison, W.P. and Maddison, D.R. 2015. Mesquite: A modular system for evolutionary analysis. Version 3.04. <http://mesquiteproject.org>
- Mannerling, A.A. and Hiller, N. 2008. An early Cenozoic neoselachian shark fauna from the Southwest Pacific. *Palaeontology*, 51:1341–1365. <https://doi.org/10.1111/j.1475-4983.2008.00812.x>
- Marples, B.J. 1952. Early Tertiary penguins of New Zealand. *New Zealand Geological Survey, Palaeontological Bulletin*, 20:1–66.
- Marples, B.J. 1953. Fossil penguins from the mid-Tertiary of Seymour Island. *Falkland Islands Dependence Survey Scientific Reports*, 5:1–15.
- Mayr, G. 2004. A partial skeleton of a new fossil loon (Aves, Gaviiformes) from the early Oligocene of Germany with preserved stomach content. *Journal of Ornithology*, 145:281–286. <https://doi.org/10.1007/s10336-004-0050-9>
- Mayr, G. 2005. The Paleogene fossil record of birds in Europe. *Biological Reviews*, 80:515–542. <https://doi.org/10.1017/s1464793105006779>
- Mayr, G. 2009. *Paleogene Fossil Birds*. Springer-Verlag, Berlin Heidelberg. <https://doi.org/10.1007/978-3-540-89628-9>
- Mayr, G. 2010. Metaves, Mirandornithes, Strisores and other novelties—A critical review of the higher-level phylogeny of neornithine birds. *Journal of Zoological Systematics and Evolutionary Research*, 49:58–76. <https://doi.org/10.1111/j.1439-0469.2010.00586.x>
- Mayr, G. 2014. The origins of crown group birds: Molecules and fossils. *Palaeontology*, 57:231–242. <https://doi.org/10.1111/pala.12103>
- Mayr, G. 2015. A new Paleogene procellariiform bird from western North America. *Neues Jahrbuch für Geologie und Paläontologie-Abhandlungen*, 275:11–17. <https://doi.org/10.1127/njgpa/2015/0445>
- Mayr, G. 2016. Variations in the hypotarsus morphology of birds and their evolutionary significance. *Acta Zoologica*, 97:196–210. <https://doi.org/10.1111/azo.12117>
- Mayr, G. 2017. *Avian Evolution: The Fossil Record of Birds and Its Paleobiological Significance*. John Wiley & Sons Ltd, Hoboken, New Jersey. <https://doi.org/10.1002/9781119020677>
- Mayr, G., De Pietri, V.L., Love, L., Mannerling, A.A., and Scofield, R.P. 2018b. A well-preserved new mid-Paleocene penguin (Aves, Sphenisciformes) from the Waipara Greensand in New Zealand. *Journal of Vertebrate Paleontology*, 37:e1398169 (1398161–1398119). <https://doi.org/10.1080/02724634.2017.1398169>

- Mayr, G., De Pietri, V.L., Love, L., Mannering, A., and Scofield, R.P. 2019. Leg bones of a new penguin species from the Waipara Greensand add to the diversity of very large-sized Sphenisciformes in the Paleocene of New Zealand. *Alcheringa: An Australasian Journal of Palaeontology*. <https://doi.org/10.1080/03115518.2019.1641619>
- Mayr, G., De Pietri, V.L., and Scofield, R.P. 2017a. A new fossil from the mid-Paleocene of New Zealand reveals an unexpected diversity of world's oldest penguins. *The Science of Nature*, 104:1–6. <https://doi.org/10.1007/s00114-017-1441-0>
- Mayr, G., De Pietri, V.L., Scofield, R.P., and Worthy, T.H. 2018a. On the taxonomic composition and phylogenetic affinities of the recently proposed clade Vegaviidae Agnolín et al., 2017—neornithine birds from the Upper Cretaceous of the Southern Hemisphere. *Cretaceous Research*, 86:178–185. <https://doi.org/10.1016/j.cretres.2018.02.013>
- Mayr, G. and Scofield, R.P. 2016. New avian remains from the Paleocene of New Zealand: The first early Cenozoic Phaethontiformes (tropicbirds) from the Southern Hemisphere. *Journal of Vertebrate Paleontology*, 36:e1031343. <https://doi.org/10.1080/02724634.2015.1031343>
- Mayr, G., Scofield, R.P., De Pietri, V.L., and Tennyson, A.J. 2017b. A Paleocene penguin from New Zealand substantiates multiple origins of gigantism in fossil Sphenisciformes. *Nature Communications*, 8:1–8. <https://doi.org/10.1038/s41467-017-01959-6>
- Mayr, G., Zvonok, E., and Gorobets, L. 2013. The tarsometatarsus of the middle Eocene loon *Colymbiculus udovichenkoi*. *Paleornithological Research 2013—Proceedings of the 8th International Meeting of the Society of Avian Paleontology and Evolution*. Verlag Naturhistorisches Museum Wien, Vienna, p. 17–22.
- Meister, W. 1962. Histological structure of the long bones of penguins. *The Anatomical Record*, 143:377–387. <https://doi.org/10.1002/ar.1091430408>
- Moreno, F.P. and Mercerat, A. 1891. Catálogo de los pájaros fósiles de la República Argentina conservados en el Museo de La Plata. *Anales del Museo de La Plata (Paleontología Argentina)*, 1:7–71.
- Mortimer, N., Campbell, H.J., Stagpoole, M., Wood, R.A., Rattenbury, M.S., Sutherland, R., and Seton, M. 2017. Zealandia: Earth's hidden continent. *GSA Today*, 27:1–8. <https://doi.org/10.1130/GSATG321A.1>
- Myrcha, A., Jadwiszczak, P., Tambussi, C.P., Noriega, J.I., Gaździcki, A., Tatur, A., and Del Valle, R. 2002. Taxonomic revision of Eocene Antarctic penguins based on tarsometatarsal morphology. *Polish Polar Research*, 23:5–46.
- Myrcha, A., Tatur, A., and Del Valle, R. 1990. A new species of fossil penguin from Seymour Island, West Antarctica. *Alcheringa: An Australasian Journal of Palaeontology*, 14:195–205. <https://doi.org/10.1080/03115519008619055>
- Norris, R.M. 1964. Sediments of Chatham Rise. *Department of Scientific and Industrial Research*, 59:1–39.
- O'Reilly, J.E., Puttick, M.N., Parry, L., Tanner, A.R., Tarver, J.E., Fleming, J., Pisani, D., and Donoghue, P.C. 2016. Bayesian methods outperform parsimony but at the expense of precision in the estimation of phylogeny from discrete morphological data. *Biology Letters*, 12:20160081 (20160081–20160085). <https://doi.org/10.1098/rsbl.2016.0081>
- O'Reilly, J.E., Puttick, M.N., Pisani, D., and Donoghue, P.C. 2018. Probabilistic methods surpass parsimony when assessing clade support in phylogenetic analyses of discrete morphological data. *Palaeontology*, 61:105–118. <https://doi.org/10.1111/pala.12330>
- Oliver, W.R.B. 1930. *New Zealand Birds*. Fine Arts (New Zealand) Ltd, Wellington, New Zealand.
- Olson, S.L. 1992. *Neogaeornis wetzeli* Lambrecht, a Cretaceous loon from Chile (Aves: Gaviidae). *Journal of Vertebrate Paleontology*, 12:122–124. <https://doi.org/10.1080/02724634.1992.10011438>
- Olson, S.L. and Parris, D.C. 1987. The Cretaceous birds of New Jersey. *Smithsonian Contributions to Paleobiology*, 63:1–22. <https://doi.org/10.5479/si.00810266.63.1>
- Pacheco, M.A., Battistuzzi, F.U., Lentino, M., Aguilar, R.F., Kumar, S., and Escalante, A.A. 2011. Evolution of modern birds revealed by mitogenomics: Timing the radiation and origin of major orders. *Molecular Biology and Evolution*, 28:1927–1942. <https://doi.org/10.1093/molbev/msr014>
- Parfitt, A.R. and Vincent, J.F.V. 2005. Drag reduction in a swimming Humboldt penguin, *Spheniscus humboldti*, when the boundary layer is turbulent. *Journal of Bionic Engineering*, 2:57–62. <https://doi.org/10.1007/BF03399481>

- Park, T., Fitzgerald, E.M.G., Gallagher, S.J., Tomkins, E., and Allan, T. 2016. New Miocene fossils and the history of penguins in Australia. *PLoS ONE*, 11:e0153915 (0153911–0153921). <https://doi.org/10.1371/journal.pone.0153915>
- Pennycuik, C.J. 1987. Flight of auks (Alcidae) and other northern seabirds compared with southern Procellariiformes: Ornithodolite observations. *Journal of Experimental Biology*, 128:335–347.
- Pinshow, B., Fedak, M.A., and Schmidt-Nielsen, K. 1977. Terrestrial locomotion in penguins: It costs more to waddle. *Science*, 195:592–594. <https://doi.org/10.1126/science.835018>
- Poe, S. and Wiens, J.J. 2000. Character selection and the methodology of morphological phylogenetics, p. 20–36. In Wiens, J.J. (ed.), *Phylogenetic Analysis of Morphological Data*. Smithsonian Institution Press, Washington, D.C.
- Ponganis, P.J., Van Dam, R.P., Levenson, D.H., Knowler, T., Ponganis, K.V., and Marshall, G. 2003. Regional heterothermy and conservation of core temperature in emperor penguins diving under sea ice. *Comparative Biochemistry and Physiology Part A: Molecular & Integrative Physiology*, 135:477–487. [https://doi.org/10.1016/S1095-6433\(03\)00133-8](https://doi.org/10.1016/S1095-6433(03)00133-8)
- R.O., Berv, J.S., Dornburg, A., Field, D.J., Townsend, J.P., Lemmon, E.M., and Lemmon, A.R. 2015. A comprehensive phylogeny of birds (Aves) using targeted next-generation DNA sequencing. *Nature*, 526:569–U247. <https://doi.org/10.1038/nature15697>
- Raikow, R.J., Bicanovsky, L., and Bledsoe, A.H. 1988. Forelimb joint mobility and the evolution of wing-propelled diving in birds. *The Auk*, 105:446–451.
- Rambaut, A., Drummond, A.J., Xie, D., Baele, G., and Suchard, M.A. 2018. Posterior summarisation in Bayesian phylogenetics using Tracer 1.7. *Systematic Biology*, 67:901–904. <https://doi.org/10.1093/sysbio/syy032>
- Reddy, S., Kimball, R.T., Pandey, A., Hosner, P.A., Braun, M.J., Hackett, S.J., Han, K.-L., Harshman, J., Huddleston, C.J., and Kingston, S. 2017. Why do phylogenomic data sets yield conflicting trees? Data type influences the avian tree of life more than taxon sampling. *Systematic Biology*, 66:857–879. <https://doi.org/10.1093/sysbio/syx041>
- Reguero, M., Goin, F., Acosta Hospitaleche, C., Dutra, T., and Marensi, S. 2013. *Late Cretaceous/Paleogene West Antarctica Terrestrial Biota and its Intercontinental Affinities*. Springer, Dordrecht. <https://doi.org/10.1007/978-94-007-5491-1>
- Ronquist, F. and Huelsenbeck, J.P. 2003. MrBayes 3: Bayesian phylogenetic inference under mixed models. *Bioinformatics*, 19:1572–1574. <https://doi.org/10.1093/bioinformatics/btg180>
- Rouillard, P., Collot, J., Sutherland, R., Bache, F., Patriat, M., Etienne, S., and Maurizot, P. 2015. Seismic stratigraphy and paleogeographic evolution of Fairway Basin, Northern Zealandia, Southwest Pacific: From Cretaceous Gondwana breakup to Cenozoic Tonga–Kermadec subduction. *Basin Research*, 29:189–212. <https://doi.org/10.1111/bre.12144>
- Schreiweis, D.O. 1982. A comparative study of the appendicular musculature of penguins (Aves: Sphenisciformes). *Smithsonian Contributions to Zoology*, 341:1–46. <https://doi.org/10.5479/si.00810282.341>
- Scotese, C.R. 2002. PALEOMAP Project. <http://www.scotese.com>
- Scotese, C.R. 2016. PALEOMAP PaleoAtlas for GPlates and the PaleoData Plotter Program, PALEOMAP Project. <https://www.earthbyte.org/paleomap-paleoatlas-for-gplates/>
- Sharpe, R.B. 1891. A review of recent attempts to classify birds: An address delivered before the Second International Ornithological Congress on the 18th of May, 1891. Pub. at the Office of the congress.
- Shufeldt, R.W. 1901. Osteology of the penguins. *Journal of Anatomy and Physiology*, 35:390–405.
- Simões, T.R., Caldwell, M.W., Palci, A., and Nydam, R.L. 2017. Giant taxon? character matrices: Quality of character constructions remains critical regardless of size. *Cladistics*, 33:198–219. <https://doi.org/10.1111/cla.12163>
- Simpson, G.G. 1946. Fossil penguins. *Bulletin of the American Museum of Natural History*, 87:7–99.
- Simpson, G.G. 1971. A review of the pre-Pliocene penguins of New Zealand. *Bulletin of the American Museum of Natural History*, 144:323–378.
- Simpson, G.G. 1976. *Penguins: Past and Present, Here and There*. Yale University Press, New Haven and London.
- Simpson, G.G. 1979. Tertiary penguins from the Duinefontein site, Cape Province, South Africa. *Annals of the South African Museum Annale Van Die Suid-Afrikaanse Museum*, 79:1–7.

- Slack, K.E., Jones, C.M., Ando, T., Harrison, G.L., Fordyce, R.E., Arnason, U., and Penny, D. 2006. Early penguin fossils, plus mitochondrial genomes, calibrate avian evolution. *Molecular Biology and Evolution*, 23:1144–1155. <https://doi.org/10.1093/molbev/msj124>
- Stilwell, J.D. 2007. First record of Late Cretaceous Gastropoda (Mollusca) from the Takatika Grit, Chatham Islands, Southwest Pacific. *New Zealand Journal of Geology and Geophysics*, 50:21–25. <https://doi.org/10.1080/00288300709509816>
- Stilwell, J.D. 2016. Zealandia's oldest volutes (Mollusca: Gastropoda: Volutidae) from the early Paleogene of South Island and Chatham Islands: Post Gondwana break-up and evolutionary divergence. *Journal of Paleontology*, 90:31–42. <https://doi.org/10.1017/jpa.2016.19>
- Stilwell, J.D. and Consoli, C.P. 2012. Tectono-stratigraphic history of the Chatham Islands, SW Pacific—The emergence, flooding and reappearance of eastern 'Zealandia'. *Proceedings of the Geologists' Association*, 123:170–181. <https://doi.org/10.1016/j.pgeola.2011.06.003>
- Stilwell, J.D., Consoli, C.P., Sutherland, R., Salisbury, S., Rich, T.H., Vickers-Rich, P.A., Currie, P.J., and Wilson, G.J. 2006. Dinosaur sanctuary on the Chatham Islands, Southwest Pacific: First record of theropods from the K-T boundary Takatika Grit. *Palaeogeography Palaeoclimatology Palaeoecology*, 230:243–250. <https://doi.org/10.1016/j.palaeo.2005.07.017>
- Stonehouse, B. 1967. The general biology and thermal balances of penguins. *Advances in Ecological Research*, 4:131–196. [https://doi.org/10.1016/S0065-2504\(08\)60321-9](https://doi.org/10.1016/S0065-2504(08)60321-9)
- Storer, R.W. 1971. Adaptive radiation of birds. *Avian Biology*, 1:149–188.
- Sutherland, R. 1999. Basement geology and tectonic development of the greater New Zealand region: An interpretation from regional magnetic data. *Tectonophysics*, 308: 341–362. [https://doi.org/10.1016/S0040-1951\(99\)00108-0](https://doi.org/10.1016/S0040-1951(99)00108-0)
- Swofford, D.L. 2003. PAUP*. Phylogenetic analysis using parsimony (* and other methods). Version 4. Sinauer Associates, Sinauer Associates, Sunderland, Massachusetts. <http://phylosolutions.com>
- Tambussi, C.P., Acosta Hospitaleche, C., Reguero, M.A., and Marensi, S.A. 2006. Late Eocene penguins from West Antarctica: Systematics and biostratigraphy. *Geological Society, London, Special Publications*, 258:145–161. <https://doi.org/10.1144/GSL.SP.2006.258.01.11>
- Tambussi, C.P., Degrange, F.J., De Mendoza, R.S., Sferco, E., and Santillana, S. 2019. A stem anseriform from the early Palaeocene of Antarctica provides new key evidence in the early evolution of waterfowl. *Zoological Journal of the Linnean Society*, 186:673–700. <https://doi.org/10.1093/zoolinnean/zly085>
- Tambussi, C.P., Reguero, M.A., Marensi, S.A., and Santillana, S.N. 2005. *Crossvallia unienwillia*, a new Spheniscidae (Sphenisciformes, Aves) from the late Paleocene of Antarctica. *Geobios*, 38:667–675. <https://doi.org/10.1016/j.geobios.2004.02.003>
- Thomas, D.B. and Fordyce, R.E. 2007. The heterothermic loophole exploited by penguins. *Australian Journal of Zoology*, 55:317–321. <https://doi.org/10.1071/ZO07053>
- Thomas, D.B., Ksepka, D.T., and Fordyce, R.E. 2011. Penguin heat-retention structures evolved in a greenhouse Earth. *Biology Letters*, 7:461–464. <https://doi.org/10.1098/rsbl.2010.0993>
- Thomas, G.H. 2015. Evolution: An avian explosion. *Nature*, 526:516–517. <https://doi.org/10.1038/nature15638>
- Tulloch, A.J., Mortimer, N., Ireland, T.R., Waight, T.E., Maas, R., Palin, J., Sahoo, T., Seebeck, H., Sagar, M.W. and Barrier, A. 2019. Reconnaissance basement geology and tectonics of South Zealandia. *Tectonics*, 38:516–551. <https://doi.org/10.1029/2018TC005116>
- van Tuinen, M., Butvill, D.B., Kirsch, J.A.W., and Hedges, S.B. 2001. Convergence and divergence in the evolution of aquatic birds. *Proceedings of the Royal Society of London B: Biological Sciences*, 268:1345–1350. <https://doi.org/10.1098/rspb.2001.1679>
- Walker, B.G. and Boersma, P.D. 2003. Diving behavior of Magellanic penguins (*Spheniscus magellanicus*) at Punta Tombo, Argentina. *Canadian Journal of Zoology*, 81:1471–1483. <https://doi.org/10.1139/z03-142>
- Watanuki, Y. and Burger, A.E. 1999. Body mass and dive duration in alcids and penguins. *Canadian Journal of Zoology*, 77:1838–1842. <https://doi.org/10.1139/z99-157>
- West, A.R., Torres, C.R., Case, J.A., Clarke, J.A., O'Connor, P.M., and Lamanna, M.C. 2019. An avian femur from the Late Cretaceous of Vega Island, Antarctic Peninsula: Removing the record of cursorial landbirds from the Mesozoic of Antarctica. *PeerJ*, 7:e7231. <https://doi.org/10.7717/peerj.7231>
- Wiens, J.J. 2003. Missing data, incomplete taxa, and phylogenetic accuracy. *Systematic Biology*, 52:528–538. <https://doi.org/10.1080/10635150390218330>

- Wiens, J.J. 2005. Can incomplete taxa rescue phylogenetic analyses from long-branch attraction? *Systematic Biology*, 54:731–742. <https://doi.org/10.1080/10635150500234583>
- Wiens, J.J. 2006. Missing data and the design of phylogenetic analyses. *Journal of Biomedical Informatics*, 39:34–42. <https://doi.org/10.1016/j.jbi.2005.04.001>
- Wiens, J.J., Fetzner Jr, J.W., Parkinson, C.L., and Reeder, T.W. 2005. Hylid frog phylogeny and sampling strategies for speciose clades. *Systematic Biology*, 54:778–807. <https://doi.org/10.1080/10635150500234625>
- Wiens, J.J. and Moen, D.S. 2008. Missing data and the accuracy of Bayesian phylogenetics. *Journal of Systematics and Evolution*, 46:307–314.
- Wiens, J.J. and Morrill, M.C. 2011. Missing data in phylogenetic analysis: Reconciling results from simulations and empirical data. *Systematic Biology*, 60:719–731. <https://doi.org/10.1093/sysbio/syr025>
- Wiens, J.J. and Reeder, T.W. 1995. Combining data sets with different numbers of taxa for phylogenetic analysis. *Systematic Biology*, 44:548–558. <https://doi.org/10.2307/2413660>
- Wiens, J.J. and Tiu, J. 2012. Highly incomplete taxa can rescue phylogenetic analyses from the negative impacts of limited taxon sampling. *PLoS ONE*, 7:e42925 (42921–42928). <https://doi.org/10.1371/journal.pone.0042925>
- Wilkinson, M. 1995. Coping with abundant missing entries in phylogenetic inference using parsimony. *Systematic Biology*, 44:501–514. <https://doi.org/10.1093/sysbio/44.4.501>
- Willener, A.S.T., Handrich, Y., Halsey, L.G., and Strike, S. 2016. Fat king penguins are less steady on their feet. *PLoS ONE*, 11:e0147784 (0147781–0147789). <https://doi.org/10.1371/journal.pone.0147784>
- Wiman, C. 1905a. Vorläufige Mitteilung über die alttertiären Vertebraten der Seymourinsel. *Bulletin of the Geological Institute of Upsala*, 6:247–253
- Wiman, C. 1905b. Über die alttertiären Vertebraten der Seymourinsel. *Wissenschaftliche Ergebnisse der Schwedischen Südpolar-Expedition 1901–1903*, 3:1–37.
- Worthy, T.H. 2012. A phabine pigeon (Aves: Columbidae) from Oligo-Miocene Australia. *Emu-Austral Ornithology*, 112:23–31. <https://doi.org/10.1071/MU11061>
- Wright, A.M. and Hillis, D.M. 2014. Bayesian analysis using a simple likelihood model outperforms parsimony for estimation of phylogeny from discrete morphological data. *PLoS ONE*, 9:e109210 (109211–109216). <https://doi.org/10.1371/journal.pone.0109210>
- Zachos, J.C., Dickens, G.R., and Zeebe, R.E. 2008. An early Cenozoic perspective on greenhouse warming and carbon-cycle dynamics. *Nature*, 451:279–283. <https://doi.org/10.1038/nature06588>
- Zinoviev, A.V. 2010. *Comparative Anatomy, Structural Modifications and Adaptive Evolution of Avian Apparatus of Bipedal Locomotion*. KMK Scientific Press Ltd, Moscow.
- Zinoviev, A.V. 2015. Comparative anatomy of the intertarsal joint in extant and fossil birds: Inferences for the locomotion of *Hesperornis regalis* (Hesperornithiformes) and *Emeus crassus* (Dinornithiformes). *Journal of Ornithology*, 156:317–323. <https://doi.org/10.1007/s10336-015-1195-4>

APPENDIX 1

Chatham Island Paleocene fossils provide insight into the palaeobiology, evolution, and diversity of early penguins (*Aves*, *Sphenisciformes*)

CT SCANNED SPECIMENS

The positioning of bones encased within the hard lithological blocks that were CT scanned (see Materials and Methods), NMNZ S.47302 and S.47303, are indicated in Figure A1 and A2 respectively. CT scanning and manipulation using *Materialise Mimics* also permitted insight into the cross-section of long bones in NMNZ S.47303 (Figure A3).

LINKING OF SPECIMENS

All specimens of *Kupoupou stilwelli* n. gen. et sp. were linked through overlapping skeletal elements (Figure A4), as well as both being found in the “bird horizon” of the Takatika Grit rock unit, and same general locality. These specimens also all share a similar size range, with intraspecific variation taken into account.

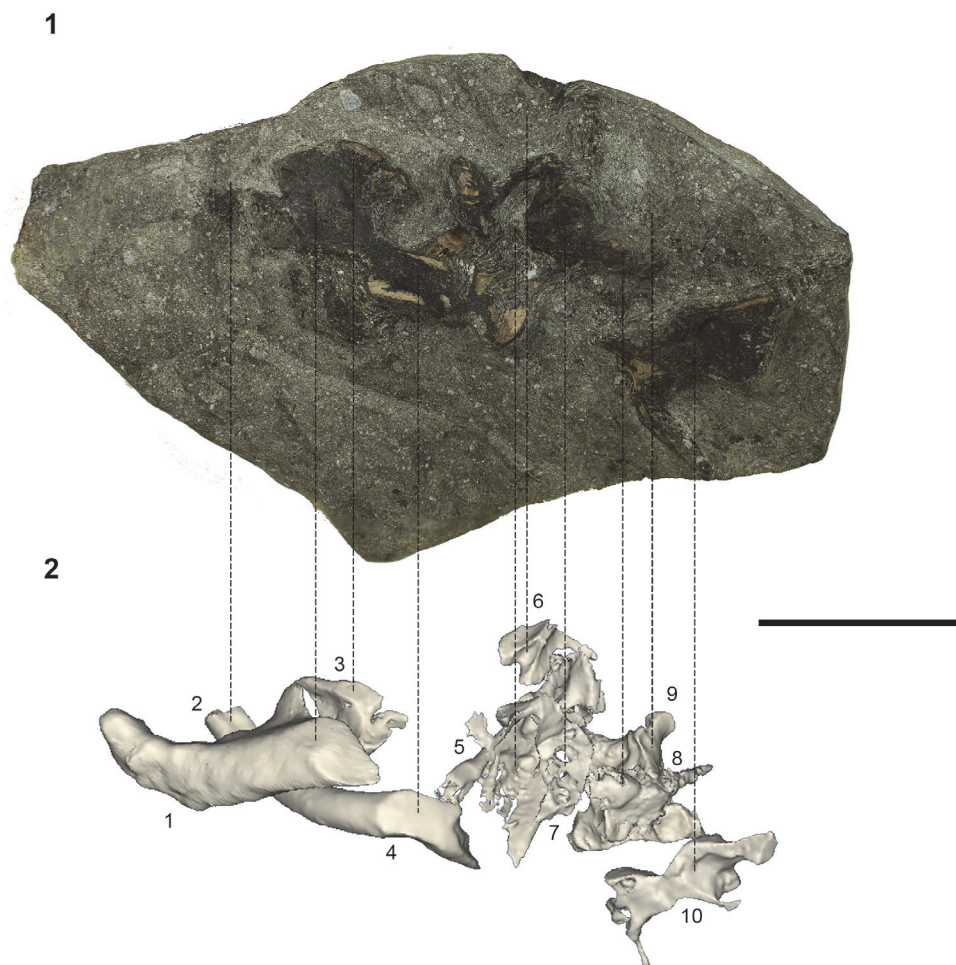


FIGURE A1. NMNZ S.47302, **1**, the extent of the specimen that has been physically prepared, **2**, the three-dimensionally rendered elements within the block. Fossils numbered in **2** are as follows: **1**, coracoid; **2**, unidentified, possibly a radiale; **3**, sternum; **4**, furcula; **5**, mandible; **6**, cervical vertebra; **7**, unidentified; **8**, unidentified; **9**, cervical vertebra IV; **10**, unidentified. Scale bar is equal to 50 mm.

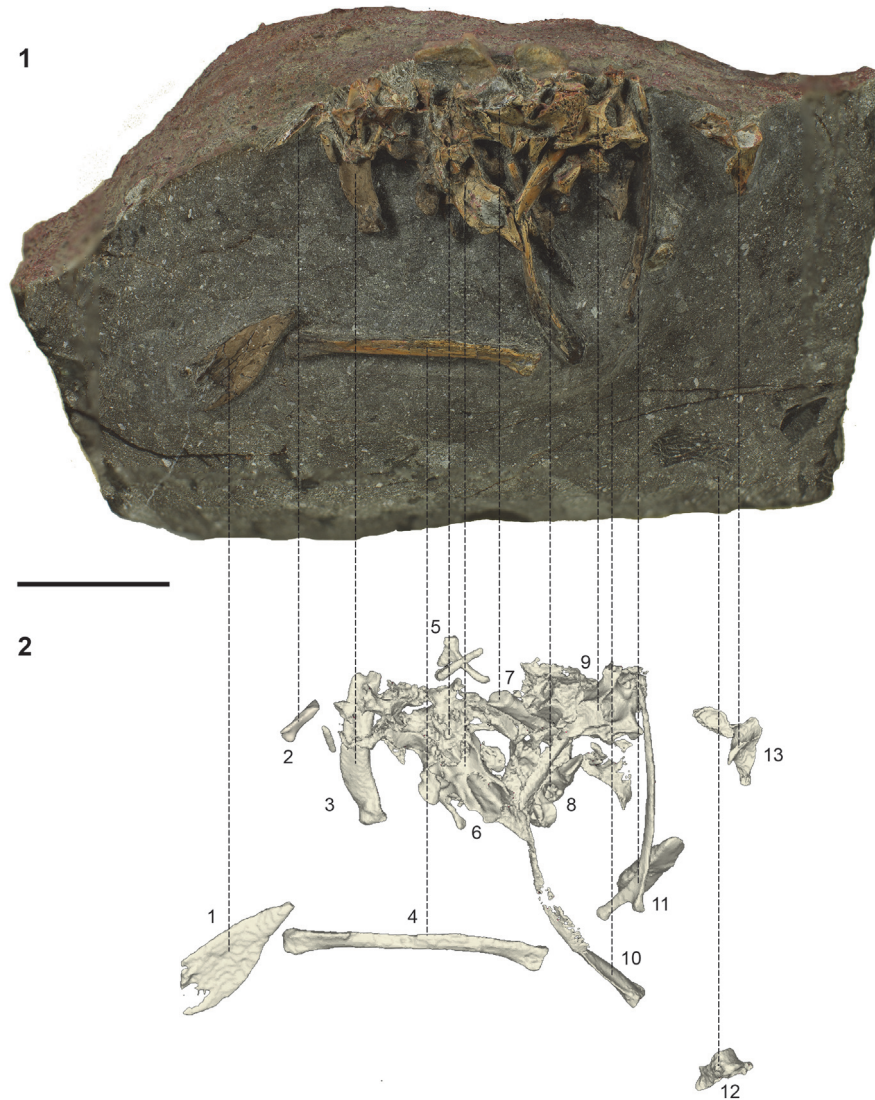


FIGURE A2. NMNZ S.47303, **1**, the extent of the specimen that has been physically prepared, **2**, the three-dimensionally rendered elements within the block. Fossils numbered in **2** are as follows: **1**, ischium; **2**, manus phalanx III-1; **3**, radius; **4**, radius; **5**, cervical vertebra, Table 1 cervical (iv), Figure 2.25-30; **6**, cervical vertebra, Table 1 cervical (iii), Figure 2.19-24; **7**, carpometacarpus; **8**, cervical vertebra, Table 1 cervical (ii), Figure 2.13-18; **9**, possibly cervical vertebra III, Table 1 cervical (i), Figure 2.7-12; **10**, manus phalanx II-1; **11**, rib; **12**, caudal vertebra; **13**, axis. Scale bar is equal to 50 mm.

UNDESCRIBED ELEMENTS

Elements that could not be confidently identified are indicated in Figure A1 and A2. Various elements were also considered too incomplete and/or too uninformative to be formally described in the main text. These elements, consisting of ribs and vertebrae, are displayed in Figure A5.

PHYLOGENETIC ANALYSES

GenBank molecular sequences

Molecular data (Table A1) were used as per the corrected dataset of Ksepka et al. (2012), available from Dryad (<http://datadryad.org>). See Ksepka et al. (2012) for references related to GenBank accession numbers. Genetic data for *Phaethon rubricauda* was added: AF158251, Stanley and Harrison (1999).

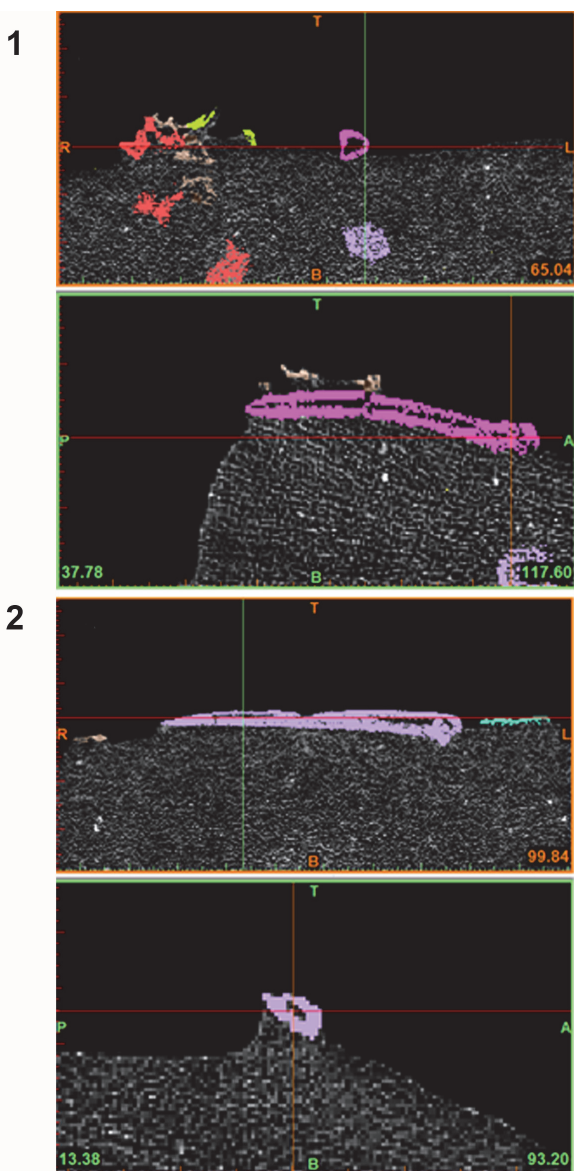


FIGURE A3. NMNZ S.47303 in *Materialise Mimics*, cross-sectional view of right radius (Figure 5.7, 5.9-10) in top two images, **1**, and left radius (Figure 5.6-11) in two lower images, **2**. Cross-sectional perspective reveals a reduced marrow-cavity compared to modern aerially flighted birds, but not as dense as extant penguins.

Parsimony analysis of larger Chatham Island specimens as separate taxa

Both NMNZ S.47302 and NMNZ S.47304 were treated as separate taxa in preliminary phylogenetic analyses to test whether they were compatible to be combined in further analyses. Except for this taxonomic modification, parsimony-based analysis using the same specifications as the primary search strategy produced 13,600 MPTs, $L = 5,245$ steps, $CI = 0.5239$, $RI = 0.7015$, $HI = 0.4761$.

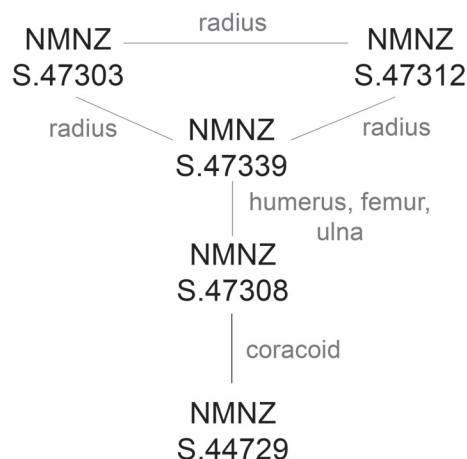


FIGURE A4. How specimens associated with *Kupou pou stilwelli* n. gen. et sp. are linked together through overlapping elements.

After pruning of taxa as per the primary analysis 9,586 non-duplicate MPTs were retained, $L = 5,233$, $CI = 0.5251$, $RI = 0.7070$, $HI = 0.4749$.

Following pruning, the strict consensus program recovered both of these specimens positioned on a large polytomy with several Eocene species and all Paleocene taxa except for *Waimanu manneringi* and *Muriwaimanu tuatahi*—which exist as a separate basal clade. The majority rule consensus (50%) tree (Figure A6) recovered better topological resolution, where the Waipara giant penguin is positioned one node crownwards of the Sphenisciformes base, and *K. stilwelli* n. gen. et sp., *C. unienwillia*, *K. maxwelli*, and a branch leading to a nested clade of *S. rosieae* and ?*C. waiparensis* are another node crownwards. NMNZ S.47304, *K. biceae*, and NMNZ S.47302 exist at separate nodes in succession respectively towards crown group Sphenisciformes.

While it is recognised that these two specimens were found at different topological positions in the majority-rule (50%) consensus tree, the recovery of *K. biceae* (and NMNZ S.47302) one node crownwards of NMNZ S.47304 was found in only 61% of MPTs, and similarly the positioning of NMNZ S.47302 a node crownwards of *K. biceae* occurred only in 53% of MPTs. This implies that a sizeable percentage of MPTs recovered these taxa in different topological positions. This uncertainty is illustrated in the poorly resolved strict consensus tree. Moreover, NMNZ S.47302 was found to have extremely high levels of taxon instability among trees, compared to other fossil and extant taxa (as well as compared to when both NMNZ S.47302

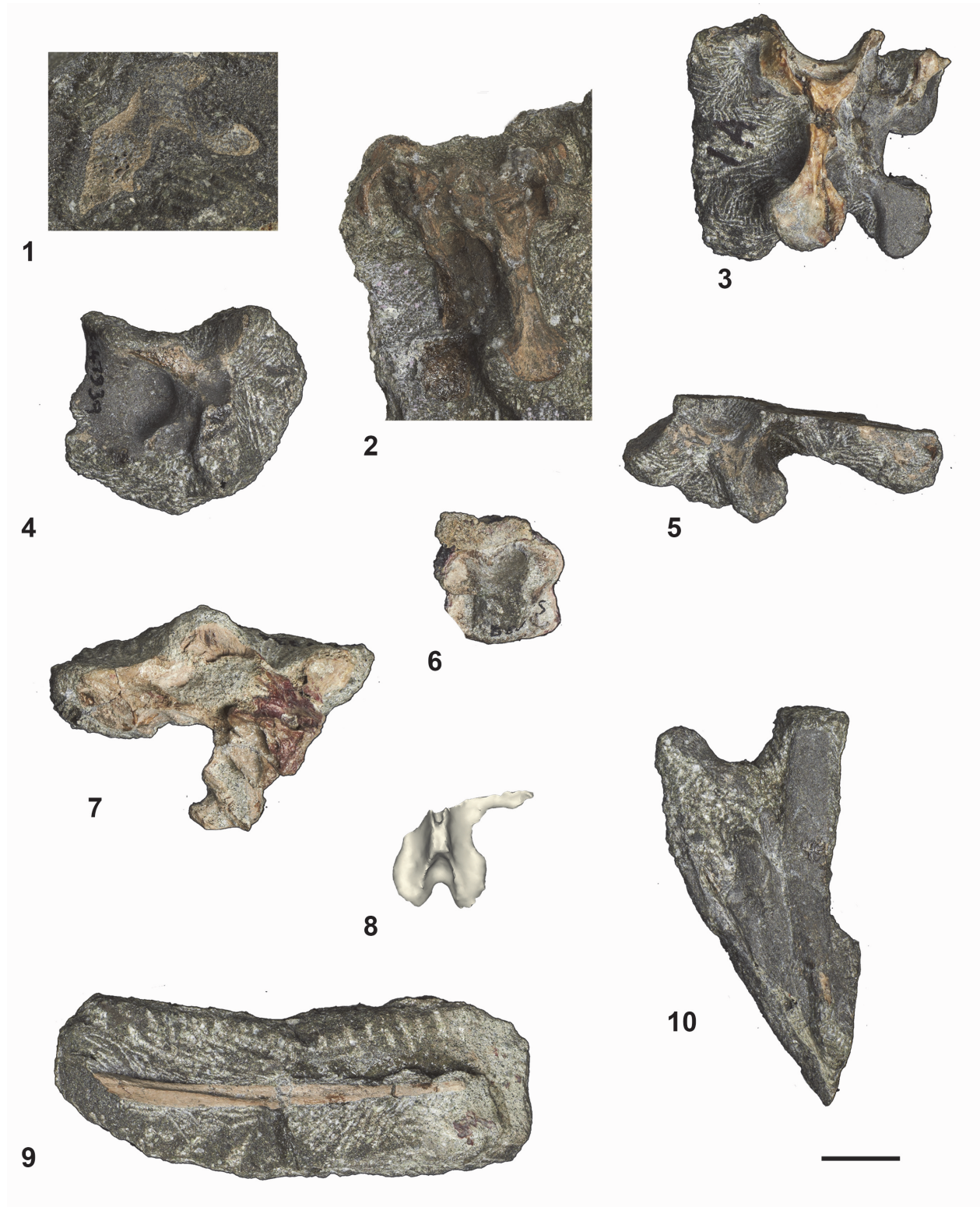


FIGURE A5. Undescribed vertebrae and ribs referred to *Kupoupou stilwelli* n. gen. et sp. **1-7**, vertebrae, NMNZ S.47339; and **9** and **10**, ribs, NMNZ S.47339. **8**, an incomplete vertebra, is part of NMNZ S.47302, associated with the larger Chatham Island form. Scale bar is equal to 10 mm.

TABLE A1. GenBank accession numbers for molecular sequences used in phylogenetic analyses.

Taxon	12S rDNA	16S rDNA	COI	Cytochrome <i>b</i>	RAG-1
<i>A. forsteri</i>	DQ137187	DQ137147	DQ137185	DQ137225	DQ137246
<i>A. patagonicus</i>	AY139221	DQ137148	DQ137186	AY138623	DQ137247
<i>D. capense</i>	X82517	—	—	AF076046	—
<i>D. exulans</i>	DQ137205	DQ137165	DQ137168	DQ137208	DQ137229
<i>E. chrysocome</i>	AY139630	—	DQ525796	—	DQ525776
<i>E. chrysolophus</i>	DQ137197	DQ137157	DQ137171	AF076052	DQ137223
<i>E. filholi</i>	DQ525741	—	DQ525781	—	DQ525761
<i>E. moseleyi</i>	DQ525746	—	DQ525786	—	DQ525766
<i>E. pachyrhynchus</i>	U88007, X82522	DQ137152	DQ137170	DQ137210	DQ137231
<i>E. robustus</i>	DQ137193	DQ137153	DQ137176	DQ137126	DQ137237
<i>E. schlegeli</i>	DQ137196	DQ137156	DQ137175	DQ137215	DQ137236
<i>E. sclateri</i>	DQ137194	DQ137154	DQ137169	DQ137309	DQ137230
<i>E. minor</i>	NC004538	DQ137164	DQ137174	NC 004538	DQ137235
<i>G. immer</i>	AF173577	DQ137166	DQ137167	DQ137207	DQ137288
<i>G. stellata</i>	AF173587	AY293618	AY666477	AF158250	—
<i>M. giganteus</i>	X82523	—	—	AF076060	—
<i>M. antipodes</i>	DQ137198	DQ137158	DQ137184	DQ137224	DQ1372245
<i>O. oceanicus</i>	—	—	DQ433048	AF076062	—
<i>O. leucorhoa</i>	—	—	AY666284	AF076064	—
<i>P. desolata</i>	—	—	—	AF076068	—
<i>P. urinatrix</i>	X82518	—	—	AF076076	DQ881818
<i>P. immutabilis</i>	—	—	DQ433933	PIU48949	—
<i>P. palpebrata</i>	—	—	—	U48943	DQ881822
<i>P. aequinoctialis</i>	—	—	—	U74350	—
<i>P. brevirostris</i>	NC007174	NC007174	NC007174	NC007174	—
<i>P. gravis</i>	AF175572	AF173752	DQ434014	U74354	—
<i>P. adeliae</i>	AF173573	DQ137149	DQ137183	DQ137223	DQ137224
<i>P. antarctica</i>	DQ137190	DQ137150	DQ137181	AF076089	DQ137242
<i>P. papua</i>	DQ137191	DQ137151	DQ137182	AF076090	DQ137243
<i>S. demersus</i>	DQ137199	DQ137159	DQ137177	DQ137217	DQ137238
<i>S. humboldti</i>	DQ137201	DQ137161	DQ137180	DQ137220	DQ137241
<i>S. magellanicus</i>	DQ137200	DQ137160	DQ137178	DQ137218	DQ137239
<i>S. mendiculus</i>	DQ137202	DQ137162	DQ137179	DQ137219	DQ137240
<i>T. melanophrys</i>	AY158677	AY158677	NC_007172	U48955	AY158677
<i>P. rubricauda</i>	—	—	—	AF158251	—

and S.47304 were merged). Relatively poor representation of NMNZ S.47302, S.47304 and most fossil taxa in the phylogenetic datamatrix compared to extant counterparts also precludes a robust phylogenetic hypothesis for stem relationships (though may be more beneficial than not having a hypothesis at all, see Wiens and Reeder, 1995; Wiens, 2003).

With the information at-hand, considering that these specimens were recovered at the same node in the strict consensus tree, we interpret these specimens as compatible to include as a single merged taxon for final analyses (larger Chatham Island form). Their merging is also supported by their recovery in the same approximate location, from the same horizon of the Takatika Grit on Chatham Island, as well as their comparable size. It



FIGURE A6. Majority-rule consensus (50%) tree treating NMNZ S.47302 and S.47304 as separate taxa (13,600 MPTs, L = 5,233 steps, CI = 0.5251, RI = 0.7020). Percentage of MPTs recovering each node is indicated at each internode in the consensus tree, and bootstrap support values (over 40% only) are numbered below them italicised in red.

should be noted, however, that without overlapping skeletal elements between specimens they cannot be considered as the same taxon with certainty.

Parsimony analyses excluding referred specimens of Seymour Island taxa

A preliminary analysis excluding scorings relating to all specimens referred to Seymour Island taxa was also performed. Removed codings pertained to the following taxa, which were effectively only represented by holotype specimens in the phylogenetic data matrix: *Marambiornis exilis*, *Mesetaornis polaris*, *Palaeudyptes klekowskii*, *Palaeudyptes gunnari*, *Anthropornis* sp. UCMP 321023, *Anthropornis nordenskjoeldi*, *Anthropornis grandis*, *Notodyptes wimani*, *Delphinornis gracilis*, *Delphinornis arctowskii*, and *Delphinornis larseni*. Testing the exclusion of these taxa was considered necessary due to the phylogenetic uncertainty many of these taxa create, in having been named on single elements, and additional bones uncertainly referred (see Jadwiszczak, 2006a; Jadwiszczak, 2006b; Ksepka and Clarke, 2010), to assess whether the removal of referred elements had a profound effect on topology and support values.

Parsimony-based analysis was conducted using the same specifications as the primary search strategy, with the exception of additionally excluded taxa. This produced 400 MPTs (L = 5256, RI = 0.7145, CI = 0.5240, HI = 0.4772), 340 of which were not duplicates following the pruning of further taxa (as per primary analysis), L = 5,212, RI = 0.7014, CI = 0.5272, HI = 0.4728. The strict consensus tree recovered *W. manningi* and *M. tuatahi* as sister taxa that branch from the base of Sphenisciformes. The Waipara giant penguin is positioned one node crownwards of the sphenisciforms base in all MPTs. All other Paleocene taxa and Eocene taxa such as *Mesetaornis*, *Delphinornis* and *Marambiornis* exist in an unresolved polytomy one node crownwards of the Waipara giant penguin in the strict consensus tree. The majority-rule (50%) consensus tree provides better resolution to this polytomy (Figure A7), where in 63% of MPTs *C. unienwillia*, *?C. waiparensis*, and *S. rosieae* form a clade that branches from this node, where the latter two have a sister taxon relationship. *K. stilwelli* n. gen. et sp. is recovered one node crownwards of this node, in 63% of MPTs. In 69% of MPTs, crownwards of this node, the larger Chatham Island form, *K. maxwelli*, *Delphinornis arctowskii* and *Delphinornis larseni* occupy an unresolved polytomy with a nested clade consist-

ing of *Delphinornis gracilis*, *Mesetaornis polaris* and *Marambiornis exilis* in 51% of shortest trees. *K. biceae* is positioned one node crownwards of this polytomy in 69% of MPTs.

In most MPTs exclusion of material referred to Seymour Island taxa revealed some novel pairings of taxa compared to the primary search strategy (Figure 13). The late early-middle Paleocene larger Chatham Island form was recovered alongside Eocene forms, and late Paleocene *K. biceae* was recovered crownwards of some Eocene sphenisciforms, which, while not implausible, would imply an evolutionary scenario where *Delphinornis*, *Marambiornis*, *Kaiika*, and *Mesetaornis* exist on long branches. However, since this relationship was not found in a supermajority of trees, and is not supported by high bootstrap values, this topology cannot be treated with confidence. More material associated with each taxon is needed to inform more completely on the skeleton of each of these early penguins, in order to substantiate relational assessments. While the Seymour Island taxa often lack definitive material compared to each taxon, we opt to include material that has been referred, to more completely sample the skeletons of these taxa as is currently understood, to better represent them in the data matrix and test them phylogenetically among other penguins. Additionally, considering the exclusion of Eocene Seymour Island penguins did not considerably improve topological resolution, nor bootstrap support values, the exclusion of material referred to Seymour Island taxa was not deemed appropriate.

Final parsimony analysis

The strict consensus tree of the 16,300 MPTs (length = 5,234) is shown in Figure A8. Of these MPTs, 6,590 different topological variations of the shortest tree were retained following pruning, a sample of which, relating to Paleocene taxa, are shown in Figure A9.

Ages for taxa

The majority of ages for taxa as illustrated in Figure 13 are based on those given in Gavryushkina et al. (2017). Ages for taxa that were not included in Gavryushkina et al. (2017) are given here:

Anthropodyptes gilli—17.6-21.0. Park and Fitzgerald (2012) list this taxon as early Miocene in age between 17.6 and 21.0 million years ago.

Anthropornis sp. UCMP 321023—34-52.5 Ma. This fossil, which represents an unique *Anthropornis* species that has not been formally named, comes from the La Meseta Formation, Seymour Island, Antarc-



FIGURE A7. Majorite-rule consensus (50%) tree excluding character scores relating to referred material of Eocene Seymour Island taxa (400 MPTs, L = 5,212, RI = 0.7014, CI = 0.5272). Percentage of MPTs recovering each node is indicated at each internode in the consensus tree, and bootstrap support values (over 40% only) are numbered below them italicised in red.



FIGURE A8. Strict consensus tree of 16,300 MPTs (length = 5,234). Bootstrap support values (over 40% only) are numbered below each node italicised in red.

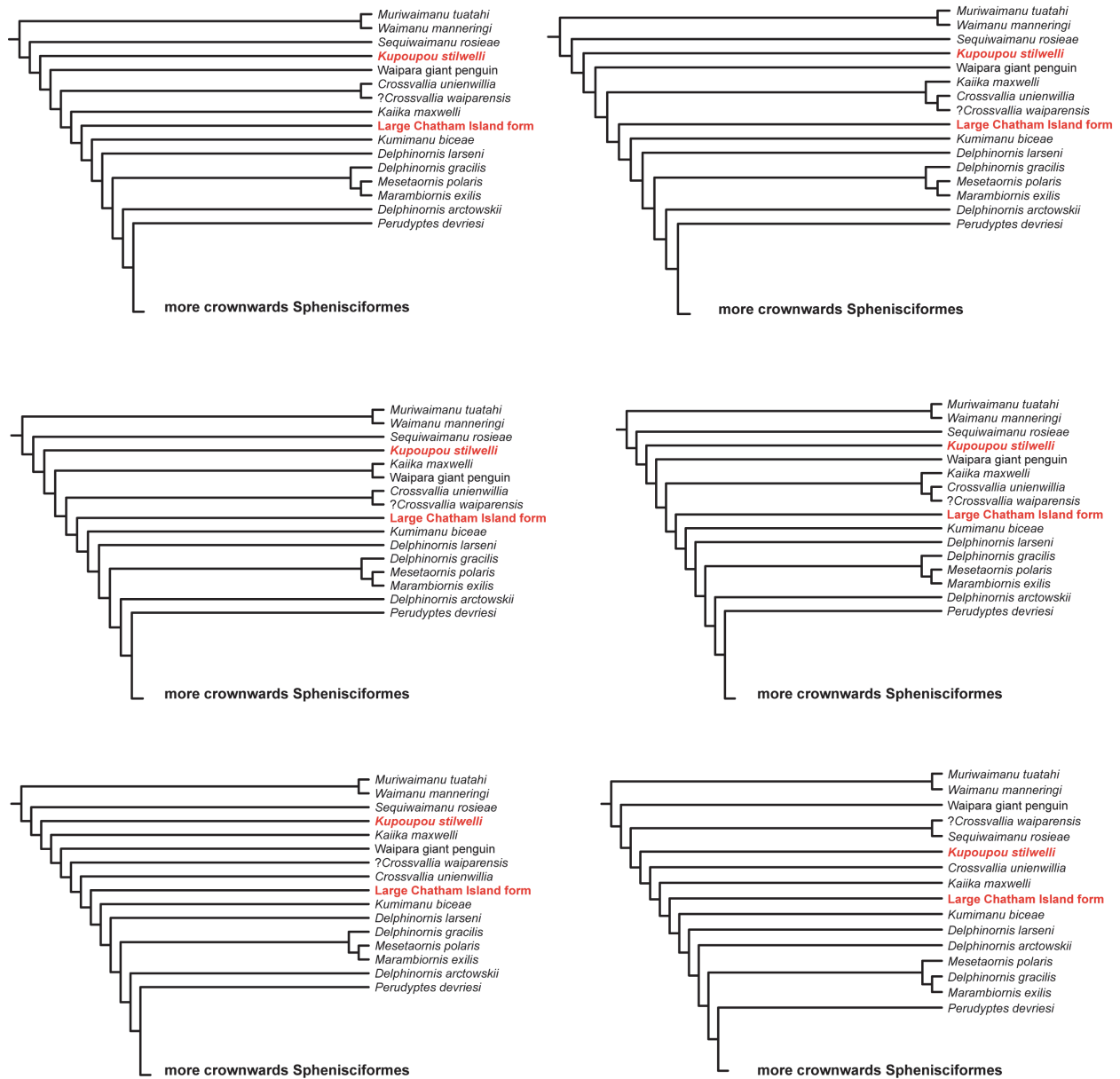


FIGURE A9. A sample of the variety of equally parsimonious phylogenetic relationships recovered between Paleocene taxa (length = 5,234).

tica (Ksepka, 2007). It is given the same age range as both *A. nordenskoeldi* and *A. grandis*.

Arthrodytes andrewsi—23.8-25.9 Ma. Bajo de San Julián (Acosta Hospitaleche and Tambussi, 2008), or lower “Patagonian Formation” (Simpson, 1972), Santa Cruz Province, Patagonia, South America, a conservative age range spans both the lower Gran Bajo Member and the upper Meseta Chica Member, and is constrained between 23.83 and 25.93 Ma after Parras et al. (2008).

Crossvallia unienwillia—56-59.2 Ma. The holotype was recovered from the Cross Valley C Allomember,

and is cited as Thanetian in age in Jadwiszczak et al. (2013).

?Crossvallia waiparensis—59-61.5 Ma. This taxon was described from fossils from site S2, of the Mt. Ellen Member concretionary member (as indicated in Mayr et al., 2018), of the Waipara Greensand, Waipara River, Canterbury, New Zealand (Mayr et al., 2019). It is therefore considered to be of within the same age range as *Sequiwaimanu rosieae*, the holotype of which was also recovered from this site (see below).

Eudyptes calauina—2.58-5.3 Ma. From the Horcon Formation, Chile, attributed to Late Pliocene in age

Chávez Hoffmeister et al. (2014). We conservatively bound the age of this taxon from the base of the Pliocene to the latest Pliocene.

Hakataramea penguin—21.7-25.2 Ma. From Hakataramea Valley, New Zealand, material associated with this taxon was recovered from the Otekaike Limestone, and is Waitakian in age (Ando, 2007).

Inguza predemersus—2.58-5.25 Ma. Associated with Langebaanweg, Cape Province, South Africa, the holotype is associated with the Muishond Fontein Phosphatic Sand Member of the Varswater Formation (Simpson, 1971a; Ksepka and Thomas, 2012), where fossils are inferred to be 5.15 ± 0.1 Ma (Roberts et al., 2011). This taxon is therefore conservatively bounded between the earliest Pliocene and the overlying Pleistocene Langebaan Formation (Roberts et al., 2011).

Kaiika maxwelli—50-63 Ma. The holotype and only known specimen was recovered in a concretion from the southern bank of the Waihao River, South Canterbury, New Zealand. The age of the specimen is uncertain, and may have originated from the Kauru Formation, as discussed in Fordyce and Thomas (2011). While the age of the Kauru Formation at the source location is problematic, the age is cited as Waipawan or Mangaorapan, but molluscs in the lower Waihao Kauru Formation characteristic of the Wangaloan Stage increases the possible age range into the Paleocene (Fordyce and Thomas, 2011). Thus, we have opted for a conservative age estimate bounded between the uppermost Mangaorapan (50 Ma) and the middle Teurian (63 Ma).

Kumimanu biceae—55.5-59.5 Ma. Mayr et al. (2017b) note that the holotype is associated with the Moeraki Formation, and is dated to the late Teurian between 55.5 and 59.5 Ma.

Nucleornis insolitus—2.58-5.25 Ma. Discovered at Koeberg Nuclear Power Station, Cape Province, South Africa, the holotype is associated with the Muishond Fontein Phosphatic Sand Member of the Varswater Formation (Simpson, 1979; Ksepka and Thomas, 2012), where fossils are inferred to be 5.15 ± 0.1 Ma (Roberts et al., 2011). This taxon is therefore conservatively bounded between the earliest Pliocene and the overlying Pleistocene Langebaan Formation (Roberts et al., 2011).

Palaeudyptes marplei—34.6-39.1 Ma. Material attributed to this species were recovered from the Burnside Mudstone, Kaiatan or Runangan in age (Simpson, 1971b). Based on Raine et al. (2015) this constrains the taxon's age between 34.6 and 39.1 Ma.

Parapternyx antarcticus—17.9-22.1 Ma. We revised the possible age range of *P. antarcticus* from what was used in Gavryushkina et al. (2017) based on $^{87}\text{Sr}/^{86}\text{Sr}$ dates of the Monte León Formation,

between 17.91 Ma at the top of the Formation, and 22.12 Ma as an older limit (Parras et al., 2012).

Parapternyx brodkorbi—23.8-25.9 Ma. From the San Julián Formation or lower "Patagonian Formation", Patagonia, South America (Simpson, 1972; Ksepka and Ando, 2011), a conservative age range spans both the lower Gran Bajo Member and the upper Meseta Chica Member, and is constrained between 23.83 and 25.93 Ma after Parras et al. (2008).

Parapternyx robustus—23.8-25.9 Ma. From the San Julián Formation or lower "Patagonian Formation", Patagonia, South America (Simpson, 1972; Ksepka and Ando, 2011), a conservative age range spans both the lower Gran Bajo Member and the upper Meseta Chica Member, and is constrained between 23.83 and 25.93 Ma after Parras et al. (2008). Material attributed to this taxon from Bahía Inglesa, Chile were shown to be unreliable by Chávez (2007).

Platydyptes amiesi—21.7-27.3 Ma. The holotype is Waitakian of the Hakataramea Valley, New Zealand (Marples, 1952), and material referred to this taxon may also be associated with the Duntroonian Stage (Simpson, 1971b). Based on the dates given in (Raine et al., 2015), this taxon is therefore constrained between the base of the Duntroonian as an older age limit (27.3 Ma), and the base of the Otaian Stage as the younger age limit (21.7 Ma).

Pseudapternyx macraei—5.0-6.0 Ma. Park and Fitzgerald (2012) list this taxon as ranging from the late Miocene (6 Ma) to early Pliocene (5 Ma).

SAM P7158 cf. *Palaeudyptes*—36.5-38 Ma. In a review of Australian fossil penguins Park and Fitzgerald (2012) list SAM P7158 as Late Eocene in age between 36.5 and 38 Ma.

Sequiwaimanu rosieae—59-61.5 Ma. Recovered from the Waipara Greensand near the position of where the holotype of *Waimanu manningi* was discovered, this material is dated to the early late Teurian (Mayr et al., 2018), about 61 Ma. A conservative age range to conform to early late Teurian dates based on Raine et al. (2015) potentially constrains the fossils between the base age of the upper Teurian of 61.5 Ma and a lower limit of 59 Ma.

Sphenisciformes indet. NMV P221273—7.25-7.92 Ma. This specimen was recovered from the lower light grey unit of the Port Campbell Limestone, Portland Bay, Victoria, Australia, and is described as Tortonian in age (Park et al., 2016).

Sphenisciformes indet. SAM P10863—23-30 Ma. The partial right humerus of SAM P10863 was recovered from the Gambier Limestone, Mt Gambier, South Australia, and is given an age of ~23-30 Ma in a review of Australian fossil penguins (Park and Fitzgerald, 2012).

Waipara Greensand giant penguin CM 2016.158.1—59-61.5 Ma. This specimen was recovered from the Waipara Greensand 11 m above those where the

holotype of *Waimanu manningi* was discovered, and is dated to the early late Teurian (Mayr et al., 2017a), about 61 Ma. A conservative age range to conform to early late Teurian dates based on Raine et al. (2015) potentially constrains the fossils between the base age of the upper Teurian of 61.5 Ma and a lower limit of 59 Ma.

COMPARATIVE MATERIAL

Specimens examined

Specimens examined for each referred species, and any coding changes for characters are listed in Table A2. Note that for species that were newly coded in full, such as *Phaethon rubricauda*, *Kupoupou stilwelli* n. gen. et sp., the Large Chatham Island form, and *?Crossvallia waiparensis*, coding of these taxa is available in the NEXUS file of the Chatham matrix.

HYPOTARSUS MORPHOLOGY

Inconsistencies exist in the literature regarding how specific features of the hypotarsus are labelled, on the proximal tarsometatarsus, in Sphenisciformes. Building on the work of Jadwiszczak (2015), we have labelled structures of hypotarsus of various sphenisciforms to conform with the terminology specified in Mayr (2016), as shown in Figure A10.

MORPHOLOGICAL CHARACTER DEFINITIONS AND STATES

Citations corresponding to where each character definition originated is indicated by the following abbreviations: New characters or those that have been modified in this study are also indicated. A, Ando (2007); AH, Acosta Hospitaleche et al. (2007); BG, Bertelli and Giannini (2005); C, Clarke et al. (2007); CHa, Chávez Hoffmeister et al. (2014); CHb, Chávez Hoffmeister (2014b); CL, Clarke et al. (2010); D, Degrange et al. (2018); GB, Giannini and Bertelli (2004); K, Ksepka et al. (2006); KC, Ksepka and Clarke (2010); KT, Ksepka and Thomas (2012); KF, Ksepka et al. (2012); LZ, Livezey and Zusi (2007); M, Mayr et al. (2017b); OH, O'Hara (1989).

Integument:

1. Tip of mandibular rhamphotheca, profile in lateral view: pointed (0); slightly truncated (1); strongly truncated, squared off (2); truncated but with a rounded margin (procellariiform-like) (3). (GB1)
2. Longitudinal grooves on base of culmen: absent (0); present (1). (GB2)
3. Longitudinal grooves on base of latericorn and ramicorn: absent (0); present (1). (GB3)
4. Feathering of maxilla: totally unfeathered (0); slightly feathered, less than half the length of maxilla feathering that reaches half the length of maxilla. (GB4) Ordered.
5. Ramicorn, inner groove at tip: absent (0); present and single (1); present and double (2). (GB5) Ordered.
6. Orange or pink plate on ramicorn: absent (0); present (1). (GB6)
7. Plates of rhamphotheca, inflated aspect: absent (0); present (1). (GB7)
8. Gape: not fleshy margin (0); narrowly fleshy margin (1); markedly fleshy (2). (GB8) Ordered.
9. Ramicorn primary colour pattern: black (0); red (1); pink (2); yellow (3); orange (4); green (5); blue (6); black rostrally but pinkish-orange caudally (7). (GB9)
10. Latericorn, ramicorn, and premaxillary nail, light distal mark: absent (0); present (1). (GB10)
11. Latericorn colour: black (0); dark red and black (1); orange (2); yellow (3); green (4); blue (5). (GB11)
12. Culminicorn: black (0); reddish orange (1); pale orange (2). (GB12)
13. Maxillary and mandibular unguis, color: black (0); reddish orange (1); yellow (2); green (3); blue-grey (4). (GB13)
14. Ramicorn, ultraviolet reflectance peak (corresponds to the orange spot): absent (0); present (1). (KC14)
15. Bill of downy chick, colour: dark (0); reddish (1); pale, variably horn to yellow (2); subtle dark reddish markings at base (3); bluish (4). (GB14)
16. Bill of immature, colour: dark (0); bicoloured red and black (1); red (2); yellow (3); grey (4). (GB15)
17. External nares: present (0); absent (1). (GB17)
18. Nostril tubes in adult: absent (0); present (1). (GB16)
19. Nostril tubes in hatchling: absent (0); present (1). (GB16)

TABLE A2. Comparative specimens examined and associated changes to characters of the phylogenetic data matrix.

Taxon	Specimens	Coding changes (with abbreviated reference to character number in brackets—see Character List)
<i>Anthropodyptes gilli</i>	NMV P 17167 (Park and Fitzgerald, 2012)	1 (BG121), 2 (BG122), 1 (CHa157), 1 (K133), 1 (CHb20), 2 (CHa176), 1 (CHa177), 0/1 (CHb31), 0 (BG126), 0 (BG128), 0 (K142), 2 (CHb37), 3 (BG127), 0 (CHb39), 2 (CHb3), 2 (C132), 0 (K128), 1 (CHb7), 1 (BG125), 1 (K134), 0/1 (K136), 0 (C143), 1 (BG128), 1 (A34), 1 (K141), 1 (K143)
<i>Anthropornis grandis</i>	IB/P/B-0483 (Myrcha et al., 2002), IB/P/B-0064, IB/P/B-0443, IB/P/B-0454, IB/P/B-0179, IB/P/B-0590 (Jadwiszczak, 2006a), specimens used within Jadwiszczak (2013)	0 (BG120), 1 (A22), 1 (CHa157), 0 (K135), 0 (KT153), 1 (CHb17), 1/2 (BG125), ? (C144), ? (CHa176), ? (CHa177), ? (BG126), ? (K142), ? (K143), ? (K141), 1 (K158), 0 (KT203), 0 (K144), 0 (CL217), 0 (K124), 0/1 (This study 266), 1 (CHb50), 0 (CHb47)
<i>Anthropornis nordenskjöldi</i>	IB/P/B-0070 (Myrcha et al., 1990; Myrcha et al., 2002), IB/P/B-0119, IB/P/B-0150, IB/P/B-0701, IB/P/B-0250b, IB/P/B-0501 (Jadwiszczak, 2006a), NHMUK A2013, USNM 402486 (Ksepka et al., 2006), NHMUK A. 3361, NHMUK A. 3348-3354, NHMUK A. 3356 (Marples, 1953), MLP 95-I-10-142 (Jadwiszczak, 2015), NRM-PZ A.45 (Wiman, 1905; Acosta Hospitaleche et al., 2017), specimens used within Jadwiszczak (2013), MLP 84-II-1-7 (cast)	0 (CL217), 1 (A22), 0 (BG120), 0 (K124), 0/1 (CHa157), 1 (CHb7), 0 (KT153), 2 (CL220), 1 (K141), 1 (K158), 1 (CHb50), 0 (KT203), 2 (This study 203), 0 (K144), 1 (K144/CHa188), 0 (K145), 1 (KC187), 1 (BG135), 0 (BG136), 1 (C169), 0 (CHb31), 2 (BG128), 1 (KC166), 0 (KF239), 0 (This study 266), 0 (CHb49), 0 (CHb47), 0/1 (C132)
<i>Aphrodroma brevirostris</i>	figure 1: Mayr (2016)	1 (K158), 0 (A72), 0 (This study 266), 0 (KT203), 0 (CHb50), 1 (CHb49), 1 (BG141) 2 (CHb47), 0 (CHb65), 0 (K163), 0 (CHb71), 0 (KT211), 1 (CHb46), 0 (CHb45), 1 (CHb44), 0 (CHb42), 1 (BG127), 1 (CHb37), 3 (K141), 3 (BG126), 0 (CL220), 0 (CHb20), 0 (K133), 0 (CHb17), 0 (CL222), 0 (CHb8), 0 (CHb3), 0 (BG122)
<i>Aptenodytes forsteri</i>	NHMUK 1905.12.30.419 (Jadwiszczak, 2015), NMV B 18320, CM AV17360	2 (K141), 2 (CHb50), 2 (K158), 0 (A72), 1 (This study 266), 0 (CHb49), 0 (BG141), 0 (CHb47), 0 (CHb64), 2 (CHb65), 2 (K163), 1 (CHb71), 0 (CHb72), 0 (KT211), 0/1 (LZ2366), 0 (CHb46), 1 (CHb45), 0 (CHb44), 2 (CHb43), 0 (CHb42), 1 (KF239), 3 (BG127), 2 (CHb37), 0 (BG126), 3 (CL220), 2 (CHb20), 3 (K133), 2 (CHb17), 1 (CHb16), 2 (CL222), 2 (CHb8), 1 (CHb7), 2 (CHb3), 2 (BG122)
<i>Aptenodytes patagonicus</i>	CM 1229, CM 1225, CM 1241, CM 1243, CM not registered, CM not registered, CM not registered, CM not registered	1 (This study 266), 1 (KF239)
<i>Archaeospheniscus lopedellorum</i>	OM C.47.21 (Marples, 1952; Simpson, 1971b), OM GL428	? (K158), 0/1 (This study 266), 2 (This study 203), 1 (M246), 0 (KF239), 1 (CHb3), 2 (C132), ? (K137)
<i>Archaeospheniscus lowei</i>	OM C.47.20 (Marples, 1952; Simpson, 1971b), OM GL407	2 (K141), 2 (This study 203), 1 (M246), 1 (M247), 0 (KF239), 1 (CHb3), 3 (CL220)
<i>Ardenna gravis</i>		0 (A72), 1 (K158), 0 (This study 266), 3 (CHb50), 2 (CHb49), 1 (BG141), 2 (CHb47), 0 (CHb61), 0 (CHb64), 0 (CHb65), 0 (K163), 0 (CHb71), 0 (CHb72), 0 (LZ2366), 0 (CHb46), 0 (CHb45), 1 (CHb44), 1 (CHb43), 0 (CHb42), 3 (K141), 3 (BG126), 0 (BG127), 0 (CHb20), 0 (K133), 0 (CHb17), 0 (CL222), 0 (CHb8), 0 (CHb3), 0 (BG122)
<i>Ardenna grisea</i>		0 (This study 266)
<i>Arthrodytes grandis</i>	MLP M-606, MLP M-607, MLP M-608 (Acosta Hospitaleche, 2005)	2 (CL223), 0 (KF235), 1 (KC137), 0 (K122), 1 (K124)
Burnside 'Palaeudyptes'	OM C48.73-81 (Marples, 1952; Simpson, 1971b; Ksepka, 2007)	0 (CHb47), 1 (M247), 1 (K141)
<i>Chauna torquata</i>	CM AV21208	

Taxon	Specimens	Coding changes (with abbreviated reference to character number in brackets—see Character List)
<i>Crossvallia unienwillia</i>	MLP 00-I-10-1 (Tambussi et al., 2005; Jadwiszczak et al., 2013)	2 (K141), 2 (K139), 1 (CL222), 1 (CL220)
? <i>Crossvallia waiparensis</i>	CM 2018.23.9, CM 2016.158.2, CM 2016.158.3	Coded in entirety, see NEXUS file
<i>Cygnus olor</i>	CM AV25436, CM AV23143	
<i>Daption capense</i>		0 (A72), 1 (K158), 1 (This study 266), 0 (KT203), 0 (CHb50), 1 (BG141), 0 (K163), 0 (CHb45), 0 (BG127), 3 (K141), 3 (BG126), 0 (CL220), 0 (K133), 0 (CHb17), 0 (CL222), 0 (CHb8), 0 (CHb3), 0 (BG122)
<i>Delphinornis arctowskii</i>	IB/P/B-0484 (Myrcha et al., 2002), IB/P/B-0115 (Jadwiszczak, 2006a)	1 (K159), 1 (K158), 1 (CHb50), 3 (CHa224), 1 (C169), 1 (This study 266), 1 (CHa229), 1 (K163), 1 (LZ2366), 2 (CHa233), 2 (CHa234)
<i>Delphinornis gracilis</i>	IB/P/B-0279a (Myrcha et al., 2002), IB/P/B-0130, IB/P/B-0408 (Jadwiszczak, 2006a)	1 (K158), 2 (CHb50), 1 (K160), 0 (This study 266), 1/2 (K163), 0 (K160), 0/1 (LZ2366), 2/3 (CHa233)
<i>Delphinornis larseni</i>	IB/P/B-0062 (Myrcha et al., 2002), IB/P/B-0444, IB/P/B-0446, IB/P/B-0090, IB/P/B-0337 (Jadwiszczak, 2006a), IB/P/B-0440 (Jadwiszczak, 2006a; 2010), NRM-PZ A.21 (holotype) (Wiman, 1905; Acosta Hospitaleche et al., 2017), MLP 93-X-1-146, MLP 93-X-1-161 (Reguero et al., 2013), NRM-PZ A.994, IB/P/B-0547 (Jadwiszczak and Mörs, 2019)	1 (CHb7), 0 (K135), 1 (K159), 2 (K144), 1 (K144/CHa188), 1 (BG121), 2 (BG122), 1 (CHb3), 0 (C132), 1 (CHa157), 0 (K128), 0 (CHb8), 2 (CL222), 1 (K129), 2 (BG123), 0 (BG124), 1 (CHb16), 2 (K133), 1 (CHb20), 0 (K136), 0 (K137), 0 (CHa176), 0 (CHa177), 0 (BG126), 2 (BG128), 3 (BG127), 0 (CHb39), 1 (M247), 1 (K158), 2 (This study 203), 1 (KC166), 0 (KF139), 0 (K145), 1 (C157), 1 (KC175), 1 (C169), 0/1 (This study 266), 1 (BG139), 0 (BG140), 1 (CHa229), 0 (K163), 0/1 (K160), 1 (LZ2366), 1 (OH16), 1 (CHb47), 0 (CHb50)
<i>Diomedea exulans</i>	CM AV7000, CM AV3351	0 (K158), 1 (This study 266), 0 (CHb50), 1 (CHb49), 1 (BG141), 1 (CHb50)
<i>Duntronornis parvus</i>	OM C.47.31 (Marples, 1952; Simpson, 1971b)	2 (K158), 0 (KF243), 2 (K158), 1 (K162), 0 (K157), 0 (K159), 2 (K160)
<i>Eretiscus tonnii</i>	MLP 81-VI-26-1, MLP 69-III-29-25 (Simpson, 1981)	1/2 (This study 266), 1 (K158), ? (CHb45), 1 (M247), 1 (K141), 0 (CHa177), 1 (CHa157), 0 (CHb16), ? (K136)
<i>Eudyptes calauina</i>	SGO-PV 21451, SGO-PV 21449, SGO-PV 21447, SGO-PV 21488, SGO-PV 21487, SGO-PV 21444 (Chávez Hoffmeister et al., 2014)	2 (BG122), 2 (CHb3), 1 (CHb7), 2 (CHb8), 1 (CHb16), 2 (CHb17), 2 (K133), 2 (CHb20), 1 (CHb31), 2 (CHb37), 3 (BG127), ? (CHb39), 0 (BG141), 1 (CHb43), 0 (CHb44), 1 (CHb45), 1 (CHb46), 1 (CHb47), 0 (CHb49), 2 (CHb50), 1 (CHb64), 2 (CHb65), 1 (CHb71), 0 (CHb72), 1 (LZ2366), 1 (This study 266), 0 (A72), 0 (CHb61), 0 (CHb42), 0 (CHb39), 3 (BG127), 2 (CHb37), 1 (CHb31), 2 (CHb20), 2 (K133), 2 (CHb17), 1 (CHb16), 1/2 (CHb8), 1 (CHb7), 2 (CHb3), 2 (BG122)
<i>Eudyptes chrysocome</i>		0 (This study 266), 0/1 (CHb46), 1 (CHb45)
<i>Eudyptes chrysolophus</i>	CM 1994-191	0 (A72), 2 (K158), 0 (This study 266), 2 (CHb50), 0 (CHb49), 0 (BG141), 1 (CHb47), 1 (CHb64), 2 (CHb65), 2 (K163), 1 (CHb71), 0 (CHb72), 0 (KT211), 1 (LZ2366), 0 (CHb46), 1 (CHb45), 0 (CHb44), 3 (BG127), 2 (CHb37), 2 (K141), 0 (BG126), 3 (CL220), 3 (K133), 2 (CHb17), 1 (CHb16), 2 (CL222), 2 (CHb8), 1 (CHb7), 2 (CHb3), 2 (BG122)
<i>Eudyptes filholi</i>		0 (A72), 1 (CHa229), 2 (K158), 0 (This study 266), 2 (CHb50), 0 (CHb49), 0 (BG141), 2 (CHb65), 2 (K163), 0 (CHb72), 0 (KT211), 1 (CHb45), 3 (BG127), 2 (CHb37), 2 (K141), 0 (BG126), 3 (CL220), 2 (CHb20), 3 (K133), 2 (CHb17), 1 (CHb16), 2 (CL222), 2 (CHb8), 1 (CHb7), 2 (CHb3), 2 (BG122)

Taxon	Specimens	Coding changes (with abbreviated reference to character number in brackets—see Character List)
<i>Eudiptes moseleyi</i>		0 (A72), 1 (CHa229), 2 (K158), 0 (This study 266), 2 (CHb50), 0 (BG141), 1 (CHb64), 2 (CHb65), 2 (K163), 1 (CHb71), 0 (CHb72), 0 (KT211), 1 (LZ2366), 0/1 (CHb46), 1 (CHb45), 0 (CHb44), 3 (BG127), 2 (CHb37), 2 (K141), 0 (BG126), 3 (CL220), 2 (CHb20), 3 (K133), 2 (CHb17), 1 (CHb16), 2 (CL222), 2 (CHb8), 1 (CHb7), 2 (CHb3), 2 (BG122), 0 (CHb49)
<i>Eudiptes pachyrhynchus</i>	OM 309 (Triche, 2007)	2 (CHb50), 2 (K158), 0 (A72), 0 (This study 266), 0 (CHb49), 0 (BG141), 2 (CHb65), 2 (K163), 0 (CHb72), 0 (KT211), 1 (CHb45), 3 (BG127), 2 (CHb37), 2 (K141), 0 (BG126), 3 (CL220), 2 (CHb20), 3 (K133), 2 (CHb17), 1 (CHb16), 2 (CL222), 2 (CHb8), 1 (CHb7), 2 (CHb3), 2 (BG122)
<i>Eudiptes robustus</i>		0 (A72), 2 (K158), 0 (This study 266), 2 (CHb50), 0 (CHb49), 0 (BG141), 2 (CHb65), 2 (K163), 0 (CHb72), 1 (CHb45), 2 (CHb37), 2 (K141), 0 (BG126), 3 (BG127), 3 (CL220), 2 (CHb20), 3 (K133), 2 (CHb17), 1 (CHb16), 2 (CL222), 2 (CHb8), 1 (CHb7), 2 (CHb3), 2 (BG122)
<i>Eudiptes schlegeli</i>		0 (BG141), 1 (CHb45), 0 (BG126), 3 (CL220), 2 (BG122)
<i>Eudiptes sclateri</i>	OM AV7861 (Triche, 2007)	2 (K158), 0 (A72), 0 (This study 266), 2 (CHb50), 0 (CHb49), 0 (BG141), 2 (CHb65), 2 (K163), 0 (CHb72), 1 (CHb45), 3 (BG127), 2 (CHb37), 2 (K141), 0 (BG126), 3 (CL220), 2 (CHb20), 3 (K133), 2 (CHb17), 1 (CHb16), 2 (CL222), 2 (CHb8), 1 (CHb7), 2 (CHb3), 2 (BG122)
<i>Eudiptula minor</i>	FUR 019, FUR 208	1 (LZ2366), 0 (This study 266), 0/1 (CHb39), 2 (K158), 2 (CHb50)
<i>Gavia immer</i>	USNM 502462	0 (K158), 3 (CHb50)
<i>Gavia stellata</i>	CM AV10284	0 (K158)
Hakataramea penguin	OU 21977 (Ando, 2007)	1 (M247), 2 (C132)
<i>Hydrobates leucorhous</i>	USNM 614217	0 (K158), 2 (This study 266), 0 (A72), 0 (K158), 3 (CHb50), 2 (CHb49), 1 (BG141), 1 (CHb47), 0 (CHb61), 0 (CHb64), 0 (CHb65), 0 (K163), 1 (CHb71), 0 (CHb72), 0 (LZ2366), 0 (CHb46), 0 (CHb45), 0 (CHb44), 1 (CHb43), 0 (CHb42), 0 (BG127), 1 (CHb37), 2 (BG126), 0 (CL220), 0 (K134), 0 (CHb20), 2 (K133), 0 (CHb17), 0 (CHb8), 0 (CHb3), 0 (BG122)
<i>Hydrobates tethys</i>		2 (This study 266)
<i>Icadyptes salasi</i>	MUSM 897 (Ksepka et al., 2008)	2 (This study 203), 0 (K141), 2/3 (CL220)
<i>Inguza predemersus</i>	ISAM L6510, ISAM PQL28195, ISAM PQL23012, ISAM PQL23003, ISAM PQL28254, ISAM PQL28251 (Ksepka and Thomas, 2012)	2 (K141), 2 (BG122), 2 (CHb3), 2 (C132), 1 (CHa157), 2 (CHb8), 1/2 (K127), 2 (CL222), 1 (CHb16), 1 (K133), 1/2 (CHb20), 3 (CL220), 1 (C143), 1/2 (CHa176), 0 (CHa177), 1 (CHb31), 2 (BG128), 2 (K142), 2 (CHb37), 3 (BG127), 0 (CHb39), 1 (KF239), 3 (K144/CHa188), 1 (M246), 0 (K145), 2 (This study 203), 1 (CHb47), 0 (CHb64), 1 (CHa229), 1 (M247), 2 (CHb17), 1/2 (K134), 1 (A34), 1 (CHb43), 0 (CHb44), 1 (CHb45), 1 (CHb46), 0 (CHb49), 2 (K158), 2 (CHa219), 1 (CHb61), 0 (A72), 2, (CHb65), 0 (This study 266), 1 (LZ2366), 1 (KT211), 0 (CHb72), 0 (CHb71), 2 (K159), 3 (CHa233), 1 (K160)
<i>Inkayacu paracasensis</i>	MUSM 1444 (Clarke et al., 2010)	1 (KF236), 1 (K141), 2 (This study 203), 2 (This study 266), 1 (K158), 1 (CHb47), 0/1 (K141), 1 (CHb3), 2/3 (CHa233), 1 (CL220), 0 (CHb50)
<i>Kaiika maxwelli</i>	OU 22402 (Fordyce and Thomas, 2011)	1/2 (BG125), 0 (A34), 2 (BG128), 1 (K135), 1 (CL222)
<i>Kairuku grebneffi</i>	OU 22094, OU 22065 (Ksepka et al., 2012)	2 (This study 203), 1 (This study 266), 1 (K158), 0/1 (CHb47), 0/1 (K141), 2/3 (CL220), 1 (C132)

Taxon	Specimens	Coding changes (with abbreviated reference to character number in brackets—see Character List)
<i>Kairuku waitaki</i>	OU 12652 (Ksepka et al., 2012)	1 (K158), 1 (This study 266), 1 (CHb47), 1 (C132)
<i>Korora oliveri</i>	OM C.50.63 (Marples, 1952; Simpson, 1971b)	Coded in entirety, see NEXUS file
<i>Kumimanu biceae</i>	NMNZ S.45877 (Mayr et al., 2017b)	1 (CHb20), 0 (CHb16), 1 (KT153), 1 (CL222)
<i>Leptoptilos</i> sp.	CM AV37491	
<i>Macronectes giganteus</i>	CM AV20407, CM AV14405	0 (A72), 1 (K158), 1 (This study 266), 0 (KT203), 1 (BG141), 0 (K163), 0 (CHb45), 0 (BG127), 3 (K141), 3 (BG126), 0 (CL220), 0 (K133), 0 (CHb17), 0 (CL222), 0 (CHb8), 0 (CHb3), 0 (BG122)
<i>Madrynornis mirandus</i>	MEF-PV 100 (Acosta Hospitaleche et al., 2007)	1/2 (K141), 1 (This study 266), 2 (This study 203), 1 (M247)
<i>Marplesornis novaezealandiae</i>	CM AV 16527	2 (This study 203), 1/3 (K144/CHa188), 1 (M246), 1 (M247), 2 (K144), 0 (KF239), 2 (K141), 0 (BG126), 3 (CL220), 3 (K133), 1 (CHb16), 0 (K135), 2 (CL222), 2 (CHb3), 2 (BG122)
<i>Marambiornis exilis</i>	IB/P/B-0490 (Myrcha et al., 2002), IB/P/B-0434, IB/P/B-0406 (Jadwiszczak, 2006a)	0 (This study 266), 0 (CHb50), 1 (LZ2366), 3 (CHa233), 2 (CHa234)
<i>Megadyptes antipodes</i>		2 (CHa233), 0/1 (This study 266)
<i>Mesetaornis polaris</i>	IB/P/B-0278 (Myrcha et al., 2002), IB/P/B-0215, IB/P/B-0207 (Jadwiszczak, 2006a)	1 (AH38), 0 (This study 266), 1 (CHa229), 1 (K158), 1 (K163), 3 (CHa233), 2 (CHa234)
<i>Muriwaimanu tuatahi</i>	CM zfa 34, CM 2008.145.3, CM 2009.99.1, OU 12651, CM 2010.108.3	1 (This study 203), 1 (K144/CHa188), 2 (K127), 2 (This study 266), 0 (CHa234), 1 (BG138), 0 (KF239), 3 (BG127), 2 (BG128), 1 (CL220), 0 (CHb16), 1 (KT153), 1 (K135), 1 (CL222), 0 (KF236), 1 (KC142), 0/1 (K124), 0/1 (CHb46), 0 (CHa157), ? (C143)
<i>Notodyptes wimani</i>	IB/P/B-0491 (Myrcha et al., 2002), IB/P/B-0176, IB/P/B-0641, IB/P/B-0110 (Jadwiszczak, 2006a), IB/P/B-0284, NHMUK A3331	1 (BG121), 2 (BG122), 1 (CHa157), 1 (CHb7), 0 (CHb8), 0 (K127), 2 (CL222), 1 (K129), 2 (BG123), 0 (BG124), 1 (CHb16), 2 (BG125), 2 (K133), 1 (CHb20), 1 (CL219), 0 (K136), 0 (CHa177), 1 (CHb31), 0 (BG126), 1/2 (BG128), 1 (K143), 0 (BG136), 1 (This study 266), 0 (CL221), 1 (K141), 2/3 (CL220), 1/2 (C132), 1 (CHb17)
<i>Nucleornis insolitus</i>	ISAM-PQ-MBD4, ISAM-PQ-MBD3 (Simpson, 1979)	2 (K158), 0 (KF243), 2 (CHb65), 0 (A72), 0 (CHa229), 3 (CHa224), 0 (CHb49), 1 (CHb43), 1/2 (CHb42), 1 (CHa219), ? (KT211), 2 (CHb50), 1/2 (CHb47), 0 (CHb44), 1 (CHb45), 0 (CHb46), 0/1 (CHb61), 0 (CHb64), 2 (K159), 3 (CHa233), 1 (LZ2366)
<i>Oceanites oceanicus</i>		0 (A72), 1 (K158), 2 (This study 266), 0 (KT203), 3 (CHb50), 1 (BG141), 0 (K163), 0 (CHb45), 1 (BG127), 3 (K141), 2 (BG126), 0 (CL220), 2 (K133), 0 (CHb17), 0 (CL222), 0 (CHb8), 0 (CHb3), 0 (BG122)
<i>Pachydyptes ponderosus</i>	NMNZ OR. 1450	1 (K141), 2/3 (CL220)
<i>Pachydyptes simpsoni</i>	P.14157, P.14158 (Jenkins, 1974)	1 (BG121), 2 (BG122), 2 (K133), 1 (CHb20), 0 (K134), 2 (CL220), 1 (CHa177), 0 (KF239)
<i>Pachyptila desolata</i>		0 (A72), 1 (K158), 0 (This study 266), 3 (CHb50), 1 (BG141), 0 (K163), 0 (CHb45), 0 (BG127), 3 (K141), 2 (BG126), 0 (CL220), 0 (K134), 0 (K133), 0 (CHb17), 0 (CL222), 0 (CHb8), 0 (CHb3), 0 (BG122)
<i>Palaeodyptes antarcticus</i>	NHMUK A.1084 (Huxley, 1859; Simpson, 1971b), OU 22167 (Ksepka et al., 2012)	1 (K158), 1 (K160), 0 (This study 266), 2 (CHa219)

Taxon	Specimens	Coding changes (with abbreviated reference to character number in brackets—see Character List)
<i>Palaeodyptes gunnari</i>	IB/P/B-0072 (Myrcha et al., 1990; Myrcha et al., 2002), IB/P/B-0306, IB/P/B-0151, IB/P/B-05896, IB/P/B-0654, IB/P/B-0103, IB/P/B-0083, IB/P/B-0455, IB/P/B-0692 (Jadwiszczak, 2006a), MLP 96-I-6-13 (Acosta Hospitaleche and Reguero, 2010), NRM-PZ A.7 (holotype) (Wiman, 1905; Chávez Hoffmeister, 2014b; Acosta Hospitaleche et al., 2017), specimens used within Jadwiszczak (2013)	0 (BG120), 1 (K158), 0 (KT203), 0/1 (K160), 2 (This study 203), 0 (CL217), 0 (K124), 0/1 (K144), 2 (K144/CHa188), 0 (BG136), 1 (C169), 0 (This study 266), 1 (C132), 2/3 (CL220)
<i>Palaeodyptes klekowskii</i>	IB/P/B-0065 (Myrcha et al., 1990), MLP 11-II-20-07 (Acosta Hospitaleche and Reguero, 2014), IB/P/B-0485 (Myrcha et al., 2002; Jadwiszczak, 2015), IB/P/B-0331, IB/P/B-0578, IB/P/B-0250a (Jadwiszczak, 2006a), MLP 94-II-15-175	1 (K158), 1 (CHb50), 0/1 (K160), 2 (This study 203), 0/1 (K144), 2 (K144/CHa188), 0 (K145), 1 (C155), 1 (C157), 0 (C158), 1 (KC175), 0 (KC176), 1 (KC187), 2 (BG135), 0 (BG136), 1 (C169), 0/1 (This study 266), 1 (C132), 3 (CL220)
<i>Palaeodyptes marplei</i>	OM C.50.28 (Simpson, 1971b)	0 (This study 266), 1 (K158), 2 (CHb47)
<i>Palaeospheniscus bergi</i>	NHMUK A694 (Jadwiszczak, 2015), <i>P. planus</i> MACN (unnumbered) (Ameghino, 1905: plate 1, 2, figure 7), <i>Paraspheniscus</i> (Ameghino, 1905: pl. 2, fig. 12)	1 (K158), 1 (M247), 0/1 (CHb50)
<i>Palaeospheniscus biloculata</i>	<i>Perispheniscus wimani</i> (Ameghino, 1905: plate 2, 3, figure 14, 15), supplemented by descriptions from Acosta Hospitaleche (2007) and Acosta Hospitaleche and Tambussi (2008)	2 (CHb50)
<i>Palaeospheniscus patagonicus</i>	AMNH No. 3297 (Simpson, 1946), MPEF-PV 3060, MPEF-PV 3070 (Acosta Hospitaleche et al., 2008)	1 (K158), 2 (This study 203), 2 (This study 266), 1 (M246), 1 (M247), 2 (CHb17), 0 (CHb50), 2 (BG128)
<i>Parapterodytes antarcticus</i>	AMNH 3338 (Bertelli et al., 2006)	2 (K141), 1 (K158), 0 (This study 266)
<i>Parapterodytes brodkorbi</i>	plate 5, figure 29a and b (Ameghino, 1905)	1 (C132)
<i>Parapterodytes robustus</i>	BM(NH) A/151 (Simpson, 1972)	1 (CL222), 1 (CHa157), 1 (C132), 1 (CHb7)
<i>Pelecanoides urinatrix</i>		1 (K158), 0 (This study 266), 3 (CHb50), 1 (BG141), 1 (BG127)
<i>Pelecanus conspicillatus</i>	CM AV37035	
<i>Perudyptes devriesi</i>	MUSM 889 (Ksepka and Clarke, 2010)	1 (K141), 1 (This study 266), ? (K163), 0 (K141), 1 (CL222), 2 (CHa233)
<i>Phaethon rubricauda</i>	NMV B12819	Coded in entirety, see NEXUS file
<i>Phalacrocorax carbo</i>	CM AV9775, CM AV19114, CM AV9774	
<i>Phoebastria immutabilis</i>		0 (A72), 0 (K158), 1 (This study 266), 0 (CHb50), 1 (BG141), 0 (K163), 0 (CHb45), 0 (BG127), 3 (K141), 3 (BG126), 0 (CL220), 0 (K133), 0 (CHb17), 0 (CL222), 0 (CHb8), 0 (CHb3), 0 (BG122)
<i>Phoebetria palpebrata</i>		0 (A72), 0 (K158), 1 (This study 266), 0 (CHb50), 1 (BG141), 0 (K163), 0 (CHb45), 0 (BG127), 3 (K141), 3 (BG126), 0 (CL220), 0 (K133), 0 (CHb17), 0 (CL222), 0 (CHb8), 0 (CHb3), 0 (BG122)
<i>Phoebastria sp.</i>	CM not registered	
<i>Platydyptes amiesi</i>	OM C.50.61, OM C.50.62 (Simpson, 1971b; Ando, 2007)	1 (M247), 1 (KF239), 1 (K141), 2 (CL222), 1 (CHb17), 1 (CL219), 0 (C143), 0 (CHb31), 1 (KC166)

Taxon	Specimens	Coding changes (with abbreviated reference to character number in brackets—see Character List)
<i>Platydyptes marplesii</i>	OM C.47.15 (Marples, 1952; Ando, 2007), OU 21946 (from Ando, 2007; used as per Chávez Hoffmeister, 2014b) Note: Ando (2007) considered the holotype of <i>Dunroornornis parvus</i> (OM C.47.31) to be synonymous with this taxon. However, because this study has not been published, this specimen has not been formally synonymised with <i>P. marplesii</i> and is referred to as <i>Dunroornornis parvus</i> here.	2 (This study 203), 1 (M246), 1 (M247), 1 (KF239), 0 (KC142), 0 (CHb7), 0 (KT153), 0 (CHb31), 2 (A34), 1 (C155), 0 (CHb44), 0 (CHb47), ? (KF243), ? CHa219, 2 (CHa233), 0 (CHb71), 1 (LZ2366), 0/2 (CHa234)
<i>Platydyptes novaezealandiae</i>	DM 1451/OU 21797 (Simpson, 1971b; Ando, 2007), OU 21805 (from Ando, 2007; used as per Chávez Hoffmeister, 2014b)	2 (This study 203), 2 (K158), 1 (M246), 1 (M247), ? (CL222), ? (K133), ? (CHb20), 1 (CL219), ? (CHb31), ? (BG128), 0 (CHb44), 0/1 (CHb47), 0 (CHb50), 1 (KT203), 1 (CHb72)
<i>Podiceps cristatus</i>	CM AV38913, CM AV10285, CM AV36143, CM AV36812	
<i>Procellaria cinerea</i>		0 (A72), 1 (K158), 0 (This study 266), 1 (BG141), 0 (K163), 0 (CHb45), 0 (BG127), 3 (K141), 3 (BG126), 0 (CL220), 0 (K133), 0 (CHb17), 0 (CL222), 0 (CHb8), 0 (CHb3), 0 (BG122)
<i>Pseudapterodytes macraei</i>	NMV P 26668, NMV P27055, NMV P27056 (Simpson, 1970; Park, 2014)	1 (BG121), 2 (BG122), 2 (CHb3), 2 (C132), 0 (CHa157), 2 (K127), 2 (CL222), 2 (K129), 1 (CHb16), 2 (K133), 2 (CHb20), 1 (C143), 0 (CHa177), 0 (K160), 1 (CHb7), 2 (CHb8), 2 (CHb17), 1/2 BG125), 1 (K134), 3 (CL220), 0 (C144), 1 (M247), 1 (C155), 0 (C156), 1 (C157), 1 (KC175), 0 (KC176), 0/1 (K137)
<i>Pygoscelis adeliae</i>	USNM 554802; Unassigned (from Jadwyszczak, 2015), CM not registered, CM not registered	2 (CHb50), 2 (K158), 1 (This study 266), 0 (A72), 0 (CHb49), 0 (BG141), 0 (CHb47), 0/1 (CHb64), 2 (CHb45), 2 (K163), 0 (CHb71), 0 (CHb72), 0 (KT211), 0/1 (CHb46), 1 (CHb45), 0 (CHb44), 1 (CHb43), 3 (BG127), 2 (CHb37), 2 (K141), 0 (BG126), 3 (CL220), 2 (CHb20), 3 (K133), 1 (CHb16), 2 (CL222), 2 (CHb8), 1 (CHb7), 2 (CHb3), 2 (BG122), 2 (CHb17)
<i>Pygoscelis antarcticus</i>		2 (CHa233), 0 (A72), 2 (K158), 0 (This study 266), 2 (CHb50), 0 (CHb49), 0 (BG141), 1 (CHb47), 0/1 (CHb64), 2 (CHb65), 2 (K163), 1 (CHb71), 0 (KT211), 1 (CHb46), 0 (CHb45), 1 (CHb43), 0 (CHb42), 3 (BG127), 2 (CHb37), 2 (K141), 0 (BG126), 3 (K133), 2 (CHb17), 1 (CHb16), 2 (CL222), 2 (CHb8), 1 (CHb7), 2 (CHb3), 2 (BG122)
<i>Pygoscelis grandis</i>	SGO-PV-1104, SGOPV-1105, SGOPV-1106, SGOPV-1107, SGOPV-1108 (Walsh and Suárez, 2006)	2 (K158), 1 (This study 266), 0 (A72), 2 (CHb50), 0 (CHb49), 0 (BG141), 0 (CHb47), 0 (CHb64), 2 (CHb65), 2 (K163), 0/1 (CHb71), 0 (CHb72), 1 (CHb45), 1 (KC137), 0 (A22), 0 (K122), 2 (BG122), 2 (CHa157), 2 (CL217), 1 (KF235), 2 (CHb8), 2 (CL222), 1 (CHb16), ? (CL220), 1 (CHb31), 0 (BG126), 0 (BG128), 2 (K141), 2 (K142), 2 (CHb37), 3 (BG127), 2 (This study 203), 1 (AH38), 1 (AH37), 0 (CHb42), 2 (CHb43), 0 (CHb44), 1 (CHb46), 2/3 (K159), 0 (KT211), 0 (LZ2366), 2 (K127), 2 (K129), 0 (K135), 2 (CHb17), 0 (CHb39), 2 (K143), 0 (K145), 0 (KC187), 1 (BG135), 0 (KF242), 0/1 (CHa219), 0 (CHb61), 2/3 (CHa233), 1 (A73)
<i>Pygoscelis papua</i>	CM 1992-224, CM 1993-90	0 (This study 266)
SAM P 7158 cf. <i>Palaeudyptes</i>	SAM P 7158 (Simpson, 1957; Park and Fitzgerald, 2012)	1 (M247), 0 (K142), 0 (K141), 1 (BG128), 1 (BG126), 0 (CHb31), 0 (CHa177), 1 (CHa176), 0 (K134), 1 (CHb20), 2 (K133), 1 (K129), 0 (K127), 0 (CHb8), 1 (CHb3), 2 (BG122), 1 (BG121), 2 (CHb37), 1 (CHb17), 1 (CHb16), 0 (K135), 1 (CL222), 0 (CHb7), 1/2 (CL222), 0/1 (K137), 3 (BG127), 0 (K143)

Taxon	Specimens	Coding changes (with abbreviated reference to character number in brackets—see Character List)
<i>Sequiwaimanu rosieae</i>	CM 2016.6.1	2 (K141), 1 (This study 203), 1/2 (K144/CHa188), 0 (K144), 2 (BG122), 1 (AH37), 0 (KF239), 0 (K143), 0 (CHb39), 3 (BG127), 2 (CHb37), 0 (K142), 0 (A34), 2 (BG128), 1 (CHb31), 0 (CHa177), 0 (CHa176), 1 (CHb20), 1 (CHb17), 0 (CHb16), 1 (KT153), 1 (CL222), 0 (CHb8), 1 (CHb7), 1 (CHa157), 1 (CHb3), 0 (C132)
<i>Sphenisciformes</i> indet.	NMV P221273 (Park et al., 2016) NMV P221273	1 (CHa177), 1 (M247), 3 (CHb37), 2 (K142), 1 (BG128), 0 (BG126), 1 (CHb31), 3 (CHa176), 1 (C143), 3 (CL220), 1 (CHb20), 2 (K133), 1 (CHb16), 0 (K135), 2 (K129), 2 (CL222), 2 (K127), 2 (CHb8), 0 (CHa157), 1 (C132), 2 (CHb3), 1 (BG122), 1 (BG121), 1 (CL222), 0 (CHb7), 2 (C132), 1 (CHb7), 2 (CL222), 2 (CHb17), 1/2 (CHb20), 1 (A34), 2 (K141), 0 (CHb39), 1 (K143)
<i>Sphenisciformes</i> indet.	SAM P 10863 (Simpson, 1957; Park and Fitzgerald, 2012) SAM P 10863	0 (CHa177), 0 (K137), 3 (CL220), 1 (CL219), 1 (K134), 1 (CHb20), 2 (K133), 2 (CL222), 0 (K127), 0 (CHb8), 1 (CHa157), 0 (C132), 1 (CHb3), 2 (BG122), 1 (BG121), 1 (M247), 1 (CHb17), 1 (CHb16), 0 (K135), 1 (CHb7), 1 (CHb3), 0 (K128), 1 (K129), ? (K134)
<i>Spheniscus demersus</i>	FUR 209	0 (A72), 2 (CHa229), 2 (K158), 1/2 (This study 266), 2 (CHb50), 0 (CHb49), 0 (BG141), 2 (CHb65), 2 (K163), 0 (CHb72), 1 (KT211), 1 (CHb46), 1 (CHb45), 1 (CHb44), 1 (CHb43), 1 (CHb42), 3 (BG127), 2 (CHb37), 1 (K141), 0 (BG126), 3 (CL220), 3 (K133), 2 (CHb17), 0 (CHb16), 2 (CL222), 2 (CHb8), 1 (CHb7), 2 (CHb3), 2 (BG122)
<i>Spheniscus humboldti</i>	CM 1993-91, CM 1994-31, CM 1997-113, NHMUK 1998.12.8	1 (This study 266), 2 (CHa229), 1 (CHb39)
<i>Spheniscus magellanicus</i>	NHMUK 2001.45.1 (Jadwiszczak, 2015)	2 (CHb50), 2 (K158), 0 (A72), 1/2 (This study 266), 0 (CHb49), 0 (BG141), 2 (CHb65), 2 (K163), 0 (CHb72), 1 (KT211), 1 (LZ2366), 0/1 (CHb46), 1 (CHb45), 1 (CHb43), 0 (CHb42), 1 (CHb39), 3 (BG127), 2 (CHb37), 0 (BG126), 3 (CL220), 3 (K133), 2 (CHb17), 0 (CHb16), 2 (CL222), 2 (CHb8), 1 (CHb7), 2 (CHb3), 2 (BG122)
<i>Spheniscus megaramphus</i>	MUSM 2087 (Chávez Hoffmeister, 2014a)	0 (A72), 0 (K157), 0 (CHb49), 0 (BG141), 2 (CHb47), 1 (B139), 0 (K157), 2 (CHb64), 2 (CHb65), 3 (K159), 2 (K163), 1 (K160), 1 (CHb71), 0 (CHb72), 1 (A73), 1 (LZ2366), 1 (CHb46), 1 (CHb45), 1 (KT211), 1 (CHb44)
<i>Spheniscus mendiculus</i>		0 (BG141), 1 (CHb45), 0 (BG126), 3 (CL220), 2 (BG122)
<i>Spheniscus muizoni</i>	MNHN PP1 147d (Göhlich, 2007)	2 (This study 203), 0 (A72), 0 (This study 266), 1/2 (CHa229), 2 (CHb50), 0 (CHb49), 0 (BG141), 2 (CHb47), 2 (CHb64), 2 (CHb65), 0 (CHb72), 1 (CHb45), 0/1 (CHb44), 1 (M246), 1 (KF239), 3 (BG127), 2 (CHb37), 1 (K141), 0 (BG126), 3 (CL220), 2 (CHb20), 3 (K133), 1 (CHb16), 2 (CL222), 1 (CHb7), 2 (CHb3), 2 (BG122)
<i>Spheniscus urbinai</i>	MUSM 898, MUSM 401 (Chávez Hoffmeister, 2014a)	1 (K141), 2 (This study 203), 0 (A72), 0 (CHb49), 0 (BG141), 2 (CHb47), 2 (CHb64), 2 (CHb65), 2 (K163), 1 (CHb71), 0 (CHb72), 0 (KT211), 0/1 (A73), 0 (LZ2366), 1 (CHb46), 1 (CHb45), 1 (CHb44), 0 (BG126), 3 (CL220), 2 (CHb17), 1 (CHb16), 2 (CHb8), 2 (BG122)
<i>Thalassarche cauta</i>	CM AV14476, CM AV36796, CM AV14738, CM AV22627	
<i>Thalassarche melanophris</i>		
<i>Waimanu manningi</i>	CM zfa 35	0 (This study 266), 0 (CHa234), 1 (BG138), 1 (AH37)
Waipara Greensand Giant penguin	CM 2016.158.1	1 (This study 266)

20. External nares: well-separated (0); fused at midline (1). (KC19)
21. Iris colour: brown (0); silvery grey (1); claret red (2); yellow (3); white (4). (GB18)
22. Scale-like feathers: absent (0); present (1). (GB19)
23. Rachis of contour feathers: cylindrical (0); flat and broad (1). (GB20)
24. Rectrices: form a functional fan (0); do not form a fan (1). (GB21)
25. Remiges: differentiated from contour feathers (0); indistinct from contour feathers (1). (GB22)
26. Apterias: present (0); absent (1). (GB23)
27. Molt of contour feathers: gradual (0); simultaneous (1). (GB24)
28. Yellow pigmentation in crown feathers (pileum): absent (0); present (1). (GB25)
29. Head plumes (cristea penna): absent (0) present (1). (GB26)
30. Head plumes: compact (0); sparse (1). (GB27)
31. Head plumes: directed dorsally (0); directed posteriorly, not drooping (1); directed posteriorly, drooping (2). (GB28)
32. Head plumes, position of origin: at base of bill close to gape (0); on the recess between latericorn and culminicorn (1); on forehead (2). (GB29) Ordered.
33. Head plumes, colour: yellow (0); orange (1). (GB30)
34. Nape (occiput), crest development: absent (0); slight (1); distinct (2). (GB31) Ordered.
35. Periocular region: black (0); white (1); yellow (2) bluish grey (3). (GB32)
36. Fleishy eyering: absent (0); present (1). (GB33)
37. White eyering: absent (0); present (1). (GB34)
38. White eyebrow (supercilium): absent (0); narrow, from postocular area (1); narrow, from preocular area (2); wide, from preocular area (3). (GB35) Ordered.
39. Loreal area (lorum): feathered (0); patch of bare skin extending from eye to base of culminicorn (1); patch of bare skin extends from eye to gape, with narrow patch of bare skin at margin of lower beak (2); patch of bare skin extends from eye to gape, with extensive patch of bare skin at margin of lower beak (3). (GB36) Ordered.
40. Auricular patch (regio auricularis): absent (0); present (1). (GB37)
41. Throat pattern: black (0); white (1); yellow (2); irregularly streaked (3); with chinstrap (4). (GB38)
42. Collar: absent (0); at most slight notch present (1); present, diffusely demarked (2); black, strongly demarked (2). (GB39) Ordered.
43. Breast, golden colour: absent (0); present (1). (GB40)
44. Dorsum: black (0); dark bluish grey (1); light bluish grey (2). (GB41)
45. Black marginal edge of dorsum between lateral collar and axillary patch, contrasting with dorsum: absent (0); present (1). (GB42)
46. Black dots irregularly distributed over white belly: absent (0) present (1). (GB43)
47. Flanks, dark lateral band reaching the breast: absent (0); present (1). (GB44)
48. Distinct dark axillary patch of triangular shape: absent (0); present (1). (GB45)
49. Flanks, extent of dorsal dark cover into the leg: incomplete, not reaching tarsus (0); complete, reaching tarsus (1). (GB46)
50. Rump, colour: indistinct in colour from dorsum (0); distinct white patch (1). (GB47)
51. Tail length: short, the quills barely emerge from the rump (0); quills distinctly developed (1). (GB48)
52. Outer rectrices, colour: same colour as inner rectrices (0); lighter than inner rectrices (1). (GB49)
53. White line connecting leading edge of flipper with white belly: absent (0); present (1). (GB50)
54. Flipper, upperside, light notch at base: absent (0); present (1). (GB51)
55. Leading edge of flipper, pattern of upperside: black (0); white (1). (GB52)
56. Leading edge of flipper, pattern of underside: white (0); incompletely dark (1); completely dark and wide (2). (GB53)
57. Flipper, underside, dark elbow patch: absent (0); present (1). (GB54)

58. Flipper, underside, tip pattern: immaculate (0); patchy, in variable extent (1); small circular dot present (2). (GB55)
59. Immature plumage, white eyebrow (supercilium): absent (0); present (1). (GB56)
60. Immature plumage, throat pattern (jugulum): black (0); mottled (1); white (2); brown (3). (GB57)
61. Immature plumage, flanks, dark lateral band: absent (0); present (1). (GB58)
62. Chicks hatch almost naked: no (0); yes (1). (GB59)
63. Dominant colour pattern of first down: pale grey (0); distinctly brown (1); bicoloured, dark above and whitish below (2); uniformly blackish grey (3). (GB60)
64. Dominant colour pattern of second down: pale grey (0); distinctly brown (1); bicoloured, dark above and whitish below (2); uniformly blackish grey (3). (GB61)
65. Chick, second down, collar: absent (0); present (1). (GB62)
66. Feet, dorsal colour: dark (0); pink (1); orange (2); white-flesh (3); blue (4). (GB63)
67. Feet, soles distinctly darker than dorsal surface: absent (0); present (1). (GB64)
68. Feet, unguis digiti: flat (0); compressed (1). (BG65)
- Reproductive Biology:**
69. Clutch size: two eggs (0); one egg (1). (GB65)
70. Incubatory sac: absent (0); present (1); (GB66)
71. Nest: no nest, incubation over the feet (0); nest placed underground, either burrowed in sand or inside natural hollow or crack (1); open nest, a shallow depression on bare ground or in midst of vegetation (3). (GB67)
72. Size of first egg relative to the second egg: similar (0); first egg smaller (1); first egg larger (2). (GB68)
73. Crèche: absent (0); small, 3-6 birds (1); formed by dozens to hundreds of immatures (2). (GB69)
74. Egg shape: oval (0); conical (1); spherical (2). (BG71)
75. Ecstatic display: absent (0); present (1). (BG72)
- Osteology:**
76. Premaxilla, tip (rostrum maxillare): pointed (0); weakly hooked (1); strongly hooked (2). (GB0) Ordered.
77. Internarial bar (pila supranasalis) shape in cross section: sub-oval (0); inverted U-shape (1). (C75)
78. Internarial bar (pila supranasalis), width: wide throughout its length (0); slender, slightly constricted laterally (1). (OH6)
79. Internarial bar (pila supranasalis), profile in lateral view: dorsal edge curves smoothly to tip of beak (0); pronounced step in dorsal edge (1). (KC78)
80. Nasal cavity, external naris (cavum nasi, apertura nasi ossea), caudal margin: extended caudal to the rostral margin of the hiatus orbitonasalis (0); not extended caudal to the rostral margin of the hiatus orbitonasalis (1). (OH5)
81. Premaxilla, frontal process, naso-premaxillary suture: visible (0); obliterated (1). (BG95)
82. Basioccipital, subcondylar fossa (fossa subcondylaris): absent or shallow (0); deep (1). (BG73)
83. Supraoccipital, paired grooves for the exit of v. occipitalis externae (sulcus vena occipitalis externae): poorly developed (0); deeply excavated (1). (BG74)
84. Frontal, shelf of bone bounding salt-gland fossa (fossa glandulae nasalis) laterally: absent (0); present (1). (OH10)
85. Squamosal, temporal fossa (fossa temporalis), size: fossae separated by considerable wide surface (at least the width of the cerebellar prominence (0); more extensive, fossae meeting or nearly meeting at midline of the skull (1). (BG76)
86. Squamosal, temporal fossa (fossa temporalis), depth of caudal region: flat (0); shallow (1); greatly deepened (2). (BG77) Ordered.
87. Squamosal, development of the opening that transmits the a. ophthalmica externa in the caudoventral area of the temporal fossa (near nuchal crest): small or vestigial (0); well-developed (1). (BG78)

88. Orbit, fonticuli orbitocraniales: small or vestigial (0); broad and conspicuous openings (1). (BG79)
89. Ectethmoid: absent (0); weakly developed, widely separate from the lacrimal (1); well developed, contacting or fused to the lacrimal (2). (BG80)
90. Lacrimal, descending process: unperforated (0); perforated (1). (OH11)
91. Lacrimal, pneumatic foramen: absent (0); present by large lacrimal foramen. (D90)
92. Lacrimal: reduced, concealed in dorsal view (0); small portion exposed in dorsal view (1); well-exposed in dorsal view (2). (BG82) Ordered.
93. Lacrimal, contact with frontal: suture (0); fusion (1). (KT89)
94. Lacrimal, dorsal process: closely applied to the nasal (0); rostral arm of dorsal process separated from the nasal by a slit-like rostro-caudally elongate opening (1). (BG83)
95. Basitemporal plate (lamina parasphenoidalis), dorsoventral position with respect to the occipital condyle: ventral to the level of the condyle (0); at the level of the condyle (1); dorsal to the level of the condyle, surface depressed (2). (BG86) Ordered.
96. Basipterygoid process (processus basipterygoideus): absent (0); vestigial or poorly developed (1); well-developed (2). (BG87) Ordered.
97. Eustachian tubes (tuba auditiva): open or very little bony covering near the caudal end of the tube (0); mostly enclosed by bone (1). (BG88)
98. Pterygoid, shape: elongated (0); slight lateral expansion of rostral end (1); rostral end broad, pterygoid sub-triangular (2). (BG89) Ordered.
99. Palatine, lamella choanalis: curved and smooth plate, slightly differentiated from main palatine blade (0); ridged, distinct from main blade by a low keel (1); extended vertically ventrally forming the crista ventralis (2). (BG90) Ordered.
100. Vomer: laterally compressed, vertical laminae and free from palatines (0); horizontally flattened laminae and ankylosed with palatines (1). (BG91)
101. Facial foramen (foramen n. facialis) (ossa otica, fossa acustica interna): absent (2); present (1). (BG92)
102. Jugal arch, bar shape in lateral view: straight (0); slightly curved (1); ventrally bowed (2); strongly curved, sigmoid shape (3). (BG93) Ordered.
103. Jugal arch, dorsal process (this pointed process is located on the caudal end of the jugal, adjacent to the condyle for articulation with the quadrate: absent (0); present (1). (BG94)
104. Quadrate, relative lengths of otic and orbital processes (processus oticus and processus orbitalis): orbital process longer (0); otic process longer (1). (KC102)
105. Quadrate, otic process (processus oticus), rostral border, tubercle for m. adductor mandibulae externus, pars profunda: absent (0); present, as a ridge (1); present, as a tubercle (2). (BG96) Ordered.
106. Quadrate, otic process (processus oticus), rostral border, tubercle for m. adductor mandibulae externus, pars profunda: contiguous with squamosal capitulum (0); separated from squamosal capitulum (1). (KC104)
107. Quadrate, processus oticus, caudal margin in lateral view: straight (0); flexed so as to be concave caudally (1). (A9)
108. Tomial edge (crista tomialis): plane of tomial edge approximately at the level of the basitemporal plate (lamina parasphenoidalis) (0); dorsal to the level of the basitemporal plate (1). (BG97)
109. Mandible, symphysis: extensive bony connection (0); short terminal bony connection (1). (C101)
110. Mandible, posteriorly projected midline spur from dentary underlying symphysis: absent (0); present (1). (KC107)
111. Mandible, rostral fenestra (fenestra mandibulae rostralis): imperforate or small opening (0); large opening (1). (OH8)
112. Mandible, caudal fenestra (fenestra mandibulae caudalis): open, can be seen through from the medial or lateral aspects (0); nearly or completely concealed by the splenial medially (i.e., fenestra not visible in the medial aspect) (1). (OH9)

113. Mandible, mandibular ramus: depth subequal over entire ramus (0); pronounced deepening at midpoint (1). (BG101)
114. Mandible, mandibular ramus: essentially straight or gently sloping (0); pronounced ventral deflection near midpoint (1). (KC112)
115. Mandible, dentary, length of dorsal edge relative to mandibular ramus length in lateral view: markedly more than half the length of ramus (0); approximately half the length of ramus (1). (BG103)
116. Mandible, articular, medial process (processus medialis): not hooked (0); hooked (1). (BG104)
117. Mandible, angular, aspect in dorsal view: sharply truncated caudally projected, forming retroarticular process (processus retroarticularis). (BG106)
118. Mandible, angular, retroarticular process (processus retroarticularis), aspect in dorsal view in relation to the articular area for the quadrate between the lateral and medial condyles (condylus lateralis and condylus medialis): broad, approximately equal to the articular area (0); moderately long, narrower than the articular area (1); very long, longer and narrower than the articular area (2). (BG105) Ordered.
119. Mandible, medial emargination between medial and retroarticular processes (processus retroarticularis and processus medialis): absent (0); weak (1); concavity (2); strong concavity (3). (K108) Ordered.
120. Mandible, coronoid process (processus coronoideus), position on the dorsal margin of the mandible with respect to caudal mandibular fenestra (fenestra mandibulae caudalis): markedly rostral (0); on the rostral end of the fenestra (1) caudal to fenestra (2). (BG98)
121. Atlas, processus ventralis: absent or slightly developed (0); well developed, high and prominent ridge on the ventral surface of the arcus atlantis (1). (BG108)
122. Transition to free cervicothoracic ribs: starting at 13th cervical vertebra (0); starting at 14th cervical vertebra (1); starting at 15th cervical vertebra (2). (BG109) Ordered.
123. Cervical vertebrae, transverse process (processus transversus) in last five cervical vertebrae: not elongated laterally (0); greatly elongated laterally (1). (BG111)
124. Thoracic vertebrae, posterior-most vertebrae: heterocoelous (0); weakly opisthocoelous (1); strongly opisthocoelous (2). (K114) Ordered.
125. Thoracic vertebrae, deep excavation on lateral face of posterior thoracic vertebrae: absent (0); present (1). (KC124)
126. Synsacrum, number of incorporated vertebrae: nine (0); eleven (1); twelve (2); thirteen (3); fourteen (4); fifteen or more (5). (C117)
127. Synsacrum, height of crista synsacri between acetabula: flat or weakly projected (0); strongly projected (1). (KC126)
128. Synsacrum, first incorporated vertebra, position of fovea costalis: caudal to level of processus transversus (0); cranial to level of transverse process (1). (KF230)
129. Synsacrum, ventral surface of first few incorporated vertebrae: rounded or flattened (0); sharp, blade-like ventral margin (1). (A63)
130. Caudal vertebrae: seven (0); eight (1); nine or more (2). (BG113) Ordered.
131. Pygostyle, shape: tapers to a narrow edge both dorsally and ventrally as in most volant birds (0); triangular in cross-section with a wide, flat ventral margin (1). (KF232)
132. Thoracic ribs, uncinat processes (costae, processes uncinati): elongate, narrow (0); wide at base, spatulate (1); extremely wide at base (2). (BG114)
133. Thoracic ribs, uncinat processes (costae, processes uncinati): fused to ribs (0); unfused (1). (KC129)
134. Sternum, external spine (spina externa rostri): absent (0); present (1). (OH13)
135. Sternum, facies articularis furculae projects as a distinctive process: absent (0); present (1). (BG116)
136. Sternum, orientation of sulcus articularis coracoideus in ventral view: sulci oriented in essentially straight horizontal line (0); sulci directed caudolaterally so as to together form an inverted U shape (1). (A15)
137. Sternum, articular facets for coracoids (sulcus articularis coracoideus): meet or over-

- lap one another at midline (0); separated by wide non-articulatary surface (1). (C122)
138. Sternum, labrum internum: continues as sharp ridge onto the base of the spina externa (0); fades away without continuing onto the base (1). (C123)
139. Sternum, caudal incisurae. none (0); two (1); four (2). (KC134)
140. Sternum, trabecula lateralis projects caudal to main body of sternum: no (0); yes (1). (KF234)
141. Furcula, hypocleidium (apophysis furculae): absent or low knob-like process (0); long, blade-like process (1). (BG117)
142. Furcula, ramus: sub-ovoid in cross-section at omal end (0); mediolaterally flattened and craniocaudally expanded at omal end (1). (CL218)
143. Scapula, acromion: craniodorsally directed, nearly parallel to long axis of scapular shaft at apex (0); forms a blunt triangular projection with apex directed approximately at 45 degree angle from long axis of scapular shaft (1); narrow and tapering, apex omally directed (2); narrow and tapering, apex directed at a right angle to scapular shaft (3). (CL223) Ordered.
144. Scapula, blade, caudal half (corpus scapulae, extremitas caudalis: blade-like (0); slightly expanded (1); broadly expanded, paddle-shaped (2). (BG118) Ordered.
145. Scapula, facies articularis humeralis: rounded, projecting from shaft of scapula (0); compressed and ovoid, projecting from shaft of scapula (1); flattened and nearly merged with shaft of scapula (2). (KF235)
146. Coracoid, length: shorter than humerus (0); greatly elongated, longer than humerus (1). (KC137)
147. Coracoid, scapular cotyle (scapula cotylaris) deep and socket-like (0); moderately concave (1); nearly flat (2). (CL217)
148. Coracoid, processus acrocoracoideus, region of tuberculum brachiale: craniocaudally compressed (0); craniocaudally expanded, with a large flat surface cranial to tuberculum brachiale (1). (A22)
149. Coracoid, medial margin, coracoidal fenestra: complete (0); incomplete (1) absent (2). (OH14)
150. Coracoid, foramen nervi supracoracoidei, Mayr (2005) cited ontogenetic evidence that this foramen is not homologous to the coracoidal fenestra of penguins: absent (0); present (1). (K122)
151. Coracoid, sternal margin (extremitas sternalis coracoidei): greatly expanded (0); moderate expansion (1). (BG120)
152. Coracoid, profile of the sternal margin (extremitas sternalis coracoidei) in ventral view: convex (0); concave (1); flat (2). (K124)
153. Coracoid, facies articularis sternalis, dorsal surface: single facet (0); two facets (1). (KF236)
154. Coracoid, lateral process (processus lateralis): absent or highly reduced (0); well-developed (1). (KC142)
155. Forelimb elements: sub-circular in cross section (0); strongly dorsoventrally compressed (1). (BG121)
156. Humerus, head, very developed and reniform, continuous with tuberculum dorsale: moderate (0); enlarged and elliptical (1); very enlarged, hemispherical to reniform (2). (BG122) Ordered.
157. Humerus, head, proximal view, respect to the cranio-caudal axis: at midline (0); dorso-caudal (1); caudal (2). (CHb3) Ordered.
158. Humerus, head, dorsal (posterior) view proximal edge shape: semicircular, apex of humeral head located near midline (0); asymmetric arch with caudal apex, slightly prominent (1); asymmetric arch with caudal apex, strongly prominent (2). (C132)
159. Humerus, head, dorsal (posterior) view, notch between head and dorsal tubercle: present (0); absent (1). (CHa157)
160. Humerus, pit for ligament insertion on proximal surface adjacent to head: absent or very shallow (0); deep (1). (K128)
161. Humerus, dorsal tubercle, insertion of minor deltoid muscle, groove on proximal dorsal surface distocaudally from dorsal tubercle towards the base of the humerus head: present, deep dorsoproximal groove (0); inconspicuous to absent (1). (CHb7) Modified: Wording in definition changed for clarification.

162. Humerus, capital groove, position: caudal (0); ventrocaudal (1); ventral (2). (CHb8) Ordered.
163. Humerus, incisura capitis (capital groove), connection with sulcus transversus (transverse groove): essentially confluent with sulcus transversus, forming a single (0); connected through a narrow groove (1); completely separated (2). (K127)
164. Humerus, secondary tricipital fossa, connection with the capital incisure (capital groove): continuous, both structures are undifferentiated (0); connected, both structures are distinctive (1); completely separated (2). (CL222) Ordered.
165. Humerus, humeral intumescencia, projection from humeral shaft: ventrally projected (0); caudally projected (1); caudoventrally projected, being well exposed in cranial view (2). (K129) Ordered.
166. Humerus, tricipital fossa, proximal view, rim, proximal margin of tricipital fossa (fossa pneumotricipitalis ventralis): not exposed to slightly exposed at the caudoventral margin (0); well-exposed along the caudal margin (1). (K135)
167. Humerus, tricipital fossa, caudal view, margin: strongly concave (0); straight to slightly concave (1). (KT153)
168. Humerus, tricipital fossa (fossa tricipitalis), developed: shallow, with penetrating pneumatic foramina (0); moderate, without pneumatic foramen (1); deep, without pneumatic foramen (2). (BG123)
169. Humerus, tricipital fossa (fossa tricipitalis): single (0); bipartite (1). (BG124)
170. Humerus, ventral tubercle (tuberculum ventrale), dorsal (caudal) view, caudal projection: long, beyond the head (0); short, at level with the head (1). (CHb16)
171. Humerus, ventral tubercle, tubercle fossa: very shallow, caudal (0); deep, caudal (1); deep, caudoventral (2). (CHb17)
172. Humerus, deltoid crest, cranial coracobrachial muscle scar (impressio m. pectoralis): superficial, poorly-defined scar (0); shallow, well-defined oblong fossa (1); deep, well-defined oblong fossa (2). (BG125) Ordered.
173. Humerus, supracoracoideus muscle scar, shape (impressio insertii m. supracoracoideus): small, semicircular scar (0); strongly protruding, greatly elongated over dorsal surface (1); flat, greatly elongated over dorsal surface (2). (K133)
174. Humerus, supracoracoideus muscle scar, position: on the dorsal tubercle, at the proximal end of the humerus (0); on shaft dorsal surface, straight to slightly oblique (1); on shaft dorsal surface, strongly oblique (2). (CHb20) Ordered. Modified: Wording was changed for character state 0, for clarification.
175. Humerus, supracoracoideus and latissimus dorsi muscle scars, separation (impressio insertii m. supracoracoideus and m. latissimus dorsi): separated by a wide gap (0); separated by a moderate gap separated by small gap or confluent. (K134) Ordered.
176. Humerus, caudal coracobrachial muscle scar (coracobrachialis caudalis scar), contact with the distal margin of head: absent (0); present (1). (CL219)
177. Humerus, caudal coracobrachial muscle attachment (coracobrachialis caudal scar): subcircular fossa (0); small tubercle (1); flattened wide ovoid scar (2); flattened narrow elongate scar (3). (CL220) Ordered.
178. Humerus, groove for coracobrachialis nerve: absent or poorly defined (0); sharp, narrow sulcus (groove) (1). (CL221)
179. Humerus, shaft, craniocaudal (dorsoventral) width: shaft thins or maintains width distally (0); shaft widens distally (1). (K136)
180. Humerus, nutrient foramen (foramen nutricum) position: situated on ventral face of shaft (0); situated on caudal face of shaft (1). (C143)
181. Humerus, shaft, ventral (anterior) view, elongate furrow along caudal margin: absent (0); present (1). (C144)
182. Humerus, shaft, ventral (anterior) view, sigmoid curvature: absent or weak (0); strong (1). (K137)
183. Humerus, shaft, shaft robustness index (proximodistal length/craniocaudal width at middle point): elongated $SRI > 7$ (0); greatly slender, $7 > SRI > 6$ (1); slender, $6 > SRI > 5$ (2); thick, $5 > SRI > 4$ (3); bulky, $SRI < 4$ (4). (CHa176) Ordered.
184. Humerus, dorsal (posterior) view, preaxial angle: absent or inconspicuous (0); well defined (1). (CHa177)

185. Humerus, dorsal (posterior) view, caudal (ventral) edge, concavity proximal to the dorsal trochlear ridge: present (0); absent (1). (CHb31)
186. Humerus, development of dorsal supracondylar tubercle (processus supracondylar dorsalis): absent (0); vestigial, compact tubercle (1); short process (2); elongate process, well exposed in distal view (3). (BG126)
187. Humerus, dorsal (posterior) view, dorsal trochlear ridge, projection in relation with the caudal (ventral) margin of the shaft: surpassing it (0); reaching the margin (1); does not reach the margin (2). (BG128)
188. Humerus, brachial muscle scar, scar for origin of m. brachialis: cranial ovoid fossa (0); inconspicuous and elongate scar on the cranial margin, between dorsal condyle and preaxial angle (1); elongate scar on the cranial margin, with deep fossa distal to the preaxial angle (2). (A34)
189. Humerus, angle between main axis of shaft and tangent of dorsal and ventral condyles (condylus dorsalis and condylus ventralis): less than 30 degrees (0); 30 to 40 degrees (1); greater than or equal to 40 degrees (2); nearly 90 degrees (3). (K141)
190. Humerus, ulnar condyle (condylus ventralis), cranial (dorsal) and distal view: spheroidal, displaced over the ventral (anterior) edge (0); spheroidal, almost parallel to dorsal condyle (1); flattened, almost parallel to dorsal condyle (2). (K142) Ordered.
191. Humerus, distal end, humerotricipital groove: absent (0); present (1); present, delimited by trochlear ridges (2). (CHb37)
192. Humerus, distal end, scapulotricipital groove (demarcation of sulcus scapulotricipitalis): not demarcated (0); well-marked groove (1); well-marked, ventrally delimited by the middle trochlea ridge (2); deep groove, delimited by the dorsal and middle trochlear ridges (3). (BG127) Ordered.
193. Humerus, distal view, scapulotricipital and humerotricipital grooves: separated (0); cranially connected (1). (CHb39)
194. Humerus, distal view, ratio ventral condyle-adjacent shelf, ratio of condyle width: large, ratio <1.3 (0); moderate, $1.3 \leq$ ratio <2 (1); greatly reduced, ratio >2 (2). (K143) Ordered.
195. Humerus, ratio of width of proximal end of humerus to width of shaft. 2.4 or more (0); <2.4 (1). (M247)
196. Radius, shaft: sub-cylindrical (0); broad and flattened (1). (KC166)
197. Radius, proximally projecting spike-like process at cranial margin: absent (0); present (1). (KF239)
198. Ulna, olecranon position: arises at level of or proximally surpassing humeral cotylae (0); slightly displaced from cotylae (1); located one fourth of length to proximal end (2). (K144) Ordered.
199. Ulna, olecranon shape: short and robust tab-like projection with a rounded posterior margin (0); tab-like projection with a squared posterior margin (1); tab-like projection with a distinctive angular posterior margin (2). (CHa188) Separation of the position and shape of the olecranon into two independent characters, previously coded together in K144.
200. Ulna, incisura radialis: concave in proximal view, so that the ulna contacts the proximal radius at both its caudal and ventral surfaces (0); obsolete, so radius and ulna abut one another at a nearly flat contact (1). (KF240)
201. Ulna, presence of processus supracondylaris dorsalis (dorsal supracondylar process of ulna): present (0); absent (1). (M246)
202. Ulna, distinct process extending toward sulcus humerotricipitalis of humerus: absent (0); present (1). (K145)
203. Ulna, shaft shape: sub-cylindrical (e.g., *Diomedea*) (0); weak dorsoventral flattening, craniocaudally narrower distally (e.g., *Sequiwaimanu*) (1); strong dorsoventral flattening, prominent craniocaudal widening (e.g., *Spheniscus*) (2). (This study) Ordered.
204. Ulnare: U-shaped (0); triangular, fan-shaped wedge (1). (KC169)
205. Ulnare, distal angle (This character refers to the distal angle in the specialized fan-shaped ulnare of penguins and is considered non-comparable for outgroup taxa): rounded (0); pointed (1). (KF241)
206. Carpometacarpus, pisiform process (processus pisiformis): well-projected round

- tubercle (0); reduced to a low ridge (1). (C155)
207. Carpometacarpus, distal facet on metacarpal I: absent (0); present (1). (C156)
208. Carpometacarpus, metacarpal II, distinct anterior bowing: absent (0); present (1). (C157)
209. Carpometacarpus, extension of metacarpals II and III: subequal or III slightly shorter (0); metacarpal III projects markedly distal of metacarpal II (1). (C158)
210. Carpometacarpus, metacarpal III, distal articular surface (*facies articularis digitalis major*): wedge shaped or broadens anteriorly in distal view (0); slightly depressed ovoid surface (1). (C158)
211. Carpometacarpus, extensor process (*processus extensorius*): present (0); absent (1). (KC175)
212. Carpometacarpus, metacarpal II, distal expansion: absent (0); present (1). (KC176)
213. Phalanx III-1, proximal process: absent (0); present (1). (BG130)
214. Manual phalanges: much shorter than phalanx II-1 (0); phalanx II-1 and phalanx III-1 subequal in length (1). (C161)
215. Phalanges of manus, length relative to carpometacarpus: long (0); short (1). (BG131)
216. Fusion of ilia to synsacrum: unfused (0); partially fused (1); well fused (2). (K149) Ordered.
217. Pelvis, preacetabular ilia: flat, well-separated (0); approach one another, but do not contact at midline (1); contact at midline forming *canalis iliosynsacralis* (2). (KC181)
218. Pelvis, foramina intervertebralia large, forming wide openings on dorsal surface of pelvis: absent (0); present (1). (KC182)
219. Ilium, projected postiliac spine: absent (0); present (1). (KC183)
220. Pelvis, size of foramen ilioischadicum and foramen acetabuli: foramen ilioischadicum smaller or similar in size (0); foramen ilioischadicum larger (1). (OH16)
221. Pelvis, fenestra ischiopubica (*pelvis et os coxae*, fenestra isquiopubica): very wide and closed at its caudal end (0); slit-like and open at its caudal end (1). (BG133)
222. Ischium, caudal extent in relation to postacetabular ilium: ischium shorter than ilium (0); ischium projects slightly beyond the ilium (1); ischium projected far caudal to ilium (2). (BG134)
223. Patella: absent, unossified, or a small ossicle (0); present as a large, block-like element (1). (KC 187)
224. Patella, sulcus *m. ambiens*: shallow groove (0); deep groove (1); perforated (2). (BG135)
225. Tibiotarsus, *crista patellaris*: slightly developed (0); well-projected (1); greatly elongated (2). (BG136)
226. Tibiotarsus, shaft, craniocaudal flattening: weak, midshaft craniocaudal depth greater than 75% mediolateral width (0); strong, midshaft craniocaudal depth equal to or less than 75% mediolateral width (1). (C169)
227. Tibiotarsus, sulcus *extensorius*: laterally positioned (0); close to midline (1); medially positioned (2). (K139)
228. Tibiotarsus, notch in distal edge of medial condyle (*condylus medialis*): present (0); absent (1). (AH38)
229. Tibiotarsus, lateral condyle (*condylus lateralis*) in lateral profile: ovoid (0); subcircular (1). (AH37)
230. Tibiotarsus, medial margin in distal view: margin is nearly straight (0); margin strongly convex (1). (KF242)
231. Tarsometatarsus, elongation index (proximodistal length/mediolateral width at proximal end): slender, $EI > 3.0$ (0); shortened, $3.0 > EI > 2.5$ (1); strongly shortened, $2.5 > EI > 2.0$ (2); very strongly shortened, $EI < 2.0$ (3). (BG138) Ordered.
232. Tarsometatarsus, proximal view, dorso-plantar compression (maximum lateromedial width/dorsoplantar width at middle point): weak, < 2 (0); strong, > 2 (1). (CHb42)
233. Tarsometatarsus, proximal view, size of cotylae: lateral bigger than medial (0); subequal (1); medial bigger than lateral (2). (CHb43)
234. Tarsometatarsus, lateral cotyla, dorsomedially expanded. In some taxa the dorsal edge of the lateral cotyla is dorsomedially deflected, expanding it slightly under the

- intercotylar prominence: absent (0); present (1). (CHb44)
235. Tarsometatarsus, lateral cotyla dorsal view, lateral projection: prominent (0); flattened (1). (CHb45)
236. Tarsometatarsus, medial cotyla, proximal view, pointed dorsal edge: absent (0); present (1). (CHb46)
237. Tarsometatarsus, medial cotyla, position: proximal (0); slightly dorsodistally deflected (1); strongly dorsodistally deflected (2). (CHb47)
238. Tarsometatarsus, enclosed hypotarsal canals (canales hypotarsi): absent (0); present (1). (BG141) Ordered. Note: While this character was modified by Chávez Hoffmeister (2014a) to associate state 1 with the enlarged hypotarsal canal present in *Gavia*, because *Gavia* was not used in our main phylogenetic analyses our character scores for this character follow Degrange et al. (2018).
239. Tarsometatarsus, proximal view, tendon of muscle flexor digitorum longus: groove (0); partially closed groove (1); canal (2). (CHb49)
240. Tarsometatarsus, proximal view, tendon of muscle flexor hallucis longus: groove, delimited medially by the crista lateralis flexor digitorum longus or the crista medialis flexor hallucis longus, and laterally by the crista lateralis flexor hallucis longus (0); groove, laterally open (1); poorly defined, inconspicuous or absent (2); canal (3). (CHb50) Modified: Wording for state 0 altered to be in accordance with terminology specified in Mayr (2016). Note that state 0 can be observed in Figures 8.5, A10.2, A10.6, state 1 in Figure A10.1, A10.4-A10.5, A10.8, A10.9-A10.10 state 2 in Figure A10.7, A10.12-A10.15 and state 3 in Figure A10.3.
241. Tarsometatarsus, crista lateralis flexor digitorum longus: present (0); absent (1). (KF243) Modified: Definition wording altered to be in accordance with hypotarsus terminology specified by Mayr (2016).
242. Tarsometatarsus, medial hypotarsal crest, proximal view, bilobulated: absent (0); present (1). (CHb52)
243. Tarsometatarsus, proximal and plantar views, hypotarsal crests, crista lateralis flexoris digitorum longus, crista medialis flexor hallucis longus and crista lateralis flexoris digitorum longus: trisulcate, both crista lateralis flexoris digitorum longus and crista medialis flexoris hallucis longus are present (0); bisulcate, crista lateralis flexoris digitorum longus present and distinct (yet may be partially fused to the crista lateralis flexoris hallucis longus), crista lateralis flexoris hallucis longus present or vestigial, crista lateralis flexoris digitorum longus has subequal or greater plantar projection to crista lateralis flexoris hallucis longus (1); monosulcate, crista lateralis flexor digitorum longus is vestigial, indistinguishable or absent, crista lateralis flexoris hallucis longus is present or vestigial, crista lateralis flexoris hallucis longus projects further plantarly than crista lateralis flexoris digitorum longus in the instance that crests are present (2). (K158) Ordered. Modified: Wording of character definition and states changed to be in accordance with hypotarsus terminology in Mayr (2016), in order to more accurately and specify and label hypotarsus morphologies, and to reflect the range of penguin hypotarsus morphologies. It should be noted that bicanaliculate morphology as described by Mayr (2016) is classified as bisulcate (state 1) in this character for simplicity. State 0 can be seen in Figures A10.1, A10.3, state 1 in Figure 10.2, A10.4-A10.11, and state 2 in Figure A10.12-A10.15.
244. Tarsometatarsus, crista lateralis flexor hallucis longus, plantar view: enlarged and connected with crista medialis flexor digitorum longus (0); well-defined and parallel to proximodistal axis of tarsometatarsus (1); reduced, poorly defined and proximal to lateral foramen forming a diagonal ridge that overhangs lateral foramen (2). (CHa224) Modified: Wording for definition and state 0 altered to be in accordance with terminology specified in Mayr (2016).
245. Tarsometatarsus, proximal view, plantar projection of crista lateralis flexor hallucis longus and/or crista lateralis flexor digitorum longus relative to crista medialis flexor digitorum longus: shorter (0); subequal (1). (KT203) Modified: Wording for definition altered to be in accordance with terminology specified in Mayr (2016).

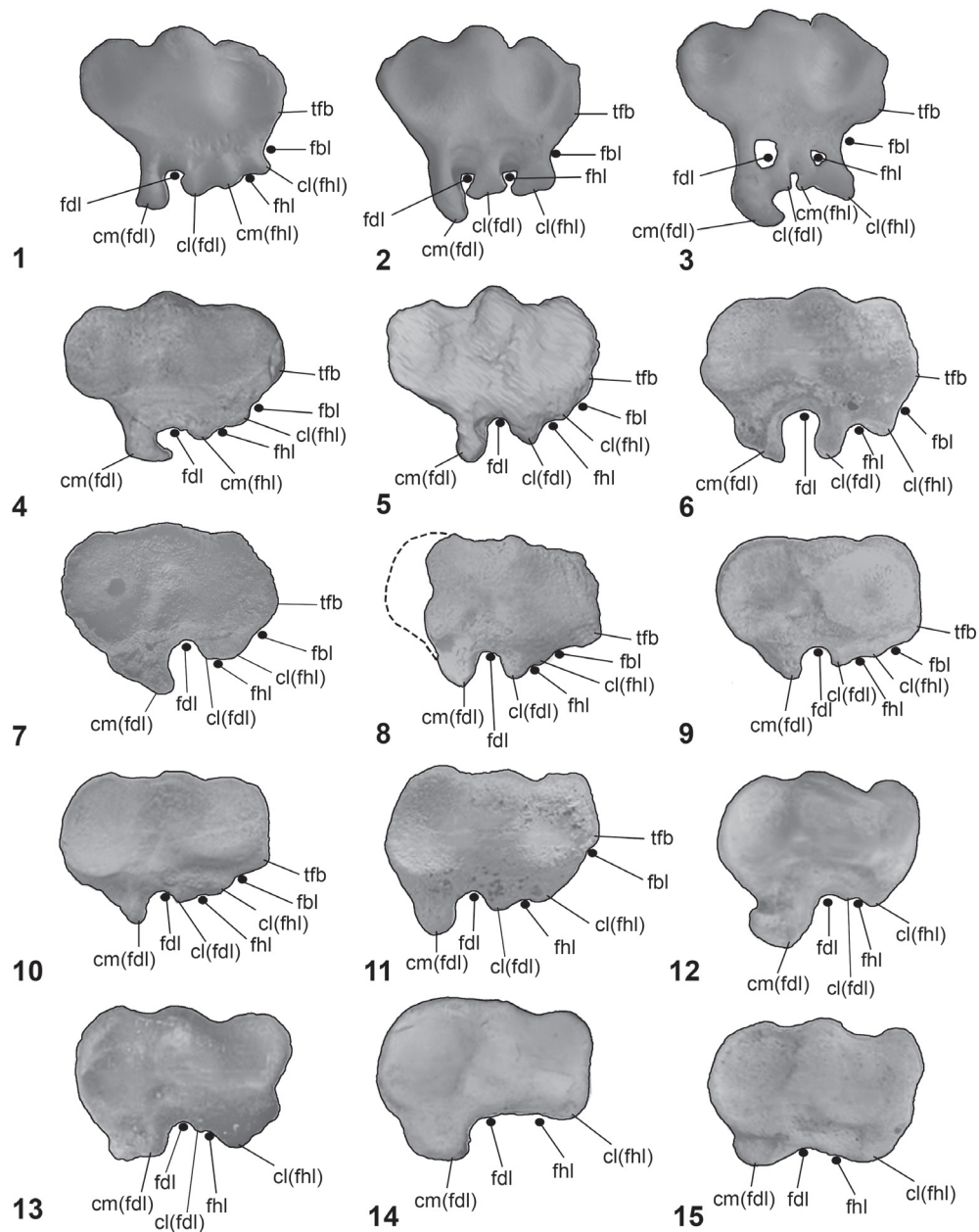


FIGURE A10. Specifics of referred hypotarsal morphology. **1**, *Diomedea antipodensis* left (mirrored, adapted from Mayr, 2016); **2**, *Aphrodroma brevirostris*, left (mirrored, adapted from Mayr, 2016); **3**, *Hydrobates castro*, left (mirrored, adapted from Mayr, 2016); **4**, *Waimanu manneringi*, right, CM zfa35; **5**, *Muriwaimanu tuatahi*, right, 2009.99.1 (.STL file, tomographic rendering); **6**, *Marambiornis exilis*, right, IB/P/B-0490 (modified from Jadwiszczak, 2015); **7**, *Delphinornis gracilis*, right, IB/P/B-0279a; **8**, *Anthropornis nordenskoeldi*, MLP 95-I-10-142 (mirrored, modified from Jadwiszczak, 2015); **9**, *Palaeudyptes klekowskii*, IB/P/B-0485 (mirrored, modified from Jadwiszczak, 2015); **10**, *Palaeudyptes antarcticus*, right, BM A.1048; **11**, *Palaeospheniscus bergi*, NHMUK A694 (mirrored, modified from Jadwiszczak, 2015); **12**, *Spheniscus magellanicus*, NHMUK 2001.45.1 (mirrored, modified from Jadwiszczak, 2015); **13**, *Eudyptes chrysocome*, NHMUK 1898.7.1.15 (mirrored, modified from Jadwiszczak, 2015); **14**, *Aptenodytes forsteri*, NHMUK 1905.12.30.419 (mirrored, modified from Jadwiszczak, 2015); **15**, *Pygoscelis adeliae*, unassigned from IB/P/B (mirrored, modified from Jadwiszczak, 2015); abbreviations: **cl(fdl)**, crista lateralis flexoris digitorum longus; **cl(fhl)**, crista lateralis flexoris hallucis longus; **cm(fdl)**, crista medialis flexoris digitorum longus; **fbl**, sulcus for musculus fibularis longus; **fdl**, sulcus/canal for tendon of musculus flexor digitorum longus; **fhl**, sulcus/canal for tendon of musculus flexor hallucis longus; **tfb**, tuberculum musculus fibularis brevis. Dotted line represents estimated extent of bone. Not to scale.

246. Tarsometatarsus, collateral lateral ligament scar (impressio lig. collat. lat.): absent or inconspicuous (0); well-defined, creating a depression over the lateral surface (1); well-defined, creating a notch on the proximolateral vertex (2). (CHa219)
247. Tarsometatarsus, proximal vascular foramina, plantar view: medial foramen present, lateral foramen absent or vestigial (0); both foramina present (1); foramen vasculare proximale laterale present, foramen vasculare proximale mediale absent or vestigial (2). (K162)
248. Tarsometatarsus, lateral foramen, dorsal view: absent or vestigial (0); small (1); enlarged (2). (CHa229)
249. Tarsometatarsus, medial foramen, plantar view, opens distally to medial crest (opening for medial foramen proximalis vascularis distal to crista medialis hypotarsi): absent (0); present (1). (BG140)
250. Tarsometatarsus, medial foramen, medial view, perforating the medial hypotarsal crest (crista medialis hypotarsi/crista medialis flexor digitorum longus) perforated by opening for the medial foramen proximalis vascularis): absent (0); present (1). (B139) Modified: Wording in definition changed in accordance with hypotarsus terminology in Mayr (2016).
251. Tarsometatarsus, lateral edge, lateral view, strongly dorsoplantarly compressed: absent (0); present (1). (CHb61)
252. Tarsometatarsus, lateral edge, dorsal view: straight (0); concave (1). (A72)
253. Tarsometatarsus, dorsal view, medial margin, pronounced convexity: absent (0); present (1). (K157)
254. Tarsometatarsus, dorsal view, medial infracotyler groove: absent or poorly defined (0); present, proximal to the medial foramen, laterally open or limited by shallow tuberosities (1); present, laterally delimited by a crest or an osseus lamina that overhangs and partially occludes the medial foramen (2). (CHb64) Modified: Wording for state 1 and 2 expanded upon as per Chávez Hoffmeister (2014b).
255. Tarsometatarsus, dorsal view, lateral dorsal groove: absent or poorly defined (0); present, distal (1); present, along all the body (2). (CHb65)
256. Tarsometatarsus, dorsal view, medial dorsal groove: absent or barely perceptible (0); shallow groove (1); moderate groove (2); deep groove (3). (K159) Ordered.
257. Tarsometatarsus, dorsal, distal and plantar aspects, incisura intertrochlearis lateralis, foramen vasculare distale and canalis interosseus distalis: present, foramen vasculare distale opens proximal to the incisura intertrochlearis lateralis on the dorsal and plantar surfaces, and also the canalis interosseus distalis opens distally within the incisura intertrochlearis lateralis, separated by osseus ridges dorsally and plantarly from the foramen vasculare distale (0); present, foramen vasculare distale opens on the dorsal surface, and also distoplantarly, openings separated by a dorsally located osseus bridge, or may be connected forming a partially closed canal (1); absent (2). (K163) Ordered. Modified: Wording for state 0 and 1 altered.
258. Tarsometatarsus, intertrochlear notches, dorsal view: medial notch absent (0); medial notch deeper than lateral (1); subequal (2); lateral notch deeper than medial (3). (CHa233)
259. Tarsometatarsus, medial and lateral trochleae, dorsal view: medial trochlea shorter than lateral (0); lateral trochlea slightly shorter than medial (1); subequal (2). (CHa234)
260. Tarsometatarsus, lateral trochlea, dorsal view: laterally projected (0); straight (1); medially deflected (2). (K160)
261. Tarsometatarsus, medial trochlea, dorsal view, medial projection: strongly projected (0); moderately projected (1); planto-laterally deflected (2). (CHb71)
262. Tarsometatarsus, medial trochlea, dorsal view, presence of a neck between the trochlea and the tarsometatarsus body: absent (0); present (1). (CHb72)
263. Tarsometatarsus, lateral trochlea, distal view: dorsally aligned with intermediate trochlea (0); dorsally deflected (1); plantarly deflected (2). (KT211)
264. Tarsometatarsus, medial trochlea, distal view, strongly plantarly deflected: absent (0); present (1). (A73)

265. Tarsometatarsus, lateral trochlea, distal view, laterally deflected: absent (0); present (1). (LZ2366)
266. Tarsometatarsus, medial trochlea, plantar view, orientation of the medial and lateral carinae on the plantar-most articulation surface of trochlea metatarsi III: strongly distoproximally tapered trochlear rims (0); weakly distoproximally tapered trochlear rims (1); parallel-sided trochlear rims (2). (This study). This character relates to a distinguishing feature described by Mayr et al., (2018), differentiating tarsometatarsi of *Waimanu manningi* and *Muriwaimanu tuatahi*.
267. Pedal digit I: small, with metatarsal I and single phalanx both present (0); metatarsal I reduced to an ossicle, claw represented by a minute ossicle or lost (1); metatarsal I absent (2). (KF245) Ordered.
- Myology:**
268. M. latissimus dorsi, pars cranialis, accessory slip: absent (0); present (1). (BG143)
269. M. latissimus dorsi, pars cranialis and pars caudalis: separated (0); fused (1). (BG144)
270. M. latissimus dorsi, pars metapatagialis, development: wide (0); intermediate (1); narrow (2). (BG145) Ordered.
271. M. serratus profundus, cranial fascicle: absent (0); present (1). (BG146)
272. M. deltoideus, pars proapatagialis, subdivision in superficial and deep layers: undivided (0); divided (1). (BG147)
273. M. deltoideus, pars major: triangular or fan-shaped (0); strap-shaped (1). (BG148)
274. M. deltoideus, pars major, caput caudale: short (0); intermediate (1); long (2). (BG149) Ordered.
275. M. deltoideus, pars minor, origin on the clavicular articulation of the coracoid: absent (0); present (1). (BG150)
276. M. ulnometacarpalis ventralis: absent (0); present (1). (BG151)
277. M. ilirotrochantericus caudalis: narrow (0); wide (1). (BG152)
278. M. iliofemoralis, origin: tendinous (0); partially tendinous and partially fleshy (1); totally fleshy (2). (BG153) Ordered.
279. M. flexor perforatus digitis IV, rami II-III: free (0); fused (1). (BG154)
280. M. flexor perforatus digitis IV, rami I-IV: free (0); fused (1). (BG155)
281. M. flexor perforatus digitis IV, insertion of middle rami: on phalanx 3 (0); on phalanx 4 (1). (BG156)
282. M. latissimus dorsi, pars caudalis, additional origin from dorsal process of vertebrae: absent (0); present (1). (BG157)
- Other soft tissue:**
283. Oral mucosa (bucca, tunica mucosa oris), buccal papillae group on the medial surface of the lower jaw (ramus mandibularis) at the level of the rictus: small number of rudimentary papillae with no clear arrangement (0); large, elongated papillae with no clear arrangement (1); two clear rows of short conical papillae (2). (BG158)
284. Tracheal rings: single (0); bifurcated (1). (KC219)

REFERENCES (APPENDIX 1)

- Acosta Hospitaleche, C. 2005. Systematic revision of *Arthrodytes* Ameghino, 1905 (Aves, Spheniscidae) and its assignment to the Paraptenodytinae. *Neues Jahrbuch für Geologie und Paläontologie-Abhandlungen*, 7:404–414.
- Acosta Hospitaleche, C. 2007. Revisión sistemática de *Palaeospheniscus biloculata* (Simpson) nov. comb. (Aves, Spheniscidae) de la Formación Gaiman (Mioceno Temprano), Chubut, Argentina. *Ameghiniana*, 44:417–426.
- Acosta Hospitaleche, C., Castro, L., Tambussi, C. and Scasso, R.A. 2008. *Palaeospheniscus patagonicus* (Aves, Sphenisciformes): New discoveries from the early Miocene of Argentina. *Journal of Paleontology*, 82:565–575. <https://doi.org/10.1666/07-014.1>

- Acosta Hospitaleche, C., Hagström, J., Reguero, M. and Mörs, T. 2017. Historical perspective of Otto Nordenskjöld's Antarctic penguin fossil collection and Carl Wiman's contribution. *Polar Record*, 53:364–375. <https://doi.org/10.1017/S0032247417000249>
- Acosta Hospitaleche, C. and Reguero, M. 2010. First articulated skeleton of *Palaeudyptes gunnari* from the late Eocene of Isla Marambio (Seymour Island), Antarctica. *Antarctic Science*, 22:289–298. <https://doi.org/10.1017/S0954102009990769>
- Acosta Hospitaleche, C. and Reguero, M. 2014. *Palaeudyptes klekowskii*, the best-preserved penguin skeleton from the Eocene–Oligocene of Antarctica: Taxonomic and evolutionary remarks. *Geobios*, 47:77–85. <https://doi.org/10.1016/j.geobios.2014.03.003>
- Acosta Hospitaleche, C. and Tambussi, C. 2008. South American fossil penguins: A systematic update. *Oryctos*, 7:109–127.
- Acosta Hospitaleche, C., Tambussi, C., Donato, M. and Cozzuol, M. 2007. A new Miocene penguin from Patagonia and its phylogenetic relationships. *Acta Palaeontologica Polonica*, 52:299–314.
- Ameghino, F. 1905. Enumeración de los impennes fósiles de Patagonia y de la Isla Seymour. *Anales del Museo Nacional de Buenos Aires*, 3:97–167.
- Ando, T. 2007. *New Zealand fossil penguins: Origin, pattern, and process*. Unpublished PhD Thesis University of Otago, Dunedin, New Zealand.
- Bertelli, S. and Giannini, N.P. 2005. A phylogeny of extant penguins (Aves: Sphenisciformes) combining morphology and mitochondrial sequences. *Cladistics*, 21:209–239. <https://doi.org/10.1111/j.1096-0031.2005.00065.x>
- Bertelli, S., Giannini, N.P. and Ksepka, D.T. 2006. Redescription and phylogenetic position of the early Miocene penguin *Parapterodytes antarcticus* from Patagonia. *American Museum Novitates*, 3525:1–36.
- Chávez Hoffmeister, M.F. 2014a. The humerus and stratigraphic range of *Palaeospheniscus* (Aves, Sphenisciformes). *Ameghiniana*, 51:159–173. <https://doi.org/10.5710/AMEGH.14.02.2014.637>
- Chávez Hoffmeister, M.F. 2014b. Phylogenetic characters in the humerus and tarsometatarsus of penguins. *Polish Polar Research*, 35:469–496. <https://doi.org/10.2478/popore-2014-0025>
- Chávez Hoffmeister, M.F., Carrillo Briceño, J.D. and Nielsen, S.N. 2014. The evolution of seabirds in the Humboldt Current: New clues from the Pliocene of central Chile. *PLoS ONE*, 9:e90043 (90041–90012). <https://doi.org/10.1371/journal.pone.0090043>
- Chávez, M.F. 2007. Sobre la presencia de *Parapterodytes* y *Palaeospheniscus* (Aves: Sphenisciformes) en la Formación Bahía Inglesa, Chile. *Revista Chilena de Historia Natural*, 80:255–259. <https://doi.org/10.4067/S0716-078X2007000200010>
- Clarke, J.A., Ksepka, D.T., Salas-Gismondi, R., Altamirano, A.J., Shawkey, M.D., D'Alba, L., Vinther, J., DeVries, T.J. and Baby, P. 2010. Fossil evidence for evolution of the shape and color of penguin feathers. *Science*, 330:954–957. <https://doi.org/10.1126/science.1193604>
- Clarke, J.A., Ksepka, D.T., Stucchie, M., Urbina, M., Giannini, N., Bertelli, S., Narvez, Y. and Boyd, C.A. 2007. Paleogene equatorial penguins challenge the proposed relationship between biogeography, diversity, and Cenozoic climate change. *Proceedings of the National Academy of Sciences of the United States of America*, 104:11545–11550. <https://doi.org/10.1073/pnas.0611099104>
- Degrange, F.J., Ksepka, D.T. and Tambussi, C.P. 2018. Redescription of the oldest crown clade penguin: Cranial osteology, jaw myology, neuroanatomy, and phylogenetic affinities of *Madrynornis mirandus*. *Journal of Vertebrate Paleontology*, 38:e1445636 (1445631–1445625). <https://doi.org/10.1080/02724634.2018.1445636>
- Fordyce, R.E. and Thomas, D.B. 2011. *Kaiika maxwelli*, a new early Eocene archaic penguin (Sphenisciformes, Aves) from Waihao Valley, South Canterbury, New Zealand. *New Zealand Journal of Geology and Geophysics*, 54:43–51. <https://doi.org/10.1080/00288306.2011.536521>
- Gavryushkina, A., Heath, T.A., Ksepka, D.T., Stadler, T., Welch, D. and Drummond, A.J. 2017. Bayesian total-evidence dating reveals the recent crown radiation of penguins. *Systematic Biology*, 66:57–73. <https://doi.org/10.1093/sysbio/syw060>
- Giannini, N.P. and Bertelli, S. 2004. Phylogeny of extant penguins based on integumentary and breeding characters. *The Auk*, 121:422–434. <https://doi.org/10.2307/4090406>
- Göhlich, U.B. 2007. The oldest fossil record of the extant penguin genus *Spheniscus* – A new species from the Miocene of Peru. *Acta Paleontologica Polonica*, 52:285–298

- Huxley, T.H. 1859. On a fossil bird and a fossil cetacean from New Zealand. *Quarterly Journal of the Geological Society of London*, 15:670–677. <https://doi.org/10.1144/GSL.JGS.1859.015.01-02.73>
- Jadwiszczak, P. 2006a. Eocene penguins of Seymour Island, Antarctica: Taxonomy. *Polish Polar Research*, 27:3–62.
- Jadwiszczak, P. 2006b. Eocene penguins of Seymour Island, Antarctica: The earliest record, taxonomic problems and some evolutionary considerations. *Polish Polar Research*, 27:287–302.
- Jadwiszczak, P. 2010. New data on the appendicular skeleton and diversity of Eocene Antarctic penguins, p. 45–51. In Nowakowski, D. (ed.) *Morphology and Systematics of Fossil Vertebrates*. DN Publishers, Wrocław. <https://doi.org/10.13140/2.1.4673.1204>
- Jadwiszczak, P. 2013. Taxonomic diversity of Eocene Antarctic penguins: A changing picture, p. 129–138. In Hambrey, M.J., Barker, P.F., Barrett, P.J.B., Davies, V. B., Smellie, J.L. and Tranter, M. (eds.), *Antarctic Palaeoenvironments and Earth-Surface Processes*. The Geological Society, London. <https://doi.org/10.1144/SP381.7>
- Jadwiszczak, P. 2015. Another look at tarsometatarsi of early penguins. *Polish Polar Research*, 36:343–354. <https://doi.org/10.1515/popore-2015-0024>
- Jadwiszczak, P., Hospitaleche, C.A. and Reguero, M. 2013. Redescription of *Crossvallia unienwillia*: The only Paleocene Antarctic penguin. *Ameghiniana*, 50:545–553. <https://doi.org/10.5710/AMGH.09.10.2013.1058>
- Jadwiszczak, P. and Mörs, T. 2019. First partial skeleton of *Delphinornis larseni* Wiman, 1905, a slender-footed penguin from the Eocene of Antarctic Peninsula. *Palaeontologia Electronica* 22.2.32A 1–31. <https://doi.org/10.26879/933>
palaeo-electronica.org/content/2019/2574-skeleton-of-an-eocene-penguin
- Jenkins, R.J.F. 1974. A new giant penguin from the Eocene of Australia. *Paleontology*, 17:291–310.
- Ksepka, D.T. 2007. *Phylogeny, histology and functional morphology of fossil penguins (Sphenisciformes)*. Unpublished PhD Thesis, Columbia University, New York, USA.
- Ksepka, D.T. and Ando, T. 2011. Penguins past, present, and future: Trends in the evolution of the Sphenisciformes, p. 155–186. In Dyke, G. and Kaiser, G.W. (eds.), *Living Dinosaurs: The Evolutionary History of Modern Birds*. John-Wiley & Sons Ltd, Hoboken, New Jersey. <https://doi.org/10.1002/9781119990475.ch6>
- Ksepka, D.T., Bertelli, S. and Giannini, N.P. 2006. The phylogeny of the living and fossil Sphenisciformes (penguins). *Cladistics*, 22:412–441. <https://doi.org/10.1111/j.1096-0031.2006.00116.x>
- Ksepka, D.T. and Clarke, J.A. 2010. The basal penguin (Aves: Sphenisciformes) *Perudyptes devriesi* and a phylogenetic evaluation of the penguin fossil record. *Bulletin of the American Museum of Natural History*, 337:1–77. <https://doi.org/10.1206/653.1>
- Ksepka, D.T., Clarke, J.A., DeVries, T.J. and Urbina, M. 2008. Osteology of *Icadyptes salasi*, a giant penguin from the Eocene of Peru. *Journal of Anatomy*, 213:131–147. <https://doi.org/10.1111/j.1469-7580.2008.00927.x>
- Ksepka, D.T., Fordyce, R.E., Ando, T. and Jones, C.M. 2012. New fossil penguins (Aves, Sphenisciformes) from the Oligocene of New Zealand reveal the skeletal plan of stem penguins. *Journal of Vertebrate Paleontology*, 32:235–254. <https://doi.org/10.1080/02724634.2012.652051>
- Ksepka, D.T. and Thomas, D.B. 2012. Multiple Cenozoic invasions of Africa by penguins (Aves, Sphenisciformes). *Proceedings of the Royal Society of London B: Biological Sciences*, 279:1027–1032. <https://doi.org/10.1098/rspb.2011.1592>
- Livezey, B.C. and Zusi, R.L. 2007. Higher-order phylogeny of modern birds (Theropoda, Aves: Neornithes) based on comparative anatomy. II. Analysis and discussion. *Zoological Journal of the Linnean Society*, 149:1–95. <https://doi.org/10.1111/j.1096-3642.2006.00293.x>
- Marples, B.J. 1952. Early Tertiary penguins of New Zealand. *New Zealand Geological Survey, Palaeontological Bulletin*, 20:1–66.
- Marples, B.J. 1953. Fossil penguins from the mid-Tertiary of Seymour Island. *Falkland Islands Dependence Survey Scientific Reports*, 5:1–15.
- Mayr, G. 2005. Tertiary plotopterids (Aves, Plotopteridae) and a novel hypothesis on the phylogenetic relationships of penguins (Spheniscidae). *Journal of Zoological Systematics and Evolutionary Research*, 43:61–71. <https://doi.org/10.1111/j.1439-0469.2004.00291.x>

- Mayr, G. 2016. Variations in the hypotarsus morphology of birds and their evolutionary significance. *Acta Zoologica*, 97:196–210. <https://doi.org/10.1111/azo.12117>
- Mayr, G., De Pietri, V.L., Love, L., Mannering, A.A. and Scofield, R.P. 2018. A well-preserved new mid-Paleocene penguin (Aves, Sphenisciformes) from the Waipara Greensand in New Zealand. *Journal of Vertebrate Paleontology*, 37:e1398169 (1398161–1398119). <https://doi.org/10.1080/02724634.2017.1398169>
- Mayr, G., De Pietri, V.L., Love, L., Mannering, A. and Scofield, R.P. 2019. Leg bones of a new penguin species from the Waipara Greensand add to the diversity of very large-sized Sphenisciformes in the Paleocene of New Zealand. *Alcheringa: An Australasian Journal of Palaeontology*. <https://doi.org/10.1080/03115518.2019.1641619>
- Mayr, G., De Pietri, V.L. and Scofield, R.P. 2017a. A new fossil from the mid-Paleocene of New Zealand reveals an unexpected diversity of world's oldest penguins. *The Science of Nature*, 104:1–6. <https://doi.org/10.1007/s00114-017-1441-0>
- Mayr, G., Scofield, R.P., De Pietri, V.L. and Tennyson, A.J. 2017b. A Paleocene penguin from New Zealand substantiates multiple origins of gigantism in fossil Sphenisciformes. *Nature Communications*, 8:1–8. <https://doi.org/10.1038/A41467-017-01959-6>
- Myrcha, A., Jadwiszczak, P., Tambussi, C.P., Noriega, J.I., Gaździcki, A., Tatur, A. and Del Valle, R. 2002. Taxonomic revision of Eocene Antarctic penguins based on tarsometatarsal morphology. *Polish Polar Research*, 23:5–46.
- Myrcha, A., Tatur, A. and Del Valle, R. 1990. A new species of fossil penguin from Seymour Island, West Antarctica. *Alcheringa: An Australasian Journal of Palaeontology*, 14:195–205. <https://doi.org/10.1080/03115519008619055>
- O'Hara, R.J. 1989. *Systematics and the study of natural history, with an estimate of the phylogeny of the living penguins (Aves: Spheniscidae)*. Unpublished PhD Thesis, Harvard University, Cambridge, Massachusetts, USA.
- Park, T. 2014. Redescription of the Miocene penguin *Pseudapterodytes macraei* Simpson (Aves: Sphenisciformes) and redefinition of the taxonomic status of *?Pseudapterodytes minor* Simpson. *Alcheringa: An Australasian Journal of Palaeontology*, 38:450–454. <https://doi.org/10.1080/03115518.2014.906177>
- Park, T. and Fitzgerald, E.M.G. 2012. A review of Australian fossil penguins (Aves: Sphenisciformes). *Memoirs of Museum Victoria*, 69:309–325. <https://doi.org/10.24199/j.mmv.2012.69.06>
- Park, T., Fitzgerald, E.M.G., Gallagher, S.J., Tomkins, E. and Allan, T. 2016. New Miocene fossils and the history of penguins in Australia. *PLoS ONE*, 11:e0153915 (0153911–0153921). <https://doi.org/10.1371/journal.pone.0153915>
- Parras, A., Dix, G.R. and Griffin, M. 2012. Sr-isotope chronostratigraphy of Paleogene–Neogene marine deposits: Austral Basin, southern Patagonia (Argentina). *Journal of South American Earth Sciences*, 37:122–135. <https://doi.org/10.1016/j.jsames.2012.02.007>
- Parras, A., Griffin, M., Feldmann, R., Casadío, S., Schweitzer, C. and Marensi, S. 2008. Correlation of marine beds based on Sr- and Ar-date determinations and faunal affinities across the Paleogene/Neogene boundary in southern Patagonia, Argentina. *Journal of South American Earth Sciences*, 26:204–216. <https://doi.org/10.1016/j.jsames.2008.03.006>
- Raine, J.I., Beu, A.G., Boyes, A.F., Campbell, H., Cooper, R.A., Crampton, J.S., Crundwell, M.P., Hollis, C.J. and Morgans, H. 2015. New Zealand Geological Timescale: NTGT2015/1. *New Zealand Journal of Geology and Geophysics*, 58:398–403. <https://doi.org/10.1080/00288306.2015.1086391>
- Reguero, M., Goin, F., Acosta Hospitaleche, C., Dutra, T. and Marensi, S. 2013. *Late Cretaceous/Paleogene West Antarctica Terrestrial Biota and its Intercontinental Affinities*. Springer, Dordrecht. <https://doi.org/10.1007/978-94-007-5491-1>
- Roberts, D.L., Matthews, T., Herries, A.I., Boulter, C., Scott, L., Dondo, C., Mtembi, P., Browning, C., Smith, R.M. and Haarhoff, P. 2011. Regional and global context of the Late Cenozoic Langebaanweg (LBW) palaeontological site: West Coast of South Africa. *Earth-Science Reviews*, 106:191–214. <https://doi.org/10.1016/j.earscirev.2011.02.002>
- Simpson, G.G. 1946. Fossil penguins. *Bulletin of the American Museum of Natural History*, 87:7–99.
- Simpson, G.G. 1957. Australian fossil penguins, with remarks on penguin evolution and distribution. *Records of the South Australian Museum*, 13:51–70.
- Simpson, G.G. 1970. Miocene penguins from Victoria, Australia, and Chubut, Argentina. *Memoirs of the National Museum of Victoria*, 31:17–24.

- Simpson, G.G. 1971a. Fossil penguin from the late Cenozoic of South Africa. *Science*, 171:1144–1145. <https://doi.org/10.1126/science.171.3976.1144>
- Simpson, G.G. 1971b. A review of the pre-Pliocene penguins of New Zealand. *Bulletin of the American Museum of Natural History*, 144:323–378.
- Simpson, G.G. 1972. Conspectus of Patagonian fossil penguins. *American Museum Novitates*, 2488:1–38.
- Simpson, G.G. 1979. Tertiary penguins from the Duinefontein site, Cape Province, South Africa. *Annals of the South African Museum Annale Van Die Suid-Afrikaanse Museum*, 79:1–7.
- Simpson, G.G. 1981. Notes on some fossil penguins, including a new genus from Patagonia. *Ameghiniana*, 18:266–272.
- Stanley, S.E. and Harrison, R.G. 1999. Cytochrome b evolution in birds and mammals: An evaluation of the avian constraint hypothesis. *Molecular Biology and Evolution*, 16:1575–1585. <https://doi.org/10.1093/oxfordjournals.molbev.a026070>
- Tambussi, C.P., Reguero, M.A., Marensi, S.A. and Santillana, S.N. 2005. *Crossvallia unienwillia*, a new Spheniscidae (Sphenisciformes, Aves) from the late Paleocene of Antarctica. *Geobios*, 38:667–675. <https://doi.org/10.1016/j.geobios.2004.02.003>
- Triche, N.E. 2007. *Systematics, biogeography, and evolutionary history of fossil and extant penguins (Aves: Sphenisciformes)*. Unpublished PhD Thesis, University of Texas, Austin, Texas, USA.
- Walsh, S.A. and Suárez, M.E. 2006. New penguin remains from the Pliocene of northern Chile. *Historical Biology*, 18:119–130. <https://doi.org/10.1080/08912960600640796>
- Wiens, J.J. 2003. Missing data, incomplete taxa, and phylogenetic accuracy. *Systematic Biology*, 52:528–538. <https://doi.org/10.1080/10635150390218330>
- Wiens, J.J. and Reeder, T.W. 1995. Combining data sets with different numbers of taxa for phylogenetic analysis. *Systematic Biology*, 44:548–558. <https://doi.org/10.2307/2413660>
- Wiman, C. 1905. Vorläufige Mitteilung über die alttertiären Vertebraten der Seymourinsel. *Bulletin of the Geological Institute of Upsala*, 6:247–253.

SUPPLEMENTARY MATERIALS

Two NEXUS files are available with additional supplementary material for this paper. They are available in a zipped file at <https://palaeo-electronica.org/content/2019/2773-chatham-island-penguins>.